Hemoglobin overexpression triggers neuronal cell death upon Parkinson's disease mimicking insults

Thesis submitted for the degree of "*Philosophiæ Doctor*"

SISSA - International School for Advanced Studies

Candidate
Marta Codrich

Supervisor
Prof. Stefano Gustincich

2013

Declaration

The work described in this thesis was carried out at International School for Advanced Studies (SISSA), Trieste, between November 2009 and October 2013 with exception of:

- FACS sorting was performed at Department of Medical and Biological Sciences (DSMB), University of Udine, Udine, Italy under the supervision professor Carlo Alberto Beltrami;
- Adeno-Associated Viruses preparation was performed at International Centre for Genetic Engineering and Biotechnology (ICGEB), Trieste, Italy under supervision of professor Mauro Giacca.

Abbreviations:

6-OHDA: 6-hydroxydopamine

AAVs: Adeno-Associated Viruses

AD: Alzheimer's disease

ALS: Amyotrophic Lateral Sclerosis

CAGE: Cap Analysis of Gene Expression

Cygb: cytoglobin

cDNA: complementary DNA

CMA: chaperone-mediated autophagy

CNS: Central Nervous System

CPu: striatum (caudatoputamen)

CTX: Cerebral cortex

DA: dopaminergic

eGFP: enhanced Green Fluorescent Protein

FACS: Fluorescent Activated Cell Sorting

GFP: Green Fluorescent Protein

Hb: hemoglobin

Hb-mut: mutant hemoglobin

HD: Huntington's disease

iMN9D: MN9D-Nurr1$^{Tet\text{-}On}$ dopaminergic neuroblastoma cells

LBs: Lewy bodies

LCM: Laser Capture Microdissection

LNs: Lewy neurites

MB: Midbrain

mDA: mesencephalic dopaminergic

MPP^+: 1-methyl-4-phenylpyridinium

MPTP: 1-methyl-4-phenyl-1,2,3,6-tetrahydropyridine

Ngb: neuroglobin

NO: Nitric Oxide

PCR: Polymerase Chain Reaction

PD: Parkinson's disease

ROS: Reactive Oxygen Species

RR: retrorubral

SN: Substantia Nigra

SNpc: Substantia Nigra pars compacta

TH: Tyrosine Hydroxilase

UPS: Ubiquitin-proteasome system

VTA: Ventral Tegmental Area

Table of contents

Zucchelli S, Codrich M, Marcuzzi F, Pinto M, Vilotti S, Biagioli M, Ferrer I, Gustincich S. TRAF6 promotes atypical ubiquitination of mutant DJ-1 and alpha-synuclein and is localized to Lewy bodies in sporadic Parkinson's disease brains. Hum Mol Genet. 2010 Oct 1;19(19):3759-70

Zucchelli S, Marcuzzi F, Codrich M, Agostoni E, Vilotti S, Biagioli M, Pinto M, Carnemolla A, Santoro C, Gustincich S, Persichetti F. Tumor Necrosis Factor Receptor Associated Factor 6 (TRAF6) associates with huntingtin protein and promotes its atypical ubiquitination to enhance aggregate formation. J Biol Chem. 2011 Jul 15;286(28):25108-17

Vilotti S, Codrich M, Dal Ferro M, Pinto M, Ferrer I, Collavin L, Gustincich S, Zucchelli S. Parkinson's Disease DJ-1 L166P alters rRNA biogenesus by exclusion of TTRAP from the nucleolus and sequestration into cytoplasmic aggregates via TRAF6. PLoS One. 2012;7(4):e35051

Russo R, Zucchelli S, Codrich M, Marcuzzi F, Verde C, Gustincich S. Hemoglobin is present as a canonical $\alpha_2\beta_2$ tetramer in dopaminergic neurons. Biochim Biophys Acta. 2013 May 17

Abstract

Parkinson's disease (PD) is the second most common neurodegenerative disease after Alzheimer's disease (AD). One of the most evident pathological hallmarks in PD is the selective loss of mesencephalic dopaminergic (mDA) neurons with the consequent decrease of dopamine in the brain. mDA neurons present two main groups of projecting cells: the A9 neurons of the Substantia Nigra (SN) and the A10 cells of the Ventral Tegmental Area (VTA). A9 neurons control the nigrostriatal pathway and are involved in regulation of voluntary movements and postural reflexes. Their selective degeneration leads to PD and the loss of DA synapses in the striatum is believed to be primary cause for the disruption of the ability to control movements. Until now, the causes of the degeneration of A9 neurons in PD are still unknown and a lot of efforts have been done to determine the molecular differences between the DA cell subpopulations that could explain the selective susceptibility of A9 neurons (Chung et al., 2005; Greene et al., 2005).

By a combination of different gene expression platforms coupled to Laser Capture Microdissection (LCM) hemoglobin α, adult chain 1 (Hba-a1) and β, adult chain 1 (Hbb-b1) transcripts have been previously identified as expressed. Furthermore, Hb protein in DA cells is present in the large majority of A9 cells, whereas only in 5% of A10 neurons. Importantly, this pattern of expression is conserved in mammals (Biagioli et al., 2009).

In this study, we aim to better understand the function of Hb in DA neurons. In particular, we assess the role of Hb in PD. To this purpose, we have taken advantage of MN9D-Nurr1$^{Tet\text{-}On}$ dopaminergic neuroblastoma cell lines (iMN9D) stably transfected with α and β chains of Hb (Biagioli et al., 2009) and their differentiated cultures as an *in vitro* model system to evaluate the effects of PD-mimicking insults, like 1-methyl-4-phenylpyridinium (MPP^+) and rotenone. In this study, we demonstrate that: 1) the impact of Hb overexpression depends on differentiation state of iMN9D cells upon MPP^+ treatment. Hb overexpression is protective in

undifferentiated cells, wheares it is toxic in differentiated cells; 2) Hb overexpression increases susceptibility to cell death upon rotenone in both undifferentiated and differentiated iMN9D cells; 3) Hb protection/toxicity doesn't depend on oxygen binding; 4) $\alpha_2\beta_2$ structure of Hb is not altered upon neurotoxic stimuli; 5) Hb-induced toxicity is concomitant with an increases of globin chains in the nucleus; 6) Hb overexpression is associated with an impairment of autophagy upon PD-like stimuli. Furthermore, we have studied the overexpression of Hb in an *in vivo* mouse model of PD. In details, we stereotaxically injected in SNpc AAV9-mediated overexpression of α and β globin in a MPTP regime. Preliminary data demonstrated that upon stimulus Hb overexpression influences DA neurons, even if there is not statistical difference. Further investigations must be done.

Our findings support a model in which Hb expression may contribute to A9-specific vulnerability in PD pathogenesis.

Introduction

Parkinson's disease

History

PD was first described by James Parkinson in 1817 in his monograph "Essay on the Shaking Palsy" as characterized by "*Involuntary tremolous motion, with lessened muscular power, in parts not in action and even when supported; with a propensity to bend the trunk forewords and to pass from a walking to a running pace: the senses and the intellect being injured*". PD was named by Jean Martin Charcot in 1862 and its clinical description was refined.

In 1912 Friedrich Lewy observed microscopic particles in affected brains later named "Lewy Bodies" (LBs). In 1997, α-synuclein was found to be the main component of LBs.

In 1919 Konstantin Tretiakoff reported that the SN is the main cerebral part affected in PD and finally in 1958, Arvid Carlsson (Nobel Prize in 2000) discovered that patients showed a massive loss of the neurotransmitter dopamine in the brain and its role in PD.

Epidemiology

PD is the second most common age-related neurodegenerative disease (six million patients worldwide) after AD. The prevalence of PD is about 0.3% of the whole population in industrialized countries. It is more common in the elderly and prevalence rises from 1% in those over 60 years of age to 4% of the population over 80 (de Lau and Breteler, 2006). The mean age of onset is around 60 years, although 5–10% of cases, classified as young onset, begin between the ages of 20 and 50 and

are probably hereditary. Some studies have proposed that it is more common in men than women, but others failed to detect any sex differences (de Lau and Breteler, 2006).

The incidence of PD is between 8 and 18 per 100,000 person/year. The precise mode of death is difficult to identify in most cases but pneumonia is the most certificated cause.

Clinical features

PD is a progressive neurodegenerative disorder and the motor symptoms result from the death of dopamine-generating cells in the SN. Clinically, any disease that includes striatal DA deficiency or direct striatal damage may lead to "parkinsonism" and PD is the most common cause of this syndrome. In 95% of cases PD is sporadic and idiopathic but in 5% the disease is genetically inherited (Fitzgerald and Plun-Favreau, 2008).

Early, in the course of the disease, the most obvious symptoms involve alteration of the ability to control movements and are characterized by tremor at rest, rigidity, slowness (bradykinesia) or absence of voluntary movement, postural instability and freezing. Later, cognitive and behavioral problems may arise, with dementia commonly occurring in the advanced stages of the disease; patients become passive or withdrawn with lacking of initiative. Depression is common.

Although PD is classically diagnosed by onset of motor manifestation, pre-motor symptoms have been observed; these include olfactory dysfunction, sleep abnormalities, cardiac sympathetic denervation, constipation and pain (O'Sullivan et al., 2008).

Clinically, the disease is heterogeneous however two major subtypes exist: a "tremor predominant form" that is often observed in younger people and a type known as "postural imbalance and gait disorder" (PIGD) often observed in older people (>70 years old), characterized by akinesia, rigidity and gait of balance impairment. In general, the first type leads to a slow decline of motor functions whereas the latter worsens more rapidly (Selikhova et al., 2009).

Therapy

PD is still incurable but therapeutic treatments improve quality of life of patients. L-dopa in combination with a peripheral dopa-decarboxylase inhibitor (benserazide or carbidopa) is the most effective therapy and allows the replace, at least in part, of the dopamine lost during degeneration of SNpc cells. Although prediction of therapeutic response in an individual is not possible, motor symptoms initially improve by 20-70%. Speech, swallowing and postural instability can also improve but these symptoms are generally less responsive and escape more readily from long-term control. The non-ergoline dopamine agonists (pramipexole, ropinirole, rotigotine and piribedil) are efficacious and in contrast to L-dopa, when used as monotherapy, do not provoke dyskinesias. They are a popular first-line treatment in patients under 55 years of age but L-dopa is usually necessary in 3 years from diagnosis. Unfortunately, dopamine agonists cause some side effects as gastrointestinal and psychiatric effects and sleep attack.

The monoamine oxidase B (MAO-B) inhibitors (selegiline and rasagiline) are well tolerated but they are less efficacious than dopamine agonists. They seem to delay disease progression. The combination of L-dopa and MAO-B inhibitor could help to eliminate early wearing-off effects (that represents the period of time between the end of the effect of one dose of medication, and the beginning of the next one) and the partial substitution of L-dopa with a dopamine agonist could also reduce dyskinesias (Lees et al., 2009).

Although the treatments for PD have improved the life expectancy and control of bradykinesia, no neuroprotective treatment can arrest the disease process and dopaminergic therapy is far from solving the motor impairments.

Some studies have proposed fetal mDA cell implantation to achieve physiological dopamine release (Paul et al., 2006). Stem cell, especially human embryonic stem cells, that can differentiate *in vitro*, provide a potentially unlimited supply of DA neurons. However it has to be considered the potential risk of tumor formation (Laguna Goya et al., 2008).

Glial-cell-line-derived neurotrophic factor has potent neurotrophic effect in DA neurons in animal models. Unfortunately, a controlled trial with monthly administration of these factors gave negative result at six months (Gill et al., 2003; Lang et al., 2006).

In conclusion, further research on the PD neurodegeneration process is needed to discover disease biomarkers and develop therapeutic interventions.

Neuropathological features of PD

The most evident pathological hallmarks of PD are the loss of the nigrostriatal DA neurons and the presence of intraneuronal proteinacious cytoplasmatic inclusions termed LBs (figure1).

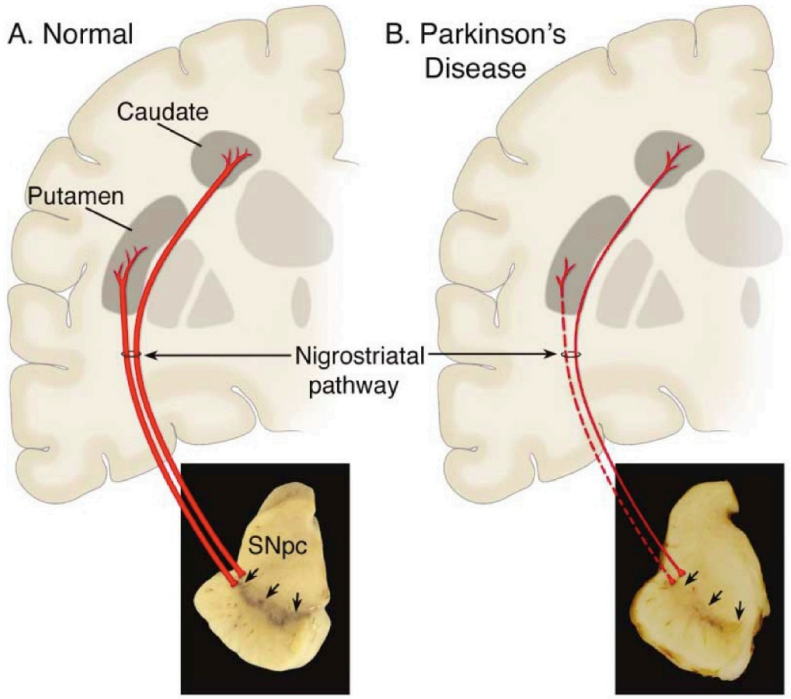

Figure 1. Neuropathology of Parkinson's disease.
(A) Schematic representation of the normal nigrostriatal pathway. (B) Schematic representation of the diseased nigrostriatal pathway. There is a marked loss of DA neurons that project to putament (dashed line) and more modest lose of those that projects to the caudate (red line). The photograph demonstrates depigmentation of SNpc due to the loss of DA neurons (adapted from Dauer and Przedborski, 2003).

Loss of DA neurons and depletion of dopamine in striatum

The characteristic motor symptoms of PD are due to the alteration of motor system in central nervous system (CNS) in particular to the gradual, selective and progressive loss of nigrostriatal DA neurons.

Voluntary movements originate at motor cortex level: signals are sent through the

encephalic trunk (mesencephalon, pons and medulla) to the brain stem and spinal cord. These signalling pathways are controlled by different sub-cortical structures (thalamus, putamen and subthalamic nuclei) that modulate movements thanks to a complex network of excitatory and inhibitory signals (figure 2). These nuclei are, in turn, innervated and modulated by ventral midbrain DA neurons, subdivided into three main groups: A8 (retrorubral field; RRF), A9 (substantia nigra pars compacta; SNpc) and A10 (ventral tegmental area; VTA). The sensorimotor striatum involved in control of movement (putamen) is mainly innervated by A9 DA cells whereas the limbic ventral striatum and the thalamus are preferentially targeted by A10 and dorsal SNc neurons.

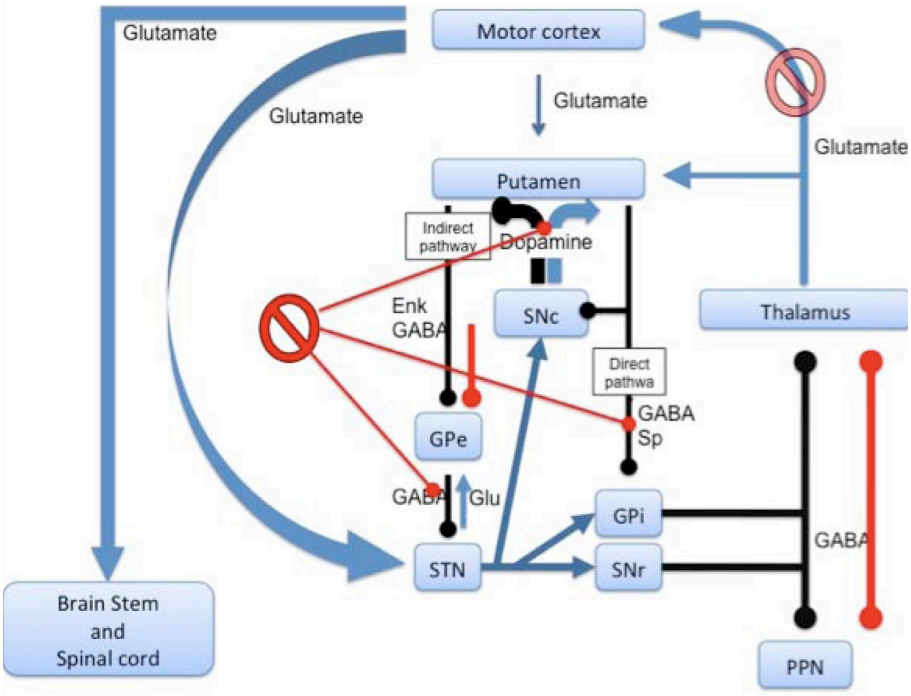

Figure 2. Schematic illustration of the basal ganglia-thalamocortical "motor" circuit and its neurotrasmitters.
Blue arrows represent excitatory transmission and black arrows inhibitory transmission, red symbols represent the pathway disregulations that happen in PD. (GPe, GPi globus pallidus external and internal segment, STN subthalamic nucleus, PPN pedunculopontine nucleus).

The cell bodies of A9 nigrostriatal neurons are in SNpc and they project primary to putamen. The loss of these neurons, which normally contain conspicuous amount of neuromelanin (Marsden, 1983), produces the classic neuropathological finding of SNpc depigmentation. The pattern of SNpc cell loss parallels with the decrease of expression level of the DA transporter (DAT) mRNA (Uhl et al., 1994) and it is

consistent with the observation that depletion of DA innervations is most pronounced in the dorsolateral putamen (Bernheimer et al., 1973).

At the onset of the symptoms, putamen is depleted about 80% and 60% of SNpc DA neurons have already been lost. The mesolimbic DA neurons, the cell bodies of which reside adjacent to the SNpc in the VTA is much less affected in PD (Uhl et al., 1985).

The loss of striatal DA pathway causes an unbalance between excitatory and inhibitory transmission in the basal ganglia thalamocortical "motor" circuit (figure 2). On one hand, decreased striatal dopamine stimulation causes the direct reduction of the inhibition of the GPi/SNr; on the other hand, decreased dopamine activity causes increased inhibition of the globus pallidus external segment (GPe), resulting in blocking the inhibition of the subtalamic nucleus (STN). Augmented STN output increases GPi/SNr inhibitory output to the thalamus that can not regulate the activity of the motor cortex any longer. The pattern of progressive cell loss displays a complex topographical and regional organization because the degeneration starts from the most lateral part of SNc and spreads to the most medialis region in different stages of the disease. The loss of the nigral DA neurons and terminals are responsible for the movement disorders associated with PD, however additional neuronal populations are affected in the disease such as medulla oblongata, pontine, tegmentum, olfactory bulb and anterior olfactory nucleus (Braak et al., 2004).

Lewy bodies

Distinct intraneuronal lesions accompany the nerve-cell loss: the LBs and the Lewy neurites (LNs). LBs and LNs are present in PD patients' brains in some of the surviving DA neurons and in other regions like dorsal motor nucleus of the vagus, locus ceruleus, thalamus, amygdala, olfactory nuclei, pediculopontine nucleus, and cerebral cortex. In late stages of PD, when patients manifest all motor and cognitive clinical symptoms, inclusion bodies decorate the entire neocortex comprising the sensory association area (Braak et al., 2004).

LBs are round cytoplasmatic eosinophilic inclusions, 5–25 μm in diameter (figure 3). The ultrastructure shows they are composed of a dense core of filamentous and granular material, surrounded by radially orientated filaments of 10–20 nm in diameter. LBs are composed by the accumulation of cytoplasmic aggregates containing a variety of proteins, like α-synuclein, the major component, parkin and UCHL1 (genes whose mutations have been correlated with PD) and many others like

Hsp-70, ubiquitin and components of the proteasome (Spillantini and Goedert, 2000). LNs are abnormal neurites that contain the same proteins and abnormal filaments found in Lewy bodies.

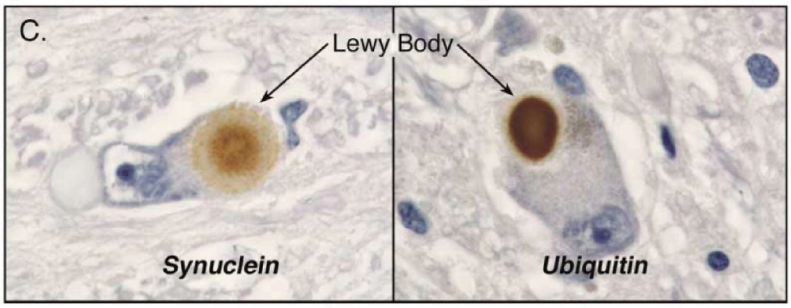

Figure 3. Immunohistochemical staining of Lewy Bodies found in DA neurons of PD patients in SNpc. Unsoluble fibrous component of aggregates are detected with anti-αsynuclein antibody and anti-ubiquitin (adapted from Dauer and Przedborski, 2003).

The mechanism causing the abnormal accumulation of proteins in Lewy bodies and Lewy neurites is not yet known and their toxic or protective role in neurodegenerative process is still matter of debate because till now there is no clear correlation between inclusion formation and neuronal cell death. According to the hypothesis that LBs are toxic, cytoplasmic protein aggregates may interfere with intracellular trafficking or sequestrate proteins important for cell survival. On the other hand, LBs are present in surviving cells that seem to be healthier than neighboring cells by morphological and biochemical analysis (Tompkins and Hill, 1997). Moreover, LBs have been found also in people without evident neuronal loss or clinical signs of PD, so they could be a protective structure in which proteins accumulate after the pathological failure of protein degradation.

Iron accumulation

In the brain, iron has different roles ranging from facilitation of cellular aerobic metabolism to synthesis and signal transduction of neurotransmitters. Through a critical component of cytochromes, enzymes and binding proteins, free iron can be cytotoxic by catalyzing the production of hydroxyl radical from hydrogen peroxide. Iron has been suggested to be responsible for nigrostriatal dopamine neuron degeneration in PD owing to its ability to produce toxic ROS and cause lipid peroxidation (Sian-Hülsmann et al., 2011).

Iron deposits in degenerating neurons of the SN and in LBs can have deleterious

effects on the extrapyramidal system and on psychomotor function. The presence of the pigment, neuromelanin, in the SN in PD also might result in iron accumulation, because neuromelanin can function like ferritin and store iron (figure 4).

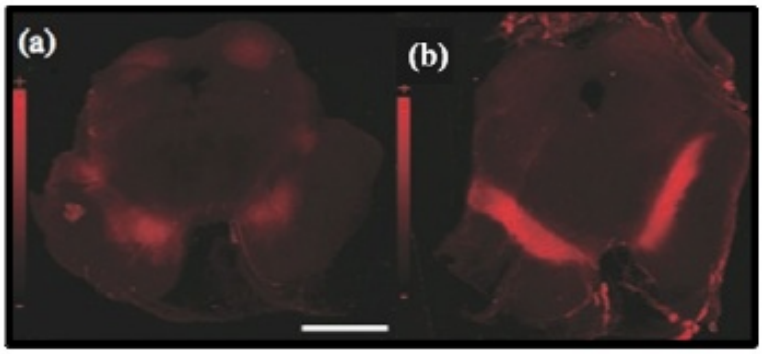

Figure 4. Iron distribution is abnormal in PD midbrain.
Transverse section of normal midbrain (a) and PD midbrain (b).

Iron may interact and interfere with the normal dopaminergic functions including α-synuclein, dopamine and TH. Moreover, it has been demonstrated that iron deficiency diet produces several expression changes in dopamine-related genes in the ventral midbrain in mice. These included dopamine receptor 2 (Drd2), Alas2, which encodes an erythroid enzyme that catalyzes heme biosynthesis, Ahsp, which gived rise to an erythroid protein that stabilizes α hemoglobin, and β hemoglobin (Hbb-b1) (Jellen et al., 2013).

All these mechanisms suggest that disturbances in iron homeostasis and metabolism in PD occur at several levels, such as iron uptake, storage, intracellular metabolism, release, and post-transcriptional control. A disturbance in iron homeostasis can provide a favorable condition in which free iron, via generation of ROS, causes permanent tissue damage.

Aetiology

The cause of sporadic PD is unknown and the role of environmental toxins and genetic factors are not yet well understood.

Environmental factors

The environmental toxin hypothesis was largely supported in the 20th century

especially because of the discovery that some toxins can mimic the pathological features of PD. Examples are the post-encephalitic PD syndromes (as described by Oliver Sacks in his book "Awakenings") and the 1-methyl-4-phenyl-1,2,3,6-tetrahydropyrydine (MPTP)-induced parkinsonism (Langston and Ballard, 1983). Moreover, the exposure to some herbicides (i.e. paraquat) and pesticides (i.e. rotenone) have been correlated to elevated risk of PD (Tanner et al., 2011).

Another possibility is that an endogenous toxin derived from distortion in the normal metabolism may be responsible for PD neurodegeneration. One source of endogenous toxins may be the normal metabolism of DA which generates reactive oxygen species (ROS) (Cohen, 1984). Consistent with this hypothesis is the fact that patients with specific polimorfisms in the gene codifying the xenobiotic detoxifying enzyme cytochrome P450 may be at greater risk of young onset-PD (Sandy et al., 1996).

Genetic factors

In the 5% of the cases, PD is a genetic disorder and 13 loci and 9 genes have been associated to both autosomal and recessive forms of disease. There is a growing list of mutations linked to PD and they account 2-3% of the late-onset cases and 50% of early-onset forms (Farrer, 2006). The most part of these mutations have been identified in genes encoding proteins that accumulate in LBs and LNs. The mutated genes associated with familial PD are SNCA, PARKIN, UCHL1, DJ-1 and LRRK2.

	Pathological aggregates	Comments
Parkinsonism		
Parkin	Substantia-nigra degeneration but usually no Lewy bodies	Recessive, young onset
PINK1	No pathology reported	Recessive, young onset
DJ-1	No pathology reported	Recessive, young onset
ATP13A2	No pathology reported	Recessive young onset
Parkinson's disease		
α-synuclein	Lewy bodies	Dominant point mutations and duplications. Genetic variability contributes to disease
LRRK-2	Usually Lewy bodies	Dominant mutations
GBA	Lewy bodies	Dominant loss of function mutations increase risk

GBA=glucocerebrosidase. *LRRK-2*=leucine rich repeat kinase 2. *PINK1*=PTEN-induced putative kinase 1.

Table: **Genes associated to L-dopa-responsive parkinsonism**

Table 1. Genes associated to L-dopa-responsive parkinsonism (adapted from Lees et al., 2009).

The study of these mutations may help to define the molecular pathways involved in neurodegeneration in PD. Genetic studies have shown that several mutation in seven genes are linked with L-dopa-responsive parkinsonism (Table 1).

SNCA (PARK1 and PARK4) gene encodes for α-synuclein. Missense mutations, gene duplications and triplication are observed in PD (Polymeropoulos et al., 1997; Ross et al., 2008; Singleton et al., 2003). α-synuclein is a natively unfolded protein because of the lack of secondary or tertiary structure and it accumulates in pre-synaptic nerve terminals associated with membranes of synaptic vesicles. It has natively a great propensity to aggregate both *in vitro* and *in vivo*, especially in the presence of oxidative stress and of several herbicide and pesticide.
The mutant forms Ala30Pro and Ala52Thr form protofibrils, an intermediate in the process of aggregation. Pesticides (such as rotenone, dieldrin and paraquat), metal ions (copper, iron) and other factors accelerate its fibrillation. The causes and consequences of α-synuclein aggregation is not yet fully understood but mutations and overexpression of this protein seem to be especially toxic to DA neurons.
Furthermore, dopamine-synuclein toxicity may inhibit chaperone-mediated autophagy (Xilouri et al., 2009). The *in vitro* expression of α-synuclein in DA neurons also results in inclusion formation and triggers pronounced (~50%) neuronal loss.
Finally, transgenic mice expressing the wild-type human gene for α-synuclein develop several of the clinic-pathological features of PD like accumulation of LBs in neurons of the neocortex, hippocampus and SN and loss of DA terminals in the basal ganglia (Masliah et al., 2000).

PARKIN (PARK2) mutations are the second most common genetic cause of disease.
Parkin encodes an E3 ubiquitin ligase that controls key step in the cycle of ubiquitin-mediated hydrolysis of damaged or misfolded proteins that are degraded via the proteosome. This form of PD is characterized by the absence of Lewy bodies and since LBs found in PD patient are immunoreactive for some of parkin substrates, it has been proposed a role of this protein in LB formation (Dawson, 2006).

Mutations in **LRRK2** (PARK8), encoding the leucine-rich repeat kinase2 (also named dardarin), represent the highest risk of development of familiar PD and the disease penetrance markedly increases with age (Healy et al., 2008; Paisán-Ruíz et al., 2004).
It is a large protein and contains both Rab-GTPase and kinase activity and also other domains involved in multi-protein scaffold interactions (Smith et al., 2005).
It has numerous roles in the secretory pathway and may contribute to adult neurogenesis, remodelling of cytoskeletal architecture and membrane and

dopaminergic signalling. Among the six pathogenic forms of LRRK2 found in PD patients, the most common mutation is Gly2019Ser with a worldwide frequency of 1% in sporadic and 4% in genetic form (Healy et al., 2008).
Transgenic mice that express the mutated form of LRRK2 (R1441G) recapitulate most of the PD motor symptoms that are reverted by the administration of Levodopa (Li et al., 2009).
Loss-of-function mutations in four genes cause recessive early-onset parkinsonism (age of onset <40 years).

UCH-L1 (Ubiquitin C-terminal hydrolase L1) (PARK5) is mainly expressed in the brain and catalyzes the hydrolysis of ubiquitin C-terminal ends. In particular UCH-L1 regulates ubiquitin-mediated proteolysis, preparing the monomers of ubiquitin that must be added to the substrates. Mutated forms of the gene have been identified in an autosomal dominant form of PD. The mutations cause a decrease of the enzymatic activity of the protein (Das et al., 2006). Deletions and missense mutations (I93M) have been identified (Setsuie et al., 2007). A polymorphism (S18Y) appears to reduce the risk of developing PD (Carmine Belin et al., 2007).
It is important to note that UCH-L1 KO mice show signs of neurodegeneration but not in the nigrostriatal dopaminergic pathway (Chen et al., 2010).

PINK1 (PTEN induced-kinase 1) (PARK6) is a mitochondrial serine/threonine protein kinase, functionally linked to parkin because their concomitant expression induces mitochondrial fission and survival of striatal neurons (Lutz et al., 2009). Parkin is recruited to dysfunctional mitochondria to promote their autophagic degradation and rescues degeneration in PINK1-null flies (Narendra et al., 2009). Moreover, PINK1 protects cells against apoptosis induced by exposure to proteosome inhibitors (Valente et al., 2004).

The function of **DJ-1** (PARK7) is not yet fully understood. It was cloned as interactor of GAPDH playing a role in mRNA regulation by stabilizing mRNA species after transcription (Hod et al., 1999). It maintains neuronal viability by modulating gene expression under cellular stress condition (Mitsumoto et al., 2001).
The L166P mutant promotes localization of the normally cytoplasmatic DJ-1 protein to mitochondria (Bonifati et al., 2003) implying that the loss of normal function of

DJ-1 is sufficient to induce PD.

DJ-1 functions as a cytoplasmic redox-sensitive molecular chaperone *in vitro* and *in vivo*, inhibiting the aggregation of α-synuclein in neuronal cell lines at an early step of the aggregation process; in fact, its loss increases the accumulation of insoluble α-synuclein. It has been hypothesized that DJ-1 may promote the degradation of misfolded proteins, either through the proteasome or through chaperone-mediated autophagy (Shendelman et al., 2004).

ATP132A (PARK9) mutation has been linked to juvenile and rare forms of PD often with atypical symptoms and no LBs or loss of DA neurons. This gene encodes for a large lysosomal P-type ATPase and mutations lead to a truncated protein that is retained in the endoplasmic reticulum instead of inserted in lysosomal membranes and degraded by proteasome. Its mutations seem to lead to a failure of autophagy execution and aggregation of α-synuclein (Ramirez et al., 2006; Di Fonzo et al., 2007).

Pathogenesis

The studies of toxic PD models, the functions of PD-related genes and the analysis of post-mortem brains of PD patients suggest two major interconnected hypothesis regarding the pathogenesis of the disease: misfolding and aggregation of proteins and mitochondrial dysfunctions and the consequent oxidative stress (figure 5).

Mitochondrial dysfunction and oxidative stress

The possibility that an oxydative phosphorylation defect plays a role in the pathogenesis of PD was supported by the discovery that MPTP blocks the mitochondrial electron transport chain by inhibiting complex I (Nicklas et al., 1987).

Other studies identified abnormalities in complex I activity in PD (Greenamyre et al., 2001) and *in vitro* experiments showed that complex I defects may induce oxidative stress and energy impairment.

In the cell, molecular oxygen is consumed by mitochondrial respiration and powerful oxydants are produced as bioproducts including hydrogen peroxide, and superoxide radicals. Inhibition of complex I increases the ROS superoxide which may form

peroxynitrite. These molecules may cause cellular damage by reacting with DNA, proteins and lipids. The electron transport chain may be a target leading to mitochondrial damage and further ROS production (Cohen, 2000). In turn, ROS increase the amount of misfolded proteins.

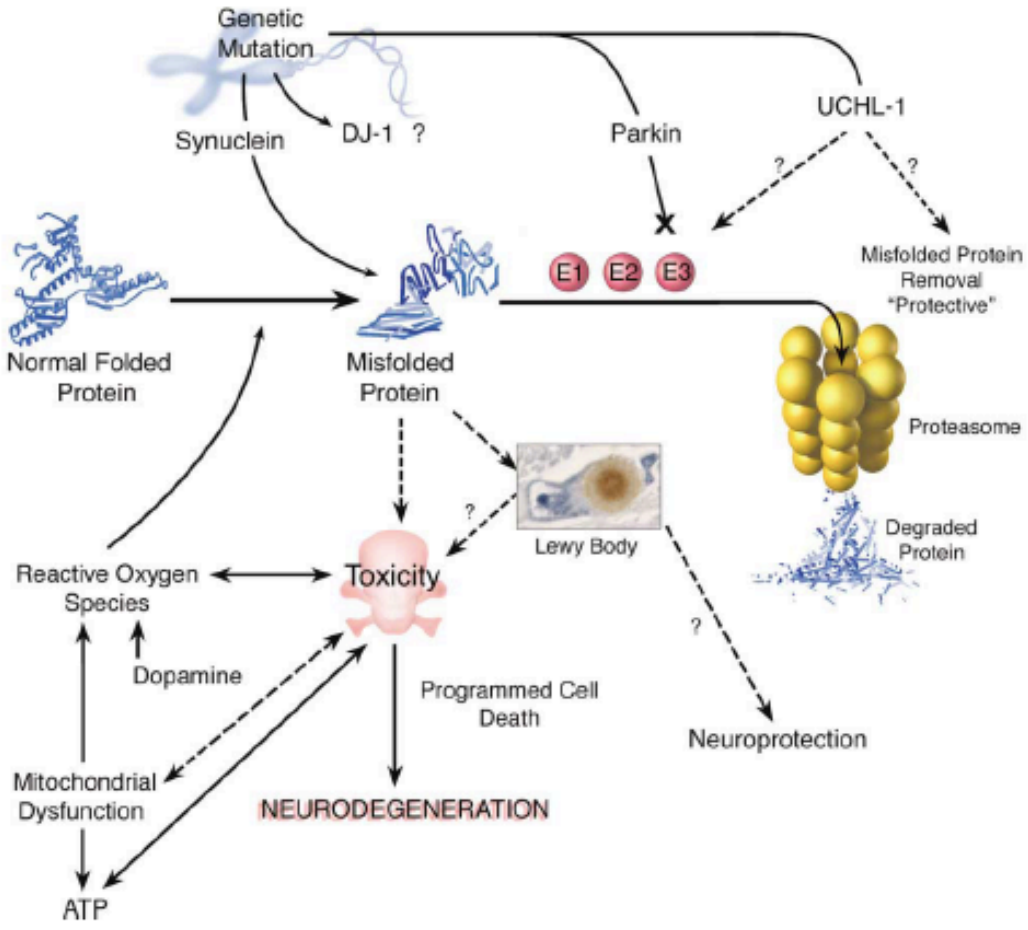

Figure 5. Mechanisms of neurodegeneration in Parkinson's disease.
A growing body of evidence suggests that the accumulation of misfolded proteins is likely to be a key event in PD neurodegeneration. Pathogenic mutations may directly induce abnormal protein conformations (as believed to be the case with α-synuclein) or damage the ability of the cellular machinery to detect and degrade misfolded proteins (Parkin, UCH-L1); the role of DJ-1 remains to be identified. Oxidative damage, linked to mitochondrial dysfunction and abnormal dopamine metabolism, may also promote misfolded protein conformations. It remains unclear whether misfolded proteins directly cause toxicity or damage cells via the formation of protein aggregates (Lewy body). Controversy exists regarding whether Lewy bodies promote toxicity or protect a cell from harmful effects of misfolded proteins by sequestering them in an insoluble compartment away from cellular elements. Oxidative stress, energy crisis (i.e., ATP depletion) and the activation of the programmed cell death machinery are also believed to be factors that trigger the death of DA neurons in Parkinson's disease (adapted from Dauer and Przedborski, 2003).

DA neurons may be important ROS generators because metabolism of DA produces hydrogen peroxide and superoxide radicals and auto-oxidation of DA produces DAquinone (Graham, 1978), which reacts with cysteines damaging proteins.

Mitochondrial-related energy failure may disrupt vesicular storage of DA, causing the free cytosolic concentration of DA to rise and allowing harmful DA-mediated reactions to damage cellular macromolecules. Accordingly, DA may be fundamental in rendering DA neurons particularly susceptible to oxidative attack.

Misfolding and aggregation of proteins

The abnormal deposition of proteins is observed in brain of patients affected by several age-related neurodegenerative disease, including PD.

Alteration of protein folding, ubiquitin-proteasome system (UPS) and autophagy are considered among the main molecular events inducing aggregate formation.

Aggregated or soluble misfolded proteins could be toxic through a variety of mechanisms: such as forming cells' damage, interfering with intracellular trafficking, sequestering proteins important for cell survival. Cytoplasmic inclusions may not result simply from precipitated misfolded proteins but rather from an active process meant to sequester soluble misfolded proteins (Kopito, 2000). Thus, inclusion formation may be a defensive measure to remove toxic soluble misfolded proteins (Warrick et al., 1999; Cummings et al., 1999, 2001; Auluck et al., 2002). This is supported by the fact that chaperons as Hsp-70 protect against neurodegeneration mediated by α-synuclein toxicity (Muchowski, 2002).

The presence of dysfunctional protein metabolism in PD may be due to oxidative stress caused by ROS. The tissues content of abnormally oxidized proteins (which may misfold) increases with age and neurons may be particularly susceptible since they are post mitotic cells. In fact, LBs contain oxidatively modified α-synuclein, which *in vitro* has a great propensity to aggregation (Giasson et al., 2002).

Moreover, some herbicides and pesticides induce misfolding and aggregation of α-synuclein (Uversky et al., 2001; Lee et al., 2002; Manning-Bog et al., 2002).

Ubiquitin-proteasome system

Cells normally respond to misfolded proteins through chaperons but if not properly refolded they are targeted to proteasomal degradation by poly-ubiquitination. Ubiquitination of a substrate requires a cascade of enzymes: ubiquitin-activating enzyme (E1), ubiquitin-conjugating enzymes (E2s) and ubiquitin-protein ligases (E3s) that are responsible for highly specific target recognition in this system through physical interactions with the substrate.

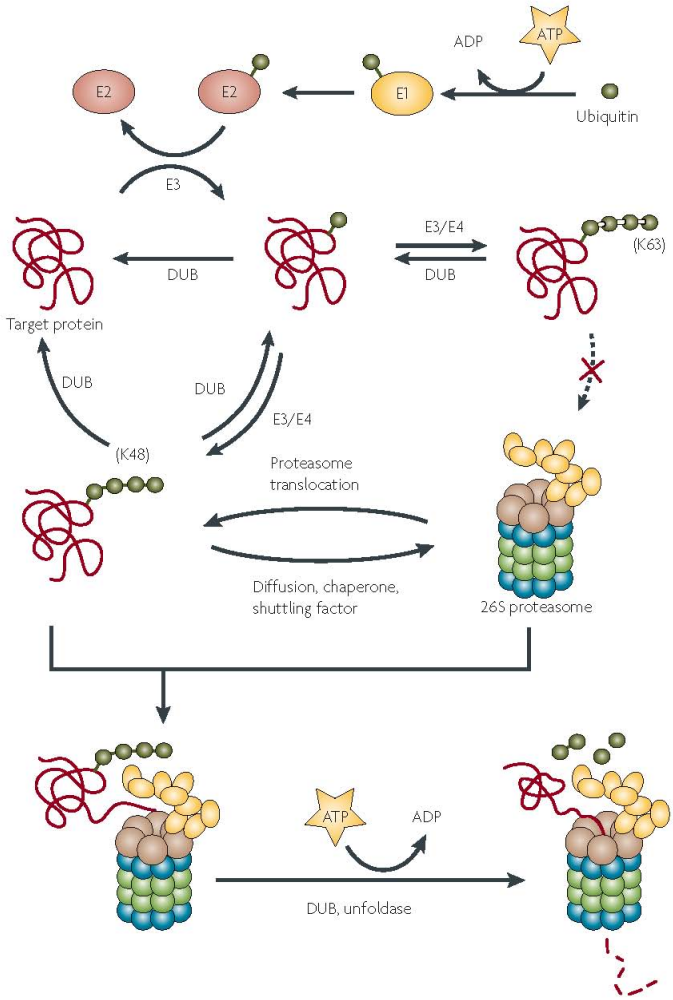

Figure 6. Schematic representation of the ubiquitin proteasome system.

Proteasome is a multi-subunit protein complex composed by a 20S core complex where proteins are degraded, a 19S regulatory complex that removes the ubiquitin and unfolds the protein for translocation into the 20S chamber and the so called 11S complex (or REG or PA28) that is thought to activate the 20S.

With age, the cells decline in their ability to manage misfolded proteins and also the ability to induce chaperons and proteosomal function is impaired (Sherman and Goldberg, 2001). Proteosomal dysfunction and consequent accumulation of misfolded proteins inhibit an already compromised proteosome. When misfolded proteins are not correctly degraded and UPS is misregulated, toxic aggregates form. It is interesting to note that LBs are immunoreactive against chaperone proteins (i.e. Hsp70), ubiquitin, and components of the 20S of the proteasome system.

Autophagy

Autophagy is another mechanism through which proteins can be degraded. Most long-lived proteins, cytoplasmic constituents, including organelles, are sequestered into double-membraned autophagosomes, which subsequently fuse with lysosomes where their contents are degraded thanks to proteolytic enzymes. There are three different types of autophagy: macroautophagy, microautophagy and chaperone-mediated autophagy (CMA) (Mizushima et al., 2008) (figure 7).

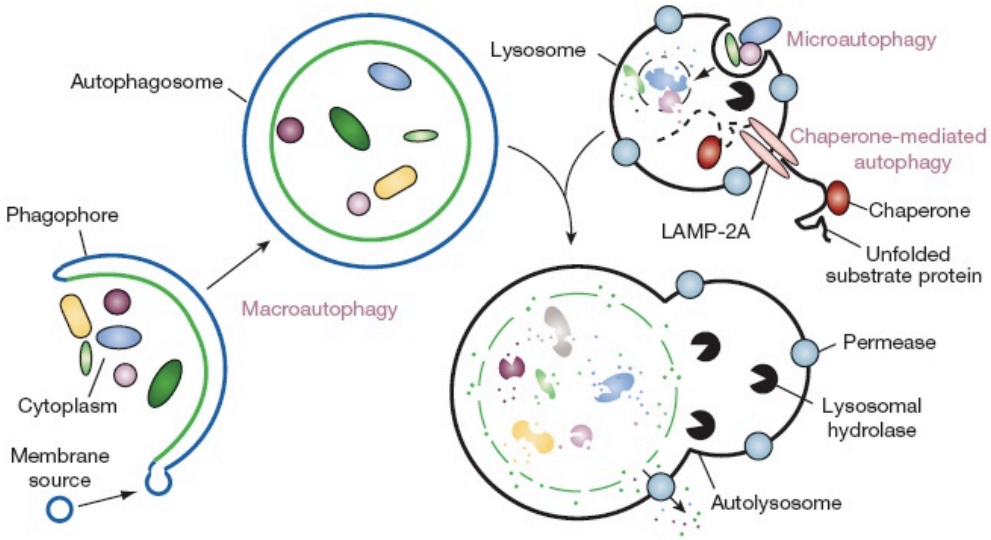

Figure 7. Different types of autophagy: macroautophagy, the microautophagy and mediated chaperone-mediated autophagy (CMA) (adapted from Mizushima et al., 2008)).

CMA involves direct translocation of unfolded substrate proteins across the lysosome membrane through the action of a cytosolic and lysosomal chaperone Hsp70 and the integral membrane receptor LAMP-2A (lysosome-associated membrane protein type 2A). CMA involves the degradation of cytoplasmic proteins that contain a consensus sequence KFERQ for lysosome association. Interestingly, many proteins involved in neurodegenerative diseases contain this sequence, as α-synuclein in PD and the amyloid precursor protein (APP) in AD (Massey et al., 2004).

Microautophagy refers to the sequestration of cytosolic components directly by lysosomes through invaginations in their limiting membrane.

Macroautophagy (also called autophagy) requires the formation of a double membrane structure called the phagosome, whose origin is unknown. The phagosome sequester portions of cytoplasm containing proteins prone to aggregation or damaged organelles. Subsequently the phagosome becames autophagosome and merges with

the lysosome to form an autolysosome, where contents will be degraded due to hydrolases.

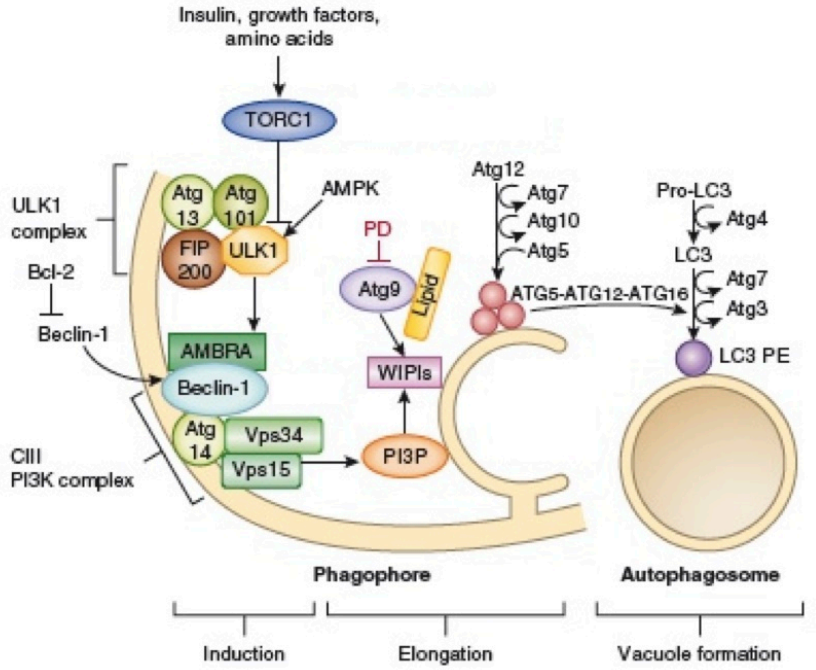

Figure 8. Autophagy induction and autophagosome biogenesis.
Autophagosome formation can be initiated via mTOR inhibition or AMPK activation. This results in the phosphorylation of ULK1 at sites that activate it and catalyze phosphorylation of other components of the Atg1–ULK complex, composed of ULK1, ULK2, Atg13, FIP200 and Atg101. ULK1 also phosphorylates AMBRA, a component of the PI3K CIII complex I (Vps34, Vps15, Atg14, and beclin-1), enabling it to relocate from the cytoskeleton to the isolation membrane. Phosphatidylinositol 3-phosphate (PI3P), generated by Vps34 activity, specifically binds the PI3P effectors WD repeat domain phosphoinositide-interacting 1 (WIPI1) and WIPI2 and catalyzes the first of two types of ubiquitination-like reactions that regulate isolation membrane elongation. In this first reaction, Atg5 and Atg12 are conjugated to each other in the presence of Atg7 and Atg10. Attachment of the fully formed complex containing Atg5, Atg12 and Atg16L on the isolation membrane induces the second complex to covalently conjugate phosphatidylethanolamine to LC3, which facilitates closure of the isolation membrane184. Atg9 (the Atg9–Atg2–Atg18 complex), another factor essential for this event, cycles between endosomes, the Golgi and the phagophore, possibly carrying lipid components for membrane expansion. Atg4 removes LC3-II from the outer surface of newly formed autophagosomes, and LC3 on the inner surface is eventually degraded when the autophagosome fuses with lysosomes. The steps known to be affected in Parkinson's diseases are indicated in red. PE, phosphatidylethanolamine. Modified from (Nixon, 2013).

Autophagy is orchestrated by a family of proteins called Atg (Autophagy related gene), which are negatively regulated by mTOR (mammalian Target Of Rapamycin).
One of the key molecular components involved in autophagy is Atg8/LC3 (microtubule associated protein 1 Light Chain 3). The conversion of soluble LC3I to lipid bound LC3II is associated with the formation of autophagosomes (Komatsu et al., 2005, 2006).
Interestingly, accumulation of autophagic vacuoles has been seen in DA neurons of

histopathological sections of PD patients post-mortem brains (Nedelsky et al., 2008). Moreover, recent evidence demonstrated protection effects of autophagy-induced drug (rapamycin) on cellular and animal models of PD (Tzeng et al., 2010; Liu et al., 2011).

It is still to clarify whether autophagy is a cause or a protective factor of neuron death. It has been suggested that the increased number of autophagic vacuoles is responsible for neuronal cell death. However, a more evident model suggests that autophagy is induced to protect neurons by enhancing degradation of abnormal proteins that might trigger injury or apoptosis in the early stages of cell death (Butler et al., 2006; Bandyopadhyay et al., 2007).

Animal model of PD

Various animal models have provided as tools to better understand PD etiology, pathology, and molecular mechanisms. For the past several decades, animal models of PD have come in a variety of forms. Typically, they can be divided into those using environmental or synthetic neurotoxins or those utilizing the *in vivo* expression of PD-related mutations.

Toxin-based models

The neurotoxins used to induce dopaminergic neurodegeneration are divided in reversible compounds, as reserpine, and irreversible compounds, as 6-hydroxydopamine (6-OHDA), MPTP, paraquat and rotenone. A common feature of all toxin-induced models is their ability to produce oxidative stress and to cause cell death in DA neuronal populations that reflect what is seen in PD (Betarbet et al., 2002; Dauer and Przedborski, 2003). Oxidative stress results from increased production of extremely reactive free radicals, including reactive oxidative species and peroxynitrite. ROS may be formed during a number of cellular processes, including mitochondrial oxidative respiration and metabolism.

MPTP

In 1982, MPTP was accidentally discovered in a synthesis process gone awry and young drug addicts developed an idiopathic parkinsonian syndrome after intravenous

injection of MPPP. After investigating the etiology of their condition, it was found that MPPP was contaminated with MPTP and this was the neurotoxic molecule responsible for the parkinsonian effect (Langston et al., 1983). Today it represents the most important and most frequently used parkinsonian toxin applied in animal models. It has been demonstrated that MPTP is indeed able to mimic oxidative stress, ROS, energy failure, and inflammation, which have been reported as hallmarks of PD (Langston et al., 1983). Unfortunately, lacking in this list is one of the characteristics of PD, LB formation (Forno et al., 1993; Halliday et al., 2009).

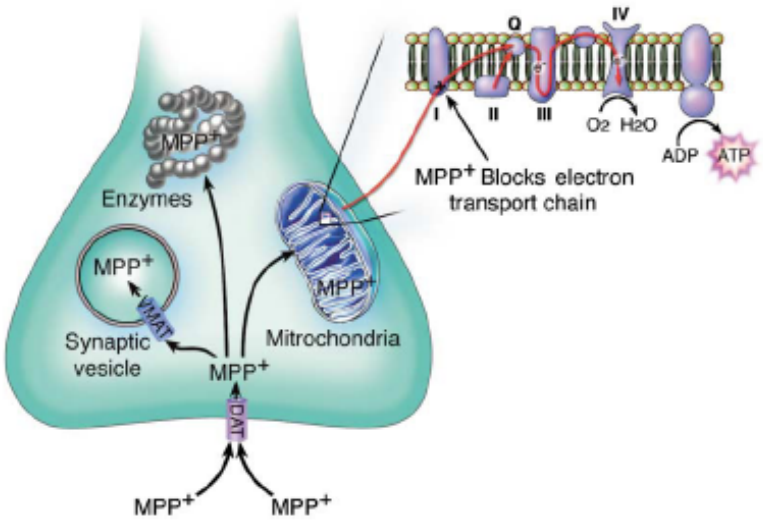

Figure 9. Schematic representation of MPP^+ intracellular pathways.
Inside DA neurons, MPP+ can follow one of three routes: (1) concentration into mitochondria through an active process (toxic); (2) interaction with cytosolic enzymes (toxic); (3) sequestration into synaptic vesicles via the vesicular monoamine transporters (VMAT; protective). Within the mitochondria, MPP+ blocks complex I (X), which interrupts the transfer of electrons from complex I to ubiquinone (Q). This perturbation enhances the production of reactive oxygen species (not shown) and decreases the synthesis of ATP (adapted from Dauer and Przedborski, 2003).

MPTP is highly lipophilic and after systemic administration rapidly crosses the blood-brain barrier. Once in the brain, MPTP enters astrocytes and is metabolized into MPP^+, its active metabolite, by monoamine oxidase B (MAO B). Once released from the astrocytes into the extracellular space via the OCT-3 transporter (Cui et al., 2009), MPP^+ is taken up into neurons by the dopamine transporter (DAT) and can be stored in vesicles via uptake by the vesicular monoamine transporter (VMAT2) (Javitch et al., 1985). Once inside the cell, MPP+ is able to inhibit complex I of the mitochondrial electron transport chain, resulting in the release of ROS as well as reduced ATP production. Additionally, MPP+ stored in vesicles is thought to expel

DA out into the intercellular space where it can be metabolized into a number of compounds, including toxic metabolites, such as superoxide radical (5-cysteinyl-DA) and hydroxyl radical (6-OHDA) attack (Burke et al., 2008; Panneton et al., 2010).
MPTP can be administered by a variety of regimens, but the most common and reproducible form is still systemic injection (subcutaneous, intravenous) (Przedborski et al., 2001).

Toxin	Mitochondrial dysfunction
MPP+/MPTP	1. Inhibits the mitochondrial complex i 2. Decreases ATP production and increases generation of ROS 3. Inhibits mitochondrial complexes III and IV 4. Decreases mitochondrial activity and mitochondrial gene expression 5. Alters mitochondrial proteins such as chaperones, metabolic enzymes, oxidative phosphorylation-related proteins, inner mitochondrial protein (mitofilin) and outer mitochondrial protein (VDAC1) 6. Alters proteins associated with mitochondrial dysfunction, dopamine signaling, ubiquitin system, calcium signaling, oxidative stress response and apoptosis 7. Causes DNA damage
Rotenone	Reduces complex I activity

Table 2. Summary of mitochondrial dysfunction by environmental toxins to PD model (adapted from Blesa et al., 2012).

6-Hydroxydopamine

6-OHDA was first isolated in the 1950s (Senoh and Witkop, 1959). Today the use of 6-OHDA remains widespread for both *in vitro* and *in vivo* investigations. Although the structure of 6-OHDA is similar to that of dopamine, the presence of an additional hydroxyl group makes it toxic to DA neurons.
This model does not mimic all of the clinical features of PD. Dopamine depletion, nigral dopamine cell loss, and neurobehavioral deficits have been successfully achieved using this model, but it does not seem to affect other brain regions, such as olfactory structures, lower brain stem areas, or locus coeruleus. Although 6-OHDA does not produce or induce proteinaceous aggregates or Lewy-like inclusions like those seen in PD, it has been reported that 6-OHDA does interact with α-synuclein (Blandini et al., 2008).
This compound does not cross the blood-brain barrier, which necessitates its direct injection into the SNpc or into striatum (Perese et al., 1989; Przedborski et al., 1995).

Rotenone

Rotenone is both an herbicide and an insecticide (Hisata et al., 2001). It is the most

potent member of the rotenoid family of neurotoxins found naturally in tropical plants.

Rotenone is highly lipophilic and freely crosses the bloodbrain barrier. Chronic exposure to low doses of rotenone results in inhibition of the mitochondrial electron transport chain in rodents.

In animals, rotenone has been administered by different ways. Oral administration appears to cause little neurotoxicity (Inden et al., 2011). Chronic systemic administration using osmotic pumps has been the most common delivery regimen (Betarbet et al., 2000). Intraperitoneal injections have been reported to elicit behavioral and neurochemical deficits, although mortality is very high (Alam et al., 2004). Intravenous administration is able to cause damage to nigrostriatal DA neurons that is accompanied by α-synuclein aggregation, Lewy-like body formation, oxidative stress, and gastrointestinal problems (Cannon et al., 2009). However, a subsequent study has found that rotenone is not specific to the DA system and has deleterious effects on other neuronal populations, as serotorinergic, noradrenergic and cholinergic neurons (Höglinger et al., 2003). Furthermore, there are no documented cases of rotenone-induced PD in humans. Thus, it is not clear that this model offers any advantage over other toxic models, such as that of 6-OHDA or MPTP.

Gene-based models

The underlying principle for studying genetic mutations of a disease is the belief that the clinical similarities between the inherited and sporadic forms of the disease share a common mechanism that can lead to the identification of molecular and biochemical pathways involved in the disease pathogenesis.

Mutations to the α-synuclein gene were the earliest evidence for genetic link to PD. Two mutations in the α-synuclein gene (A53T, A30P) cause a dominantly inherited form of PD (Krüger et al., 1998) and have been used to create transgenic mice in an effort to recapitulate the pathophysiology of PD. Studies done using α-synuclein transgenic mice have yielded considerable progress, showing that A53T mutations in mice can result in a severe motor phenotype which can eventually lead to paralysis and death (Giasson et al., 2002). Additionally, mutations to the α-synuclein gene in mice produce inclusions that resemble LBs (Masliah et al., 2000). However this phenotype is restricted to the A53T mutation and not found in A30P transgenic mice. Furthermore, it has been shown that knocking out α-synuclein does not affect DA

neuron development or maintenance (Abeliovich et al., 2000; Thomas et al., 2011). Some of the α-synuclein transgenic mice have olfactory impairments and colonic dysfunction, and it seems that there are other nonmotor abnormalities (Wang et al., 2008). However, since the function of α-synuclein has yet to be figured out, the actual role of α-synuclein in PD still remains elusive.

Mutations to parkin, DJ1 and PINK1 cause autosomal recessive forms of PD. Knock-out rodent models of these genes do not demonstrate any nigrostriatal degeneration and intranuclear inclusions (only PINK1 knockout mice display reduced DA release in the striatum) (Moore and Dawson, 2008). However, recently it has been shown that knocking out parkin in mice at adult age causes neurodegeneration in the SNc (Shin et al., 2011).

Overall, this genetic mouse models are able to recapitulate specific aspects of PD, although none produce the neuronal degeneration associated with PD; therefore these themselves may be defective and may require additional modulations or modifications (Peng et al., 2010).

The selective vulnerability of SNpc cells

mDA neurons and their projections

The largest assembly of DA neurons is found in the ventral midbrain. A distinction is usually made between nigral (A9) and non-nigral (A8 and A10) DA neurons, although there is no clear definable boundary between them and these groups can be seen as a continuous cell system (Björklund and Lindvall, 1984, from Handbook of Chemical Neuroanatomy). Nigral neurons are confined to the pars compacta and pars lateralis of the SN. Few A9 cells are scattered ventrally in the pars reticulata. The A10 cell group is largely confined to the VTA and is positioned medially to the SN proper (figure 10). A8 cell group is located in the retrorubral field, caudally to the SN proper and it can be considered as a caudal extension of the A9 cell group as they too project to the striatum.

The DA cells of the A10 group are implicated in the control of emotional balance, reward-associated and addictive behaviour, attention and memory. The A9 cells play an essential role in the control of postural reflexes and initiation of voluntary movement. Finally, the A8 dopamine neurons are thought to influence orofacial

movements.

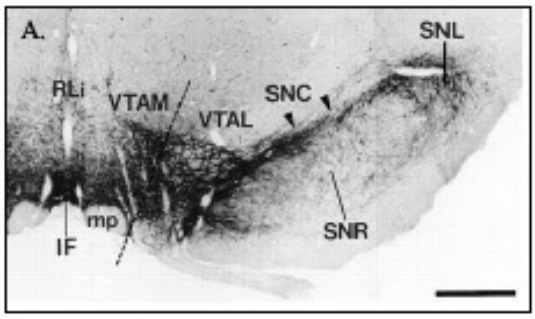

Figure 10. Rappresentation of ventral midbrain (VMB).
TH-immunocytochemistry in the midbrain dopaminergic areas, showing the Substantia Nigra (SN), the Ventral Tegmental Area (VTA), interfascicular nucleus (IF), the rostral linear nucleus (RLi). The ventral tegmental area is divided into the medial (VTAM) and lateral (VTAL) parts by a dotted line between the lateral edge of the mamillary peduncle (mp) and the medial edge of medial lemniscus.

It has become evident that mDA neurons are not a simple system but they are organized in a complex circuit that comprises subpopulations of neurons exhibiting differences in their morphology, but also in several molecular markers and patterns of forebrain projections. Although the projections of the three DA pathways (nigrostriatal, mesolimbic and mesocortical) are both anatomically and functionally distinct and confined to their projection targets with a very limited degree of collateralization, their cells of origin are more intermixed than originally thought. More specifically, A9 cells project to the sensorimotor striatum through the "nigrostriatal" pathway, in the strict sense of the term. Lateral VTA (A10) and RR (A8) project to the limbic part of the striatum, which includes the nucleus accumbens rostrally and the central nucleus of the amygdala and adjacent parts of the caudal striatum. It follows that the term mesostriatal DA pathway may be more appropriate to describe all components of the midbrain DA system projecting to the striatum. Therefore, often the three DA projections arising from mDA are described with the terms mesostriatal and mesocorticolimbic pathways.

Cellular diversity in SN DA cells

One key question is why only specific subsets of dopamine neurons die in PD. Neurons in the ventral and lateral SN are much more sensitive to neurodegeneration than neurons in the VTA (figure 11). This differential vulnerability is a key characteristic of the disease and it is well recapitulated in PD animal models like rodents or primates (Dawson and Dawson, 2002).

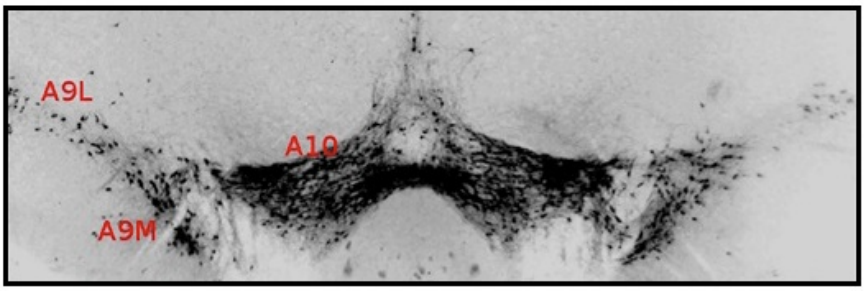

Figure 11. DA neurons of mouse midbrain.
From the left different groups of DA neurons: A9 lateralis (A9L) and medialis (A9M) neurons forming Substantia Nigra (SN) and A10 neurons, forming Ventral Tegmental Area (VTA). The progressive neurodegeneration observed in PD affects first A9L and then spreads to A9M. Notably, A10 neurons are almost spared even in severe cases of the disease.

A9 and A10 cells have many common features. They present long and thin axons and these have little or no myelination (Braak et al., 2004). They have a high-energy demand, feature that renders these neurons particularly dependent on proper mitochondrial dynamics. However, Liang and collegues found that the cytoplasmic area occupied by mitochondria in the DA neurons in the SN is lower than in neighbouring nondopaminergic neurons or in dopaminergic neurons of VTA (resistant in PD), suggesting the possibility that the vulnerable neurons may be more susceptible to subtle changes in mitochondrial maintenance (Liang et al., 2007).
Other factors that may selectively affect SNpc neurons include their less capacity for calcium buffering (Esteves et al., 2010) and in their expression of specific transcription factors that regulate cell fate and survival (Alavian et al., 2008). However, these characteristics are not sufficient to explain the different susceptibility of SNpc neurons to neurodegeneration.

Transcriptional anatomy of DA neurons

In the last decade, a lot of efforts have been done in order to determine the critical molecular differences between A9 and A10 neurons. In particular, the advantage to use new tools and techniques like LCM (that permits the isolatation of A9 and A10 cells) and high-throughput gene expression methods, such as Affymetrix array analysis, CAGE and nanoCAGE technologies coupled to next generation sequencing, has represented a new approach to analyze differences between A9 and A10, obtaining gene expression profiles of the two DA neuronal populations.
In comparison to A10 neurons, A9 cells show higher expression of genes related to

metabolism and genes encoding mitochondrial proteins as well as genes involved in protein, lipid and vesicle-mediated transport. Interestingly, the level of metabolic transcripts correlates directly with susceptibility to complex I toxins (Greene et al., 2005). Several genes related to small GTPase-mediated signaling and synaptic vesicle recycling, including RAB and RAS proteins, are elevated in A9 cells. Transcripts related to neuropeptide signalling and neurotrophic factors like BDNF, NGF or VGF were also markedly different between A9 and A10 cells. Several genes related to hormone activity and axon guidance are elevated in A10 neurons (Chung et al., 2005; Greene et al., 2005).

Hemoglobin in DA neurons

As mentioned above, gene expression profiles of A9 and A10 DA neurons has been performed to evaluate differences between the two subpopulations. In the laboratory of professor Gustincich, combination of different gene expression platforms unveiled transcripts of α hemoglobin, adult chain 1 (Hba-a1), and β hemoglobin, adult chain 1 (Hbb-b1) in A9 neurons. Interestingly, Hb immunoreactivity decorated the large majority of A9 cells, whereas it stained only 5% of A10 neurons. Hb is expressed in almost all oligodendrocytes and cortical and hippocampal astrocytes. This pattern of expression was conserved in mammals and in human post-mortem brain.

In addition, by gene expression analysis of mouse DA cell stably transfected with α and β chains of Hb, changes in genes involved in oxygen homeostasis as well as in mitochondrial oxidative phosphorylation were observed. Other variations involved genes in oxidative stress, iron metabolism as well as in Nitric Oxide (NO) synthesis. Genes that encode for subunits of mitochondrial complex I-V were upregulated with a marked induction of complex I transcripts. Furthermore, the mitochondrial proton carrier Uncoupling Protein 2 (Ucp2), was also strongly up-regulated. Genes well known as detoxifying agents from cellular free radicals as SOD2, Prdx5, Gpx4, Trn2 and Txnrd2 were also up-regulated as well as neuronal nitric oxide synthase 1 (Nos1). Among genes involved in iron metabolism, an up-regulation of ferritin heavy chain (Fth1) was observed while transferrin receptor (Tfrc) transcript was decreased.

These results open a new scenario for hemoglobin role in brain physiology and in PD pathogenesis.

Hemoglobin

Globin family

Globin family members are characterized by the coordination of heme group and by the consequent binding with oxygen that is the essential ligand for their function.

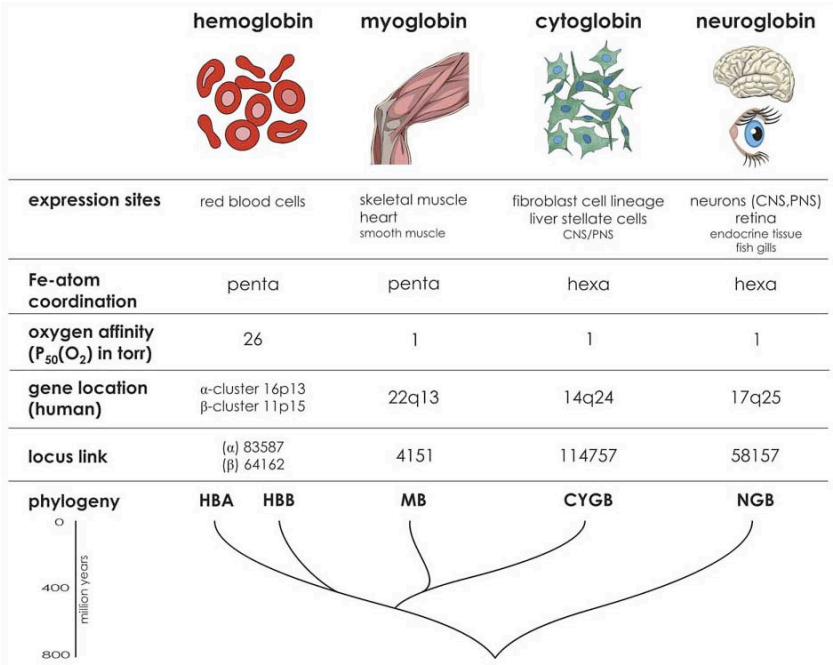

Figure12. Human globins family characteristics: tissue distribution, biochemical and phylogenetics aspects (adapted from Hankeln et al., 2005).

Globins have been identified in different organisms like in plants (leghemoglobin) where single-chain globins are involved with electron tranfer, oxygen storage and scavenging, in yeast (flavohemoglobin) or in bacteria where they seem to be primarily NO dioxygenases for detoxifying NO (Hardison, 1998).

Beside their role of transport and storage of oxygen, other functions have been identified like enzymatic and detoxifying functions (Minning et al., 1999).

Four main components of the family have been discovered and characterized in mammals up to now: hemoglobin, myoglobin, cytoglobin and neuroglobin (figure 12) (Hankeln et al., 2005).

All these proteins share a similar tertiary structure even though their primary sequences have less than 50% of homology. The residues responsible for heme

binding are conserved.

Myoglobin

Myoglobin is a monomeric protein strongly resembling one single hemoglobin chain. It coordinates an heme group and its oxygen binding site has an higher affinity for the ligand in comparison to the other globins. It is mainly expressed by the striated muscules and cardiac tissue and its classical function is to store oxygen and to release it instantaneously under high request of energy by muscular tissue, in particular it facilitates oxygen diffusion to mitochondria. It also helps maintaining nitric oxide homeostasis (acting as a NO dioxygenase and nitrite reductase), and scavenge reactive oxygen species (Garry et al., 2003). Although it has been studied since 40′s, a detailed understanding of its function has still not been achieved; interestingly, knockout mice for myoglobin have almost normal physiology (Gödecke et al., 1999).

Cytoglobin

Cytoglobin (Cygb) is one of the newly discovered oxygen-binding members of the globin family (Burmester et al., 2002). It′s monomeric and very similar to myoglobin in the tertiary structure. Mammalian Cygb is longer than most globins and covers 190 amino acids instead of the typical 140–150 aminoacids. This is due to two 20 amino acid extensions at both the N- and the C- terminal. Its affinity for oxygen is similar to myoglobin and it can bind CO and NO like hemoglobin but with a weaker affinity.

It is prevalently cytoplasmic and is ubiquitously expressed, in particular in eyes, liver, heart, skeletal muscle and neurons, where its subcellular localization is both cytoplasmic and nuclear (Schmidt et al., 2004).

Its function is still unknown and many hypotheses have been made on a possible implication in oxygen sensing or storage and in ROS scavenging. Up to now several studies show that it is over-expressed under hypoxic conditions (Singh et al., 2009), Cygb is correlated with cell respiration and proliferation in fibroblasts via NO dioxygenation (Halligan et al., 2009) and with collagen synthesis. It also seems to be a tumor suppressor, in fact it has been demonstrated that its down-regulation is a key event in a familial cancer syndrome of the upper aerodigestive tract (Shivapurkar et al., 2008).

Neuroglobin

Neuroglobin (Ngb) was first observed in vertebrate brain (Burmester and Hankeln, 2004), now it is known how it is widely expressed in vertebral central and peripheral nervous system as well as in retina, endocrine tissues and gastrointestinal tract (Reuss et al., 2002; Schmidt et al., 2004). Recently, Ngb has also been detected in human glioblastoma cell lines and in quiescent and reactive astrocytes (Brunori and Vallone, 2006; DellaValle et al., 2010; Emara et al., 2010). Like myoglobin and cytoglobin, it is monomeric but unlike cytoglobin, it is exclusively cytoplasmic.

Ngb binds several ligands such as O_2, CO and NO (Brunori and Vallone, 2006). Besides small ligands, Ngb has been reported to interact with several proteins, modulating their functions (Yu et al., 2012a).

Previous studies demonstrated that expression of Ngb increases in response to oxygen deprivation and that it is neuroprotective against hypoxic/ischemic brain injuries (Sun et al., 2001, 2003; Liu et al., 2009). It's important to note that metabolically most active oxygen-consuming cell types express Ngb, including neurons that are particularly sensitive to hypoxic/ischemic insults. In this contex it has been observed that increased levels of Ngb protect neurons from neurodegerative disorders, as AD, modulating the activation of the apoptotic cascade (Yu et al., 2012b). Recently it has been identified an endogenous modulators that up-regulates Ngb levels. In details, Ngb is part of the 17β-estradiol signalling mechanism that is activated to exert protective effects against H_2O_2-induced neurotoxicity (De Marinis et al., 2010). Ngb can also act as a guanine nucleotide dissociation inhibitor (GDI) regulating signal transduction (Wakasugi et al., 2003).

Hemoglobin

The oxygen-carrying protein hemoglobin was discovered by Friedrich Ludwig Hünefeld in 1840. In 1851, Otto Funke published a series of articles in which he described growing hemoglobin crystals by successively diluting red blood cells with a solvent such as pure water, alcohol, or ether, followed by slow evaporation of the solvent from the resulting protein solution. Hemoglobin's reversible oxygenation was described a few years later by Felix Hoppe-Seyler. In 1962 Perutz won Nobel Prize for Chemistry for his studies of the structures of hemoglobin and globular proteins.

Hemoglobin structure

Hemoglobin is a hetero-tetrameric protein composed of two couples of identical subunits. Human hemoglobin coding genes are distinguished in two groups: alpha (α) and zeta (ζ) chains belong to the first group, on the chromosome 16, beta (β), epsilon (ε), gamma (γ) and delta (δ) chains belong to the second, on the chromosome 11. During development, different couples of genes are expressed, forming at least five different hemoglobin tetramers: in temporal order, the first is composed by two ζ and two ε chains and it's called Gower Hb ($\zeta_2\varepsilon_2$), the second is called Portland Hb ($\zeta_2\gamma_2$), the third is the fetal Hb, HbF ($\alpha_2\gamma_2$). During adult life both β and δ chains are expressed, forming adult Hb, HbA ($\alpha_2\beta_2$) and HbA2 ($\alpha_2\delta_2$). In adulthood, HbA accounts for approximately 97% of the protein molecules, HbA2 for about 2% and HbF for only 1% (Collins and Weissman, 1984).

HbA is composed by two α chains of 141 aminoacids and two β chains of 146 aminoacids, held together by non-covalent interactions. Each chain is folded around a heme group that coordinates an iron atom, responsible for the binding with oxygen. The primary and secondary structures of the two chains do not share a high similarity, but the tertiary one is much conserved. Each polypeptide chain is made up of eight or nine α-helical segments and an equal number of non-helical ones placed at the corners between them and at the ends of the chain. The helices are named A-H, starting from the amino acid terminal (figure 13).

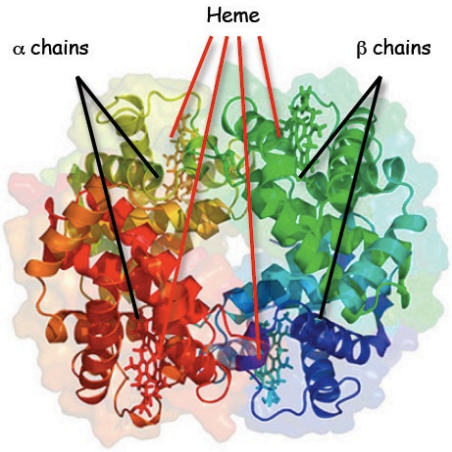

Figure 13. Terameric structure of adult hemoglobin.

The most conserved aminoacids are the proximal histidines (87th residue in α chain and 92nd in the β chain), involved in the binding with heme, and the distal histidines

(58^{th} residue in α chain and 63^{rd} in β chain), involved in the interaction between the four chains.

The heme consists of an organic part, porphyrin, and an iron atom. Porphyrin is made up of four pyrrole groups that are linked by methane bridges to form a tetrapyrrole ring. The porphyrin found in hemoglobin is protoporphyrin IX, which contains four methyl, two vinyl, and two propionate side chains. The iron atom (Fe^{2+}) in deoxyhemoglobin is pentacoordinated: four of its ligands are nitrogens residues in the centre of the protoporphyrin ring, the fifth is the nitrogen atom of the proximal His. In the oxyhemoglobin the iron atom is exacoordinated because it also binds an oxygen atom. The second oxygen atom is linked to the distal His through a hydrogen bond. The hydrophobic environment in which the heme group is located prevent the iron atom from oxidation; if hemoglobin comes in contact with air, the iron atom become oxidized (Fe^{3+}), forming the so called methemoglobin in which the oxygen binding site is occupied from H_2O and becomes inactive (Spiro et al., 1990).

Hemoglobin genes

In human

The α-like globin genes are located in chromosome 16 near the telomere. The β-like genes (chromosome 11) are in a region that contains multiple DNA sequences that act as strong tissue and developmental stage-specific enhancers of transcription.

The α globin gene cluster is composed by only 3 coding genes (ζ, α1, α2) and at least 4 pseudogenes whereas, in β globin gene cluster, there are 5 coding genes (ε, Gγ, Aγ, δ, β) and only one pseudogene (Schechter, 2008) (figure 14).

The expression of the different genes is controlled by multiple cis-acting elements like promoters, enhancers, silencer, insulators, MARs/SAR/s and LCR, because of their fine regulation from embryonic to adult life. The β globin cluster is the most regulated one because it has to control the perfect switch between 5 genes during development: in particular its proximity to a group of 5 LCRs contribute significantly to regulation of the sequential 5'-to-3' expression of the globin genes during development, as well as their very high level of expression, with matched contributions from the α locus, in normal erythrocyte. Interestingly, sequencing of the globin gene clusters has revealed an enormous number of additional DNA motifs,

which appear to be binding sites for many other proteins and may contribute to enhancing or silencing transcription.

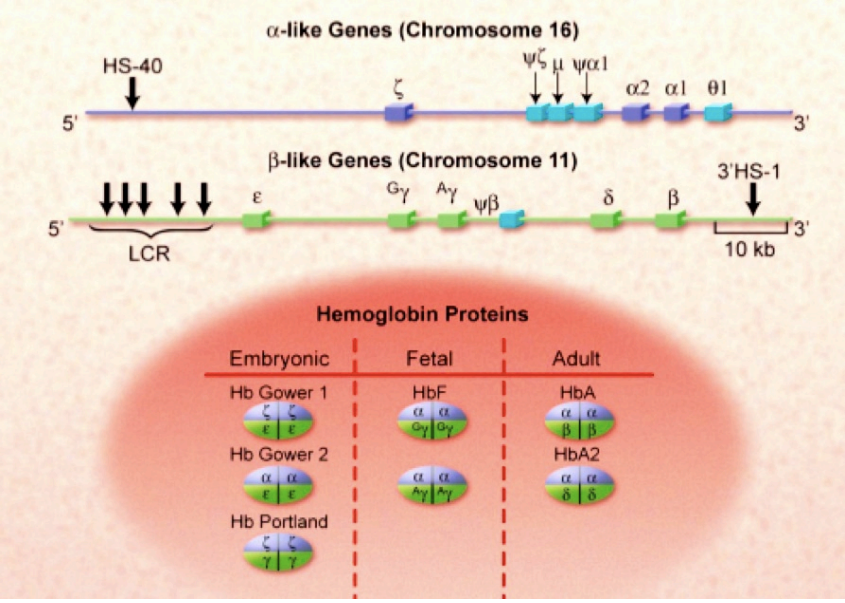

Figure 14. The genomic structure of α and β globin clusters.
The functional α-like and β-like genes are respectively in dark blue and light green. Pseudogenes are in light blue. The important control elements, HS-40 and the LCR, are also shown at their approximate locations. The various hemoglobin species formed from these genes, with their prime developmental stages, are shown in the lower part of the figure (Schechter, 2008).

The molecular mechanisms of the β globin LCR have been only partially elucidated: they are major regulators of globin gene expression, both as a strong general enhancer of transcription and as a specific mediator of developmental control. They are supposed to "open" the chromatin allowing the transcription initiation complex and other trans-acting factors to bind at the appropriate gene.

The most studied transcription regulatory protein with a strong erythroid specificity is GATA-1 but many others like FOG-1, TAL-1, EKLF, Gfi-1b and BCL11A, have a role in fine control of individual globin genes or their sequential expression (Mahajan et al., 2007).

In mouse

Murin α and β clusters have some differences compared to human's: α cluster is on chromosome 11 and is composed by 3 coding genes (Hba-x, Hba-a1 and Hba-a2) that encode for X embryonic chain and α adult chains and 2 pseudogenes. There are also two added genes (Hbq1 and Hbq2) encoding for adult θ globins that in homo sapiens are evolved in a pseudogene (Storz et al., 2008). β cluster is on chromosome 7 and is

composed by 4 coding genes (Hbb-y, Hbb-bh1, Hbb-b1 and Hbb-b2) that encode for Y, Z embryonic chains and β^{minor}, β^{major} adult chains and 3 pseudogenes.
In mouse embryo three different types of tetramers are expressed: X_2Y_2, α_2Y_2 and α_2Z_2; the switch to adult hemoglobin occurs between 14^{th} and 15^{th} gestation day.

Hemoglobin function

Oxygen

In mammals, the most studied function of hemoglobin is to transport oxygen from the lungs to tissues and the most abundant sites of expression are the red blood cells. The binding with oxygen for α and β subunits does not happen contemporary: when the first oxygen molecule binds to the iron atom of one chain, it "pulls" the proximal His and induces a conformational change that propagates to all the chain structure. This change induces, in turn, conformational rearrangements of the other chains and the consequent increase of their affinity for oxygen. In this way the binding of the other three oxygen molecules is much faster. The vice versa, the release of oxygen, follows the same mechanism.
The cooperative binding of hemoglobin by its ligand oxygen dramatically increases its physiological oxygen-carrying capacity: in the lungs the partial pressure of oxygen (pO_2) is relatively high (100 torr) and hemoglobin becomes nearly saturated with oxygen (98% of the oxygen-binding sites are occupied); in the tissues pO_2 is much lower (20 torr) and hemoglobin saturation level drops to 32%. The cooperative binding of oxygen by hemoglobin enables it to deliver about two times as much oxygen as it would if sites were independent.
However, the cooperative binding only partially explains the behaviour of hemoglobin in efficiently transporting oxygen: other allosteric effectors like CO_2, pH and 2,3-bisphosphoglycerate (2,3-BPG) regulate hemoglobin structural changes and function. CO_2 stabilizes deoxyhemoglobin by reacting with the terminal amino groups to form carbamate groups, so the presence of CO_2 in tissues decreases hemoglobin affinity for oxygen, facilitating its release. On the other hand, in lungs, the high concentration of oxygen stabilizes the oxyhemoglobin, inducing the release of CO_2.
Moreover, a portion of CO_2 reacts with H_2O becoming HCO_3^- with the release of a H^+, responsible of the Bohr effect. In fact the oxygen affinity of hemoglobin

decreases as pH decreases. As hemoglobin moves into a region of low pH, for example from lungs to tissues, its tendency to release oxygen increases due to conformational changes in the four chains.

Another allosteric effector is 2,3-diphosphoglycerate (2,3-DPG). This highly anionic compound is present in red blood cells and gives to hemoglobin the capacity to act as an extremely efficient oxygen transporter. Single molecules of DPG bind to deoxyhemoglobin and stabilize it, reducing the oxygen affinity and increasing the capacity to release oxygen. DPG binding to hemoglobin has other crucial physiological consequences in the passage of oxygen from maternal to fetal red blood cells. Fetal hemoglobin tetramers include two α chains and two γ chains in which there is the substitution of a serine residue for His143 of the β chain of the DPG-binding site. This change reduces the affinity of DPG for fetal hemoglobin, thereby increasing the oxygenbinding affinity of fetal hemoglobin relative to that of maternal (adult) hemoglobin. This difference in oxygen affinity allows oxygen to be effectively transferred from maternal to fetal red blood cells.

Nitric oxide

Nitric oxide is present in all the tissues of the organism and its concentration increases in ischemic conditions. It is a ubiquitously produced cell signalling molecule, acting via soluble guanylyl cyclase production of cyclic GMP and through other mechanisms. It is especially important in mammals in the regulation of vascular tone, cell interactions, and neural function.

Under basal conditions, in blood vessels, NO are produced by endothelial NO synthase enzymes to activate soluble guanylyl cyclase (sGC) to produce cyclic GMP and regulate vascular tone.

In neurons it is synthesised by NO synthase (NOS type1) and acts as a neuromodulator in different processes like memory, neuronal plasticity or nociception. It is also a toxic molecule at high concentration and in presence of ROS: it reacts in particular with anion superoxide ($O_2^{\bullet -}$) to form peroxinitrite ($ONOO^-$), a highly reactive molecule that oxidise cellular molecules and inhibits Glutamate transporter (Trotti et al., 1996).

The presence of nitrosilated molecules in post-mortem human brains of PD, SLA and Alzheimer patients lead to the hypothesis of a role of NO in neurodegenerative diseases (Good et al., 1996;Beal et al., 1997).

NO can bind hemoglobin in different ways: it can react with iron atom of deoxyhemoglobin to form nitrosyl(heme)hemoglobin (NO-hemoglobin) and it can also bind the cystein in position 93 of the β chain to form S-nitrosylhemoglobin (SNO-hemoglobin) (figure 15). The first reaction had generally been assumed to be irreversible, however, there is now evidence that NO-hemoglobin in the circulating red blood cell may release NO molecules, potentially allowing a mechanism for hemoglobin-based, endocrine-like transport of NO from one tissue to another within the body.

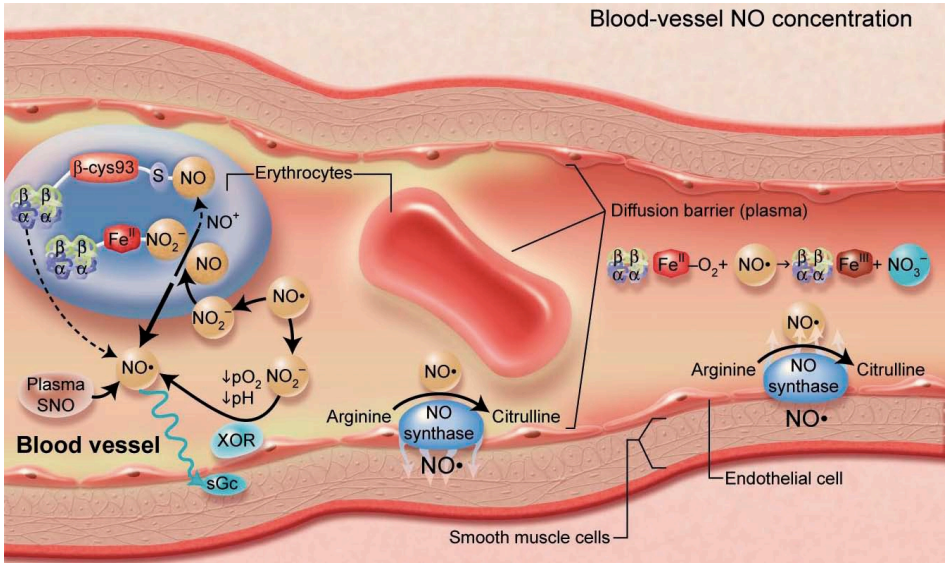

Figure 15. A representation of nitric oxide (NO)/hemoglobin reactions in the arterial microcirculation (adapted from Schechter, 2008).

SNO-hemoglobin seems to be able to dissociate and to release NO at low oxygen concentration. This could be a mechanism for homeostatic control of blood flow to tissues, because NO promotes vascular dilatation and increases blood flow and oxygen delivery, but this hypothesis is still controversial (Singel and Stamler, 2005).

NO reacts also with oxyhemoglobin to produce methemoglobin, with ferric iron (Fe^{3+}) and nitrate ions. Recent work suggests that most of the methemoglobin circulating in red blood cells is derived from this oxidation process which is normally reversed by the erythrocytic methemoglobin reductase system.

More recently, an alternative hypothesis to account for the transport of NO by erythrocytes has been proposed. It has been suggested that nitrite ions within erythrocytes could be reduced to NO by deoxyhemoglobin in regions of relative hypoxia (Dejam et al., 2004).

It is important to consider that the interactions of NO, produced by endothelial cells under physiological condition, with red cells is limited by several barriers. Whereas, in case of hemolysis, cell-free oxyhemoglobin acts as an efficient scavenger of NO, causing vasoconstriction and perhaps pathological organ conditions.

Atypical localization of hemoglobin

In the last years it has becoming clear that hemoglobin expression is not restricted to erythrocytes and his precursors. For this reasons other potential functions have been postulated.

In 1999, Liu et al. described the expression of β^{min} chain of hemoglobin in murine macrophages (Liu et al., 1999): they showed that both an immortalized macrophagic cell line and primary macrophages expressed β^{min} chain of hemoglobin after treatment with IFN-γ and LPS, inducers of inflammatory response. The role of this induction is still unknown but it suggests alternative functions for globins in mammalian cells and challenges the prevailing view that the expression of α and β globin genes is always balanced and coordinated. The functional properties of the single chains compared to those of the tetramer, are very different: α chain monomer is very unstable and doesn't aggregate in tetramers; on the contrary β chain can form tetramers (known as HbH), isolated from the blood of α-thalassemic or HbH disease patients (Tongsong et al., 2009) with a high affinity for oxygen. β_4 tetramer biochemical properties can be affected by pH and by BPG like hemoglobin. However, its physiological role, if any, is still under investigation.

In 2006, Newton et al. demonstrated the expression of both α and β chains in alveolar epithelial cells and Clara cells, the primary producers of pulmonary surfactant, implicating then in the physiology and pathology of the lung (Newton et al., 2006).

Moreover, in 2008 Nishi et al. observed an up-regulation of hemoglobin in the hypoxic kidney, in particular in rat glomerular mesangial cells. With the support of *in vitro* studies, they hypothesized a protective role of this protein against oxidative stress induced by hydrogen peroxide and superoxide anion (Nishi et al., 2008).

Other sites of globin subunits mRNAs expression have been reported included the pituitary of neonatal rats after exposure to estrogen and human cardiac ventricular tissue after ischemia-reperfusion (Leffers et al., 2006).

Moreover, α and β chains of hemoglobin were found in human hepatocytes cells and oxidative stress upregulated its expression (Liu et al., 2011b).
Futhermore, hemoglobin was found in thyroid cancer cells, breast cancer and cervical carcinoma cells (Onda et al., 2005; Capulli et al., 2012; Li et al., 2013). In these cases hemoglobin awards to the tumours a more aggressive phenotype.
Finally, in the laboratory of professor Gustincich, it has been demonstrated the presence of hemoglobin in mammalia DA neurons as well as in a subpopulation of hippocampus and cortex astrocytes and in almost all oligodendrocytes. Similarly, Richter and colleagues showed the existence of Hb in mammalia brain neurons (Richter et al., 2009).

Hemoglobin disorders

Hemoglobin disorders consist of two different groups, the structural hemoglobin variants and the thalassemias.

Hemoglobinopathy

Hemoglobinopathies are diseases related to mutations in globin chain, which alter the structure of hemoglobin or lead to a drastic decrease in the production of a type of chain. The structural hemoglobin variants typically are based on the point mutations in the α or β globin chain that result in a single-amino acid substitution in the corresponding globin chain. There are more than hundreds genetic variants of hemoglobin. The most common Hb variants worldwide are HbS, HbE, HbC, and HbD. All of these Hb variants have single amino acid substitutions in the Hb β chain. In details, HbS has a valine for glutamic acid substitution at position 6 of the β chain. HbC is a different variant mutation (lysine substituted for glutamic acid) at the same site as HbS mutation on the β chain. HbE contains a substitution of lysine for glutamic acid at position 26 of the β chain, and HbD Punjab (also called HbD Los Angeles) contains a substitution of glutamine for glutamic acid at position 121 of the β-globin chain. The presence of any of these four variants does affect the ionic charge of the Hb molecule (Little and Roberts, 2009). These hereditary blood disorders are named as Sickle-cell anemia (SCA) and causes abnormal, rigid, sickle shape red blood cells. Sickling decreases the cells' flexibility and results in a risk of various

complications. In particular, homozygosity for HbS (SCA) causes a serious disease with vascular obstruction and consequent tissue infarction. Those with HbC disease (also called HbCC disease) may have a normal hemoglobin concentration or be mildly or moderately anemic. Subjects with HbSC disease (also called sickle-hemoglobin C disease) can be affected mildly or moderately with chronic hemolytic anemia. Subjects with homozygous E disease (also called HbEE disease) are usually completely asymptomatic, and those with HbD Punjab disease may have mild hemolysis and sometimes a mild hemolytic anemia. Heterozygous individuals for any of these Hb variants are usually asymptomatic and have normal red cell survival.

Thalassemia

Thalassemias are due to a large number of mutations that cause abnormal globin gene expression and result in total absence or quantitative reduction of globin chain synthesis (Steinberg and Brugnara, 2003).

They are divided according to which globin chain is produced in reduced amounts: α thalassemia, in which α globin chain is reduced or absent, and β thalassemia, in which β globin chain is reduced or absent.

The two main problems of thalassemias are decreased hemoglobin synthesis and an imbalance between the α and β globin chains. In the absence of the complementary globin chains, the excess unbound globin protein aggregates and precipitates, damaging cell membranes and leading to premature destruction (Schrier, 2002). When this occurs in immature erythroid precursors it results in ineffective erythropoiesis, wheares in mature blood cells it results in hemolysis. Both result in anemia. Other factors may involve iron overload and oxidative stresses (Shinar and Rachmilewitz, 1993; Weatherall and Clegg, 2001).

The thalassemias are widespread in areas that in the past were malarial (Mediterranean, Middle East, India) because of the thalassemia trait that confers protection against malaria. The parasite that causes malaria in fact colonize erythrocytes and its survival is linked to the "health" of the erythrocytes themselves.

Hemoglobin and its implication in other diseases

Over the last years there has been increasing evidence of the direct involvement of hemoglobin and its derivatives in many diseases, such as cancer and

neurodegererative diseases.

Recently it has been demonstrated that increased expression of a set of genes involved in oxygen metabolism, including β hemoglobin, confer a more aggressive metastatic phenotype in breast cancer cells (Capulli et al., 2012). Moreover, the expression of hemoglobin, in cervical carcinoma cells, may have important implications in the pathology of solid tumors because of the functions inherent to the structure of the Hb molecule, including gas exchange, and protection against oxidative and nitrosative stress (Li et al., 2013).

It has been demonstrated the involvement of Hb in neurodegeneration. Interestingly, the levels of Hb are positively correlated with age in rats and negatively correlated to their learning and memory performances (Blalock et al., 2003).

Concerning AD, Hb and Hb-derived peptides have been isolated from human cerebrospinal fluid and brain tissues of AD patients (Slemmon et al., 1994; Raymackers et al., 2000; Schonberger et al., 2001). In particular, it has been shown that Hb is present in neurons, glial cells and amyloid plaques of post-mortem AD brains (Wu et al., 2004). Furthermore, Hb induces the formation of structure composed of amyloid-beta in a transgenic mouse model of AD, suggesting its involvement in the AD pathogenesis (Chuang et al., 2012).

Iron deposition occurs in the SN with normal aging but its accumulation is markedly higher in PD post-mortem brains (Kaur and Andersen, 2004; Bartzokis et al., 2007). Since Hb is the major source of iron in the brain, it has been proposed that toxic levels of brain iron may cause neurodegeneration by promoting oxidative stress through a Hb-induced iron homeostasis dysregulation (Kaur and Andersen, 2004). Furthermore, the presence of Hb formations (nitrosyl-Hb) in the SN could explain brain iron dysregulation, reduction of nigral glutathione levels and increase of dopaminergic nitric oxide (Cammack et al., 1998; Chinta et al., 2007; Shergill et al., 1996). Moreover, brain iron may aggregate with α-synuclein. Indeed in humans it has been found α-synuclein in red blood cells (Barbour et al., 2008). By metal binding and α-synuclein interaction, Hb may have an important role in formation of Lewy bodies, which are the major hallmark of PD pathogenesis (Wolozin and Golts, 2002). Lastly, epidemiologic studies demonstrated that Hb, that remains high in elderly men, is associated with an increase risk of PD (Abbott et al., 2012).

In this thesis we aim to elucidate the role of hemoglobin in PD.

Materials and methods

Constructs

We used pBudCE4.1 vector (Invitrogen), designed for the independent expression of two genes from a single plasmid, in order to express α and β chains of mouse hemoglobin, as described previosly (Biagioli et al., 2009). Briefly, a fragment composed by β globin-MYC-IRES-eGFP was cloned into the MCS1 (SalI/XbaI) whether 2xFLAG-α globin was placed into MCS2 (KpnI/XhoI). We called this vector pBudCE4.1-β globin-MYC-IRES-eGFP, 2xFLAG-α globin. A control vector containing only IRES-eGFP in CMV-MCS (SalI/XhoI) was also created. We called this vector pBudCE4.1-IRES-eGFP.

From pBudCE4.1-β globin-MYC-IRES-eGFP, 2xFLAG-α globin we generated a mutated Hb (Hb-mut). In particular we mutated the proximal hystidine of α and β chains into a glycine (respectively His87Gly and His92Gly). We used QuickChange Site-Directed Mutagenesis Kit (Stratagene) according to the manufacturer's instructions. We designed the indicated primers:

Primers		Sequence	Tm
α globin H87G	FW	GCTCTGAGCGACCTGGGTGCCCACAAGCTGCGTG	83,5 °C
	REV	CACGCAGCTTGTGGGCACCCAGGTCGCTCAGAGC	
β globin H92G	FW	CAGCCTCAGTGAGCTCGGCTGTGACAAGCTGCATG	81,1 °C
	REV	CATGCAGCTTGTCACAGCCGAGCTCACTGAGGCTG	

We used pcDNA3-2xFLAG-α globin and pcDNA3.1$^-$-β globin-MYC, already present in the laboratory of professor Gustincich.

We used pAAV-MCS (Agilent Technologies), designed for the production of AAVs, in order to express α and β chains of mouse Hb. Briefly, from pcDNA3-2xFLAG-α globin, the fragment composed by 2xFLAG-α globin was cloned into the MCS (HindIII/XhoI) of pAAV-MCS. We called this vector pAAV-2xFLAG-α globin.

Meanwhile from pcDNA3.1^{-}-β globin-MYC we generated another construct, in particular the fragment corresponding to β globin-MYC was placed in the MCS (EcoRI/HindIII) of pAAV-MCS. We called this vector pAAV-β globin-MYC.

Generation and purification of recombinant Adeno-Associated Viruses

We decided to use Adeno-Associated Viruses (AAVs) serotypes 9 for our experiments because of its high-expression level and its brain tropism (Zincarelli et al., 2008).

As previously described, the fragments corresponding to 2xFLAG-α globin and β globin-MYC were cloned into the pAAV-MCS vector (Agilent Technologies), which was used to produce recombinant AAV vectors. In addition we use the vector alone as control. Recombinant AAV vectors were prepared, as described previously (Eulalio et al., 2012). Briefly, AAV vectors of serotype 9 were generated in HEK 293T cells, using a triple-plasmid co-transfection for packaging. Viral stocks were obtained by $CsCl_2$ gradient centrifugation. Titration of AAV viral particles was performed by real-time PCR quantification of the number of viral genomes. The viral preparations had the following titres: AAV9-α globin 5×10^{13} viral genome particles/ml, AAV9-β globin $6{,}7\times10^{13}$ viral genome particles/ml and AAV9-control $2{,}2\times10^{13}$ viral genome particles/ml. AAV9-α globin and AAV9-β globin were diluted in PBS 1X at the concentration of $2{,}2\times10^{13}$ viral genome particles/ml before use in order to have the same ratio of infection of AAV9-control.

In addition, we used also an AAV9-GFP (3×10^{12} viral genome particles/ml).

Cell cultures

HEK 293T cells were grown in Gibco® DMEM (Life Technlogies) supplemented with 10% fetal bovine serum (Sigma–Aldrich), 100 μg/ml penicillin (Sigma–Aldrich), and 100 μg/ml streptomycin (Sigma–Aldrich) at 37 °C in a humidified CO_2 incubator. MN9D-Nurr1$^{Tet\text{-}On}$ (iMN9D) cell line (Hermanson et al., 2003) was obtained from Dr. Perlmann (Ludwig Institute for Cancer Research, Stockholm, Sweden). Cells were maintained in culture using DMEM/F12 medium (Life Technlogies) supplemented with 10% fetal bovine serum (Sigma–Aldrich), 100 μg/ml penicillin (Sigma–Aldrich), 100 μg/ml streptomycin (Sigma–Aldrich) and neomycin selection (Life Technlogies)

(250 mM) at 37 °C in a humidified CO_2 incubator. Nurr1 expression in iMN9D cell lines was induced by addition of 3 μg/ml doxycycline (Sigma–Aldrich) to the culture medium every 48 hours. Cells were grown as above except that the 10% fetal bovine serum was changed to 5% (Hermanson et al., 2003). The same condition were used for iMN9D cell line stably transfected with pBUD-IRES-GFP (that we called control cells) or with pBUD-β globin-MYC IRES-GFP, 2xFLAG-α globin (that we called Hb cells) or with pBUD-β globin mutated-MYC IRES-GFP, 2xFLAG-α globin mutated (that we called Hb-mut cells) with the exemption of zeocyn (Life Technologies) selection (150 μg/ml).

Cell transfections

Cells were transfected with Lipofectamine 2000 (Life Technologies) according to the manufacturer's instructions.

Cell infections

Cells were detached, counted and plated. After 24 hours doxycycline were added to the colture medium in order to induce differentiation. Doxycycline was added every 48 hours. After 96 hours cells were treated with 50 mU/ml of Neuroaminidase in serum-free medium for 3 hours at 37 °C and then washed with sereum-free medium. Cells were infected with AAV9s (10^8 MOI) in serum-free medium for 3 hours at 37 °C and then washed with sereum-free medium. 3 days after infection cells were recovered.

Cell treatments

For treatments, the following reagents were used: MPP^+ (Sigma–Aldrich) and Rotenone (Sigma–Aldrich) for 16 hours at different concentrations.

FACS sorting

iMN9D cell line was transfected with pBUD-β globin mut-IRES-GFP, 2xFLAG-α

globin mut. After 24 hours from transfection, cells were collected. 7-Amino-actinomycin D (7-AAD) (Beckman-Coulter) was added to the cell suspension before sorting: it is excluded by viable cells but can penetrate membranes of dying or dead cells and it intercalates into double-stranded nucleic acids. A high-speed cell sorter (MoFlo) was used to sort a population of cells expressing GFP. Sorting parameters used are described previously (Biagioli et al., 2009). Briefly, we first excluded from the analysis cell doublets and debris on the basis of their Pulse Width vs. Forward Scatter (PW/FSC) dot plot. Physical parameters such as FSC and Side Scatter (SSC) were then used to remove a part of dead cells and debris. 7-AAD exclusion was also employed in order to exclude cells with loss in the membrane integrity and, finally, a subpopulation of cells with increased GFP emission was identified and sorted. After sorting, cells were re-plated and 48 hours later, zeocyn (300μg/ml) was added for selection. After 3 weeks polyclonal cell populations expressing mutated tagged α and β chains of mouse Hb was obtained.

Animals

All animal experiments were performed in accordance with European guidelines for animal care and following SISSA Ethical Committee permissions (DM 2/2012-B, January 9th 2012). Mice were housed and bred in SISSA animal facility, with 12 hours dark/light cycles and controlled temperature and humidity. Food and water were provided *ad libitum*.

Stereotaxic surgery

The stereotaxic procedure followed were according to (Cetin et al., 2006). Adult (8–12 weeks old) male C57BL/6 mice weighing 25g ± 3g were used for experiments. Mice were pre-anaesthetised with Tramadolo i.p. (30 mg/kg body weight, intraperitoneally) and anaesthetised with a mixture of Xylazina (15 mg/kg body weight) and Zoletil (15 mg/kg body weight) i.p.. A stereotaxic injection of 2 μl of viral vector suspension (AAV9-GFP or AAV9-control or a mixture of AAV9-2xFLAG-α globin and AAV9-β globin-MYC) was delivered to the left SNpc. The coordinates were: anterior/posterior (A/P) -3.2 mm from bregma, medio/lateral (M/L)

-1,2 mm from bregma and (D/V) dorso/ventral -4,5 mm from the dura (Cao et al., 2010; St Martin et al., 2007). The coordinates used were accorded with the Franklin and Paxinos Mouse Atlas. The injection rate was 0,2 μl/30 seconds using a 10 μl syringe with 26 gauge needle (SGE).

MPTP treatment

MPTP (Sigma-Aldrich) was handled according to the published safety recommendations (Przedborski et al., 2001). Mice were injected i.p. with 35,1 mg/kg of MPTP hydrochloride (corresponding to 30 mg/kg free base MPTP) daily for five consecutive days (Jackson-Lewis and Przedborski, 2007).

Tissue collection and processing

At the indicated number of weeks after injection of AAVs into SN and MPTP treatment (see Results), animals were sacrified. Animals were anesthetized with an overdose of a mixture of Xylazina and Zoletil. Following induction of deep anesthesia, animals were intensively perfused transcardially with PBS 1X. For biochemical analysis, ventral midbrain, striatum and cortex were dissected and immediately put in liquid nitrogen, stored at -80°C and subsequently processed. For immunohistochemistry analysis, after the intensively transcardially perfusion with PBS 1X, animals were perfused with 4% paraformaldehyde diluted in PBS 1X. Brains were immediately dissected with the Mouse Brain Matrix instrument and separated into two pieces, the anterior part containing CPu and the posterior one containing SN. Brains were post-fixed in 4% paraformaldehyde for 1h at room temperature. The regions containing CPu and SN were cut in 40 μm free floating slides with a vibratome (Vibratome Series 1000 Sectioning System). Five consecutive series were collected, in order to represent the whole area of interest.

Western blot

Proteins derivated from adherent and floating cells were collected, washed intensely with PBS 1X and lysed in SDS sample buffer 2X or in Nonidet P-40 (NP-40) lysis

buffer (150 mM NaCl, 50 mM Tris-Cl pH 7.5 and 0.5% NP-40) with the addition of protease inhibitor mixture (Roche). Proteins derivated from tissue were obtained using TRIzol reagent (Life Technologies) following the manufacturer's instructions.
In SDS-PAGE proteins were separated in 10–17% SDS polyacrylamide gel as needed. Native PAGE was performed on gradient polyacrylamide gel electrophoresis (10–12–17% of acrylamide). Standard proteins were loaded using Native Mark Unstained Protein Standard (Sigma-Aldrich). The proteins supplied in the kit have a molecular mass range of 14.2–545 kDa. After the separation on gel, proteins were transferred to nitrocellulose membrane (Schleicher & Schuell). Membrane was blocked with 5% nonfat milk in TBST solution (TBS + 0.1% Tween20), then incubated with primary antibodies overnight at 4 °C or at room temperature for 2 h. The following antibodies were used: anti-Hb 1:1000 (Cappel), anti-FLAG 1:2000 (Sigma–Aldrich), anti-MYC 1:2000 (Cell Signaling), anti-cleaved Caspase-3 1:1000 (Cell Signaling), anti-GFP 1:1000 (Life Technologies), anti-LC3b 1:1000 (Cell Signaling), anti-TH 1:1000 (Sigma–Aldrich), anti-UBF 1:1000 (SantaCruz) and anti-βactin 1:10000 (Sigma–Aldrich). For development, secondary antibodies conjugated with horseradish peroxidase (Dako) were used in combination with ECL reagent (GE Healthcare).

FACS analysis

For FACS analysis, both adherent and floating cells were collected and fixed in ice-cold 70% ethanol. After rehydration, cells were resuspended in PBS + 0.1% NP40 + 200 μg/ml o 2 μg/mL RNaseA and treated with 40 o 10 μg/mL propidium iodide and analyzed on a flow cytometer (FacsCalibur; BD). At least 10^4 green fluorescent protein (GFP)-positive cells were analyzed in each acquisition. FACS data were processed using FlowJo software, and cell cycle profiles were determined using the Watson pragmatic model (Tree Star).

WST-1 analysis

Cell viability was assayed using WST-1 reagent (Roche), according to the manufacturer's protocol. In details absorbance was measured on a microplate ELISA reader (Thermo Scientific) at a 450 nm and 620 nm detection wavelength. Normalized

WST was calculated as follows: WST(%) = [(A_{450nm} − A_{620nm} of treated sample – A_{450nm} − A_{620nm} of blank)/(A_{450nm} − A_{620nm} of untreated sample – A_{450nm} − A_{620nm} of blank)] × 100. Blank represents wells containing culture medium only (Lunardi et al., 2010).

Cellular fractionation

Nucleo-cytoplasmic separation was performed using Nucleo-Cytoplasmic separation kit (Norgen) according to the manufacturer's instruction. The effectiveness of cellular separation were controlled with cytoplasmatic and nuclear markers, respectivately TH and UBF.

RNA isolation and reverse transcription

Total RNA was extracted from cells and mouse tissue samples (cortex, striatum and substantia nigra) using the TRIzol reagent (Life Technologies) following the manufacturer's instructions. All tissues were homogenized using a glass-Teflon® (Thomas Scientific). A fraction of the total RNA samples were subjected to DNase I treatment (Ambion) at 37°C for 1 hour and the sample was then purified on RNAeasy mini kit columns (Qiagen). The final quality of RNA sample was tested on agarose gel. Single-strand cDNA was obtained from 1 μg of purified RNA using the iSCRIPT cDNA synthesis kit (Bio-Rad) according to the manufacturer's instructions.

PCR

To amplify transcripts the polymerase chain reaction mix was prepared by adding 1μl of first strand reaction to a mix containing 0,5μl of Ex Taq DNA polymerase, 10X buffer, dNTPs mix 2,5mM each (all reagents from Takara), 10μM of each oligonucleotide primer and water to a final volume of 50μl. All products were analyzed on agarose gel.

The oligonucleotide primer pairs designed to amplify the transcripts are listed below:

Primers		Sequence	Expected product size
FLAG-α globin	FW	GCGCAAGCTTATGGACTACAAGGA	500 bp
	REV	ATATCTCGAGTTAACGGTACTTGG	
B globin-MYC	FW	GCGCATGGTGCACCTGACtGAtGC	500 bp
	REV	ATATTTACAGGTCCTCCTCGCTGA	
TH	FW	CCGTCTCAGAGCAGGATACC	200 bp
	REV	CGAATACCACAGCCTCCAATG	

Immunocytochemistry and immunohistochemistry

For immunocytochemistry experiments, cells were fixed in 4% paraformaldehyde for 10 minutes, then washed with PBS 1X, treated with 0.1M glycine for 4 minutes in PBS 1X and permeabilized with 0.1% Triton X-100 in PBS 1X for another 4 minutes. After washing with PBS 1X and blocking with 0.2% BSA, 1% NGS, 0.1% Triton X-100 in PBS 1X, cells were incubated with the indicated antibodies diluted in blocking solution for 90 minutes at room temperature. After washes in PBS 1X, cells were incubated with labeled secondary antibodies for 60 minutes. For nuclear staining, cells were incubated with 1μg/ml DAPI for 5 minutes. Cells were washed and mounted with Vectashield mounting medium (Vector). The following antibodies were used: anti-Hb 1:1000 (Cappel), anti-FLAG 1:1000 (Sigma–Aldrich) and anti-MYC 1:2000 (Cell Signaling). For detection, Alexa Fluor -488, -594 or -405 (Life Technologies) antibodies were used.

For immunohistochemistry, slides were treated with 1% SDS in PBS 1X for 1 minutes at RT and blocked with 10% NGS, 1% BSA, 1% Fish gelatin in PBS 1X (filtered) for 1h at RT, the primary and secondary antibodies were diluted in 1% BSA, 0.1% Fish gelatin, 0.3% triton X-100 in PBS 1X. Incubation with primary antibodies was performed for 16h at RT; incubation with secondary antibodies was performed for 2h at RT. Nuclei were labeled with DAPI. Slides were mounted with mounting medium for fluorescence Vectashield (Vector Lab.). The following antibodies were used: anti-GFP (Life Technologies), anti-Hb 1:1000 (Cappel), anti-FLAG 1:100 (Sigma–Aldrich), anti-MYC 1:100 (Cell Signaling) and anti-TH 1:1000 (Sigma–Aldrich). For detection, Alexa Fluor -488, -594 or -405 (Invitrogen) antibodies were used.

All images were collected using a confocal microscope (LEICA TCS SP2 and Nikon).

Lysotracker

Cell were stained without fixation with 50nM Lysotracker Red (Molecular Probes) in growth medium for 1 hour. Stained cells were immediately fixed with 4% paraformaldeide and follow a standard immunofluorescence protocol (Wu et al., 2009). Lysotracker stainining were visualized with confocal microscope (Nikon). Using Volocity 3D Image Analysis Software (PelkinElmer), Lysotracker Red foci per cell were counted. Autophagy activity was defined as follows: high: >10 Lysotracker Red foci/cell; medium: 6–10 Lysotracker Red foci/cell; low: <6 Lysotracker Red foci/cell. The values were represented as percentage of the total.

Quantification of DA neurons in the SNpc

One out of five series of 40 μm freefloating slides was stained for anti-TH antibody. SNpc was outlined under a low magnification objective (10X) following landmarks from the Franklin and Paxinos Mouse Atlas and the analysis was performed under the 40X objective of a Leica DM6000 microscope. Cells were counted throughout the whole SNpc area and through the entire section thickness. TH^+ cells were counted manually. All counts were performed blind to the experimental status of the animals. The orientation for each brain was determined by marking one side of each brain by performing an incision through one side of the brain. The TH^+ cells values were expresses relative to the controlateral side of control-injected mice treated with saline.

Determination of striatal DA density

DA innervation in the striatum was estimated via optical density determination of fluorescent immunostaining using Leica DM6000 microscope. Briefly, striatal sections were immunostained with anti-TH antibody. Scans of three different section were acquired corresponding to a frontal, media and caudal area of striatum. Using Volocity 3D Image Analysis Software (PelkinElmer), the region of interest on the section was outlined and the mean of fluorescence value for the region determined (St Martin et al., 2007). A background value, corresponding to corpus callosum, was subtracted from the fluorescence values (Diaz-Ruiz et al., 2009). The optical density values were expresses as a percentage relative to the controlateral side of control-injected mice treated with saline.

Statistical analysis

All data were obtained by at least three independent experiments. Data represent the mean ± S.D., each group was compared individually with reference control group using Student's t test (Microsoft Excel software). Significance to reference samples were indicated. Regarding statistical analysis of *in vivo* experiments, data represent the mean ± SEM, each group was compared individually with reference control group using ANOVA. Statistical significance was assessed using one-way ANOVA. Significance was set at $p<0.05$.

Results

Preliminary data in the laboratory of Professor Gustincich

Hemoglobin is a well-known blood-associated protein, where it transports oxygen throughout the body. In the last few years, expression of Hb has been found in atypical sites, including the brain. α and β chains of Hb have been detected in the majority of A9 DA neurons (Biagioli et al., 2009), the site of neurodegeneration in PD. Therefore, we asked whether Hb could have a role in PD.

To address this hypothesis, we took advantage of the iMN9D that, under the control of doxocycline, are inducible for the pro-dopaminergic transcription factor Nurr1 (Hermanson et al., 2003). As Hb acts as heterotetramer of two different subunits, we took advantage of pBUDCE4.1 vector to overexpress tagged α and β chains of mouse Hb in iMN9D cells, as previously described (Biagioli et al., 2009). Briefly, by the use of an Internal Ribosomal Entry Site (IRES) driving the expression of eGFP, two stable polyclonal cell lines were obtained by FACS and zeocyn selection: iMN9D cells expressing tagged α and β chains of mouse Hb together with eGFP (Hb cells) and iMN9D cells expressing eGFP only (control cells).

The impact of Hb overexpression depends on the differentiation state of iMN9D cells upon MPP^+ treatment

In order to investigate the function of Hb and its involvement in PD, we analyzed Hb overexpresssion upon typical PD-mimicking insults. We studied cell death induced by the administration of MPP^+, the active ion of the Parkinson-inducing neurotoxin 1-methyl-4-phenyl-1,2,3,6-tetrahydropyride. MPP^+ is reported to induce damage in cells (Chee et al., 2005) resulting in the activation of caspases cascade. Therefore, we analyzed the expression of cleaved Caspase 3 in undifferentiated and differentiated Hb and control cells. Moreover, we tested cell viability through FACS and WST-1 (for technical details see material and methods). We must note that we used different

techniques to measure viability/mortality that are based on different features of viable/death cells. Clevead Caspase 3 expression and FACS monitor cell mortality, while WST-1 analyzes the metabolic activity of viable cells.

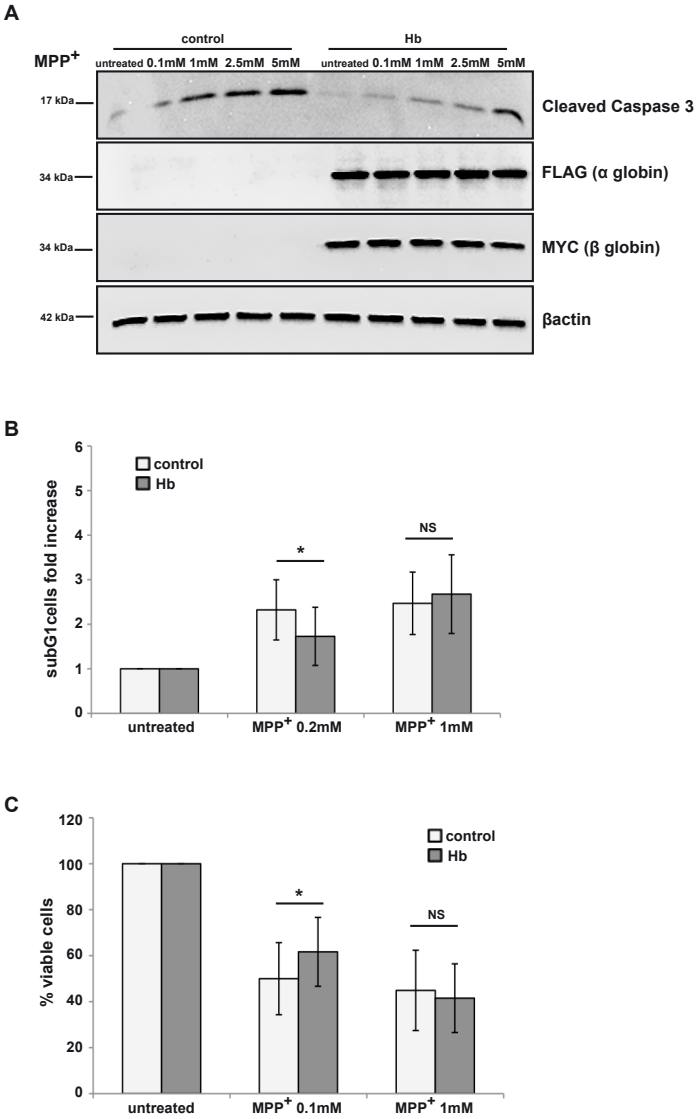

Figure 16. In undifferentiated cells overexpression of Hb is protective upon MPP^+.
Undifferentiated Hb cells (Hb) and control cells (control) were treated with MPP^+ (at the indicated concentrations) for 16 hours. A. Western blot analysis of cleaved Caspase 3 expression. α and β globin were detected with anti-FLAG and anti-MYC antibodies respectively. βactin was used as loading control. (n=5) B. FACS analysis. Percentage of subG1 cells is expressed as fold increased relative to controls, arbitrary set as 1. (n=3) C. WST-1 analysis. In graph are represented the percentage of viable cells. (n=4) Value are mean ± SD. Data were evaluated statistically by Student's *t*-test. Statistical analysis is indicated as: * = p value ≤ 0.05, * *= p value ≤ 0.01, *** = p value ≤ 0.001, NS=non-significance.

First, we focused our attention on undifferentiated cells. In these conditions, cells were detached, counted and plated. After 24 hours, when cells were to approximately

80% confluence, MPP^+ was added and cells were collected 16 hours later for analysis. We decided to use MPP^+ at concentrations of 0.1 mM, 1 mM, 2.5 mM or 5 mM for 16 hours.

As shown in figure 16A, upon MPP^+ treatment Hb cells showed lower levels of cleaved Caspase 3 expression than controls. Untreated cells didn't express cleaved Caspase 3, as expected. In addition we observed a dose-dependent cleavage of Caspase 3 in response to increased concentration of MPP^+, in according to literature data (Nicotra and Parvez, 2002). We also performed FACS analysis in order to discriminate subG1 cells, which represent death cells. The amount of death cells was higher in control cells than Hb cells upon 0.2 mM MPP^+, confirming previous data (figure 16B). Upon 1mM MPP^+ we didn't observe any difference. In addition, we evaluated viable cells through WST-1 assay (figure 16C). Upon MPP^+ treatment we observed about 50% decrease of viability. Furthermore, Hb cells were more viable of about 10% in comparison to control cells upon 0.1 mM MPP^+. Upon 1mM MPP^+ there was no difference. In conclusion, these data suggest that overexpression of Hb protects undifferentiated iMN9D cells from MPP^+ treatment.

We then analyzed differentiated Hb and control cells. In differentiated condition, cells were detached, counted and plated. 24 hours later, doxycycline was added to the colture medium to induce dopaminergic differentiation. The drug was added 56 hours later (cells at approximately 80% confluence) and after 16 hours cells were collected (72 hours after differentiation induction). We used MPP^+ at the concentrations of 0.1 mM, 0.2 mM, 0.5 mM or 1 mM for 16 hours.

Surprisingly, in differentiated conditions, expression of cleaved Caspase 3 was higher in Hb cells than controls (figure 17A). We noticed a dose-dependent cleavage of Caspase 3. In addition, FACS analysis demonstrated that in Hb cells cell death was clearly more evident in comparison to control cells upon 1mM MPP^+ (figure 17B). Upon 0.2 MPP^+ there wasn't statistical difference even if the trend was maintained ($p=0.11$). Moreover, the analysis of viable cells through WST-1 assay showed that in general there was a 30-40% decrease of viability. Furthermore, Hb cells presented about 20% less viability in comparison to control cells upon MPP^+ treatments (figure 17C). All these results suggest a toxic role of Hb after MPP^+ treatment in differentiated conditions.

In conclusion, upon MPP^+ the impact of the overexpression of Hb depends on iMN9D cells' differentiation state.

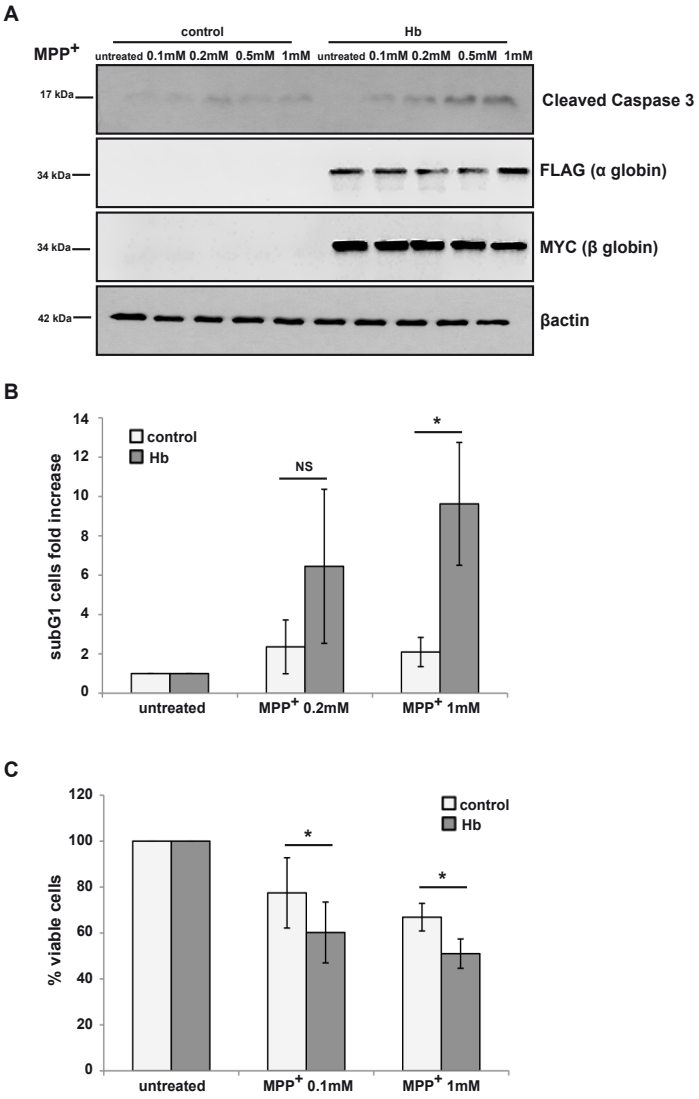

Figure 17. In differentiated cells overexpression of Hb is toxic upon MPP^+.
Differentiated Hb cells (Hb) and control cells (control) were treated with MPP^+ (at the indicated concentrations) for 16 hours. A. Western blot analysis of cleaved Caspase 3 expression. α and β globin were detected with anti-FLAG and anti-MYC antibodies respectively. βactin was used as loading control. (n=10) B. FACS analysis. Percentage of subG1 cells is expressed as fold increased relative to controls, arbitrary set as 1. (n=3) C. WST-1 analysis. In graph are represented the percentage of viable cells. (n=4) Value are mean ± SD. Data were evaluated statistically by Student's *t*-test. Statistical analysis is indicated as: * = p value ≤ 0.05, * *= p value ≤ 0.01, *** = p value ≤ 0.001, NS=non-significance.

In order to understand when Hb overexpression turns out to be toxic upon MPP^+ treatment, we decided to study the expression of cleaved Caspase 3 at different intervals of differentiation. In details, cells were detached, counted and plated at different densities. After 24 hours, doxycycline was added to the colture medium to induce dopaminergic differentiation. After 16 hours from MPP^+ addition, cells were collected at exactly 24, 48 and 72 hours after differentiation induction. We decided to

use 1 mM MPP^+ based on previous data. As shown in figure 18B, after 48 hours of dopaminergic differentiation the effect of Hb overexpression switched from protective to toxic upon MPP^+ treatment. Untreated cells didn't express cleaved Caspase 3, as expected (figure 18A). We hypothesize that there may be some different gene expressions that influence the healthy state of iMN9D cells upon Hb overexpression.

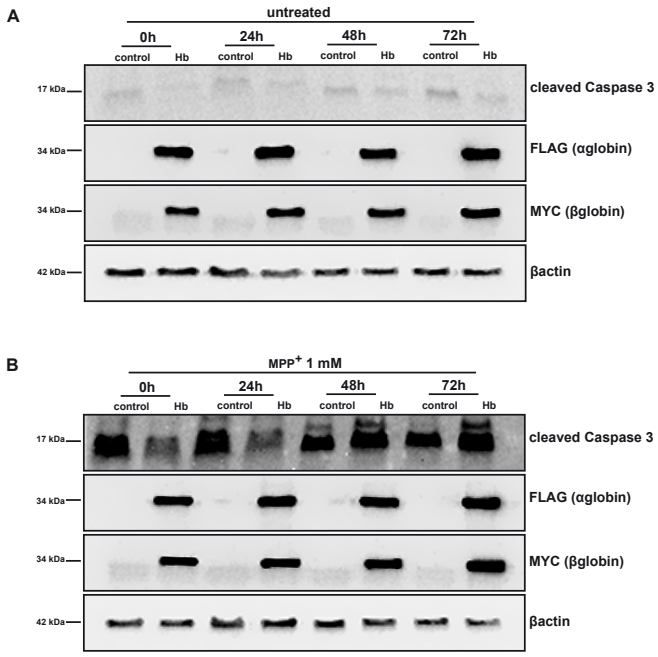

Figure 18. Hb protection/toxicity depends on differentiated state of iMN9D cells.
Differentiation time course of Hb cells (Hb) and control cells (control) untreated (A) or treated with 1mM MPP^+ for 16 hours (B). A, B. Western blot analysis of cleaved Caspase 3 expression. α and β globin were detected with anti-FLAG and anti-MYC antibodies respectively. βactin was used as loading control. (n=4)

Hb overexpression is toxic upon rotenone treatment on both undifferentiated and differentiated iMN9D cells

We then decided to analyze the effects of Hb upon another PD-mimicking drug, that is rotenone. Rotenone, together with MPP^+, is one of the common drugs used to induce neuronal cell death (Panov et al., 2005). The experimental procedure was described above with the unique difference that we used rotenone instead of MPP^+.

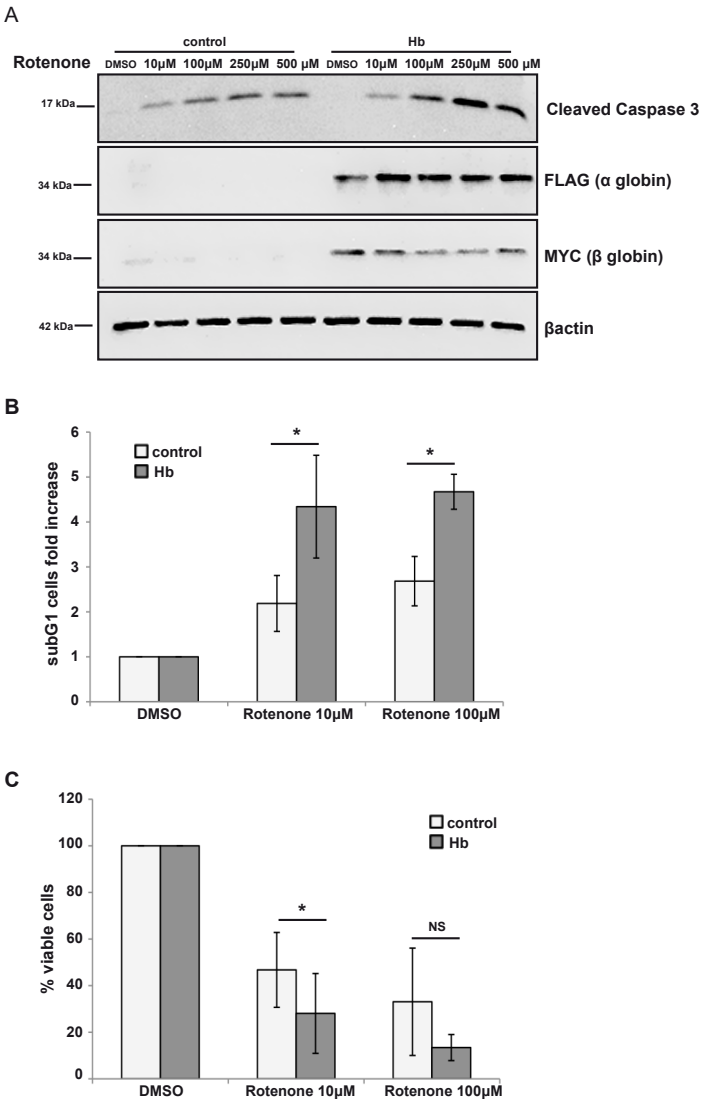

Figure 19. In undifferentiated cells overexpression of Hb is toxic upon Rotenone.
Undifferentiated Hb cells (Hb) and control cells (control) were treated with Rotenone (at the indicated concentrations) for 16 hours. A. Western blot analysis of cleaved Caspase 3 expression. α and β globin were detected with anti-FLAG and anti-MYC antibodies respectively. βactin was used as loading control. (n=6) B. FACS analysis. Percentage of subG1 cells is expressed as fold increased relative to controls, arbitrary set as 1. (n=3) C. WST-1 analysis. In graph are represented the percentage of viable cells. (n=4) Value are mean ± SD. Data were evaluated statistically by Student's *t*-test. Statistical analysis is indicated as: * = p value ≤ 0.05, * *= p value ≤ 0.01, *** = p value ≤ 0.001, NS=non-significance.

As shown in figure 19A, in undifferentiated cells there was a higher expression of cleaved Caspase 3 in Hb cells in comparison to controls upon rotenone treatments. Cleaved Caspase 3 expression was rotenone dose-dependent. The percentage of subG1 cells measured with FACS demonstrated a higher cell death count in Hb cells upon drug treatment (figure 19B). Furthermore, WST-1 experiment proved about 50% of mortality. Interestingly, lower viability was evident in Hb cells (figure 19C).

There was no statistical difference between Hb and control cells upon 100 µM rotenone, although the trend was maintained (p=0.08). All these data suggest that Hb overexpression is toxic upon Rotenone treatment in undifferentiated condition.

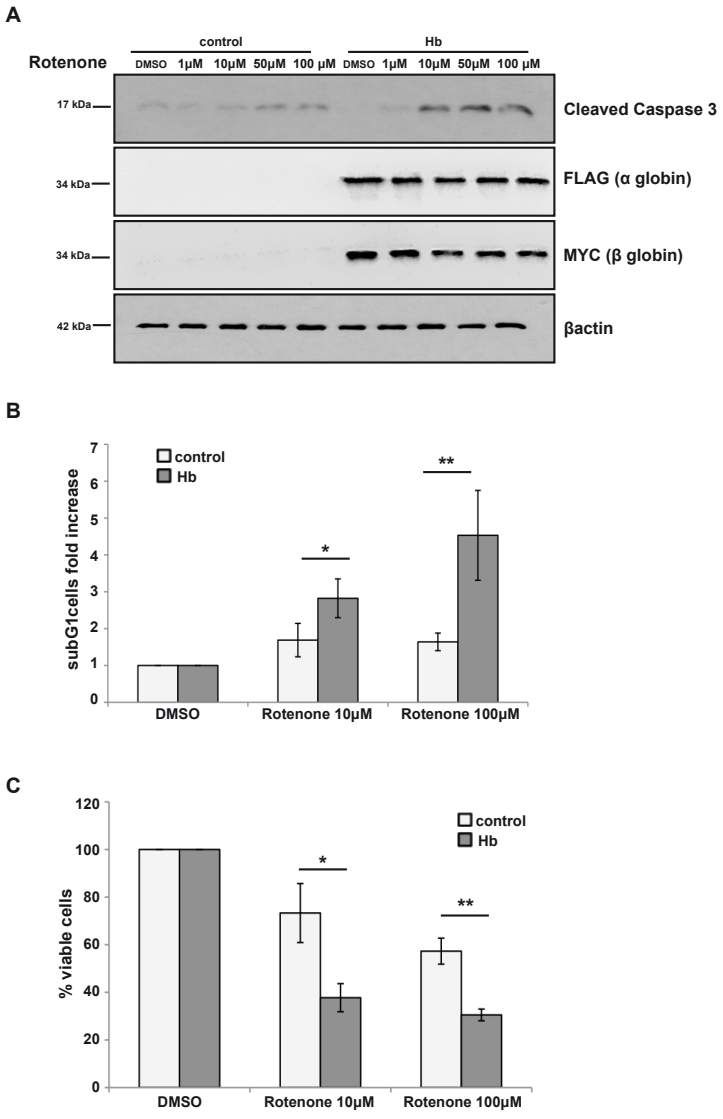

Figure 20. In differentiated cells overexpression of Hb is toxic upon rotenone.
Differentiated Hb cells (Hb) and control cells (control) were treated with Rotenone (at the indicated concentrations) for 16 hours. A. Western blot analysis of cleaved Caspase 3 expression. α and β globin were detected with anti-FLAG and anti-MYC antibodies respectively. βactin was used as loading control. (n=8) B. FACS analysis. Percentage of subG1 cells is expressed as fold increased relative to controls, arbitrary set as 1. (n=4) C. WST-1 analysis. In graph are represented the percentage of viable cells. (n=3) Value are mean ± SD. Data were evaluated statistically by Student's *t*-test. Statistical analysis is indicated as: * = p value ≤ 0.05, * *= p value ≤ 0.01, *** = p value ≤ 0.001, NS=non-significance.

We then analyzed differentiated Hb and control cells. There was a higher expression of cleaved Caspase 3 in Hb cells in comparison to control cells upon Rotenone treatment (figure 20A). The expression of cleaved Caspase 3 was again dose-

dependent. Furthermore, FACS analysis showed higher death ratio in Hb cells than control cells upon stimuli (figure 20B). Moreover, WST-1 assay indicated about 50% of cell death upon rotenone. We noted that Hb cells presented about 30% less viability in comparison to control cells upon drug treatments. (figure 20C). Furthermore, all these experiments indicated that in differentiated cells Hb overexpression is toxic upon rotenone treatment. In summary, differently from MPP^+ stimulus, Hb cells appear to be more susceptible to rotenone in both undifferentiated and differentiated conditions.

Cloning of mutant Hb

To understand if protective and toxic functions of Hb were due to oxygen, we created a stable cell line overexpressing a mutant Hb that is unable to bind oxygen (Hb-mut). In details, we mutated the proximal histidine (F8) that is involved in the binding with heme on both α and β chains. Starting from pBUDCE4.1-β globin-MYC-IRES-eGFP, 2xFLAG-α globin we mutated histidine 87 (nucleotide sequence CAT) on α chain in glycine (GGT) and histidine 92 (CAC) on β chain in glycine (GGC), as indicated in literature (Barrick et al., 1997). We decided to replace histidine by glycine because is the smallest and non-ligand aminoacid, creating a cavity in the proximal heme pocket. Glycine doesn't allow the covalent bond with the iron of the heme group, which in physiological conditions is mediated by the ionic charges of histidine. In the presence of glycine, the binding site is altered, causing significant changes in the affinity for oxygen. In these conditions, it is believed that Hb is not working as oxygen carrier.

The generation of pBUDCE4.1-β globin-MYC mut-IRES-eGFP, 2xFLAG-α globin mut was obtained by two progressive steps of mutagenesis (for technical details see material and methods). At each step, the effectiveness of the mutagenesis reaction was evaluated by sequencing the gene of interest.

It was then possible to proceed with the analysis of the expression of the construct, carried out in HEK 293T cell line that lacks endogenous Hb. Cells have been transiently transfected with pBUDCE4.1-IRES-eGFP (control construct), pBUDCE4.1-β globin-MYC-IRES-eGFP, 2xFLAG-α globin (Hb construct) and pBUDCE4.1-β globin-MYC mut-IRES-eGFP, 2xFLAG-α globin mut (Hb-mut construct). 48 hours after transfection, we evaluated protein expression by Western

blot analysis. To discriminate α and β chains of Hb, two different antibodies were used: anti-FLAG antibody recognized specifically α globin while anti-MYC antibody recognized β globin. Moreover a third antibody anti-Hb was used to identify the global amount of Hb. Finally, anti-GFP antibody was used to evaluate the efficiency of transfection.

As shown in figure 21A, transfected Hb and Hb-mut constructs gave rise to 34 kDa bands, as expected. It is important to note that, as in the case of Hb, also the Hb-mut protein has a band at 34 kDa. This molecular weight is higher than what we expected after a SDS-PAGE (17 kDa) and is compatible with the weight of Hb chains dimer. Previous studies in the laboratory have shown that the bicistronic vector pBUDCE4.1 promotes the formation of a dimer resistant to denaturation. Moreover, the dimer contains α and β chains, as demonstrated by Biagioli and colleagues (Biagioli et al., 2009). All together, these results indicate that the construct Hb-mut is able to express the protein correctly.

Many of the functions of a protein depend on its cellular localization. Therefore, we performed an immunofluorescence experiment to verify the localization of Hb proteins. HEK 293T cells were transiently transfected with the vectors: Hb, Hb-mut and control. The cellular localization of Hb was analyzed 48 hours after transfection by immunofluorescence with anti-Hb antibody. As expected, control transfected cells were negative to staining with anti Hb (figure 21B). A clear signal for the expression of Hb was present both in the cells with Hb and Hb-mut contructs (Figure 21B). This result confirms that Hb-mut was expressed properly. Moreover, proteins were localized in the cytoplasm and in the nucleus (identified by DAPI staining). These data confirm earlier analysis carried out in HEK 293T cells (Biagioli et al., 2009). The localization of Hb does not change in the presence of histidine mutations and Hb-mut is expressed both in the nucleus and in the cytoplasm of cells, as wild type Hb. We also analyzed localization of Hb single chains. We performed double immunofluorescence in which individual chains were localized with anti-FLAG (α chain specific) and anti-MYC (specific for the β chain) antibodies. As shown in Figure 21C, α and β chains were both expressed in cells transfected with Hb and Hb-mut constructs. The signal was absent in cells transfected with the vector only, as expected. α and β chains colocalized and were present in the cytoplasm and in the cells nucleus.

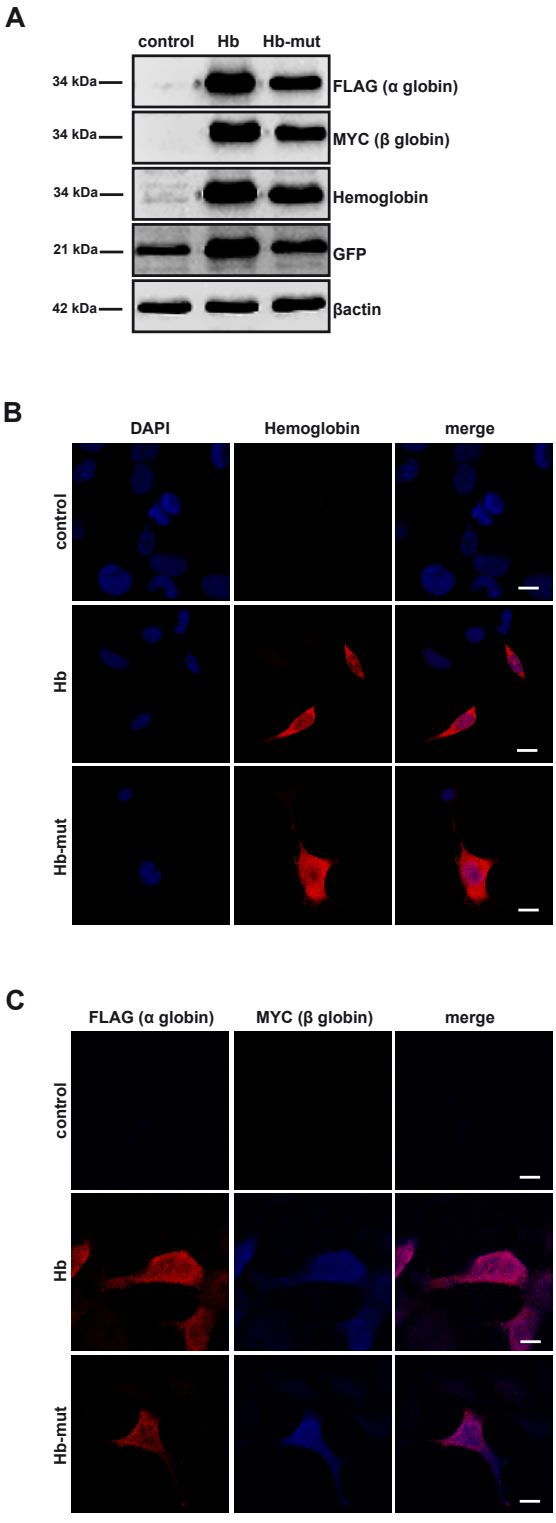

Figure 21. Expression of Hb, Hb-mut and control constructs in HEK 293T cells.
HEK 293T cells were transfected with control, Hb and Hb-mut contructs. A. Western blot analysis of cell lysates. Immunoblot was carried out with anti-FLAG (that recognize α globin specifically), anti-MYC (that recognize β globin specifically), anti-Hb (that recognize both α and β globins), anti-GFP (as control of transfection) and βactin (as loading control). B. Immunofluorescence performed with anti-Hb antibody (red). Nuclei are marked by DAPI. Scale bar 10 μm. C. Double immunofluorescence performed with anti-FLAG (red) and anti-MYC (blue) antibodies. Scale bar 10 μm.

These data confirm previous results obtained with anti-Hb antibodies and demonstrate that Hb-mut maintains the expression and cellular localization of wild type Hb.

Generation of Hb-mut iMN9D stable cell line

In collaboration with professor Carlo Alberto Beltrami at the Department of Medical and Biological Sciences (DSMB), University of Udine in Udine, we decided to generate an iMN9D cell line that overexpresses Hb-mut construct, that we called Hb-mut cells. We applied the same procedure that Biagioli and collegues used to create Hb and control cells (for technical details see material and methods).

In order to verify the correct expression of Hb in Hb-mut cells, first of all we proceeded with Western blot analysis. The lysates were prepared from Hb cells, Hb-mut cells and control cells. We tested the expression of Hb, α chain, β chain and GFP with specific antibodies. The expression of GFP was analyzed in order to verify the effectiveness of sorting and subsequent selection of positive cells. As shown in figure 22A, the specific antibodies used (anti-FLAG, anti-MYC and anti-Hb) recognized a clear band at 34 kDa in Hb cells and Hb-mut cells, as expected. No bands in control cells were detected using anti-FLAG and anti-MYC antibodies. In control cells a weak band was detected with anti-Hb antibody, as expected because iMN9D cells expresses endogenous Hb. The observed molecular weight for the single chains was 34 kDa. Furthermore, comparing the expressing levels of single chains with those of Hb, we observed that Hb-mut cells espressed lower levels of Hb, even if the GFP levels was comparable between Hb cells and Hb-mut cells. Probably this was due to the mutations inserted in the sequence of Hb-mut. Finally, it is interesting to note that control cells presented lower levels of GFP, although sorted by FACS with the same parameters. Biagioli and collegues had previously observed this aspect. Altogether these results demonstrate that Hb-mut cells correctly express mutant α and β chains, even if expressing levels were lower than Hb cells.

In order to study the localization of mutant Hb in Hb-mut cells, we carried out immunofluorescence experiments, as previously described. First, we analyzed Hb staining. As shown in figure 22B, Hb levels were very low in control cells, as expected. Overexpressed Hb was present in the cytoplasm and in the nucleus of Hb cells. The same distribution was observed in Hb-mut cells. We then analyzed the localization of single globin chains. As shown in figure 22C, control cells didn't

express FLAG and MYC tags. In Hb cells and Hb-mut cells tagged α and β chains (recognized by specific antibody) colocalized and were present in cytoplasm and nucleus of cells.

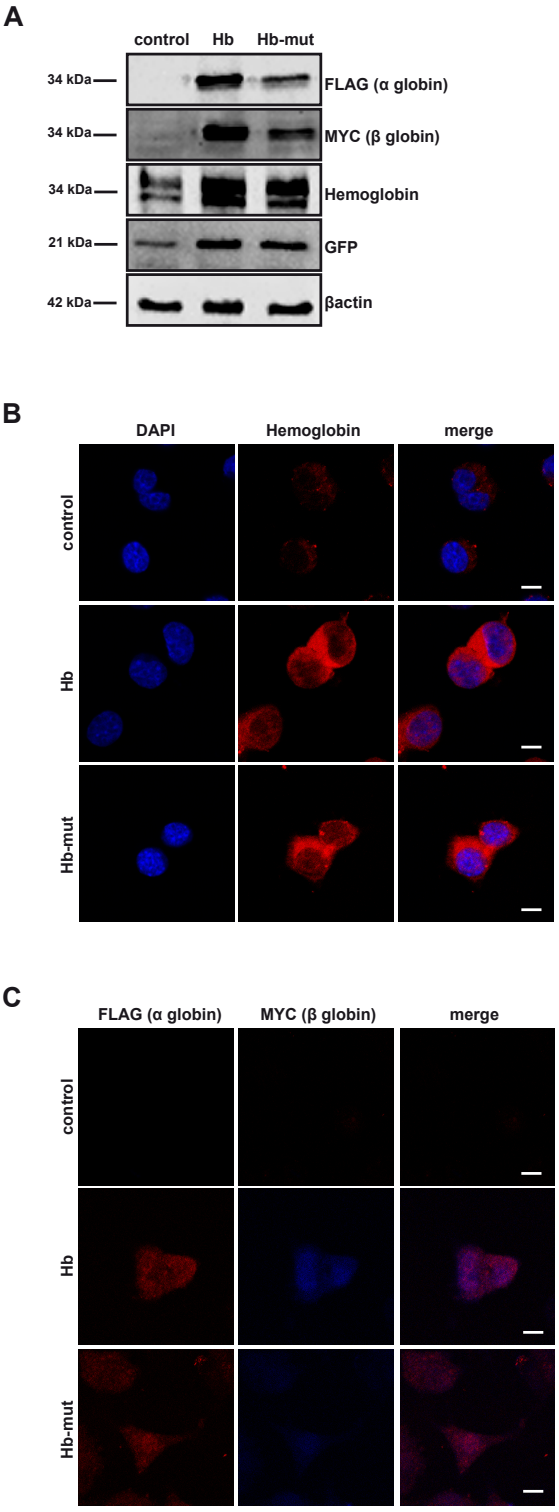

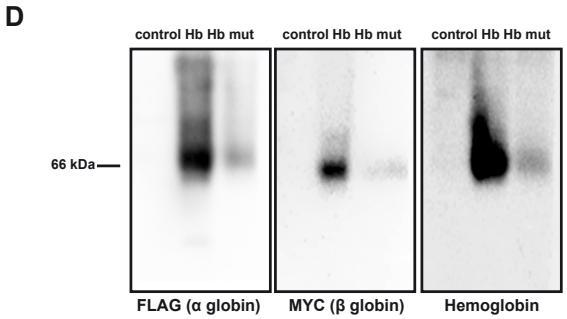

Figure 22. Analysis of Hb, Hb-mut and control cells.
iMN9D cell lines stable transfected with Hb, Hb-mut and control constructs. A. Western blot analysis of cell lysates. Immunoblot was carried out with anti-FLAG (that recognize α globin specifically), anti-MYC (that recognize β globin specifically), anti-Hb (that recognize both α and β globins), anti-GFP (as internal control) and βactin (as loading control). B. Immunofluorescence performed with anti-Hb antibody (red). Nuclei are marked by DAPI. Scale bar 10 μm. C. Double immunofluorescence performed with anti-FLAG (red) and anti-MYC (blue) antibodies. Scale bar 10 μm. D. Native PAGE of cell lysates. Immunoblot was carried out with anti-FLAG, anti-MYC and anti-Hb.

We have recently showed that in Hb cells overexpressed Hb exists as an $\alpha_2\beta_2$ tetramer (Russo et al., 2013). Therefore, we analyzed the tertiary structure of mutant Hb in Hb-mut cells. We used anti-FLAG and anti-MYC antibodies to discriminate between the two chains in order to determine the presence of each chain within the Hb quaternary structure. In contrast to SDS–PAGE, native PAGE was performed in non-denaturing conditions allowing the separation of intact non-covalent protein complexes (for technical details see material and methods). We used this technique to determine the native molecular mass of Hb overexpressed in Hb-mut cells. As controls, we included protein extracts prepared from Hb and control cells. In Hb cells and Hb-mut cells both anti-FLAG and anti-MYC antibodies detected a single band with an estimated mass of 64 kDa, based on its mobility relative to native molecular weight markers (Figure 22D). As expected, no bands were observed in control cells. These data indicate that overexpressed Hb-mut folds as a tetramer that contains two α and two β chains. The same result was obtained when the lysates were stained with an anti-Hb antibody, thus confirming that anti-tag antibodies detected Hb-containing bands.

In conclusion, all these data demonstrated that Hb-mut cells express mutant Hb, even if the expressing levels were lower in comparison with Hb cells. Moreover, despite the presence of histidine mutations, Hb-mut is present a $\alpha_2\beta_2$ tetramer and localizes both in the cytoplasm and in the nucleus of the cells, as wild type Hb in Hb cells.

Hb protection/toxicity does not depend on oxygen binding

We then decided to compare the mortality of Hb, Hb-mut and control cells upon PD-mimicking stimuli. Undifferentiated and differentiated cells were treated with MPP^+ or rotenone. We analyzed mortality through the expression of cleaved Caspase 3, as a marker of neuronal death.

As shown in figure 23A, Hb-mut maintained the protective capacity. Furthermore, Hb-mut didn't revert Hb toxicity in comparison to controls (figure 23B,C,D). This result suggests that oxygen binding is not required in the protective/toxic process. We have to note that there was a slightly higher expression of cleaved Caspase 3 in Hb cells than Hb-mut cells. We hypothesised that this is due to the fact that Hb-mut cells expressed lower protein levels. Further investigation must be done in order to confirm that Hb protection/toxicity does not depend on oxygen binding.

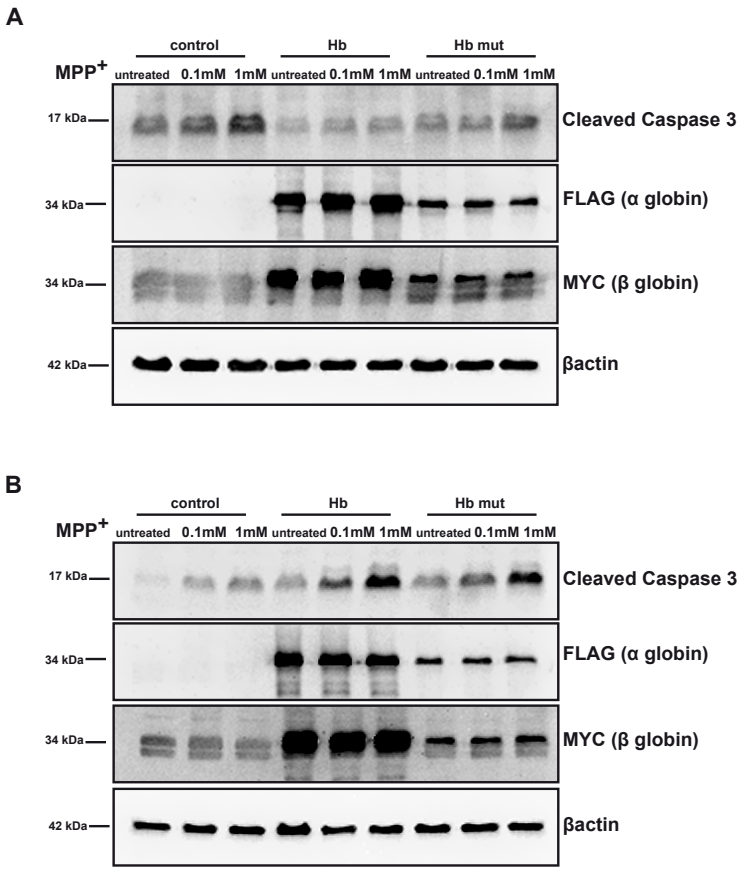

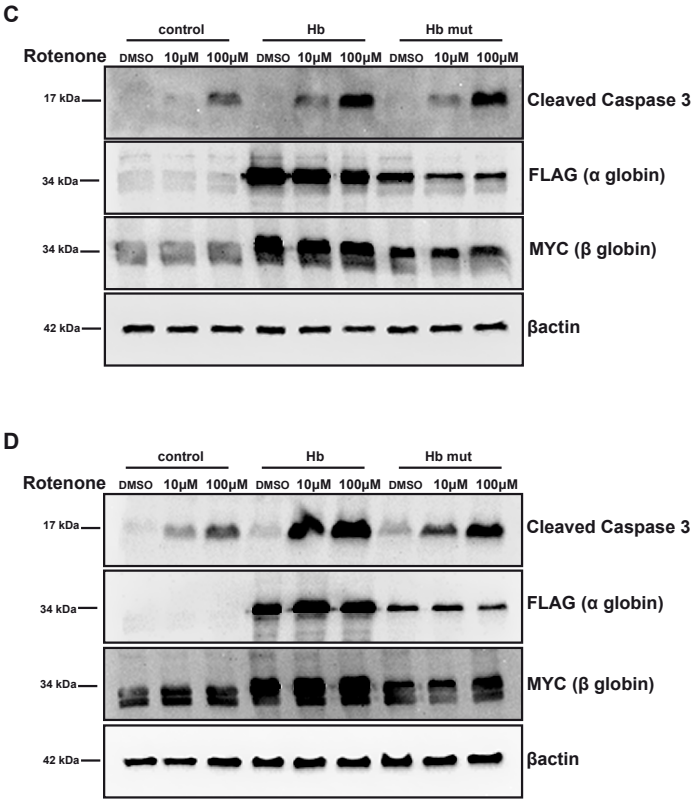

Figure 23. Hb protection/toxicity doesn't depend on oxygen binding.
Undifferentiated (A,C) and differentiated (B,D) Hb cells (Hb), Hb-mut cells (Hb-mut) and control cells (control) were treated for 16 hours with 0.1mM and 1mM MPP^+ (A,B) or with 10μM and 100 μM rotenone (C,D). A,B,C,D. Western blot analysis of cleaved Caspase 3 expression. α and β globin were detected with anti-FLAG and anti-MYC antibodies respectively βactin was used as loading control. (n=3)

Quaternary structure of Hb ($\alpha_2\beta_2$) is not altered upon neurotoxic stimuli

In the blood Hb presents $\alpha_2\beta_2$ tetrameric structure. This structure is essential for Hb function. We recently demonstrated that in Hb cells, overexpressed Hb exists as an $\alpha_2\beta_2$ tetramer (Russo et al., 2013). We thus analyzed the quaternary structure of overexpressed Hb in Hb cells upon PD-mimicking insults.

As shown in figure 24, quaternary structure of Hb did not change neither upon MPP^+ nor upon rotenone treatments. This result indicates that $\alpha_2\beta_2$ tetramer of Hb is maintained upon toxic stimuli.

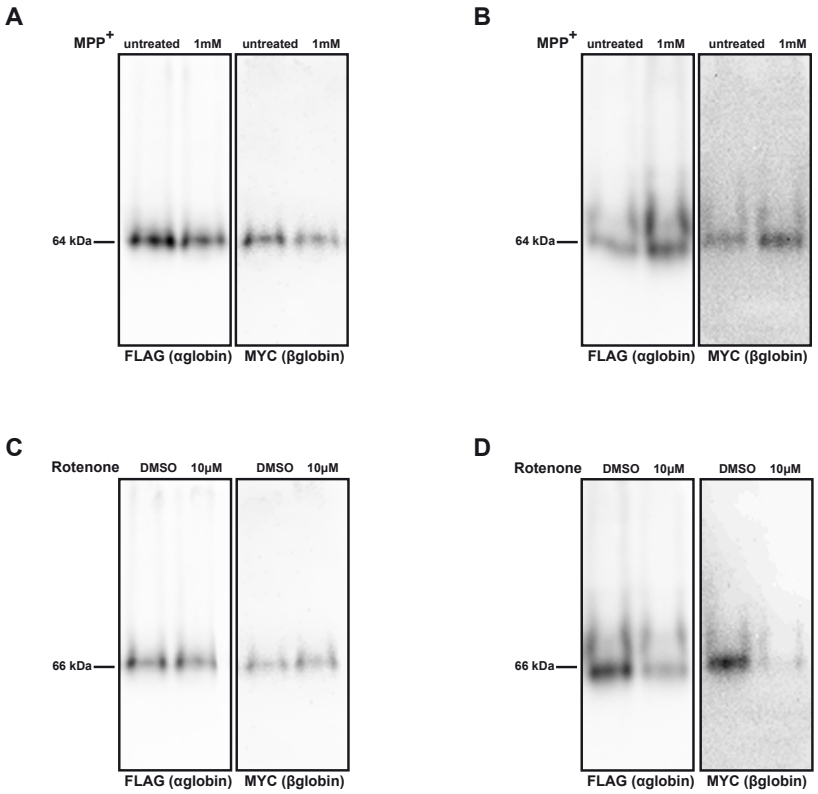

Figure 24. Quaternary structure of Hb upon toxic stimuli in Hb cells.
A. Undifferentiated Hb cells were treated for 16 hours with 1mM MPP^+. Immunoblot of native PAGE of cell lysates was carried out with anti-FLAG and anti-MYC antibodies. (n=3) B. Differentiated Hb cells were treated for 16 hours with 1mM MPP^+. Immunoblot of native PAGE of cell lysates was carried out with anti-FLAG and anti-MYC antibodies. (n=3) C. Undifferentiated Hb cells were treated for 16 hours with 10 μM rotenone. Immunoblot of native PAGE of cell lysates was carried out with anti-FLAG and anti-MYC antibodies. (n=3) D. Differentiated Hb cells were treated for 16 hours with 10 μM rotenone. Immunoblot of native PAGE of cell lysates was carried out with anti-FLAG and anti-MYC antibodies. (n=3)

Hb accumulates in the nucleus upon neurotoxic stimuli

The cellular localization of proteins is important for their functions. Previous data (Biagioli et al., 2009) demonstrated that Hb is localized in the cytoplasm and in the nucleus of DA neurons *in vivo*. This was recapitulated in Hb cells where overexpressed Hb is present in both cell compartments. Therefore we decided to perform cellular fractionation experiments in order to study the cellular distribution of Hb upon PD-mimicking insults (for technical details see material and methods). First, we decided to focus our attention on differentiated cells, as in previous experiments. We analyzed Hb cells upon MPP^+ and rotenone treatments. Cellular fractionation

experiments demonstrated that in untreated conditions α and β globins were present both in the cytoplasm and in the nucleus, confirming previous data (figure 25A,B).

Upon MPP^+ treatment, α globin (visualized with anti-FLAG antibody) and β globin (visualized with anti-MYC antibody) increased in the nucleus, as confirmed by 34 kDa band. Furthermore, in these conditions, α globin also showed a 17 kDa band, that, upon treatments, decreased in the cytoplasm and increased in the nucleus. Interestingly upon toxic stimuli a band of about 20 kDa appeared in the nucleus. This band was probably due to a post-translational modification and this modification may be associated with the toxic role of Hb in these conditions.

In order to confirm cellular fractionation data, we carried out immunofluorescence experiments with identical experimental settings. As shown in figure 25C,D, untreated Hb cells presented α and β globins both in the cytoplasm and in the nucleus, confirming previous data.

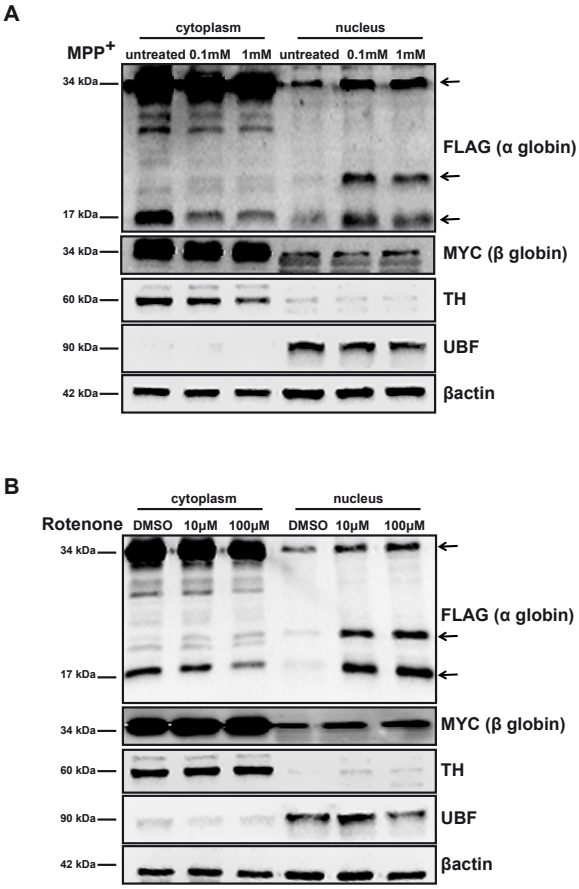

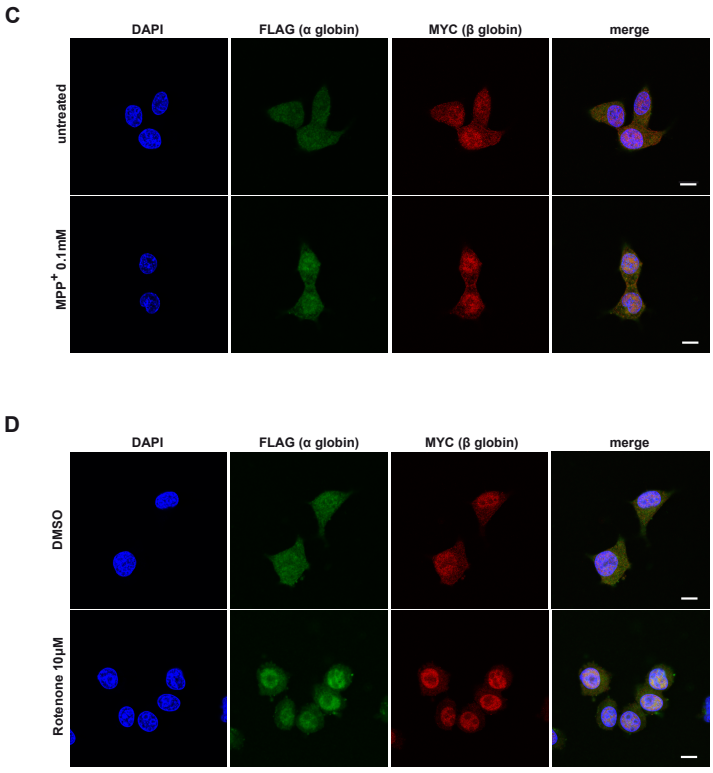

Figure 25. Hb accumulates in the nucleus upon toxic stimuli in differentiated Hb cells.
Differentiated Hb cells were treated for 16 hours with 0.1mM MPP^+ (A,C) or with 10µM rotenone (B,D). A,B. Immunoblot of cellular fractionation was carried out with anti-FLAG (that recognized specifically α globin) and anti-MYC (that recognized specifically β globin) antibodies. Anti-TH and anti-UBF antibodies were used to visualize specifically cytoplasm and nucleus comportment respectively. βactin was used as loading control. (n=4) C,D. Representative images of double immunofluorescence performed with anti-FLAG (green) and anti-MYC (red) antibodies. Nuclei are marked by DAPI. Scale bar 10 µm. (n=3)

Upon toxic stimuli α and β globins increased in the nucleus compartment, confirming cellular fractionation experiments. In conclusion, in differentiated Hb cells overexpressed Hb accumulates in the nucleus of cells upon exposure with MPP^+ and rotenone.

In order to exclude artefacts derivate from immonoblot analysis, we decided to performed cellular fractionation experiments. As shown in figure 26, anti-FLAG antibody revealed bands at different weights such as 17 kDa, 20 kDa and 34 kDa in Hb cells and not in control cells, demonstrating that these bands were specific. Anti-MYC antibody recognized a single band at 34 kDa in Hb cells, proving the specificity of bands.

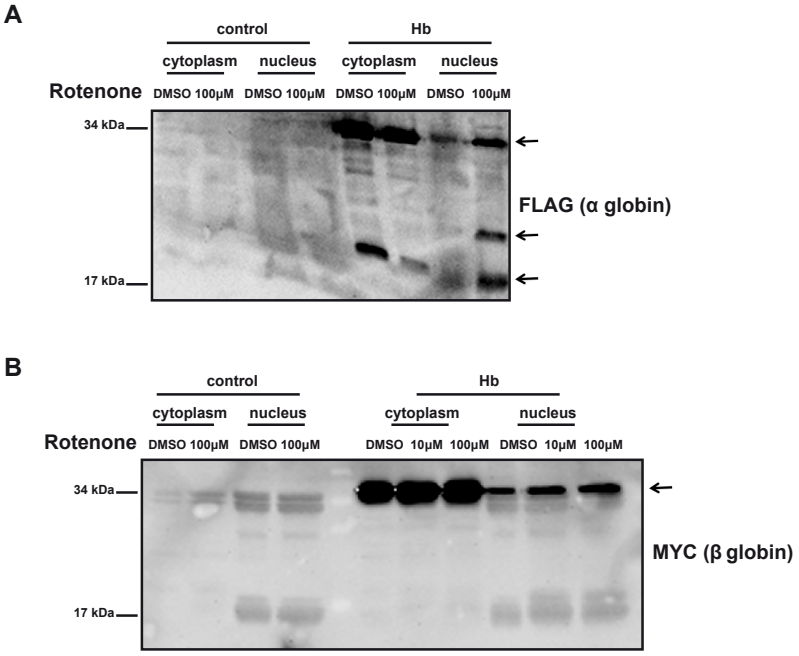

Figure 26. Exclusion of artefacts derivate from immoblot analysis.
Differentiated Hb cells (Hb) and control cells (control) were treated for 16 hours with 10μM Rotenone. A. Immunoblot of cellular fractionation was carried out with anti-FLAG antibody that recognized specifically α globin. B. Immunoblot of cellular fractionation was carried out with anti-MYC antibody that recognized specifically β globin.

Accumulation in the nucleus is associated to a toxic effect of overexpressed Hb

Increased nuclear Hb may be associated to Hb toxicity upon neurotoxic stimuli. In order to confirm this hypothesis we performed cellular fractionation experiments in undifferentiated Hb cells, as described previously. In particular, we compared Hb cellular localization upon rotenone, where we demonstrated that Hb overexpression was toxic, and upon MPP^+, where we demonstrated that Hb overexpression was protective. In undifferentiated Hb cells, α globin accumulated in the nuclear compartment upon rotenone (figure 27A). On the other hand, α globin did not increase in the nucleus upon MPP^+ (figure 27B). These results suggest that increased nuclear Hb is associated to its toxic effects upon PD-mimicking drugs.

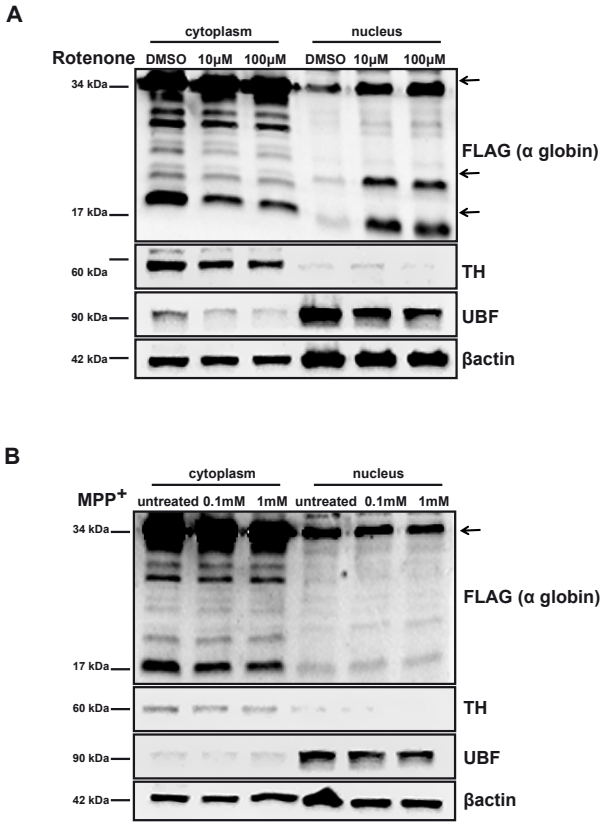

Figure 27. In undifferentiated Hb cells Hb accumulates in the nucleus upon rotenone and not upon MPP^+.
Undifferentiated Hb cells were treated for 16 hours with 10μM rotenone (A) or with 0.1mM MPP^+ (B). A,B. Immunoblot of cellular fractionation was carried out with anti-FLAG (that recognized specifically α globin) antibody. Anti-TH and anti-UBF antibodies were used to visualize specifically cytoplasm and nucleus comportment respectively. βactin was used as loading control. (n=4)

Accumulation of mutant Hb in the nucleus upon neurotoxic treatments

In order to confirm that protection/toxicity of Hb upon neurotoxic stimuli is not oxygen dependent, we decided to analyze cellular compartment distribution of Hb-mut upon PD-mimicking drugs. As shown in figure 28B,C,D, α globin accumulated in the nucleus of cells upon neurotoxin stimuli. These data confirmed our previous observation that Hb toxicity was not due to oxygen binding. Furthermore, we didn't observe such accumulation in undifferentiated cells treated with MPP^+ (figure 28A).
In conclusion Hb protective/toxic mechanisms do not require oxygen binding.

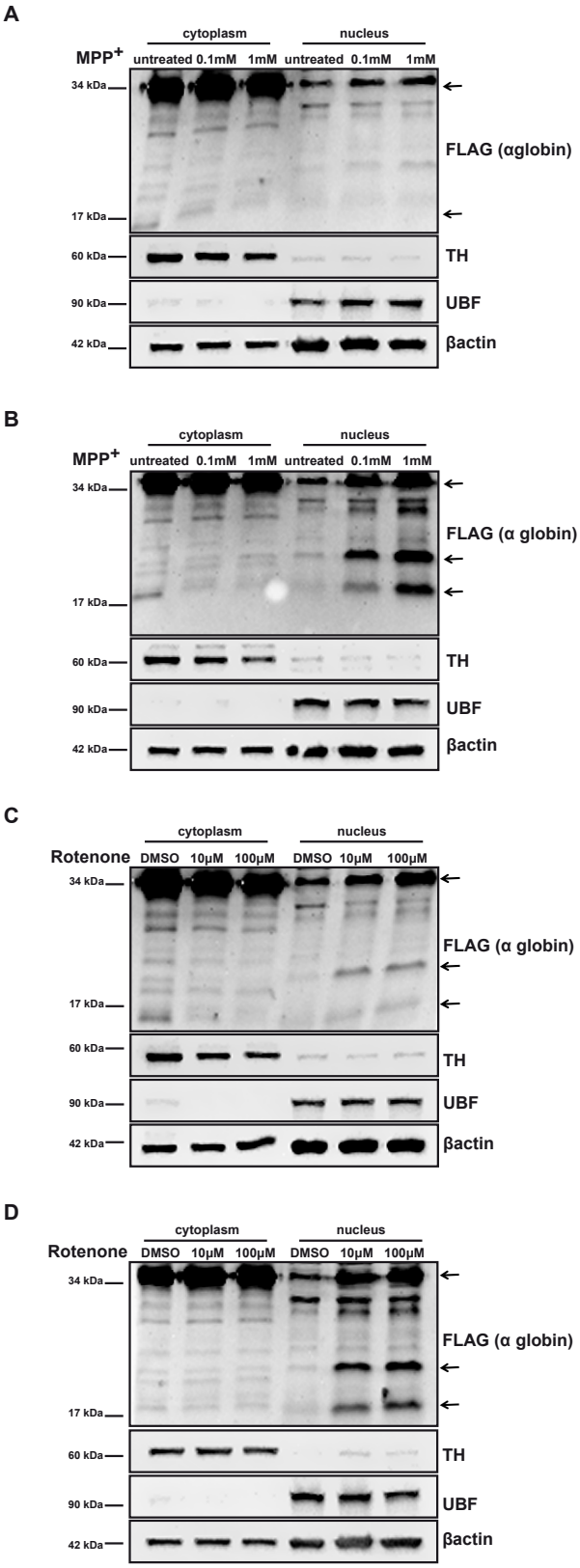

Figure 28. Cellular compartment distribution of Hb-mut upon MPP^+ and rotenone treatments in undifferentiated and differentiated Hb-mut cells.
Undifferentiated (A,C) and differentiated (B,D) Hb-mut cells were treated for 16 hours with MPP^+ (A,B) or with 10μM rotenone (C,D). A,B,C,D. Immunoblot of cellular fractionation was carried out with anti-FLAG (that recognized specifically α globin) antibody. Anti-TH and anti-UBF antibodies

were used to visualize specifically cytoplasm and nucleus comportment respectively. βactin was used as loading control. (n=3)

Overexpression of Hb is associated with an impairment of autophagy upon neurotoxic stimuli

Autophagy is a process responsible for the degradation of intracellular material. Recent reports indicate that autophagy plays a crucial role in many different neuropathologies, such as HD, AD and PD (Nixon, 2013). If cells cannot activate autophagy, protein synthesis predominates over protein degradation. Activation of autophagy could also be an effective way of eliminating altered agents that are present in the cytosol. Furthermore, in the laboratory of professor Gustincich microarray data indicated that in a thalassemic mouse model, in which β globin gene was deleted in heterozigosity, Atg4 gene, a major regulator of autophagy, was differentially expressed (Marcuzzi et al., unpublished data).

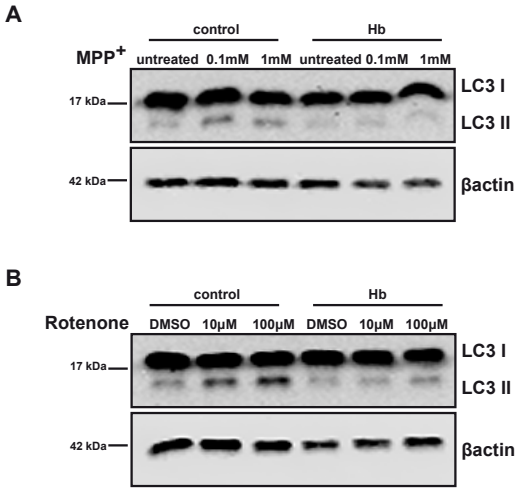

Figure 29. Overexpression of Hb is associated with an impairment of autophagy upon neurotoxic stimuli in differentiated cells.
Differentiated Hb cells (Hb) and control cells (control) were treated with MPP^+ (A) and rotenone (B) for 16 hours. A,B. Western blot analysis of cell lysates. Immunoblot was carried out with anti-LC3. βactin was used as loading control. (n=6)

Therefore, we decided to study the autophagy pathway in our cells' system. In particular, we analyzed differentiated Hb and control cells upon MPP^+ and rotenone treatments. First, we studied the expression of LC3 by Western blot analysis. LC3 is one of the key molecular components involved in autophagy. To date, LC3 is the only reliable marker of autophagosomes. Tracking LC3II expression is indicative of

autophagic activity. As shown in figure 29, in control cells it was observed an evident increased expression of LC3II upon both toxic stimuli, indicating an activation of autophagy; whereas in Hb cells we didn't observe such increase. Our results suggest that Hb overexpression impairs autophagy induction upon PD-mimicking treatments. We then stained cells with Lysotracker RED, which permits to label acidic organelles in live cells, such autophagosome.

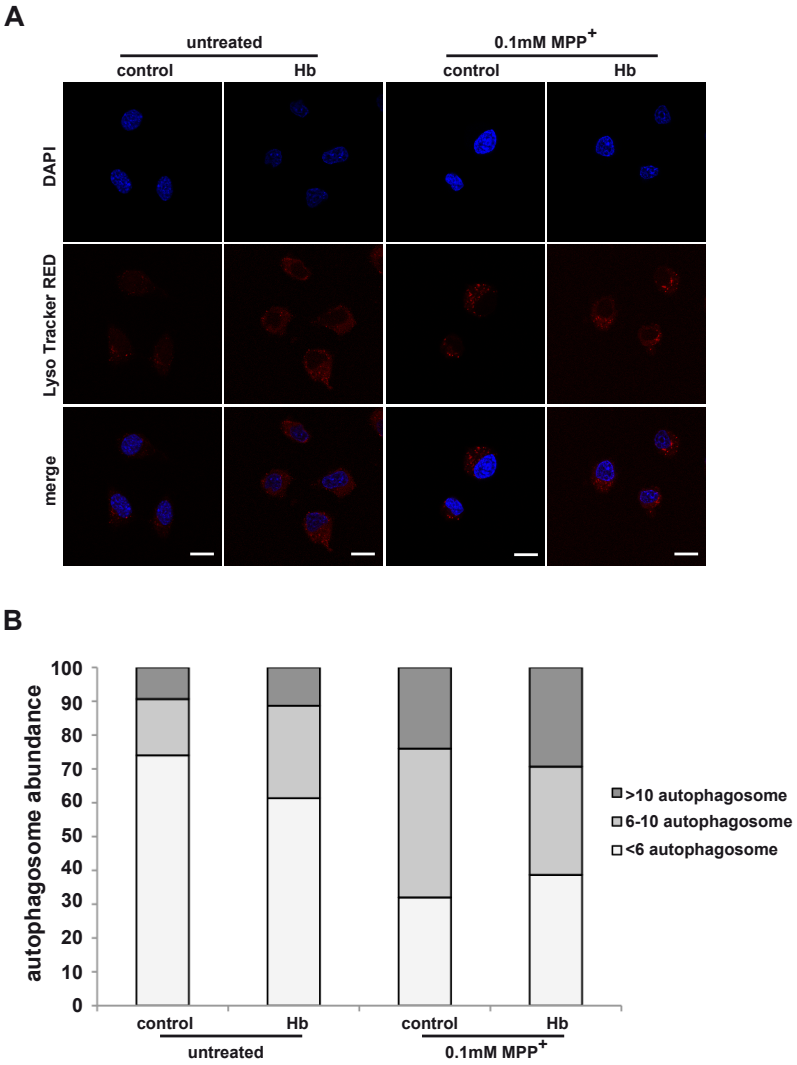

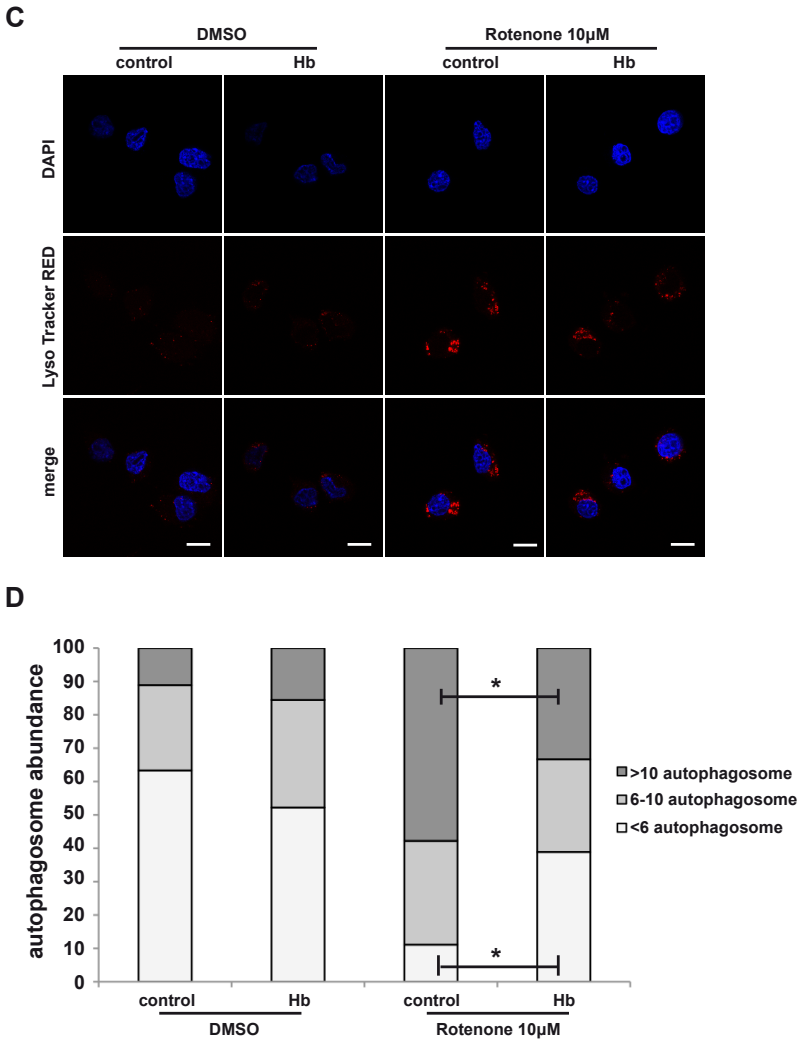

Figure 30. Overexpression of Hb is associated with an impairment of autophagy upon neurotoxic stimuli in differentiated cells .
Differentiated Hb cells (Hb) and control cells (control) were treated with MPP^+ and rotenone for 16 hours. A,C. Lysotracker Red staining. Nuclei are marked by DAPI. Scale bar 10 µm. B,D. Quantification of autophasome. Autophagy activity was defined as follows: high: >10 Lysotracker RED foci/cell; medium: 6–10 Lysotracker RED foci/cell; low: <6 Lysotracker RED foci/cell. Lysotracker RED-positive foci in 100 randomly chosen cells were counted for quantification. Value are mean ± SD. Data were evaluated statistically by Student's *t*-test. Statistical analysis is indicated as: * = p value ≤ 0.05, * *= p value ≤ 0.01, *** = p value ≤ 0.001.

As shown in figure 30, quantification analysis of the number of Lysotracker RED-positive foci per cell demonstrated a prominent rise of autophagosome density in control cells in comparison to Hb cells upon Rotenone treatment. Even if the trend was maintained there was no statistical difference in Hb and control cells upon MPP^+. These results suggest that Hb overexpression impairs autophagy upon PD-mimicking insults. Further investigation must be done in order to assess if autophagy impairment is linked to Hb-mediated toxicity.

Cloning and generation of AAV9-2xFLAG-α globin and AAV9- β globin-MYC

AAVs are commonly used to study the function of a protein in an *in vivo* model. To this purpose we decided to produce AAVs that encode for 2xFLAG-α globin and β globin-MYC to assess the role of Hb in a mouse model. Furthermore, we decided to use AAVs serotype 9 for its high affinity for neuronal cells (Zincarelli et al., 2008). In particular, we wanted to overexpress Hb in DA neurons of SNpc in the mouse brain to better understand what is the physiological role of Hb in DA neurons *in vivo* and what happens upon PD-mimicking stress conditions as well as MPTP treatment.

Starting from pcDNA3-2xFLAG-α globin and pcDNA3.1-β globin-MYC we subcloned each coding sequences in pAAV-MCS vector (for technical details see material and methods). We tested the expression of the obtained constructs (pAAV-2xFLAG-α globin and pAAV-β globin-MYC) by Western blot. We transiently transfected HEK 293T cells with pAAV-2xFLAG-α globin and pAAV-MCS, as control, and 48 hours later lysates were prepared. As show in figure 31A, pcDNA3-2xFLAG-α globin correctly encoded for tagged α globin detected by anti-FLAG and anti-Hb antibodies. At the same time we carried out the same experiment to test pAAV-β globin-MYC. As shown in figure 31B, pAAV-β globin-MYC expressed tagged β globin detected by anti-MYC and anti-Hb antibodies. We observed that α and β globin presented a molecular weight of 17 kDa, as expected from a denaturated SDS-PAGE. We then proceeded with the generation of AAV9s, that we called AAV9-2xFLAG-α globin, AAV9-β globin-MYC and AAV9-control (for technical details see material and methods).

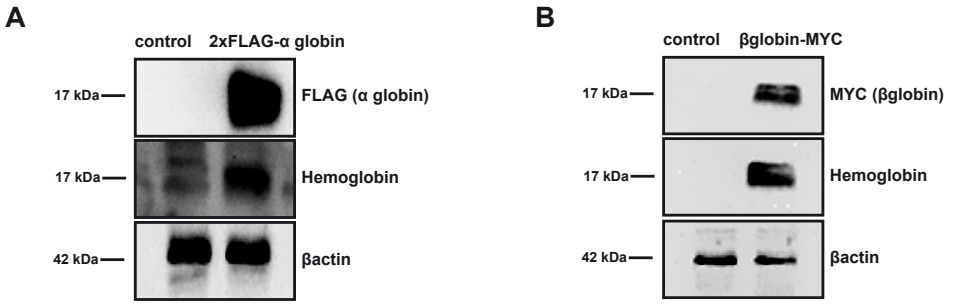

Figure 31. Expression of pAAV-2xFLAG-α globin and pAAV-β globin-MYC in HEK 293T cells.
A. HEK 293T cells were transfected with pAAV or pAAV-2xFLAG-α globin contructs. Western blot analysis was carried out using anti-FLAG and anti-Hb antibodies. βactin was used as loading control.
B. HEK 293T cells were transfected with pAAV or pAAV- β globin-MYC contructs. Western blot analysis was carried out using anti-MYC and anti-Hb antibodies. βactin was used as loading control.

Once obtained the AAV9-control, AAV9-2xFLAG-α globin and AAV9-β globin-

MYC from the laboratory of professor Mauro Giacca at ICGEB in Trieste, we decided to test the expression of the AAV9s *in vitro* before performing *in vivo* experiments (see materials and methods for technical approach). In details, cells were detached, counted and plated. After 24 hours doxycycline were added to the colture medium to induce differentiation. After 96 hours cells were treated with Neuroaminidase and infected with AAV9-2xFLAG-α globin, AAV9-β globin-MYC or AAV9-control with a MOI of 10^8. 3 days after infection cells were recovered, cell lysates prepared and Western blot analysis performed. We used iMN9D cells transfected with pAAV-2xFLAG-α globin or pAAV-β globin-MYC as positive control and cells infected with AAV9-control as negative control. As shown in figure 32, iMN9D cells were correctly infected by AAV9-2xFLAG-α globin or by AAV9-β globin-MYC and presented a clear band, as expected.

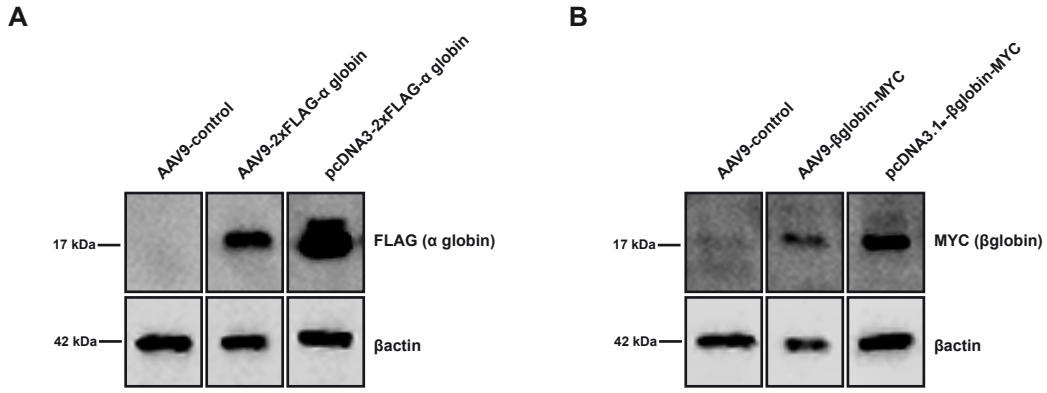

Figure 32. Infection of iMN9D cells with AAV9-2xFLAG-α globin and AAV9-β globin-MYC.
A. iMN9D cells were infected with AAV9-2xFLAG-α globin or AAV9-control. Western blot analysis was carried out using anti-FLAG antibody. iMN9D cells transfected with pcDNA3-2xFLAG-α globin were used as positive control. βactin was used as loading control. B. iMN9D cells were infected with AAV9-β globin-MYC or AAV9-control. Western blot analysis was carried out using anti-MYC antibody. iMN9D cells transfected with pcDNA3.1$^-$-β globin-MYC were used as positive control. βactin was used as loading control.

Settings of stereotactic surgery

Stereotactic surgery is a form of surgical intervention, which makes use of a three-dimensional coordinates system to locate small targets inside the brain and to perform on them some actions as injection of viruses. We decided to use this technique in order to precisely infect DA neurons of SNpc of mouse brain (figure 33).

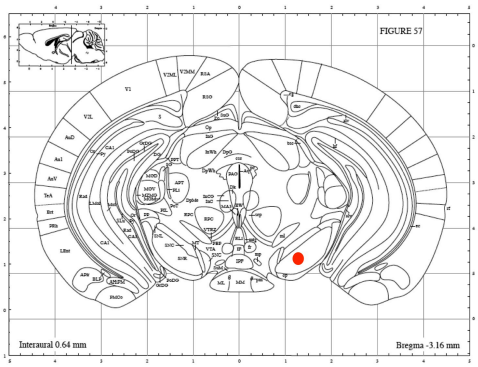

Figure 33. Schematic representation of stereotactic surgery.
Red spot indicates the site of AAV9s injection, that corresponded to Substantia Nigra pars compacta (SNpc). This brain side is called ipsilateral side. The non-injected side is called controlateral side.

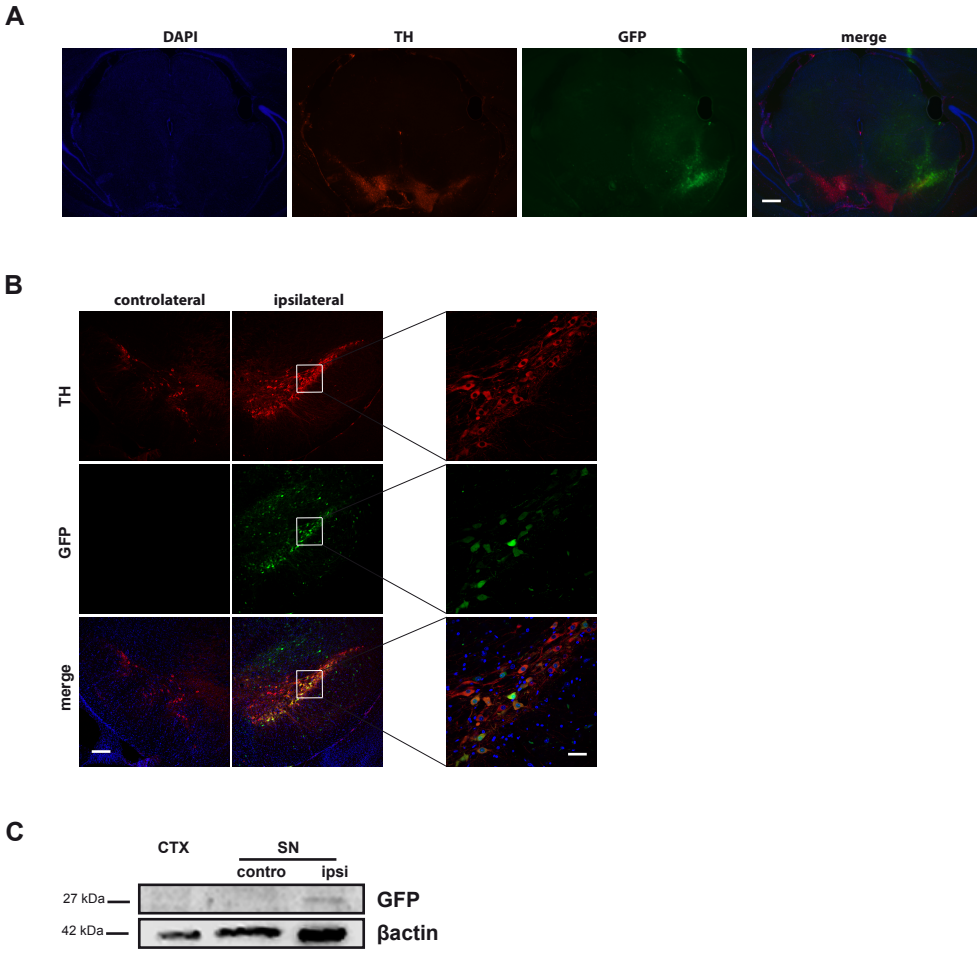

Figure 34. Infection of SNpc of mouse brain with AAV9-GFP.
A. Images of coronal sections of mouse brain. Substantia nigra was stained with anti-TH antibody (red). Infected cells were stained with anti-GFP antibody (green). Nuclei were visualized with DAPI. Scale bar 800 μm. B. Immunohistochemistry of coronal sections of mouse brain. SN was stained with anti-TH antibody (red). Infected cells were stained with anti-GFP antibody (green). Nuclei were visualized with DAPI. Scale bar 200 μm. Enlargement of ipsilateral side (scale bar 50 μm). C. Western blot analysis of dissected controlateral (contro) and ispilateral (ipsi) side of Substantia Nigra (SN) and of cortex (CTX). Immunoblot carried out with anti-GFP antibody. CTX was used as negative control. βactin was used as loading control.

We set up the stereotactic surgery using an AAV9-GFP, kindly provided by professor Mauro Giacca. Adult male C57Bl/6 mice were used for the study. Under anesthesia, the mice were injected stereotaxically with 2 µl of AAV9-GFP ($3x10^{12}$ genome viral/ml) into the right SNpc (for technical details see material and methods). Animals were sacrificed after 3 weeks following AAV9-GFP infection. Brain tissue was processed for immunohistochemistry or for protein extraction using Trizol. As shown in figure 34B, we infected DA neurons of SNpc with AAV9-GFP. In particular, in the ipsilateral side about 50% of DA neurons were GFP positive. The controlateral side didn't present any GFP positive cells. Moreover, Western blot analysis of dissected SN demonstrated the effective AAV9-GFP infection of SN ipsilateral (figure 34C).

AAV9-mediated overexpression of α and β globin in SNpc

We then tested the expression of AAV9-2xFLAG-α globin and of AAV9-β globin-MYC in the SNpc of mouse brain. In details, 1µl AAV9-2xFLAG-α globin ($2,2\times10^{13}$ viral genome particles/ml) and 1µl of AAV9-β globin-myc ($2,2\times10^{13}$ viral genome particles/ml) were injected together unilaterally into the right SNpc of C57Bl/6 mice. Three weeks after viruses injections, expression of 2xFLAG-α globin and β globin-MYC was analyzed by histochemistry, biochemical and molecular analysis. In order to perform PCR and Western blot analysis we extracted protein and RNA using TRIzol from ipsilatreal and controlateral side of SN, CPu and CTX.

First of all we studied mRNA expression of AAV9-2xFLAG-α globin and of AAV9-β globin-MYC by PCR. RNA extracted were retrotranscribed into cDNA. Oligos were specific for the coding sequence of tagged-globins. Figure 35A shows the expression of the transcripts in the ipsilateral SN. Furthermore, we noticed that SN controlateral and ipsilateral CPu express globin transcripts, while CTX did not. We hypothesized the presence of viral migration though brain neuronal connections. Furthermore, we performed PCR using oligos direct against TH transcript.

Then, we analyzed protein extracted by Western blot (figure 35B). Immunoblot was carried out using an anti-FLAG antibody that discriminates α globin, an anti-MYC antibody that recognizes β globin and an anti-Hb antibody. SN ipsilateral expressed both α and β globins. Furthermore, controlateral SN and CTX didn't express viral proteins. Moreover, Hb staining was evident in SN ipsilateral. In controlateral SN and CTX, a less intense band was also detected with anti-Hb antibody, as expected

because DA neurons and cortical astrocytes express endogenous Hb.

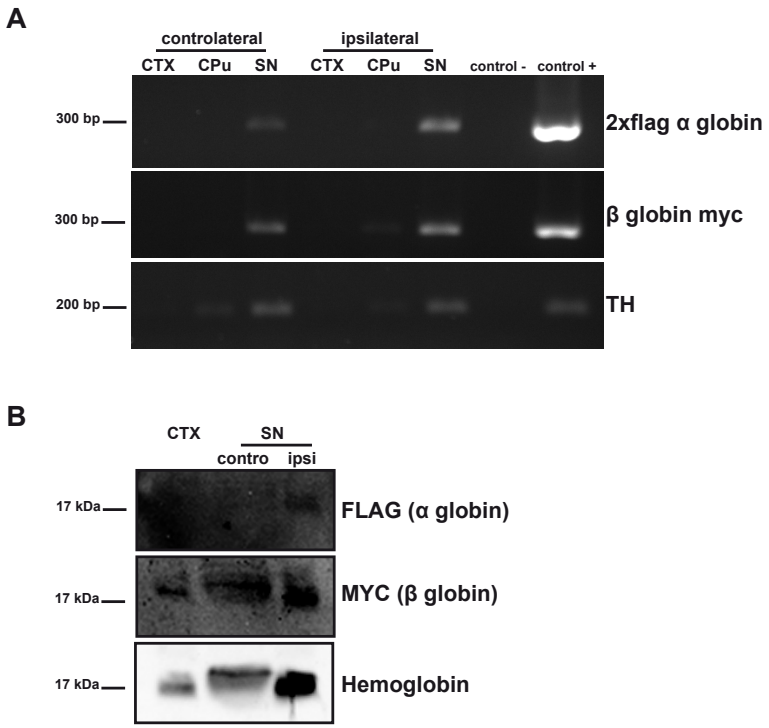

Figure 35. Infection of SNpc of mouse brain with AAV9-2xFLAG-α globin and AAV9-β globin-MYC. A. PCR analysis of dissected controlateral and ispilateral side of Substantia Nigra (SN), striatum (CPu). Cortex (CTX) was used as negative control. Additional control were used: pcDNA3-2xFLAG-α globin and pcDNA3.1$^-$-β globin-MYC (control +) were used for the efficiently of PCR amplification; negative control of retrotranscription (control -) was included. B. Western blot analysis of dissected controlateral (contro) and ispilateral (ipsi) side of SN and CTX. Immunoblot carried out with anti-FLAG, anti-MYC and anti-Hb antibodies.

Then we studied the expression of the viruses by immunohistochemistry using antibodies direct against FLAG (specific for α globin) and MYC (specific for β globin). Figure 36A,B shows representative panels, demonstrating widespread expression of the virally transferred genes 2xFLAG-α globin and β globin-MYC in DA neurons of the injected side. The ratio of infection was about 40%. We observed that globins were present both in the cytoplasm and in the nucleus of the neuronal cells, demonstrating our previous results in iMN9D cells. Moreover, α and β globins colocalized in TH$^+$ cells, proving the efficiency of coinfection (figure 36C).

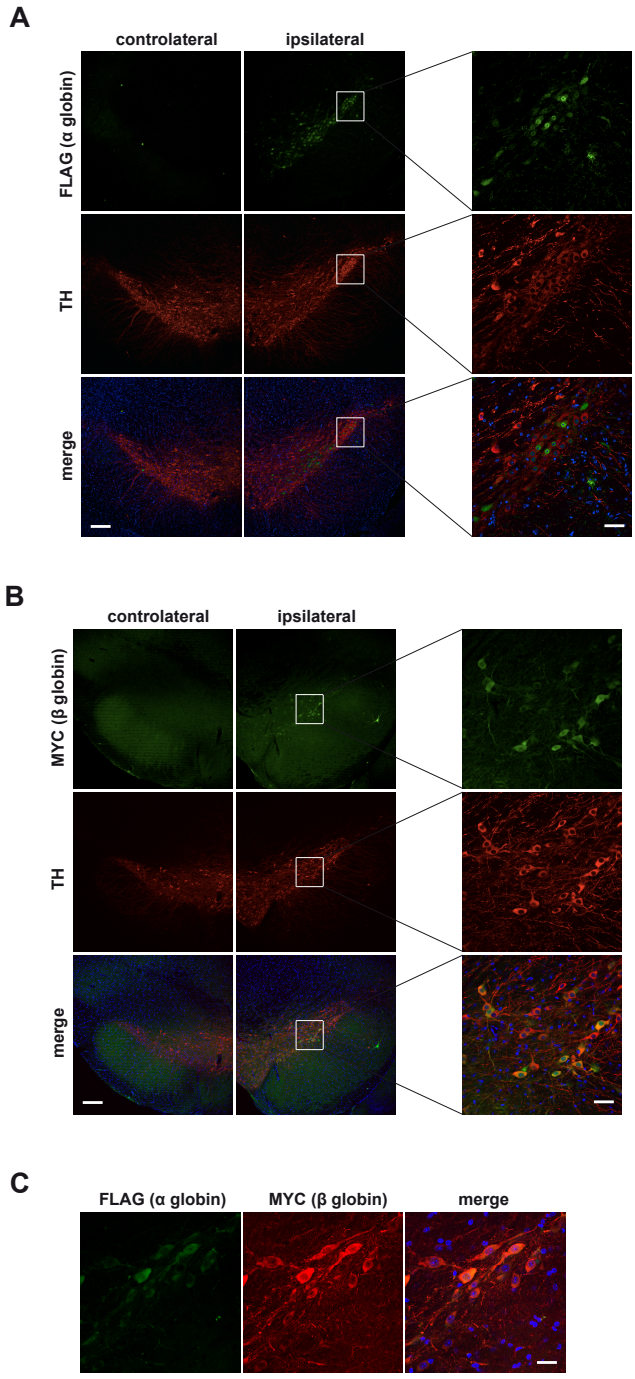

Figure 36. Infection of SNpc of mouse brain with AAV9-2xFLAG-α globin and AAV9-β globin-MYC. A. Immunohistochemistry of coronal sections of mouse brain. SN was stained with anti-TH antibody (red). Infected cells were stained with anti-FLAG antibody (green). Nuclei were visualized with DAPI. Scale bar 200 μm. Enlargement of ipsilateral side (scale bar 50 μm). B. Images of coronal sections of mouse brain. SN was stained with anti-TH antibody (red). Infected cells were stained with anti-MYC antibody (green). Nuclei were visualized with DAPI. Scale bar 200 μm. Enlargement of ipsilateral side (scale bar 50 μm). C. Double immunohistochemistry performed with anti-FLAG (green) and anti-MYC (red) antibodies. Nuclei were visualized with DAPI. Scale bar 50 μm.

Finally, we analyzed Hb staining. As shown in figure 37, in ipsilateral side the fluorescent intensity of Hb-staining in TH^+ cells was more evident in comparison to controlateral side, demonstrating that AAV9s infection took place correctly.

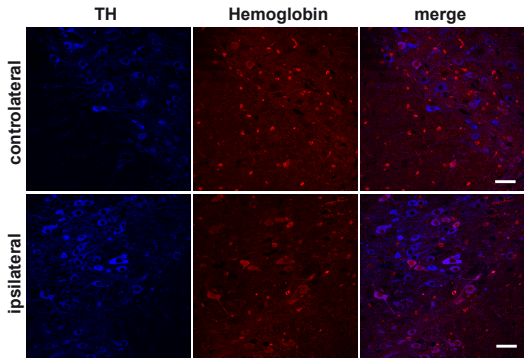

Figure 37. Infection of SNpc of mouse brain with AAV9-2xFLAG-α globin and AAV9-β globin-MYC. A. Immunohistochemistry of coronal sections of mouse brain. SN was stained with anti-TH antibody (blue) and anti-Hb (red). Scale bar 50 μm.

In conclusion, these results demonstrate that AAV9-2xFLAG-α globin and AAV9-β globin-myc are correctly expressed in DA neurons, even though the ratio of infection is about 40%. Moreover, we observe a partially migration of AAVs transcripts from ipsilateral side to controlateral side.

AAV9-mediated overexpression of α and β globin does not increase MPTP-induced DA neuron loss

We decided to investigate the influence of Hb on MPTP-induced DA neuron loss *in vivo*. In details, male C57Bl/6 mice were injected with 1 μl of AAV9-2xFLAG-α globin ($2{,}2\times10^{13}$ viral genome particles/ml) and 1μl of AAV9-β globin-myc ($2{,}2\times10^{13}$ viral genome particles/ml) together or 2 μl AAV9-control ($2{,}2\times10^{13}$ viral genome particles/ml) into SNpc of mouse brain. The contralateral SNpc remained uninjected. Three weeks after viruses injections, mice were divided into two subgroups, one treated with saline and the other with a subchronic regimen of MPTP. At 6 weeks after viruses delivery (9 days after the last MPTP injection) all mice were sacrificed. Brain tissue was processed for immunohistochemistry or for biochemical analysis. We first quantified DA neuron survival counting TH^+ cells in SNpc, since the major effect of PD-mimicking drugs (MPTP) was the degeneration of DA neurons. First of all, we observed that the injection *per se* didn't cause damage, since the number of

TH^+ cells in ipsilateral and controlateral side of control-injected mice was equal (figure 38A,B). Moreover, MPTP-treated mice showed about 50% less DA neurons in both sides when compared to saline-treated mice. Hb infected-mice did not show statistical difference in comparison to control infected-mice both in saline and MPTP regime. In addition, we didn't observe significance side effect in Hb-injected mice. However, there were more TH^+ cells in Hb-injected side in comparison to non-injected side in saline-treated mice, whereas there were less TH^+ cells in Hb-injected side in comparison to non-injected side upon MPTP treatment.

We then performed a densitometric analysis of TH^+ fibres of striatum, since the striatum receives profuse DA innervation from the SN. In the striatum, MPTP injection led to a dramatic reduction in TH immunoreactivity (figure 38C,D). This reduction was not modified by overexpression of Hb.

In conclusion, AAV9-mediated overexpression of α and β globin doesn't alter MPTP-induced DA neuron loss, even if there are some not statistical side-effects differences.

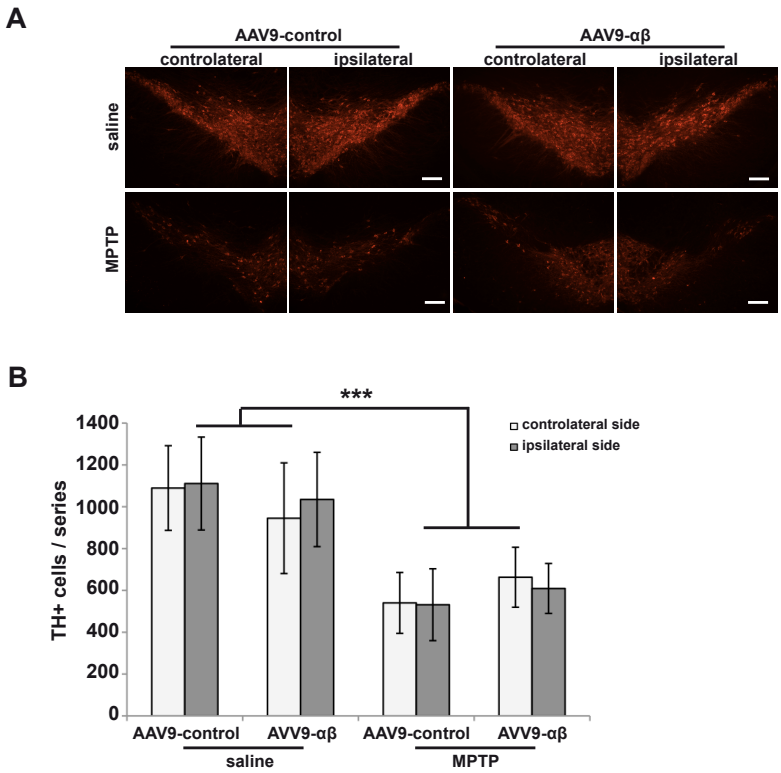

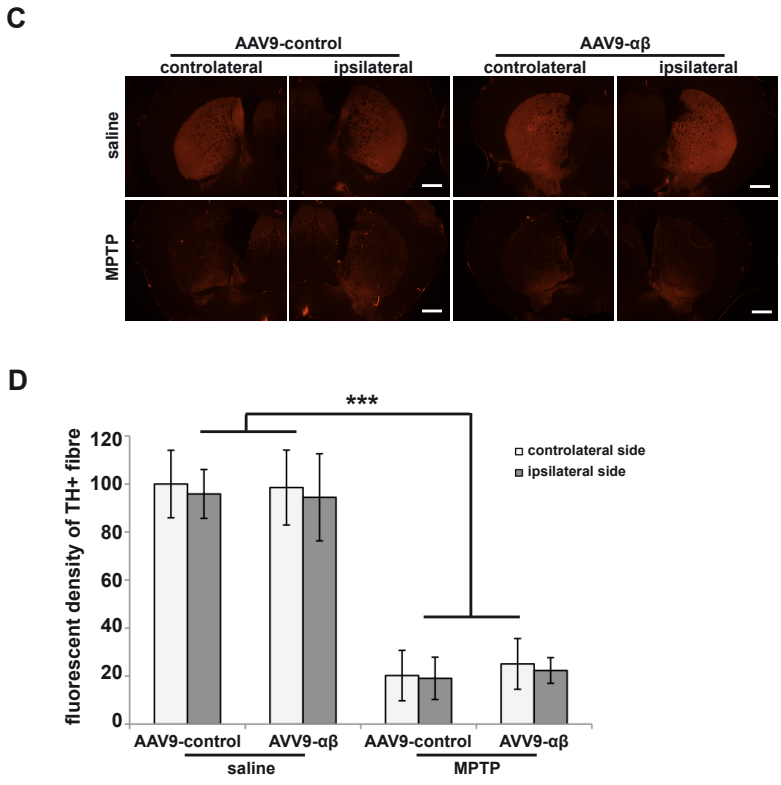

Figure 38. AAV9-mediated overexpression of α and β globin does not increase MPTP-induced DA neuron loss.
A. Immunohistochemistry of coronal sections of mouse brain. SN was stained with anti-TH antibody (red). Scale bar 200 µm. B. Quantitative analysis of TH^+ cells number. Values are expresses as number of TH^+ cells/series relative to the controlateral side of control-injected mice treated with saline. Data are represented as mean±SEM (n= 8 mice/group). C. Immunohistochemistry of coronal sections of mouse brain. TH^+ fibres in CPu were stained with anti-TH antibody (red). Scale bar 800 µm. D. Densitometric analysis of TH^+ cells. Values are expresses as a percentage relative to the controlateral side of control-injected mice treated with saline (set arbitrary at 100%). Data are represented as mean±SEM (n= 8 mice/group). Data were evaluated statistically by ANOVA. Statistical analysis is indicated as: * = p value ≤ 0.05, * *= p value ≤ 0.01, *** = p value ≤ 0.001.

In addition, we performed Western blot analysis to investigate changes in cleaved fragments of Caspase 3 in saline/MPTP-treated mice injected with AAV9-2xFLAG-α globin and AAV9-β globin-myc or AAV9-control. In saline-treated mice we didn't reveal the expression of cleaved Caspase 3, as expected (figure 39A). In MPTP-treated mice, Hb injected-mice manifest a trend, which exhibits an increase of cleaved Caspase 3 expression in comparison to control-injected mice. However no statistical difference was found (figure 39B,C).

In conclusion, the overexpression of α and β globin does not change the susceptibly to neuronal loss caused by MPTP; even if we observed a trend, looking both at the number of TH^+ cells and at the expression of cleaved Caspase 3. Further

investigations are needed to fully assess the issue.

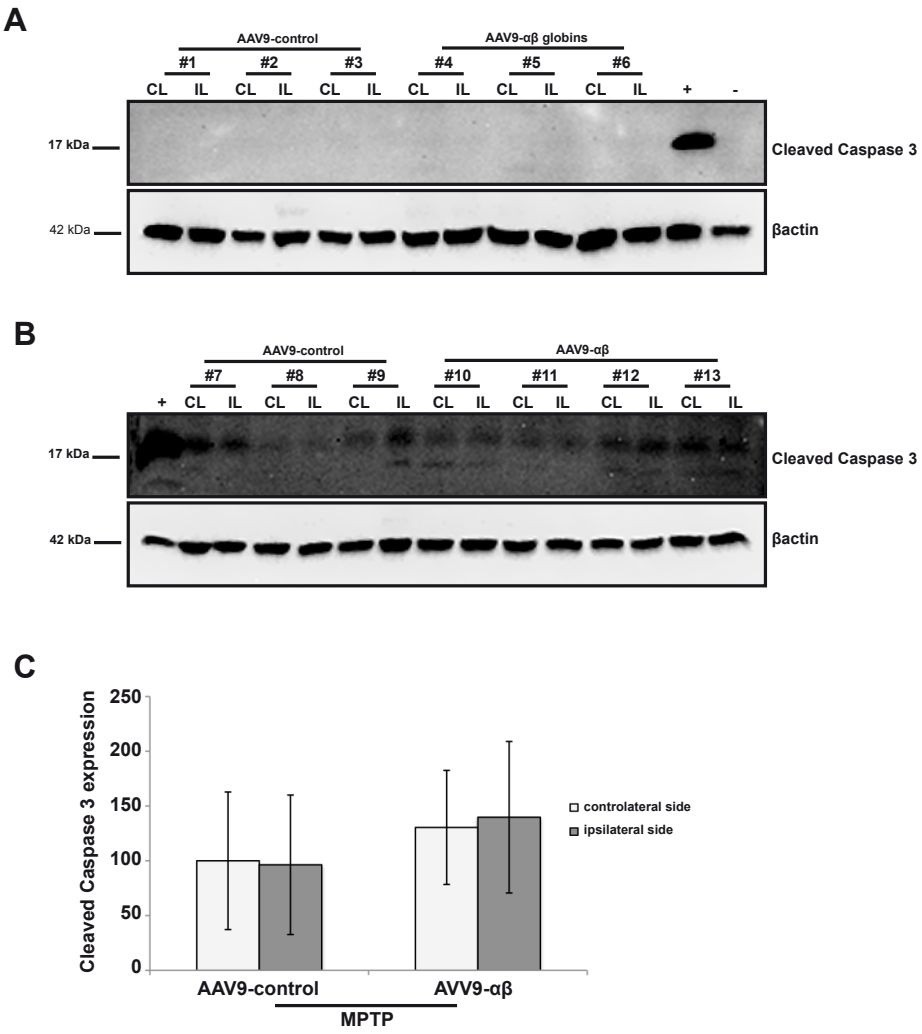

Figure 39. AAV9-mediated overexpression of α and β globin does not increase MPTP-induced cleavage of Caspase 3.
A. Western blot analysis of cleaved Caspase 3 expression in saline-treated mice. βactin was used as loading control. (n=3 mice/group) B. Western blot analysis of cleaved Caspase 3 expression in MPTP-treated mice. βactin was used as loading control. (n=3 control-injected mice and n=4 Hb-injected mice) C. Quantitative analysis of cleaved Caspase 3 expression. Values are expresses as a percentage relative to the controlateral side of control-injected mice treated with saline (set arbitrary at 100%). Data are represented as mean±SD. Data were evaluated statistically by Student's *t*-test. Statistical analysis is indicated as: * = p value ≤ 0.05, * *= p value ≤ 0.01, *** = p value ≤ 0.001.

Discussion

PD is a progressive worsening neurodegenerative disorder whose causes are still unknown. Its most evident neuropathological manifestation is the selective loss of neurons of SNpc. Despite the large amount of studies, the molecular aspects of the selective degeneration of A9 neurons in PD have not yet been elucidated.

Therefore, in order to better understand the physiology of DA cells and the molecular differences or commonalities between A9 and A10 neurons, a detailed transcriptome analysis on RNA extracted from these cells was performed in the laboratory of Prof. Gustincich. By taking advantage of gene expression analysis, it has been found that transcripts of α and β chains of Hb were expressed in mDA neurons in the mouse brain. Moreover, Hb immunoreactivity decorated the majority of A9 cells, whereas only 5% of A10 neurons are Hb positive (Biagioli et al., 2009).

Hb is a well-known blood-associated protein. The main function of Hb is the transport of oxygen throughout the body recovering the consequent carbon dioxide. The concept that globins have a functional role only as oxygen transporters was challenged in recent studies in which, in addition to blood cells, expression of Hb was observed in other districts. In particular, Hb was found in macrophages (Liu et al., 1999), lung (Newton et al., 2006), kidney (Nishi et al., 2008), liver (Liu et al., 2011b), brain (Biagioli et al., 2009; Leffers et al., 2006; Richter et al., 2009) and tumours (Onda et al., 2005; Capulli et al., 2012; Li et al., 2013). Hb function in these tissues remains to be investigated.

In this study, we have provided a model in which Hb expression may contribute to A9 specific vulnerability in PD pathogenesis. We took advantages of dopaminergic neuroblastoma cell lines stably transfected with α and β chains of hemoglobin (Biagioli et al., 2009) and their differentiated cultures to evaluate the mechanism(s) involved in PD-mimicking insults, like MPP^+ and rotenone. We used iMN9D cells because represents a well-accepted *in vitro* model to study dopaminergic cell physiology and dysfunction (Choi et al., 1991, 1999).

First, here we demonstrated that the impact of Hb overexpression depends on differentiation state of iMN9D cells upon MPP+ treatment (Langston et al., 1983). In particular, we observed that upon stimulus in undifferentiated iMN9D cells the presence of Hb is protective, whereas is toxic in differentiated cultures. Moreover, we showed that hemoglobin behaviour changes 48 hours after differentiation induction. We hypothesize that Hb overexpression influences gene expression profile conditioning the healthy state of iMN9D cells. This is extremely important because it allows us to understand what are the specific prosurvival mechanisms.

Furthermore, we analyzed the involvement of Hb in PD using another PD-mimicking drug that is rotenone. Rotenone, together with MPP^+, is one of the common drugs used to induce neuronal cell death (Panov et al., 2005; Sherer et al., 2003). In details, we observed that Hb overexpression increases susceptibility to cell death in both undifferentiated and differentiated DA cells. Together with previous data, this is strong evidence that the presence of Hb in DA cells is detrimental upon typical PD-stimuli. This may be a suggestive mechanism to explain why only A9 neurons degenerate in PD.

Furthermore, we observed a caspase3-dependent cell death in every conditions we tested (Giordano et al., 2012), suggesting a common cell death mechanism in iMN9D cells.

Moreover, in undifferentiated iMN9D cells Hb overexpression triggers diverse cell fate depending on the type of treatment. As mentioned before, Hb overexpression-induced cell death takes place only in the presence of rotenone and not of MPP^+. Both drugs are known to inhibit complex I of the mitochondrial electron transport chain concomitant with a decrease of ATP reserve (Panov et al., 2005; Choi et al., 2011). However, there are conflicting studies regarding ROS generation (Lotharius and O'Malley, 2000; Li et al., 2005). Rotenone induced significant cell death, whereas MPP^+ exhibited a different behaviour with less pronounced effects. Interestingly, it is well known that MPP^+, unlike rotenone, stimulates bioenergetics reserve capacity (Giordano et al., 2012). It remains to clarify the precise mechanism of toxicity and the main difference of action of the two drugs. Our *in vitro* model could provide a system to study differences between these PD-mimicking drugs.

The main function of hemoglobin is the transport of oxygen. We generated mutant hemoglobin that theoretically does not bind oxygen. In particular the replacement of the highly conserved proximal histidine F8 residue by a glycine should result in a low

affinity for the heme group and a loss of the allosteric properties (Barrick et al., 1997). In these conditions, we observed that Hb protection/toxicity doesn't depend on oxygen binding. In details, mutant Hb doesn't revert the characteristic phenotype of Hb, which we previously described. These results confirm the idea that Hb doesn't have a functional role exclusively as oxygen transporter or storage.

Hb acts as $\alpha_2\beta_2$ structure. Our results demonstrated that the quaternary structure of Hb is not altered upon neurotoxic stimuli. This result indicates that $\alpha_2\beta_2$ tetramer of Hb is maintained upon toxic stimuli, probably indicating that Hb-mediated protection or toxicity is managed by its structure.

The localization of a protein is an indicator of its potential function. Hb is present in cytoplasmic and nuclear compartments both *in vitro* models and *in vivo*. Furthermore, Hb-induced toxicity is concomitant with an increase in the nucleus of globin chains. The nucleus is the place where gene expression regulation takes place. In addition we observe a hypothetical post-translational modification of α globin upon stimuli. It's well known that some post-translational modifications, such as glycosylation, monoubiquitination and SUMOylation, are signal for the nuclear transport of cytosolic proteins (Guinez et al., 2005; Trotman et al., 2007; Truong et al., 2012). In literature there are a lot of examples of modifications that occurs in Hb, like glycosylation (Bunn, 1984; Woodi et al., 2009). We thus speculate that upon PD-mimicking insults Hb is modified, moves to the nucleus and there acts as transcription factor or cofactor in order to regulate gene expression positively or negatively. Further investigation must be done in order to confirm this hypothesis.

Recently, many works have come out demonstrating the relationship between PD and autophagy. In details, dysregulation of the autophagy pathway has been observed in the brains of PD patients and in animal models of PD, indicating the emerging role of autophagy in this disease (Lynch-Day et al., 2012). Indeed, autophagy is increasingly implicated in a number of pathophysiologies, including various neurodegenerative diseases such as AD, HD and ALS (Nixon, 2013). Furthermore, it has been demonstrated that rapamycin (a drug that is an autophagy enhancer) protects against cell death caused by MPTP and rotenone (Pan et al., 2009; Liu et al., 2011). In our study we show that Hb overexpression is associated with autophagy impairment upon PD-like stimuli. For the time being we couldn't assess if autophagy impairment is linked to Hb-mediated toxicity. However we analyzed potential interactors of Hb by Ingenuity Systems, which is a software that analyze complex biological systems. One

of these interactors may be GATE-16. GATE-16 together with LC3 and GABARAP belong to mammalian Atg8-related proteins. The role of this family remains to be fully elucidated. However LC3, GABARAP and GATE-16 are indispensable for the autophagic process. Briefly, LC3 is involved in elongation of the autophagic membrane whereas GABARAP/GATE-16 are essential for a later stage in autophagosome maturation (Weidberg et al., 2010). Therefore we can hypothesis that Hb sequesters GATE-16, through binding, causing an alter autophagosome biogenis.

Finally, we studied the overexpression of Hb in an *in vivo* mouse model of PD. Preliminary data demonstrated that upon stimulus Hb overexpression doesn't influence significantly DA cell death, even if there is a trend. This phenotype could be due to a low expression of AAV9-overexpressing Hb in A9 cells. Moreover, AAV9-overexpressing Hb infects A9 neurons and, to a less extent, closer cells, such as astrocytes and oligodentrocytes. Indeed these type of cells present endogenues Hb (Biagioli et al., 2009) and the presence of exogenous Hb may interfere with the surrounding environment influencing the survival of DA neurons. Further investigations must be done.

Our findings support a model in which Hb expression may contribute to A9 specific vulnerability in PD pathogenesis. It will thus be extremely interesting to asses the relationship between Hb levels *in vivo* and PD susceptibility in positioning Hb as an unexpected new therapeutic target.

Bibliography

Abbott, R.D., Ross, G.W., Tanner, C.M., Andersen, J.K., Masaki, K.H., Rodriguez, B.L., White, L.R., and Petrovitch, H. (2012). Late-life hemoglobin and the incidence of Parkinson's disease. Neurobiol. Aging *33*, 914–920.

Abeliovich, A., Schmitz, Y., Fariñas, I., Choi-Lundberg, D., Ho, W.H., Castillo, P.E., Shinsky, N., Verdugo, J.M., Armanini, M., Ryan, A., et al. (2000). Mice lacking alpha-synuclein display functional deficits in the nigrostriatal dopamine system. Neuron *25*, 239–252.

Alam, M., Mayerhofer, A., and Schmidt, W.J. (2004). The neurobehavioral changes induced by bilateral rotenone lesion in medial forebrain bundle of rats are reversed by L-DOPA. Behav. Brain Res. *151*, 117–124.

Alavian, K.N., Scholz, C., and Simon, H.H. (2008). Transcriptional regulation of mesencephalic dopaminergic neurons: the full circle of life and death. Mov. Disord. Off. J. Mov. Disord. Soc. *23*, 319–328.

Auluck, P.K., Chan, H.Y.E., Trojanowski, J.Q., Lee, V.M.Y., and Bonini, N.M. (2002). Chaperone suppression of alpha-synuclein toxicity in a Drosophila model for Parkinson's disease. Science *295*, 865–868.

Bandyopadhyay, U., Bandhyopadhyay, U., and Cuervo, A.M. (2007). Chaperone-mediated autophagy in aging and neurodegeneration: lessons from alpha-synuclein. Exp. Gerontol. *42*, 120–128.

Barbour, R., Kling, K., Anderson, J.P., Banducci, K., Cole, T., Diep, L., Fox, M., Goldstein, J.M., Soriano, F., Seubert, P., et al. (2008). Red blood cells are the major source of alpha-synuclein in blood. Neurodegener. Dis. *5*, 55–59.

Barrick, D., Ho, N.T., Simplaceanu, V., Dahlquist, F.W., and Ho, C. (1997). A test of the role of the proximal histidines in the Perutz model for cooperativity in haemoglobin. Nat. Struct. Mol. Biol. *4*, 78–83.

Bartzokis, G., Tishler, T.A., Lu, P.H., Villablanca, P., Altshuler, L.L., Carter, M., Huang, D., Edwards, N., and Mintz, J. (2007). Brain ferritin iron may influence age- and gender-related risks of neurodegeneration. Neurobiol. Aging *28*, 414–423.

Beal, M.F., Ferrante, R.J., Browne, S.E., Matthews, R.T., Kowall, N.W., and Brown, R.H., Jr (1997). Increased 3-nitrotyrosine in both sporadic and familial amyotrophic lateral sclerosis. Ann. Neurol. *42*, 644–654.

Bernheimer, H., Birkmayer, W., Hornykiewicz, O., Jellinger, K., and Seitelberger, F. (1973). Brain dopamine and the syndromes of Parkinson and Huntington. Clinical, morphological and neurochemical correlations. J. Neurol. Sci. *20*, 415–455.

Betarbet, R., Sherer, T.B., MacKenzie, G., Garcia-Osuna, M., Panov, A.V., and Greenamyre, J.T. (2000). Chronic systemic pesticide exposure reproduces features of Parkinson's disease. Nat. Neurosci. *3*, 1301–1306.

Betarbet, R., Sherer, T.B., and Greenamyre, J.T. (2002). Animal models of Parkinson's disease. BioEssays News Rev. Mol. Cell. Dev. Biol. *24*, 308–318.

Biagioli, M., Pinto, M., Cesselli, D., Zaninello, M., Lazarevic, D., Roncaglia, P., Simone, R., Vlachouli, C., Plessy, C., Bertin, N., et al. (2009). Unexpected expression of alpha- and beta-globin in mesencephalic dopaminergic neurons and glial cells. Proc. Natl. Acad. Sci. U. S. A. *106*, 15454–15459.

Blalock, E.M., Chen, K.-C., Sharrow, K., Herman, J.P., Porter, N.M., Foster, T.C., and Landfield, P.W. (2003). Gene microarrays in hippocampal aging: statistical profiling identifies novel processes correlated with cognitive impairment. J. Neurosci. Off. J. Soc. Neurosci. *23*, 3807–3819.

Blandini, F., Armentero, M.-T., and Martignoni, E. (2008). The 6-hydroxydopamine model: news from the past. Parkinsonism Relat. Disord. *14 Suppl 2*, S124–129.

Blesa, J., Phani, S., Jackson-Lewis, V., and Przedborski, S. (2012). Classic and new animal models of Parkinson's disease. J. Biomed. Biotechnol. *2012*, 845618.

Bonifati, V., Rizzu, P., van Baren, M.J., Schaap, O., Breedveld, G.J., Krieger, E., Dekker, M.C.J., Squitieri, F., Ibanez, P., Joosse, M., et al. (2003). Mutations in the DJ-1 gene associated with autosomal recessive early-onset parkinsonism. Science *299*, 256–259.

Braak, H., Ghebremedhin, E., Rüb, U., Bratzke, H., and Del Tredici, K. (2004). Stages in the development of Parkinson's disease-related pathology. Cell Tissue Res. *318*, 121–134.

Brunori, M., and Vallone, B. (2006). A globin for the brain. FASEB J. Off. Publ. Fed. Am. Soc. Exp. Biol. *20*, 2192–2197.

Bunn, H.F. (1984). Post-translational modifications of hemoglobin. Haematologia (Budap.) *17*, 179–186.

Burke, W.J., Kumar, V.B., Pandey, N., Panneton, W.M., Gan, Q., Franko, M.W., O'Dell, M., Li, S.W., Pan, Y., Chung, H.D., et al. (2008). Aggregation of alpha-synuclein by DOPAL, the monoamine oxidase metabolite of dopamine. Acta Neuropathol. (Berl.) *115*, 193–203.

Burmester, T., and Hankeln, T. (2004). Neuroglobin: a respiratory protein of the nervous system. News Physiol. Sci. Int. J. Physiol. Prod. Jointly Int. Union Physiol. Sci. Am. Physiol. Soc. *19*, 110–113.

Burmester, T., Ebner, B., Weich, B., and Hankeln, T. (2002). Cytoglobin: a novel globin type ubiquitously expressed in vertebrate tissues. Mol. Biol. Evol. *19*, 416–421.

Butler, D., Nixon, R.A., and Bahr, B.A. (2006). Potential compensatory responses through autophagic/lysosomal pathways in neurodegenerative diseases. Autophagy *2*, 234–237.

Cammack, R., Shergill, J.K., Ananda Inalsingh, V., and Hughes, M.N. (1998). Applications of electron paramagnetic resonance spectroscopy to study interactions of iron proteins in cells with nitric oxide. Spectrochim. Acta. A. Mol. Biomol. Spectrosc. *54A*, 2393–2402.

Cannon, J.R., Tapias, V., Na, H.M., Honick, A.S., Drolet, R.E., and Greenamyre, J.T. (2009). A highly reproducible rotenone model of Parkinson's disease. Neurobiol. Dis. *34*, 279–290.

Cao, S., Theodore, S., and Standaert, D.G. (2010). Fcγ receptors are required for NF-κB signaling, microglial activation and dopaminergic neurodegeneration in an AAV-synuclein mouse model of Parkinson's disease. Mol. Neurodegener. *5*, 42.

Capulli, M., Angelucci, A., Driouch, K., Garcia, T., Clement-Lacroix, P., Martella, F., Ventura, L., Bologna, M., Flamini, S., Moreschini, O., et al. (2012). Increased expression of a set of genes enriched in oxygen binding function discloses a predisposition of breast cancer bone metastases to generate metastasis spread in multiple organs. J. Bone Miner. Res. Off. J. Am. Soc. Bone Miner. Res. *27*, 2387–2398.

Carmine Belin, A., Westerlund, M., Bergman, O., Nissbrandt, H., Lind, C., Sydow, O., and Galter, D. (2007). S18Y in ubiquitin carboxy-terminal hydrolase L1 (UCH-L1) associated with decreased risk of Parkinson's disease in Sweden. Parkinsonism Relat. Disord. *13*, 295–298.

Cetin, A., Komai, S., Eliava, M., Seeburg, P.H., and Osten, P. (2006). Stereotaxic gene delivery in the rodent brain. Nat. Protoc. *1*, 3166–3173.

Chee, J.L.Y., Guan, X.L., Lee, J.Y., Dong, B., Leong, S.M., Ong, E.H., Liou, A.K.F., and Lim, T.M. (2005). Compensatory caspase activation in MPP+-induced cell death in dopaminergic neurons. Cell. Mol. Life Sci. CMLS *62*, 227–238.

Chen, F., Sugiura, Y., Myers, K.G., Liu, Y., and Lin, W. (2010). Ubiquitin carboxyl-terminal hydrolase L1 is required for maintaining the structure and function of the neuromuscular junction. Proc. Natl. Acad. Sci. U. S. A. *107*, 1636–1641.

Chinta, S.J., Kumar, M.J., Hsu, M., Rajagopalan, S., Kaur, D., Rane, A., Nicholls, D.G., Choi, J., and Andersen, J.K. (2007). Inducible alterations of glutathione levels in adult dopaminergic midbrain neurons result in nigrostriatal degeneration. J. Neurosci. Off. J. Soc. Neurosci. *27*, 13997–14006.

Choi, H.K., Won, L.A., Kontur, P.J., Hammond, D.N., Fox, A.P., Wainer, B.H., Hoffmann, P.C., and Heller, A. (1991). Immortalization of embryonic mesencephalic dopaminergic neurons by somatic cell fusion. Brain Res. *552*, 67–76.

Choi, W.-S., Palmiter, R.D., and Xia, Z. (2011). Loss of mitochondrial complex I activity potentiates dopamine neuron death induced by microtubule dysfunction in a Parkinson's disease model. J. Cell Biol. *192*, 873–882.

Choi, W.S., Yoon, S.Y., Oh, T.H., Choi, E.J., O'Malley, K.L., and Oh, Y.J. (1999). Two distinct mechanisms are involved in 6-hydroxydopamine- and MPP+-induced dopaminergic neuronal cell death: role of caspases, ROS, and JNK. J. Neurosci. Res. *57*, 86–94.

Chuang, J.-Y., Lee, C.-W., Shih, Y.-H., Yang, T., Yu, L., and Kuo, Y.-M. (2012). Interactions between amyloid-β and hemoglobin: implications for amyloid plaque formation in Alzheimer's disease. PloS One *7*, e33120.

Chung, C.Y., Seo, H., Sonntag, K.C., Brooks, A., Lin, L., and Isacson, O. (2005). Cell type-specific gene expression of midbrain dopaminergic neurons reveals molecules involved in their vulnerability and protection. Hum. Mol. Genet. *14*, 1709–1725.

Cohen, G. (1984). Oxy-radical toxicity in catecholamine neurons. Neurotoxicology *5*, 77–82.

Cohen, G. (2000). Oxidative stress, mitochondrial respiration, and Parkinson's disease. Ann. N. Y. Acad. Sci. *899*, 112–120.

Collins, F.S., and Weissman, S.M. (1984). The molecular genetics of human hemoglobin. Prog. Nucleic Acid Res. Mol. Biol. *31*, 315–462.

Cui, M., Aras, R., Christian, W.V., Rappold, P.M., Hatwar, M., Panza, J., Jackson-Lewis, V., Javitch, J.A., Ballatori, N., Przedborski, S., et al. (2009). The organic cation transporter-3 is a pivotal modulator of neurodegeneration in the nigrostriatal dopaminergic pathway. Proc. Natl. Acad. Sci. U. S. A. *106*, 8043–8048.

Cummings, C.J., Reinstein, E., Sun, Y., Antalffy, B., Jiang, Y., Ciechanover, A., Orr, H.T., Beaudet, A.L., and Zoghbi, H.Y. (1999). Mutation of the E6-AP ubiquitin ligase reduces nuclear inclusion frequency while accelerating polyglutamine-induced pathology in SCA1 mice. Neuron *24*, 879–892.

Cummings, C.J., Sun, Y., Opal, P., Antalffy, B., Mestril, R., Orr, H.T., Dillmann, W.H., and Zoghbi, H.Y. (2001). Over-expression of inducible HSP70 chaperone suppresses neuropathology and improves motor function in SCA1 mice. Hum. Mol. Genet. *10*, 1511–1518.

Das, C., Hoang, Q.Q., Kreinbring, C.A., Luchansky, S.J., Meray, R.K., Ray, S.S., Lansbury, P.T., Ringe, D., and Petsko, G.A. (2006). Structural basis for conformational plasticity of the Parkinson's disease-associated ubiquitin hydrolase UCH-L1. Proc. Natl. Acad. Sci. U. S. A. *103*, 4675–4680.

Dauer, W., and Przedborski, S. (2003). Parkinson's disease: mechanisms and models. Neuron *39*, 889–909.

Dawson, T.M. (2006). Parkin and defective ubiquitination in Parkinson's disease. J. Neural Transm. Suppl. 209–213.

Dawson, T.M., and Dawson, V.L. (2002). Neuroprotective and neurorestorative strategies for Parkinson's disease. Nat. Neurosci. *5 Suppl*, 1058–1061.

Dejam, A., Hunter, C.J., Schechter, A.N., and Gladwin, M.T. (2004). Emerging role of nitrite in human biology. Blood Cells. Mol. Dis. *32*, 423–429.

DellaValle, B., Hempel, C., Kurtzhals, J.A.L., and Penkowa, M. (2010). In vivo expression of neuroglobin in reactive astrocytes during neuropathology in murine models of traumatic brain injury, cerebral malaria, and autoimmune encephalitis. Glia *58*, 1220–1227.

Diaz-Ruiz, O., Zapata, A., Shan, L., Zhang, Y., Tomac, A.C., Malik, N., de la Cruz, F., and Bäckman, C.M. (2009). Selective Deletion of PTEN in Dopamine Neurons Leads to Trophic Effects and Adaptation of Striatal Medium Spiny Projecting Neurons. PLoS ONE *4*, e7027.

Emara, M., Turner, A.R., and Allalunis-Turner, J. (2010). Hypoxic regulation of cytoglobin and neuroglobin expression in human normal and tumor tissues. Cancer Cell Int. *10*, 33.

Esteves, A.R., Arduíno, D.M., Swerdlow, R.H., Oliveira, C.R., and Cardoso, S.M. (2010). Dysfunctional mitochondria uphold calpain activation: contribution to Parkinson's disease pathology. Neurobiol. Dis. *37*, 723–730.

Eulalio, A., Mano, M., Ferro, M.D., Zentilin, L., Sinagra, G., Zacchigna, S., and Giacca, M. (2012). Functional screening identifies miRNAs inducing cardiac regeneration. Nature *492*, 376–381.

Farrer, M.J. (2006). Genetics of Parkinson disease: paradigm shifts and future prospects. Nat. Rev. Genet. *7*, 306–318.

Fitzgerald, J.C., and Plun-Favreau, H. (2008). Emerging pathways in genetic Parkinson's disease: autosomal-recessive genes in Parkinson's disease--a common pathway? FEBS J. *275*, 5758–5766.

Di Fonzo, A., Chien, H.F., Socal, M., Giraudo, S., Tassorelli, C., Iliceto, G., Fabbrini, G., Marconi, R., Fincati, E., Abbruzzese, G., et al. (2007). ATP13A2 missense mutations in juvenile parkinsonism and young onset Parkinson disease. Neurology *68*, 1557–1562.

Forno, L.S., DeLanney, L.E., Irwin, I., and Langston, J.W. (1993). Similarities and differences between MPTP-induced parkinsonsim and Parkinson's disease. Neuropathologic considerations. Adv. Neurol. *60*, 600–608.

Garry, D.J., Kanatous, S.B., and Mammen, P.P.A. (2003). Emerging roles for myoglobin in the heart. Trends Cardiovasc. Med. *13*, 111–116.

Giasson, B.I., Duda, J.E., Quinn, S.M., Zhang, B., Trojanowski, J.Q., and Lee, V.M.-Y. (2002). Neuronal alpha-synucleinopathy with severe movement disorder in mice expressing A53T human alpha-synuclein. Neuron *34*, 521–533.

Gill, S.S., Patel, N.K., Hotton, G.R., O'Sullivan, K., McCarter, R., Bunnage, M., Brooks, D.J., Svendsen, C.N., and Heywood, P. (2003). Direct brain infusion of glial cell line-derived neurotrophic factor in Parkinson disease. Nat. Med. *9*, 589–595.

Giordano, S., Lee, J., Darley-Usmar, V.M., and Zhang, J. (2012). Distinct effects of rotenone, 1-methyl-4-phenylpyridinium and 6-hydroxydopamine on cellular bioenergetics and cell death. PloS One *7*, e44610.

Gödecke, A., Flögel, U., Zanger, K., Ding, Z., Hirchenhain, J., Decking, U.K., and Schrader, J. (1999). Disruption of myoglobin in mice induces multiple compensatory mechanisms. Proc. Natl. Acad. Sci. U. S. A. *96*, 10495–10500.

Good, P.F., Werner, P., Hsu, A., Olanow, C.W., and Perl, D.P. (1996). Evidence of neuronal oxidative damage in Alzheimer's disease. Am. J. Pathol. *149*, 21–28.

Graham, D.G. (1978). Oxidative pathways for catecholamines in the genesis of neuromelanin and cytotoxic quinones. Mol. Pharmacol. *14*, 633–643.

Greenamyre, J.T., Sherer, T.B., Betarbet, R., and Panov, A.V. (2001). Complex I and Parkinson's disease. IUBMB Life *52*, 135–141.

Greene, J.G., Dingledine, R., and Greenamyre, J.T. (2005). Gene expression profiling of rat midbrain dopamine neurons: implications for selective vulnerability in parkinsonism. Neurobiol. Dis. *18*, 19–31.

Guinez, C., Morelle, W., Michalski, J.-C., and Lefebvre, T. (2005). O-GlcNAc glycosylation: a signal for the nuclear transport of cytosolic proteins? Int. J. Biochem. Cell Biol. *37*, 765–774.

Halliday, G., Herrero, M.T., Murphy, K., McCann, H., Ros-Bernal, F., Barcia, C., Mori, H., Blesa, F.J., and Obeso, J.A. (2009). No Lewy pathology in monkeys with over 10 years of severe MPTP Parkinsonism. Mov. Disord. Off. J. Mov. Disord. Soc. *24*, 1519–1523.

Halligan, K.E., Jourd'heuil, F.L., and Jourd'heuil, D. (2009). Cytoglobin is expressed in the vasculature and regulates cell respiration and proliferation via nitric oxide dioxygenation. J. Biol. Chem. *284*, 8539–8547.

Hankeln, T., Ebner, B., Fuchs, C., Gerlach, F., Haberkamp, M., Laufs, T.L., Roesner, A., Schmidt, M., Weich, B., Wystub, S., et al. (2005). Neuroglobin and cytoglobin in search of their role in the vertebrate globin family. J. Inorg. Biochem. *99*, 110–119.

Hardison, R. (1998). Hemoglobins from bacteria to man: evolution of different patterns of gene expression. J. Exp. Biol. *201*, 1099–1117.

Healy, D.G., Falchi, M., O'Sullivan, S.S., Bonifati, V., Durr, A., Bressman, S., Brice, A., Aasly, J., Zabetian, C.P., Goldwurm, S., et al. (2008). Phenotype, genotype, and worldwide genetic penetrance of LRRK2-associated Parkinson's disease: a case-control study. Lancet Neurol. *7*, 583–590.

Hermanson, E., Joseph, B., Castro, D., Lindqvist, E., Aarnisalo, P., Wallén, A., Benoit, G., Hengerer, B., Olson, L., and Perlmann, T. (2003). Nurr1 regulates

dopamine synthesis and storage in MN9D dopamine cells. Exp. Cell Res. *288*, 324–334.

Hisata, J.S., Wildlife, W. (State) D. of F. and, and Division, F.P. (Wash) F.M. (2001). Lake and Stream Rehabilitation: Rotenone Use and Health Risks : Final Supplemental Environmental Impact Statement (Washington Department of Fish and Wildlife).

Hod, Y., Pentyala, S.N., Whyard, T.C., and El-Maghrabi, M.R. (1999). Identification and characterization of a novel protein that regulates RNA-protein interaction. J. Cell. Biochem. *72*, 435–444.

Höglinger, G.U., Féger, J., Prigent, A., Michel, P.P., Parain, K., Champy, P., Ruberg, M., Oertel, W.H., and Hirsch, E.C. (2003). Chronic systemic complex I inhibition induces a hypokinetic multisystem degeneration in rats. J. Neurochem. *84*, 491–502.

Inden, M., Kitamura, Y., Abe, M., Tamaki, A., Takata, K., and Taniguchi, T. (2011). Parkinsonian rotenone mouse model: reevaluation of long-term administration of rotenone in C57BL/6 mice. Biol. Pharm. Bull. *34*, 92–96.

Jackson-Lewis, V., and Przedborski, S. (2007). Protocol for the MPTP mouse model of Parkinson's disease. Nat. Protoc. *2*, 141–151.

Javitch, J.A., D'Amato, R.J., Strittmatter, S.M., and Snyder, S.H. (1985). Parkinsonism-inducing neurotoxin, N-methyl-4-phenyl-1,2,3,6 -tetrahydropyridine: uptake of the metabolite N-methyl-4-phenylpyridine by dopamine neurons explains selective toxicity. Proc. Natl. Acad. Sci. U. S. A. *82*, 2173–2177.

Jellen, L.C., Lu, L., Wang, X., Unger, E.L., Earley, C.J., Allen, R.P., Williams, R.W., and Jones, B.C. (2013). Iron deficiency alters expression of dopamine-related genes in the ventral midbrain in mice. Neuroscience *252C*, 13–23.

Kaur, D., and Andersen, J. (2004). Does cellular iron dysregulation play a causative role in Parkinson's disease? Ageing Res. Rev. *3*, 327–343.

Komatsu, M., Waguri, S., Ueno, T., Iwata, J., Murata, S., Tanida, I., Ezaki, J., Mizushima, N., Ohsumi, Y., Uchiyama, Y., et al. (2005). Impairment of starvation-induced and constitutive autophagy in Atg7-deficient mice. J. Cell Biol. *169*, 425–434.

Komatsu, M., Kominami, E., and Tanaka, K. (2006). Autophagy and neurodegeneration. Autophagy *2*, 315–317.

Kopito, R.R. (2000). Aggresomes, inclusion bodies and protein aggregation. Trends Cell Biol. *10*, 524–530.

Krüger, R., Kuhn, W., Müller, T., Woitalla, D., Graeber, M., Kösel, S., Przuntek, H., Epplen, J.T., Schöls, L., and Riess, O. (1998). Ala30Pro mutation in the gene encoding alpha-synuclein in Parkinson's disease. Nat. Genet. *18*, 106–108.

Laguna Goya, R., Tyers, P., and Barker, R.A. (2008). The search for a curative cell therapy in Parkinson's disease. J. Neurol. Sci. *265*, 32–42.

Lang, A.E., Gill, S., Patel, N.K., Lozano, A., Nutt, J.G., Penn, R., Brooks, D.J., Hotton, G., Moro, E., Heywood, P., et al. (2006). Randomized controlled trial of intraputamenal glial cell line-derived neurotrophic factor infusion in Parkinson disease. Ann. Neurol. *59*, 459–466.

Langston, J.W., and Ballard, P.A., Jr (1983). Parkinson's disease in a chemist working with 1-methyl-4-phenyl-1,2,5,6-tetrahydropyridine. N. Engl. J. Med. *309*, 310.

Langston, J.W., Ballard, P., Tetrud, J.W., and Irwin, I. (1983). Chronic Parkinsonism in humans due to a product of meperidine-analog synthesis. Science *219*, 979–980.

De Lau, L.M.L., and Breteler, M.M.B. (2006). Epidemiology of Parkinson's disease. Lancet Neurol. *5*, 525–535.

Lee, H.-J., Shin, S.Y., Choi, C., Lee, Y.H., and Lee, S.-J. (2002). Formation and removal of alpha-synuclein aggregates in cells exposed to mitochondrial inhibitors. J. Biol. Chem. *277*, 5411–5417.

Lees, A.J., Hardy, J., and Revesz, T. (2009). Parkinson's disease. Lancet *373*, 2055–2066.

Leffers, H., Navarro, V.M., Nielsen, J.E., Mayen, A., Pinilla, L., Dalgaard, M., Malagon, M.M., Castaño, J.P., Skakkebaek, N.E., Aguilar, E., et al. (2006). Increased expression of alpha- and beta-globin mRNAs at the pituitary following exposure to estrogen during the critical period of neonatal sex differentiation in the rat. J. Steroid Biochem. Mol. Biol. *99*, 33–43.

Li, J., Spletter, M.L., Johnson, D.A., Wright, L.S., Svendsen, C.N., and Johnson, J.A. (2005). Rotenone-induced caspase 9/3-independent and -dependent cell death in undifferentiated and differentiated human neural stem cells. J. Neurochem. *92*, 462–476.

Li, X., Wu, Z., Wang, Y., Mei, Q., Fu, X., and Han, W. (2013). Characterization of adult α- and β-globin elevated by hydrogen peroxide in cervical cancer cells that play a cytoprotective role against oxidative insults. PloS One *8*, e54342.

Li, Y., Liu, W., Oo, T.F., Wang, L., Tang, Y., Jackson-Lewis, V., Zhou, C., Geghman, K., Bogdanov, M., Przedborski, S., et al. (2009). Mutant LRRK2(R1441G) BAC transgenic mice recapitulate cardinal features of Parkinson's disease. Nat. Neurosci. *12*, 826–828.

Liang, C.-L., Wang, T.T., Luby-Phelps, K., and German, D.C. (2007). Mitochondria mass is low in mouse substantia nigra dopamine neurons: implications for Parkinson's disease. Exp. Neurol. *203*, 370–380.

Little, R.R., and Roberts, W.L. (2009). A review of variant hemoglobins interfering with hemoglobin A1c measurement. J. Diabetes Sci. Technol. *3*, 446–451.

Liu, J., Yu, Z., Guo, S., Lee, S.-R., Xing, C., Zhang, C., Gao, Y., Nicholls, D.G., Lo, E.H., and Wang, X. (2009). Effects of neuroglobin overexpression on mitochondrial

function and oxidative stress following hypoxia/reoxygenation in cultured neurons. J. Neurosci. Res. *87*, 164–170.

Liu, K., Liu, C., Shen, L., Shi, J., Zhang, T., Zhou, Y., Zhou, L., and Sun, X. (2011a). WITHDRAWN: Therapeutic effects of rapamycin on MPTP-induced Parkinsonism in mice. Neurochem. Int.

Liu, L., Zeng, M., and Stamler, J.S. (1999). Hemoglobin induction in mouse macrophages. Proc. Natl. Acad. Sci. U. S. A. *96*, 6643–6647.

Liu, W., Baker, S.S., Baker, R.D., Nowak, N.J., and Zhu, L. (2011b). Upregulation of hemoglobin expression by oxidative stress in hepatocytes and its implication in nonalcoholic steatohepatitis. PloS One *6*, e24363.

Lotharius, J., and O'Malley, K.L. (2000). The parkinsonism-inducing drug 1-methyl-4-phenylpyridinium triggers intracellular dopamine oxidation. A novel mechanism of toxicity. J. Biol. Chem. *275*, 38581–38588.

Lunardi, A., Di Minin, G., Provero, P., Dal Ferro, M., Carotti, M., Del Sal, G., and Collavin, L. (2010). A genome-scale protein interaction profile of Drosophila p53 uncovers additional nodes of the human p53 network. Proc. Natl. Acad. Sci. U. S. A. *107*, 6322–6327.

Lutz, A.K., Exner, N., Fett, M.E., Schlehe, J.S., Kloos, K., Lämmermann, K., Brunner, B., Kurz-Drexler, A., Vogel, F., Reichert, A.S., et al. (2009). Loss of parkin or PINK1 function increases Drp1-dependent mitochondrial fragmentation. J. Biol. Chem. *284*, 22938–22951.

Lynch-Day, M.A., Mao, K., Wang, K., Zhao, M., and Klionsky, D.J. (2012). The role of autophagy in Parkinson's disease. Cold Spring Harb. Perspect. Med. *2*, a009357.

Mahajan, M.C., Karmakar, S., and Weissman, S.M. (2007). Control of beta globin genes. J. Cell. Biochem. *102*, 801–810.

Manning-Bog, A.B., McCormack, A.L., Li, J., Uversky, V.N., Fink, A.L., and Di Monte, D.A. (2002). The herbicide paraquat causes up-regulation and aggregation of alpha-synuclein in mice: paraquat and alpha-synuclein. J. Biol. Chem. *277*, 1641–1644.

De Marinis, E., Ascenzi, P., Pellegrini, M., Galluzzo, P., Bulzomi, P., Arevalo, M.A., Garcia-Segura, L.M., and Marino, M. (2010). 17β-estradiol--a new modulator of neuroglobin levels in neurons: role in neuroprotection against H_2O_2-induced toxicity. Neurosignals *18*, 223–235.

Marsden, C.D. (1983). Neuromelanin and Parkinson's disease. J. Neural Transm. Suppl. *19*, 121–141.

Masliah, E., Rockenstein, E., Veinbergs, I., Mallory, M., Hashimoto, M., Takeda, A., Sagara, Y., Sisk, A., and Mucke, L. (2000). Dopaminergic loss and inclusion body formation in alpha-synuclein mice: implications for neurodegenerative disorders. Science *287*, 1265–1269.

Massey, A., Kiffin, R., and Cuervo, A.M. (2004). Pathophysiology of chaperone-mediated autophagy. Int. J. Biochem. Cell Biol. *36*, 2420–2434.

Minning, D.M., Gow, A.J., Bonaventura, J., Braun, R., Dewhirst, M., Goldberg, D.E., and Stamler, J.S. (1999). Ascaris haemoglobin is a nitric oxide-activated "deoxygenase."Nature *401*, 497–502.

Mitsumoto, A., Nakagawa, Y., Takeuchi, A., Okawa, K., Iwamatsu, A., and Takanezawa, Y. (2001). Oxidized forms of peroxiredoxins and DJ-1 on two-dimensional gels increased in response to sublethal levels of paraquat. Free Radic. Res. *35*, 301–310.

Mizushima, N., Levine, B., Cuervo, A.M., and Klionsky, D.J. (2008). Autophagy fights disease through cellular self-digestion. Nature *451*, 1069–1075.

Moore, D.J., and Dawson, T.M. (2008). Value of genetic models in understanding the cause and mechanisms of Parkinson's disease. Curr. Neurol. Neurosci. Rep. *8*, 288–296.

Muchowski, P.J. (2002). Protein misfolding, amyloid formation, and neurodegeneration: a critical role for molecular chaperones? Neuron *35*, 9–12.

Narendra, D., Tanaka, A., Suen, D.-F., and Youle, R.J. (2009). Parkin-induced mitophagy in the pathogenesis of Parkinson disease. Autophagy *5*, 706–708.

Nedelsky, N.B., Todd, P.K., and Taylor, J.P. (2008). Autophagy and the ubiquitin-proteasome system: collaborators in neuroprotection. Biochim. Biophys. Acta *1782*, 691–699.

Newton, D.A., Rao, K.M.K., Dluhy, R.A., and Baatz, J.E. (2006). Hemoglobin is expressed by alveolar epithelial cells. J. Biol. Chem. *281*, 5668–5676.

Nicklas, W.J., Youngster, S.K., Kindt, M.V., and Heikkila, R.E. (1987). MPTP, MPP+ and mitochondrial function. Life Sci. *40*, 721–729.

Nicotra, A., and Parvez, S. (2002). Apoptotic molecules and MPTP-induced cell death. Neurotoxicol. Teratol. *24*, 599–605.

Nishi, H., Inagi, R., Kato, H., Tanemoto, M., Kojima, I., Son, D., Fujita, T., and Nangaku, M. (2008). Hemoglobin is expressed by mesangial cells and reduces oxidant stress. J. Am. Soc. Nephrol. JASN *19*, 1500–1508.

Nixon, R.A. (2013). The role of autophagy in neurodegenerative disease. Nat. Med. *19*, 983–997.

O'Sullivan, S.S., Williams, D.R., Gallagher, D.A., Massey, L.A., Silveira-Moriyama, L., and Lees, A.J. (2008). Nonmotor symptoms as presenting complaints in Parkinson's disease: a clinicopathological study. Mov. Disord. Off. J. Mov. Disord. Soc. *23*, 101–106.

Onda, M., Akaishi, J., Asaka, S., Okamoto, J., Miyamoto, S., Mizutani, K., Yoshida, A., Ito, K., and Emi, M. (2005). Decreased expression of haemoglobin beta (HBB)

gene in anaplastic thyroid cancer and recovery of its expression inhibits cell growth. Br. J. Cancer *92*, 2216–2224.

Paisán-Ruíz, C., Jain, S., Evans, E.W., Gilks, W.P., Simón, J., van der Brug, M., López de Munain, A., Aparicio, S., Gil, A.M., Khan, N., et al. (2004). Cloning of the gene containing mutations that cause PARK8-linked Parkinson's disease. Neuron *44*, 595–600.

Pan, T., Rawal, P., Wu, Y., Xie, W., Jankovic, J., and Le, W. (2009). Rapamycin protects against rotenone-induced apoptosis through autophagy induction. Neuroscience *164*, 541–551.

Panneton, W.M., Kumar, V.B., Gan, Q., Burke, W.J., and Galvin, J.E. (2010). The neurotoxicity of DOPAL: behavioral and stereological evidence for its role in Parkinson disease pathogenesis. PloS One *5*, e15251.

Panov, A., Dikalov, S., Shalbuyeva, N., Taylor, G., Sherer, T., and Greenamyre, J.T. (2005). Rotenone model of Parkinson disease: multiple brain mitochondria dysfunctions after short term systemic rotenone intoxication. J. Biol. Chem. *280*, 42026–42035.

Paul, G., Ahn, Y.H., Li, J.-Y., and Brundin, P. (2006). Transplantation in Parkinson's disease: The future looks bright. Adv. Exp. Med. Biol. *557*, 221–248.

Peng, J., Oo, M.L., and Andersen, J.K. (2010). Synergistic effects of environmental risk factors and gene mutations in Parkinson's disease accelerate age-related neurodegeneration. J. Neurochem. *115*, 1363–1373.

Perese, D.A., Ulman, J., Viola, J., Ewing, S.E., and Bankiewicz, K.S. (1989). A 6-hydroxydopamine-induced selective parkinsonian rat model. Brain Res. *494*, 285–293.

Polymeropoulos, M.H., Lavedan, C., Leroy, E., Ide, S.E., Dehejia, A., Dutra, A., Pike, B., Root, H., Rubenstein, J., Boyer, R., et al. (1997). Mutation in the alpha-synuclein gene identified in families with Parkinson's disease. Science *276*, 2045–2047.

Przedborski, S., Levivier, M., Jiang, H., Ferreira, M., Jackson-Lewis, V., Donaldson, D., and Togasaki, D.M. (1995). Dose-dependent lesions of the dopaminergic nigrostriatal pathway induced by intrastriatal injection of 6-hydroxydopamine. Neuroscience *67*, 631–647.

Przedborski, S., Jackson-Lewis, V., Naini, A.B., Jakowec, M., Petzinger, G., Miller, R., and Akram, M. (2001). The parkinsonian toxin 1-methyl-4-phenyl-1,2,3,6-tetrahydropyridine (MPTP): a technical review of its utility and safety. J. Neurochem. *76*, 1265–1274.

Ramirez, A., Heimbach, A., Gründemann, J., Stiller, B., Hampshire, D., Cid, L.P., Goebel, I., Mubaidin, A.F., Wriekat, A.-L., Roeper, J., et al. (2006). Hereditary parkinsonism with dementia is caused by mutations in ATP13A2, encoding a lysosomal type 5 P-type ATPase. Nat. Genet. *38*, 1184–1191.

Raymackers, J., Daniels, A., De Brabandere, V., Missiaen, C., Dauwe, M., Verhaert, P., Vanmechelen, E., and Meheus, L. (2000). Identification of two-dimensionally separated human cerebrospinal fluid proteins by N-terminal sequencing, matrix-assisted laser desorption/ionization--mass spectrometry, nanoliquid chromatography-electrospray ionization-time of flight-mass spectrometry, and tandem mass spectrometry. Electrophoresis *21*, 2266–2283.

Reuss, S., Saaler-Reinhardt, S., Weich, B., Wystub, S., Reuss, M.., Burmester, T., and Hankeln, T. (2002). Expression analysis of neuroglobin mRNA in rodent tissues. Neuroscience *115*, 645–656.

Richter, F., Meurers, B.H., Zhu, C., Medvedeva, V.P., and Chesselet, M.-F. (2009). Neurons express hemoglobin alpha- and beta-chains in rat and human brains. J. Comp. Neurol. *515*, 538–547.

Ross, O.A., Braithwaite, A.T., Skipper, L.M., Kachergus, J., Hulihan, M.M., Middleton, F.A., Nishioka, K., Fuchs, J., Gasser, T., Maraganore, D.M., et al. (2008). Genomic investigation of alpha-synuclein multiplication and parkinsonism. Ann. Neurol. *63*, 743–750.

Russo, R., Zucchelli, S., Codrich, M., Marcuzzi, F., Verde, C., and Gustincich, S. Hemoglobin is present as a canonical α2β2 tetramer in dopaminergic neurons. Biochim. Biophys. Acta BBA - Proteins Proteomics.

Sandy, M.S., Armstrong, M., Tanner, C.M., Daly, A.K., Di Monte, D.A., Langston, J.W., and Idle, J.R. (1996). CYP2D6 allelic frequencies in young-onset Parkinson's disease. Neurology *47*, 225–230.

Schechter, A.N. (2008). Hemoglobin research and the origins of molecular medicine. Blood *112*, 3927–3938.

Schmidt, M., Gerlach, F., Avivi, A., Laufs, T., Wystub, S., Simpson, J.C., Nevo, E., Saaler-Reinhardt, S., Reuss, S., Hankeln, T., et al. (2004). Cytoglobin is a respiratory protein in connective tissue and neurons, which is up-regulated by hypoxia. J. Biol. Chem. *279*, 8063–8069.

Schonberger, S.J., Edgar, P.F., Kydd, R., Faull, R.L., and Cooper, G.J. (2001). Proteomic analysis of the brain in Alzheimer's disease: molecular phenotype of a complex disease process. Proteomics *1*, 1519–1528.

Schrier, S.L. (2002). Pathophysiology of thalassemia. Curr. Opin. Hematol. *9*, 123–126.

Selikhova, M., Williams, D.R., Kempster, P.A., Holton, J.L., Revesz, T., and Lees, A.J. (2009). A clinico-pathological study of subtypes in Parkinson's disease. Brain J. Neurol. *132*, 2947–2957.

Senoh, S., and Witkop, B. (1959). Non-enzymatic Conversions of Dopamine to Norepinephrine and Trihydroxyphenethylamines. J. Am. Chem. Soc. *81*, 6222–6231.

Setsuie, R., Wang, Y.-L., Mochizuki, H., Osaka, H., Hayakawa, H., Ichihara, N., Li, H., Furuta, A., Sano, Y., Sun, Y.-J., et al. (2007). Dopaminergic neuronal loss in

transgenic mice expressing the Parkinson's disease-associated UCH-L1 I93M mutant. Neurochem. Int. *50*, 119–129.

Shendelman, S., Jonason, A., Martinat, C., Leete, T., and Abeliovich, A. (2004). DJ-1 is a redox-dependent molecular chaperone that inhibits alpha-synuclein aggregate formation. PLoS Biol. *2*, e362.

Sherer, T.B., Betarbet, R., Testa, C.M., Seo, B.B., Richardson, J.R., Kim, J.H., Miller, G.W., Yagi, T., Matsuno-Yagi, A., and Greenamyre, J.T. (2003). Mechanism of toxicity in rotenone models of Parkinson's disease. J. Neurosci. Off. J. Soc. Neurosci. *23*, 10756–10764.

Shergill, J.K., Cammack, R., Cooper, C.E., Cooper, J.M., Mann, V.M., and Schapira, A.H. (1996). Detection of nitrosyl complexes in human substantia nigra, in relation to Parkinson's disease. Biochem. Biophys. Res. Commun. *228*, 298–305.

Sherman, M.Y., and Goldberg, A.L. (2001). Cellular defenses against unfolded proteins: a cell biologist thinks about neurodegenerative diseases. Neuron *29*, 15–32.

Shin, J.-H., Ko, H.S., Kang, H., Lee, Y., Lee, Y.-I., Pletinkova, O., Troconso, J.C., Dawson, V.L., and Dawson, T.M. (2011). PARIS (ZNF746) repression of PGC-1α contributes to neurodegeneration in Parkinson's disease. Cell *144*, 689–702.

Shinar, E., and Rachmilewitz, E.A. (1993). Haemoglobinopathies and red cell membrane function. Baillières Clin. Haematol. *6*, 357–369.

Shivapurkar, N., Stastny, V., Okumura, N., Girard, L., Xie, Y., Prinsen, C., Thunnissen, F.B., Wistuba, I.I., Czerniak, B., Frenkel, E., et al. (2008). Cytoglobin, the newest member of the globin family, functions as a tumor suppressor gene. Cancer Res. *68*, 7448–7456.

Sian-Hülsmann, J., Mandel, S., Youdim, M.B.H., and Riederer, P. (2011). The relevance of iron in the pathogenesis of Parkinson's disease. J. Neurochem. *118*, 939–957.

Singel, D.J., and Stamler, J.S. (2005). Chemical physiology of blood flow regulation by red blood cells: the role of nitric oxide and S-nitrosohemoglobin. Annu. Rev. Physiol. *67*, 99–145.

Singh, S., Manda, S.M., Sikder, D., Birrer, M.J., Rothermel, B.A., Garry, D.J., and Mammen, P.P.A. (2009). Calcineurin activates cytoglobin transcription in hypoxic myocytes. J. Biol. Chem. *284*, 10409–10421.

Singleton, A.B., Farrer, M., Johnson, J., Singleton, A., Hague, S., Kachergus, J., Hulihan, M., Peuralinna, T., Dutra, A., Nussbaum, R., et al. (2003). alpha-Synuclein locus triplication causes Parkinson's disease. Science *302*, 841.

Slemmon, J.R., Hughes, C.M., Campbell, G.A., and Flood, D.G. (1994). Increased levels of hemoglobin-derived and other peptides in Alzheimer's disease cerebellum. J. Neurosci. Off. J. Soc. Neurosci. *14*, 2225–2235.

Smith, W.W., Pei, Z., Jiang, H., Moore, D.J., Liang, Y., West, A.B., Dawson, V.L., Dawson, T.M., and Ross, C.A. (2005). Leucine-rich repeat kinase 2 (LRRK2) interacts with parkin, and mutant LRRK2 induces neuronal degeneration. Proc. Natl. Acad. Sci. U. S. A. *102*, 18676–18681.

Spillantini, M.G., and Goedert, M. (2000). The alpha-synucleinopathies: Parkinson's disease, dementia with Lewy bodies, and multiple system atrophy. Ann. N. Y. Acad. Sci. *920*, 16–27.

Spiro, T.G., Smulevich, G., and Su, C. (1990). Probing protein structure and dynamics with resonance Raman spectroscopy: cytochrome c peroxidase and hemoglobin. Biochemistry (Mosc.) *29*, 4497–4508.

St Martin, J.L., Klucken, J., Outeiro, T.F., Nguyen, P., Keller-McGandy, C., Cantuti-Castelvetri, I., Grammatopoulos, T.N., Standaert, D.G., Hyman, B.T., and McLean, P.J. (2007). Dopaminergic neuron loss and up-regulation of chaperone protein mRNA induced by targeted over-expression of alpha-synuclein in mouse substantia nigra. J. Neurochem. *100*, 1449–1457.

Steinberg, M.H., and Brugnara, C. (2003). Pathophysiological-based approaches to treatment of sickle cell disease. Annu. Rev. Med. *54*, 89–112.

Storz, J.F., Hoffmann, F.G., Opazo, J.C., and Moriyama, H. (2008). Adaptive functional divergence among triplicated alpha-globin genes in rodents. Genetics *178*, 1623–1638.

Sun, Y., Jin, K., Mao, X.O., Zhu, Y., and Greenberg, D.A. (2001). Neuroglobin is up-regulated by and protects neurons from hypoxic-ischemic injury. Proc. Natl. Acad. Sci. U. S. A. *98*, 15306–15311.

Sun, Y., Jin, K., Peel, A., Mao, X.O., Xie, L., and Greenberg, D.A. (2003). Neuroglobin protects the brain from experimental stroke in vivo. Proc. Natl. Acad. Sci. U. S. A. *100*, 3497–3500.

Tanner, C.M., Kamel, F., Ross, G.W., Hoppin, J.A., Goldman, S.M., Korell, M., Marras, C., Bhudhikanok, G.S., Kasten, M., Chade, A.R., et al. (2011). Rotenone, paraquat, and Parkinson's disease. Environ. Health Perspect. *119*, 866–872.

Thomas, B., Mandir, A.S., West, N., Liu, Y., Andrabi, S.A., Stirling, W., Dawson, V.L., Dawson, T.M., and Lee, M.K. (2011). Resistance to MPTP-neurotoxicity in α-synuclein knockout mice is complemented by human α-synuclein and associated with increased β-synuclein and Akt activation. PloS One *6*, e16706.

Tompkins, M.M., and Hill, W.D. (1997). Contribution of somal Lewy bodies to neuronal death. Brain Res. *775*, 24–29.

Tongsong, T., Srisupundit, K., and Luewan, S. (2009). Outcomes of pregnancies affected by hemoglobin H disease. Int. J. Gynaecol. Obstet. Off. Organ Int. Fed. Gynaecol. Obstet. *104*, 206–208.

Trotman, L.C., Wang, X., Alimonti, A., Chen, Z., Teruya-Feldstein, J., Yang, H., Pavletich, N.P., Carver, B.S., Cordon-Cardo, C., Erdjument-Bromage, H., et al.

(2007). Ubiquitination regulates PTEN nuclear import and tumor suppression. Cell *128*, 141–156.

Trotti, D., Rossi, D., Gjesdal, O., Levy, L.M., Racagni, G., Danbolt, N.C., and Volterra, A. (1996). Peroxynitrite inhibits glutamate transporter subtypes. J. Biol. Chem. *271*, 5976–5979.

Truong, K., Lee, T.D., Li, B., and Chen, Y. (2012). Sumoylation of SAE2 C terminus regulates SAE nuclear localization. J. Biol. Chem. *287*, 42611–42619.

Tzeng, Y.W., Lee, L.Y., Chao, P.L., Lee, H.C., Wu, R.T., and Lin, A.M.Y. (2010). Role of autophagy in protection afforded by hypoxic preconditioning against MPP+-induced neurotoxicity in SH-SY5Y cells. Free Radic. Biol. Med. *49*, 839–846.

Uhl, G.R., Hedreen, J.C., and Price, D.L. (1985). Parkinson's disease: loss of neurons from the ventral tegmental area contralateral to therapeutic surgical lesions. Neurology *35*, 1215–1218.

Uhl, G.R., Walther, D., Mash, D., Faucheux, B., and Javoy-Agid, F. (1994). Dopamine transporter messenger RNA in Parkinson's disease and control substantia nigra neurons. Ann. Neurol. *35*, 494–498.

Uversky, V.N., Li, J., and Fink, A.L. (2001). Pesticides directly accelerate the rate of alpha-synuclein fibril formation: a possible factor in Parkinson's disease. FEBS Lett. *500*, 105–108.

Valente, E.M., Abou-Sleiman, P.M., Caputo, V., Muqit, M.M.K., Harvey, K., Gispert, S., Ali, Z., Del Turco, D., Bentivoglio, A.R., Healy, D.G., et al. (2004). Hereditary early-onset Parkinson's disease caused by mutations in PINK1. Science *304*, 1158–1160.

Wakasugi, K., Nakano, T., and Morishima, I. (2003). Oxidized human neuroglobin acts as a heterotrimeric Galpha protein guanine nucleotide dissociation inhibitor. J. Biol. Chem. *278*, 36505–36512.

Wang, D., Tang, B., Zhao, G., Pan, Q., Xia, K., Bodmer, R., and Zhang, Z. (2008). Dispensable role of Drosophila ortholog of LRRK2 kinase activity in survival of dopaminergic neurons. Mol. Neurodegener. *3*, 3.

Warrick, J.M., Chan, H.Y., Gray-Board, G.L., Chai, Y., Paulson, H.L., and Bonini, N.M. (1999). Suppression of polyglutamine-mediated neurodegeneration in Drosophila by the molecular chaperone HSP70. Nat. Genet. *23*, 425–428.

Weatherall, D.J., and Clegg, J.B. (2001). Inherited haemoglobin disorders: an increasing global health problem. Bull. World Health Organ. *79*, 704–712.

Weidberg, H., Shvets, E., Shpilka, T., Shimron, F., Shinder, V., and Elazar, Z. (2010). LC3 and GATE-16/GABARAP subfamilies are both essential yet act differently in autophagosome biogenesis. EMBO J. *29*, 1792–1802.

Wolozin, B., and Golts, N. (2002). Iron and Parkinson's disease. Neurosci. Rev. J. Bringing Neurobiol. Neurol. Psychiatry *8*, 22–32.

Woodi, M., Mondal, A.K., Padmanabhan, B., and Rajagopalan, K.P. (2009). Analysis of protein posttranslational modifications by mass spectrometry: With special reference to haemoglobin. Indian J. Clin. Biochem. IJCB *24*, 23–29.

Wu, C.-W., Liao, P.-C., Yu, L., Wang, S.-T., Chen, S.-T., Wu, C.-M., and Kuo, Y.-M. (2004). Hemoglobin promotes Abeta oligomer formation and localizes in neurons and amyloid deposits. Neurobiol. Dis. *17*, 367–377.

Wu, H., Wang, M.C., and Bohmann, D. (2009). JNK protects Drosophila from oxidative stress by trancriptionally activating autophagy. Mech. Dev. *126*, 624–637.

Xilouri, M., Vogiatzi, T., Vekrellis, K., Park, D., and Stefanis, L. (2009). Abberant alpha-synuclein confers toxicity to neurons in part through inhibition of chaperone-mediated autophagy. PloS One *4*, e5515.

Yu, Z., Liu, N., Wang, Y., Li, X., and Wang, X. (2012a). Identification of neuroglobin-interacting proteins using yeast two-hybrid screening. Neuroscience *200*, 99–105.

Yu, Z., Liu, N., Liu, J., Yang, K., and Wang, X. (2012b). Neuroglobin, a Novel Target for Endogenous Neuroprotection against Stroke and Neurodegenerative Disorders. Int. J. Mol. Sci. *13*, 6995–7014.

Zincarelli, C., Soltys, S., Rengo, G., and Rabinowitz, J.E. (2008). Analysis of AAV serotypes 1-9 mediated gene expression and tropism in mice after systemic injection. Mol. Ther. J. Am. Soc. Gene Ther. *16*, 1073–1080.

HMG Advance Access published July 28, 2010

Human Molecular Genetics, 2010 **1–12**
doi:10.1093/hmg/ddq290

TRAF6 promotes atypical ubiquitination of mutant DJ-1 and alpha-synuclein and is localized to Lewy bodies in sporadic Parkinson's disease brains

Silvia Zucchelli[1,2,3], Marta Codrich[1], Federica Marcuzzi[1], Milena Pinto[1], Sandra Vilotti[1], Marta Biagioli[1,3], Isidro Ferrer[4] and Stefano Gustincich[1,2,3,*]

[1]Sector of Neurobiology, International School for Advanced Studies (SISSA), AREA Science Park, s.s. 14, Km 163.5, Basovizza, 34012 Trieste, Italy, [2]SISSA Unit, Italian Institute of Technology (IIT), AREA Science Park, s.s. 14, Km 163.5, Basovizza, 34012 Trieste, Italy, [3]The Giovanni Armenise-Harvard Foundation Laboratory, International School for Advanced Studies (SISSA), AREA Science Park, s.s. 14, Km 163.5, Basovizza, 34012 Trieste, Italy and [4]Institute of Neuropathology, Institut d'Investigacio Biomedica de Bellvitge – University Hospital Bellvitge, University of Barcelona, 08907 Hospitalet de LLobregat, Spain

Received April 9, 2010; Revised and Accepted July 7, 2010

Parkinson's disease (PD) is a neurodegenerative disorder characterized by loss of dopaminergic neurons in the Substantia Nigra and the formation of ubiquitin- and alpha-synuclein (aSYN)-positive cytoplasmic inclusions called Lewy bodies (LBs). Although most PD cases are sporadic, families with genetic mutations have been found. Mutations in PARK7/DJ-1 have been associated with autosomal recessive early-onset PD, while missense mutations or duplications of aSYN (PARK1, PARK4) have been linked to dominant forms of the disease. In this study, we identify the E3 ubiquitin ligase tumor necrosis factor-receptor associated factor 6 (TRAF6) as a common player in genetic and sporadic cases. TRAF6 binds misfolded mutant DJ-1 and aSYN. Both proteins are substrates of TRAF6 ligase activity *in vivo*. Interestingly, rather than conventional K63 assembly, TRAF6 promotes atypical ubiquitin linkage formation to both PD targets that share K6-, K27- and K29- mediated ubiquitination. Importantly, TRAF6 stimulates the accumulation of insoluble and polyubiquitinated mutant DJ-1 into cytoplasmic aggregates. In human post-mortem brains of PD patients, TRAF6 protein colocalizes with aSYN in LBs. These results reveal a novel role for TRAF6 and for atypical ubiquitination in PD pathogenesis.

INTRODUCTION

Parkinson's disease (PD) is one of the most common neurodegenerative disorders. It is characterized by loss of dopaminergic (DA) neurons in the Substantia Nigra (SN) and the presence of cytoplasmic inclusions called Lewy bodies (LBs) (1). Most PD cases are sporadic, but a minority of forms is associated to familial transmission. Among them, PARK7/DJ-1 has been linked to autosomal recessive PD, whereas PARK1/PARK4/alpha-synuclein (aSYN) is found in dominant forms. aSYN is a major component of LBs providing a molecular link between sporadic and genetic cases. The accumulation of misfolded proteins into cellular aggregates is a prominent feature common to most neurodegenerative diseases. These insoluble proteinaceous deposits contain ubiquitin and components of the ubiquitin–proteasome system, including those encoded by genes mutated in familiar cases, like the ubiquitin ligase parkin/PARK2 and ubiquitin C-terminal hydrolase-L1 (UCH-L1/PARK5) (2–5). These data suggest that cellular handling of misfolded and aggregation-prone proteins play a central role in PD pathogenesis.

Substrate ubiquitination is a signal for diverse cellular functions. Polyubiquitin chains can be formed through covalent conjugation using any of the seven lysines present in the ubiquitin moiety. Ubiquitination through K48 generally targets proteins for degradation, whereas K63 linkage plays a role in signaling and protein trafficking (6). Recent data indicate

*To whom correspondence should be addressed. Tel: +39 0403756505; Fax: +39 0403756502; Email: gustinci@sissa.it

that degradative and nondegradative functions of protein ubiquitination can be also associated with atypical chain formation. All lysine residues, with the exception of K63, accumulate in response to proteasome inhibition (7). K11 has been implicated in endoplasmic reticulum-associated degradation (7), while K27 and K29 appear to be connected to lysosomal localization and degradation (8,9). K6, K27, K29 and K33 have also been proven to have nondegradative functions on selected substrates (10–12).

We previously showed that tumor necrosis factor-receptor associated factor 6 (TRAF6)-binding protein TRAF- and TNF-receptor associated protein (TTRAP) (13) is a novel interactor of DJ-1 able to bind the PD-associated mutant L166P more strongly than wild type (wt) (14). TRAF6 is an E3 ubiquitin ligase that promotes K63-specific chain assembly in the signal transduction pathway that ultimately leads to nuclear factor-kB (NFkB) activation (15). Although in the immune system it has an essential role in tumor necrosis factor and interleukin-1/Toll-like receptors signaling, in the brain, TRAF6 activity has been associated with the transduction cascade of the neurotrophin receptors p75 and TrkA (16–18). So far, the only evidence that supports a role for TRAF6 in neurodegeneration has been limited to its colocalization with tau in brains of Alzheimer's disease (AD) patients (19).

In the current study, we provide evidence that TRAF6 interacts with and ubiquitinates mutant DJ-1 and aSYN. Unexpectedly, TRAF6 promotes an atypical mode of polyubiquitin chain formation onto its PD-associated target proteins that share K6, K27 and K29 ubiquitination. We also show that TRAF6-mediated ubiquitination stimulates the accumulation of mutant DJ-1 into insoluble aggregates. In post-mortem brains of sporadic PD patients, TRAF6 is present in LBs.

Altogether, our data imply a novel role for TRAF6 in mediating atypical ubiquitination of proteins relevant for sporadic and familial PD.

RESULTS

TRAF6 binds to and ubiquitinates misfolded mutant DJ-1

We have previously shown that TTRAP is a potent interactor of PD-associated mutant DJ-1, with misfolded L166P being the stronger partner (14). Since TTRAP was originally identified as a TRAF-interacting protein with highest selectivity for TRAF6 (13), we analyzed whether TRAF6 itself could associate with DJ-1.

We performed coimmunoprecipitation experiments using HEK cells transfected with HA–TRAF6 and FLAG–DJ-1 wt or PD-linked L166P mutant. Although protein levels were significantly lower than those of wt protein, misfolded DJ-1 mutant could specifically associate with TRAF6 in untreated conditions (Fig. 1A). Since proteasome inhibition stabilizes L166P levels, we then analyzed the binding capabilities of wt and mutant proteins in conditions of proteasome block. Coimmunoprecipitation in cells treated with MG132 revealed an enhanced binding of TRAF6 to L166P and confirmed not detectable binding with wt DJ-1, proving that TRAF6 is able to discriminate misfolded mutant DJ-1. Interaction data were confirmed by reverse immunoprecipitation with HA–TRAF6 and FLAG–DJ-1 (Fig. 1B) as well as by the use of different protein tags (Fig. 1C). To identify which portion of TRAF6 binds to misfolded DJ-1, we expressed wt and mutant form of TRAF6 lacking the N-terminal RING domain in HEK cells and verified binding to L166P. Similar to other TRAF6-binding proteins (16), the C-terminal TRAF domain was sufficient to mediate its association with mutant DJ-1 (Fig. 1D). Together, our data indicate that TRAF6 binds misfolded mutant DJ-1, but not wt protein.

Since TRAF6 is an E3 ubiquitin ligase, we investigated whether mutant DJ-1 might be substrate of TRAF6 activity. To test this hypothesis, we performed *in vivo* ubiquitination assays. HEK cells were transfected with MYC–DJ-1 wt or L166P with HA–ubiquitin in the presence or absence of FLAG–TRAF6. Controls were included with HA–ubiquitin alone or with FLAG–TRAF6 to avoid artifacts due to a general increase in polyubiquitination. We found that, in the absence of exogenous TRAF6, both wt and mutant DJ-1 could be ubiquitinated, even though at very low levels (Fig. 2A). Overexpression of TRAF6 had no effect on the ubiquitination of wt DJ-1, but significantly enhanced ubiquitination of L166P, as expected from their interaction pattern. Mutant DJ-1 was mainly observed in the polyubiquitinated form. To provide further support on the role of TRAF6 in mediating misfolded DJ-1 ubiquitination, we performed *in vivo* ubiquitination assays with a form of TRAF6 lacking the N-terminal ubiquitin ligase RING domain (DN) (Supplementary Material, Fig. S1A). The effects on wt DJ-1 were used as internal control. We found that overexpression of TRAF6–DN abolished L166P ubiquitination (Fig. 2B). Therefore, E3 ligase activity of TRAF6 is required for mutant DJ-1 polyubiquitination.

To examine the specificity of TRAF6-mediated effects on L166P, we compared TRAF6 activity with that of TRAF2, another E3 ligase that belongs to the TRAF family. MYC–L166P was transfected with HA–ubiquitin and FLAG–TRAF2 wt or DN mutant. FLAG–TRAF6 wt and DN were included in the same experiment as internal reference. The amount of polyubiquitinated L166P by TRAF2 was much less than by TRAF6 (Fig. 2C). These results indicate that the effects of TRAF6 are specific, but not exclusive.

TRAF6-mediated ubiquitination of L166P involves atypical chain linkage

E3 ligases can promote the formation of polyubiquitin chains on target substrates through any of the lysines present on ubiquitin molecules. TRAF6 activity has been widely associated with chain formation mainly via K63-specific linkage. Therefore, we investigated whether K63 or canonical K48 linkages were used for mutant DJ-1 ubiquitination by TRAF6. We used ubiquitin mutants in which either of these residues was substituted with an arginine (K48R and K63R). An ubiquitin mutant with all lysines substituted with arginine was also included as negative control (K0). HEK cells were thus transfected with MYC–L166P with HA–wt or mutant ubiquitin in the presence of FLAG–TRAF6. As expected, a robust polyubiquitination of L166P with wt ubiquitin was promoted by TRAF6 overexpression, while it was abolished in the presence of K0 mutant. Strikingly, we found that TRAF6-mediated ubiquitination of L166P was maintained with K48R and K63R

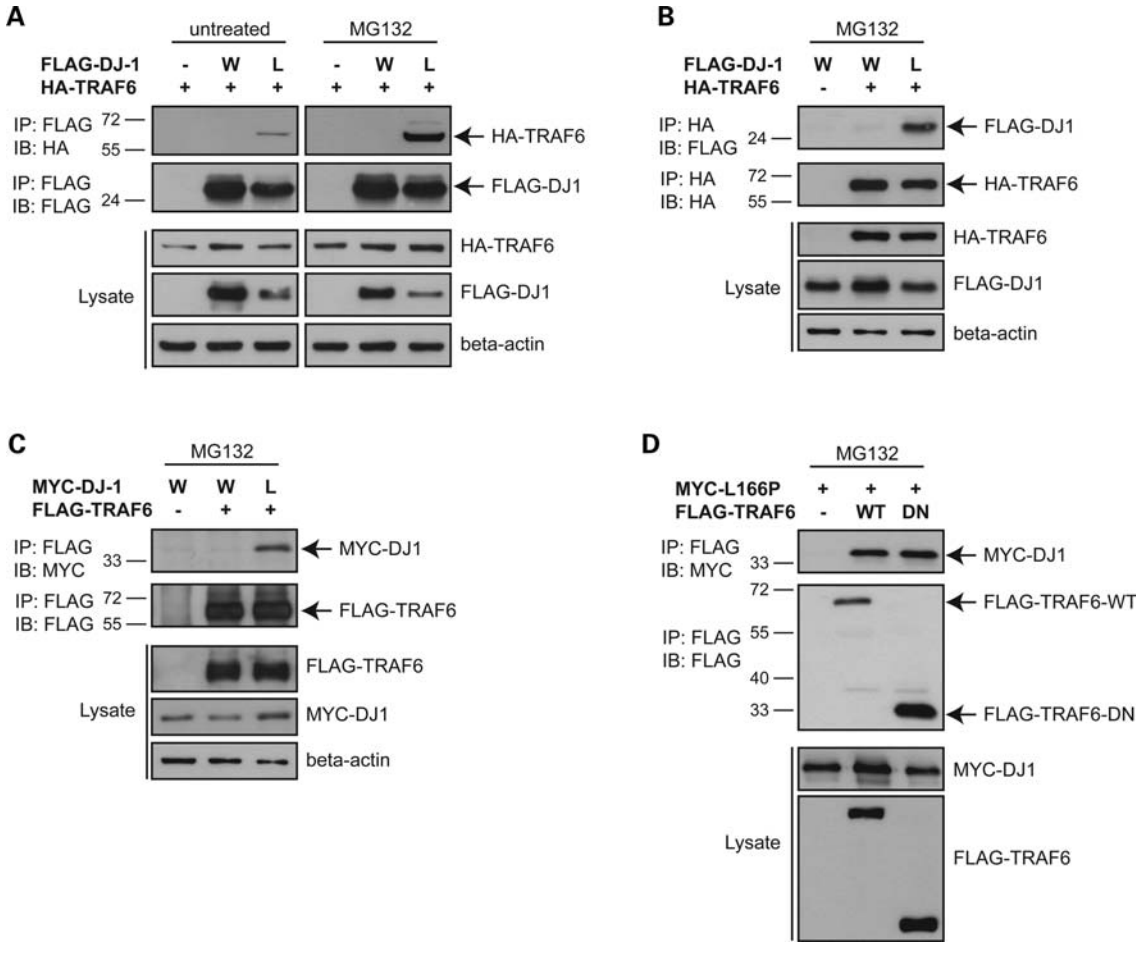

Figure 1. TRAF6 interacts with mutant DJ-1. (**A**) HEK cells were transfected with HA-TRAF6 alone or with FLAG-DJ-1 wt (W) or L166P (L) and left untreated or incubated with 5 μM MG132 for 16 h. Lysates were immunoprecipitated (IP) with anti-FLAG agarose beads and bound proteins were revealed by immunoblot (IB) with anti-HA and anti-FLAG antibodies. Lysates were tested for the expression of TRAF6 and DJ-1 proteins. β-actin was used as loading control. (**B**) Cells were transfected with FLAG–DJ-1 wt (W) or L166P (L) and HA–TRAF6 and treated with MG132. Lysates were subjected to coimmunoprecipitation with anti-HA antibody. Immunoprecipitates and lysates were analyzed with anti-FLAG, anti-HA and beta-actin antibodies. (**C**) Coimmunoprecipitation with FLAG–TRAF6 and MYC–DJ-1 constructs. Experiment was performed as in (A) with HEK cells treated with MG132. (**D**) Cells were transfected with MYC–L166P alone or with full length (WT) or N-terminally deleted (DN) FLAG–TRAF6. Lysates were immunoprecipitated with anti-FLAG agarose beads. Bound proteins and lysates were analyzed with anti-MYC and anti-FLAG antibodies.

mutants (Fig. 3A). We then generated ubiquitin mutants with only one lysine available for polymerization. Consistent with the data obtained with K48R and K63R, neither K63 nor K48 were used by TRAF6 for mutant DJ-1 ubiquitination. Instead, TRAF6 promoted a robust polyubiquitination of L166P in the presence of K27 and K29 mutants. Weaker but reproducible ubiquitination was also induced with K6 and K33 ubiquitins. Background signals were observed with K0 (Fig. 3B).

Altogether, our data indicate that TRAF6 promotes atypical polyubiquitination of misfolded mutant DJ-1 by using K6, K27, K29 and K33 as isotype linkages.

TRAF6 ubiquitination promotes the accumulation of mutant DJ-1 into insoluble aggregates

One fundamental question was to determine whether TRAF6-mediated atypical ubiquitination of L166P might trigger its degradation. Human neuroblastoma SH–SY5Y cells stably expressing FLAG–L166P were transfected with FLAG–TRAF6 wt or DN, and the steady-state levels of misfolded DJ-1 were followed by western blot. TRAF6 had no effect on L166P protein levels, indicating that its activity has a non-degradative role (Supplementary Material, Fig. S2A). Similarly, pulse chase experiments with cyclohexamide showed no evident effects of TRAF6 ubiquitination on L166P stability (Supplementary Material, Fig. S2B). Since nondegradative ubiquitination has been previously associated with altered solubility of PD-associated aSYN and synphilin-1 (20,21), we next investigated whether TRAF6-mediated ubiquitination of L166P might have an impact on its biochemical status. MYC–L166P and HA–ubiquitin were co-expressed in HEK cells in the presence or absence of FLAG–TRAF6 wt or DN. Lysates were separated into Triton X-100 soluble and insoluble fractions. We found that nonubiquitinated forms of L166P were distributed in both fractions and TRAF6 had no effect on total levels of soluble mutant DJ-1. In contrast, polyubiquitinated misfolded DJ-1

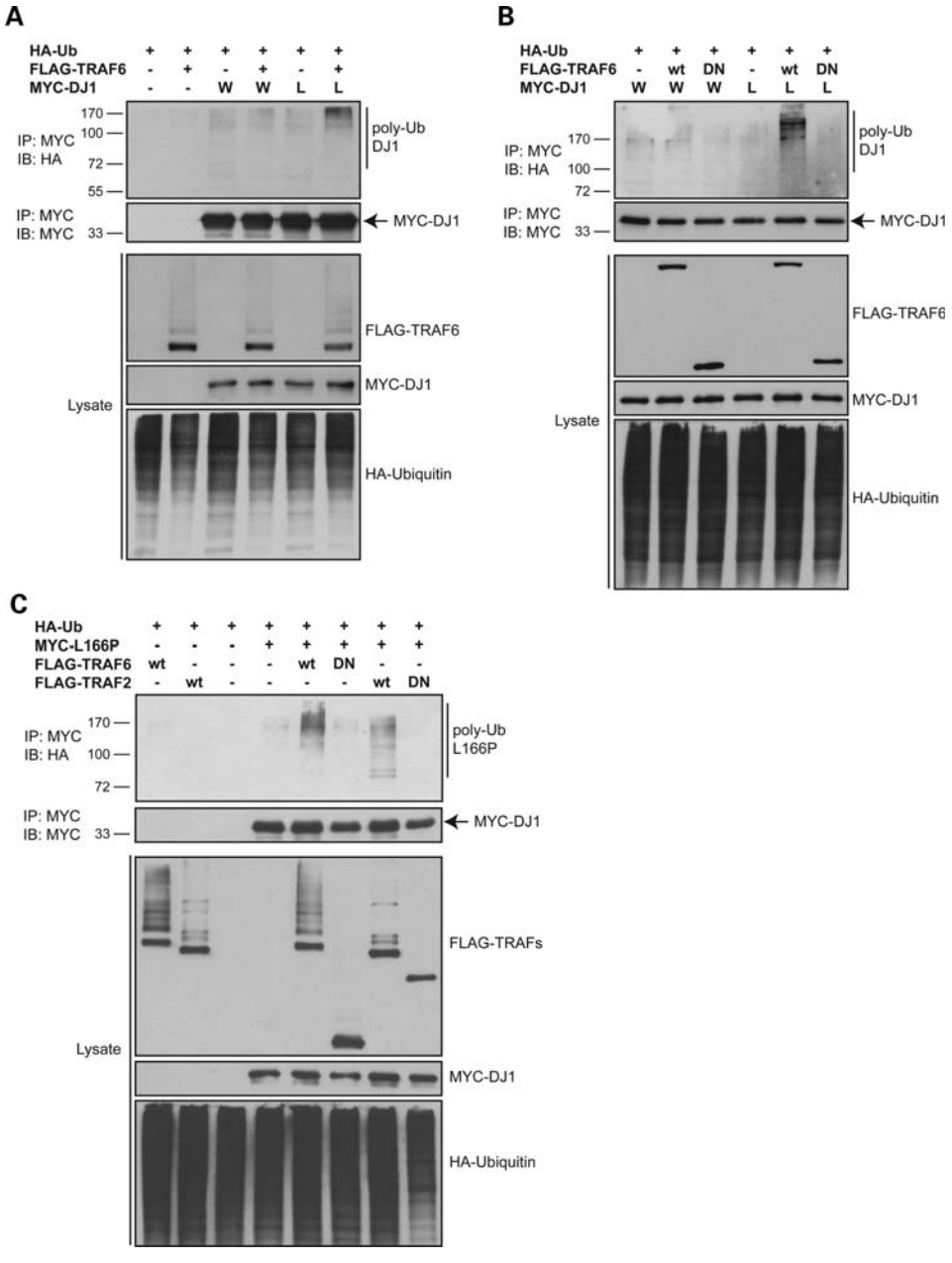

Figure 2. Mutant DJ-1 is substrate of TRAF6 ubiquitin ligase activity. (**A**) For *in vivo* ubiquitination assay, HEK cells were transfected with HA–ubiquitin, FLAG–TRAF6 and MYC–DJ-1 wt (W) or L166P (L) and treated with 10 μM MG132 for 3 h. Ubiquitinated DJ-1 was visualized with anti-HA antibody after immunoprecipitation with anti-MYC. Immunoprecipitated DJ-1 was verified by anti-MYC immunoblot. Inputs were checked with anti-FLAG, ant-MYC and anti-HA antibodies. (**B**) Cells were transfected with HA–ubiquitin and MYC–DJ-1 wt or L166P with WT or DN FLAG–TRAF6. Ubiquitination assay was performed as in (A). (**C**) Ubiquitination experiment was done with HA–ubiquitin, MYC–L166P and FLAG–TRAF6 (wt and DN) or FLAG–TRAF2 (wt and DN). Immunoprecipitates and lysates were analyzed with anti-HA, anti-MYC and anti-FLAG antibodies.

was present only in Triton-insoluble fraction (Fig. 4A). Consistent with our *in vivo* ubiquitination data, we observed a potent increase in the amount of ubiquitinated L166P only when TRAF6 wt, but not DN, was overexpressed.

To assess whether the increased insolubility of L166P induced by TRAF6 is associated with a propensity to form protein aggregates, we monitored the effects of TRAF6 overexpression on L166P inclusion formation. We created wt–TRAF6 and DN–TRAF6 fused to GFP (Supplementary Material, Fig. S1B) and used these constructs with FLAG–L166P and HA–ubiquitin. The formation of ubiquitin- and L166P-positive aggregates was followed by double immunofluorescence coupled with GFP autofluorescence. To detect only insoluble inclusions, a permeabilization protocol was performed (14). L166P showed a diffused pattern when expressed alone or with ubiquitin (Fig. 4B). Addition of ligase-competent TRAF6 generated larger insoluble L166P-containing aggregates in >90% of the cells. These were positively stained for TRAF6 and ubiquitin. No aggregates were observed when TRAF6 DN was used, proving that inclusion

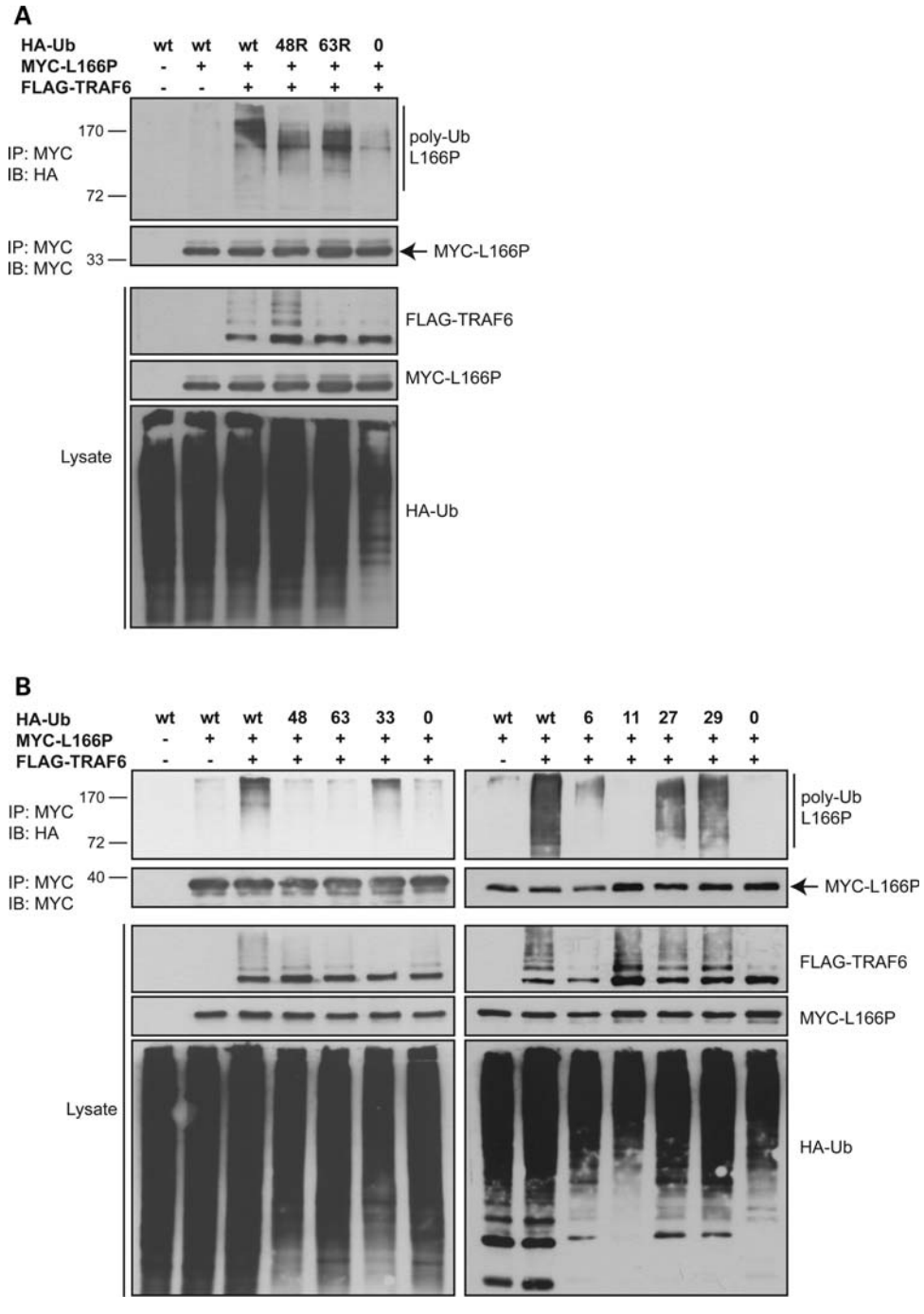

Figure 3. TRAF6 mediates atypical ubiquitin chain formation on mutant DJ-1. (**A**) HA–ubiquitin constructs with either wt or mutated K48 (48R) and K63 (63R) lysine residues were used for ubiquitination assay with MYC–L166P and FLAG–TRAF6. A polyubiquitination incompetent mutant (K0) was used as control. Immunoprecipitates and lysates were analyzed with anti-FLAG, anti-MYC and anti-HA antibodies. (**B**) HA–ubiquitin mutants in which only the indicated lysine residue is available for chain formation were used. Wt and K0 ubiquitin constructs were used as positive and negative controls. Ubiquitination assay was performed as in (A).

formation is a consequence of TRAF6 activity on mutant DJ-1. As expected, wt DJ-1 staining was not altered by ubiquitin or TRAF6 expression (Fig. 4B). To prove that TRAF6 action on L166P involved atypical ubiquitination, we carried out analogous experiments with ubiquitin mutants that were shown to be involved in L166P ubiquitination (K27 and K29). As controls, K0 was used as well as K11 and K48 ubiquitins. These are mutants that mediate poly-chain formation, but are not TRAF6 substrates. K27 and K29, but not K0, K11 and K48, were able to recapitulate the phenotype observed with wt ubiquitin, proving the specificity of TRAF6 activity (Fig. 4C). Experiments were also carried out with differentially tagged mutant DJ-1 and all the remaining ubiquitin mutants (Supplementary Material, Fig. S3). Together, these

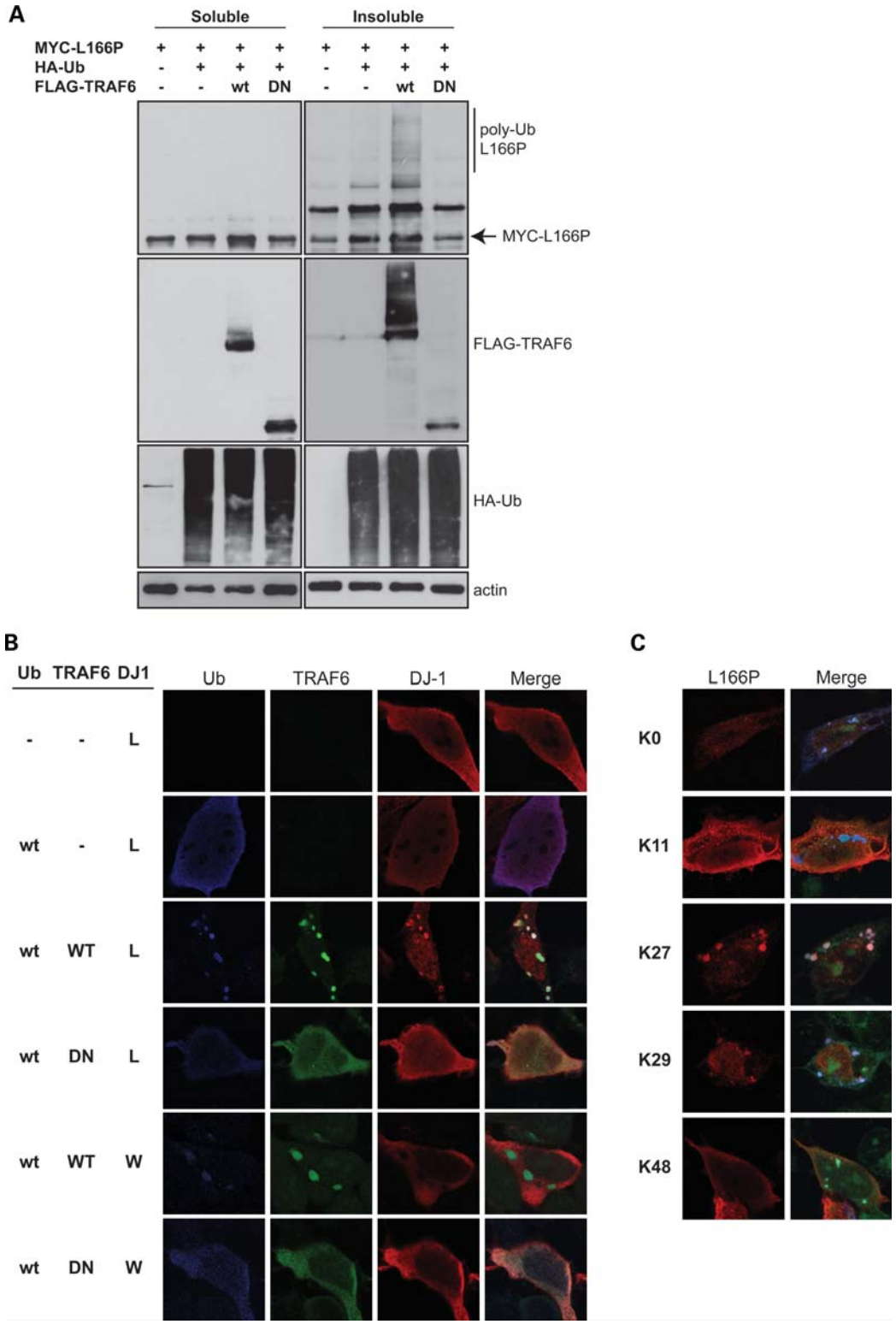

Figure 4. TRAF6 promotes the accumulation of ubiquitinated mutant DJ-1 in insoluble aggregates. (**A**) HEK cells were transfected with HA–ubiquitin, MYC–L166P and FLAG–TRAF6 (wt or DN). After treatment with 10 μM MG132 for 3 h, Triton X-100 soluble and insoluble fractions were separated. Lysates were analyzed with anti-MYC, anti-HA, anti-FLAG and anti-actin antibodies. (**B**) Cells were transfected with HA–ubiquitin wt, FLAG–L166P and GFP–TRAF6 (wt or DN) and treated as in (A). Before fixation, cells were permeabilized with Triton X-100. Insoluble aggregates were analyzed by double immunofluorescence coupled with GFP autofluorescence. (**C**) HA–ubiquitin wt or K0, K11 K27, K29 and K48 mutants were used with FLAG–L166P and GFP–TRAF6 wt to follow insoluble aggregate formation. Double immunofluorescence coupled with GFP autofluorescence was performed as in (B) on permeabilized cells.

data provide evidence that TRAF6-mediated atypical ubiquitination of DJ-1 L166P increases its propensity to accumulate into insoluble aggregates.

TRAF6 binds to and ubiquitinates aSYN with atypical linkage formation

It has been shown that the ubiquitin ligase seven in absentia homolog (SIAH)-1 binds to and ubiquitinates aSYN and aSYN-binding protein synphilin-1 (4). Structural studies proved that members of the SIAH family possess a domain highly similar to the TRAF-C region of TRAF proteins (22). To study a potential role of TRAF6 in PD sporadic cases, we analyzed the interplay between TRAF6 and aSYN. Coimmunoprecipitation experiments were carried out using MYC–aSYN and FLAG–TRAF6. Both wt and PD-associated A53T mutant aSYN constructs were tested. aSYN was found to specifically interact with TRAF6 (Fig. 5A). No preferential binding toward the wt or mutant form of aSYN could be observed, suggesting a potential role of TRAF6 in both sporadic and aSYN-linked genetic cases.

The interaction between TRAF6 and aSYN raised the possibility that aSYN might be an additional PD-associated target of TRAF6 ligase activity. We thus performed *in vivo* ubiquitination assay with HA–ubiquitin and MYC–aSYN wt or A53T with or without FLAG–TRAF6 wt and DN. In this experiment, the level of aSYN polyubiquitinated species was significantly enhanced by TRAF6 overexpression (Fig. 5B). No accumulation of ubiquitinated aSYN was observed when TRAF6 DN was used. Both wt and A53T mutant were targets of TRAF6.

We then evaluated whether TRAF6 activity on aSYN might involve atypical ubiquitin chain formation (Fig. 5C). We thus performed ubiquitination assay with all ubiquitin mutants. TRAF6 supported aSYN ubiquitination mainly via K6, K27 and K29 chains. Importantly, these are shared motifs with misfolded mutant DJ-1.

TRAF6 is present in LBs and accumulates in PD brains

To gain further insights into the relevance of TRAF6 for PD pathogenesis, we analyzed the presence of endogenous TRAF6 in SN DA neurons in human post-mortem brains. As shown in Fig. 6A, TRAF6 is expressed in the cytoplasm of DA neurons, as identified by tyrosine hydroxylase (TH) staining. Some TRAF6 immunoreactivity was also found in non-DA neurons, proving a quite broad distribution in midbrain cell populations.

Several E3 ligases, including Parkin, carboxyl terminus of Hsc70-interaction protein (CHIP) and SIAH, have been shown to be part of LBs in surviving DA neurons in PD brains. Therefore, we examined human post-mortem brains of pathologically confirmed cases of sporadic PD. Experiments were performed on brain samples from two different patients. LBs were identified using an aSYN antibody. Interestingly, virtually all nigral LBs were immunoreactive for an anti-TRAF6 antibody in both individuals (Fig. 6B and Supplementary Material, Fig. S4). TRAF6 was expressed throughout the cytoplasm, but the protein was clearly accumulated at the border of LBs, a site where aSYN staining was more prominent. The specificity of TRAF6 accumulation in LBs was verified using three antibodies directed against N- or C-terminal epitopes of the protein (Supplementary Material, Fig. S4). No immunoreactivity was detected with unrelated IgG (data not shown).

In response to an excess burden of misfolded proteins, neurons tend to increase the expression of E3 ligases and downregulate the level of deubiquitinating enzymes as previously shown in PD post-mortem brains for Parkin and UCH-L1 (23–26). Therefore, we tested TRAF6 mRNA levels in sporadic PD ($n = 6$) and healthy control ($n = 3$) brains (27). RNA was extracted selectively from SN, the site of PD pathogenesis. Quantitative real-time polymerase chain reaction (qPCR) amplification showed that the amount of TRAF6 mRNA was statistically increased in sporadic PD samples when compared with normal controls ($P < 0.02$), with an average 1.7-fold upregulation (Fig. 6C).

To strengthen the significance of the increased amount of TRAF6 expression in PD, we also checked for the status of regulators of TRAF6 activity. By qPCR analysis, we found no significant differences in the expression of p62, CYLD and A20 between PD and control samples (Supplementary Material, Fig. S5). Overall, our results show that the ubiquitin ligase TRAF6 is present in DA neurons in the midbrain of both normal and PD brains. In sporadic patients, TRAF6 colocalizes with aSYN within LBs and the amount of its mRNA seems increased in SN.

DISCUSSION

The description of the molecular components of LBs and the discovery of new players in the recruitment of these molecules to aggregates are important for the understanding of the molecular mechanisms of PD and for the identification of new drug targets. More than 76 proteins have been described so far as localized in LBs (28–30) and the significance of their relocalization may depend on protein identity.

Ubiquitin ligases are responsible for the formation of polyubiquitin chains in substrate proteins and are frequently associated with neurodegenerative diseases for their presence in intracellular aggregates and their role in aggregate formation. The E3 ligases Parkin, CHIP and SIAH have been found to accumulate in LBs of PD patients (2,4,5). While their enzymatic activities may be important for protein recruitment into the aggregates, their sequestration may decrease the quantity of soluble, active enzymes inducing a ‘loss of function’ phenotype for the lack of appropriate physiological ubiquitination of targets. Interestingly, they ubiquitinate misfolded L166P DJ-1 and aSYN with degradative or nondegradative effects on either of PD substrates (4,5,21,31).

Structural studies proved that members of the SIAH family possess a domain highly similar to the TRAF-C region of TRAF proteins (22). In this study, we demonstrate that the ubiquitin E3 ligase TRAF6 is a component of LBs. Virtually all LBs in the post-mortem brains of two individuals were positive for TRAF6. Three different antibodies against both the N- and C-terminals of the protein have been used.

TRAF6 ligase activity has been extensively characterized in the context of NFkB activation (15). In the brain, TRAF6 has

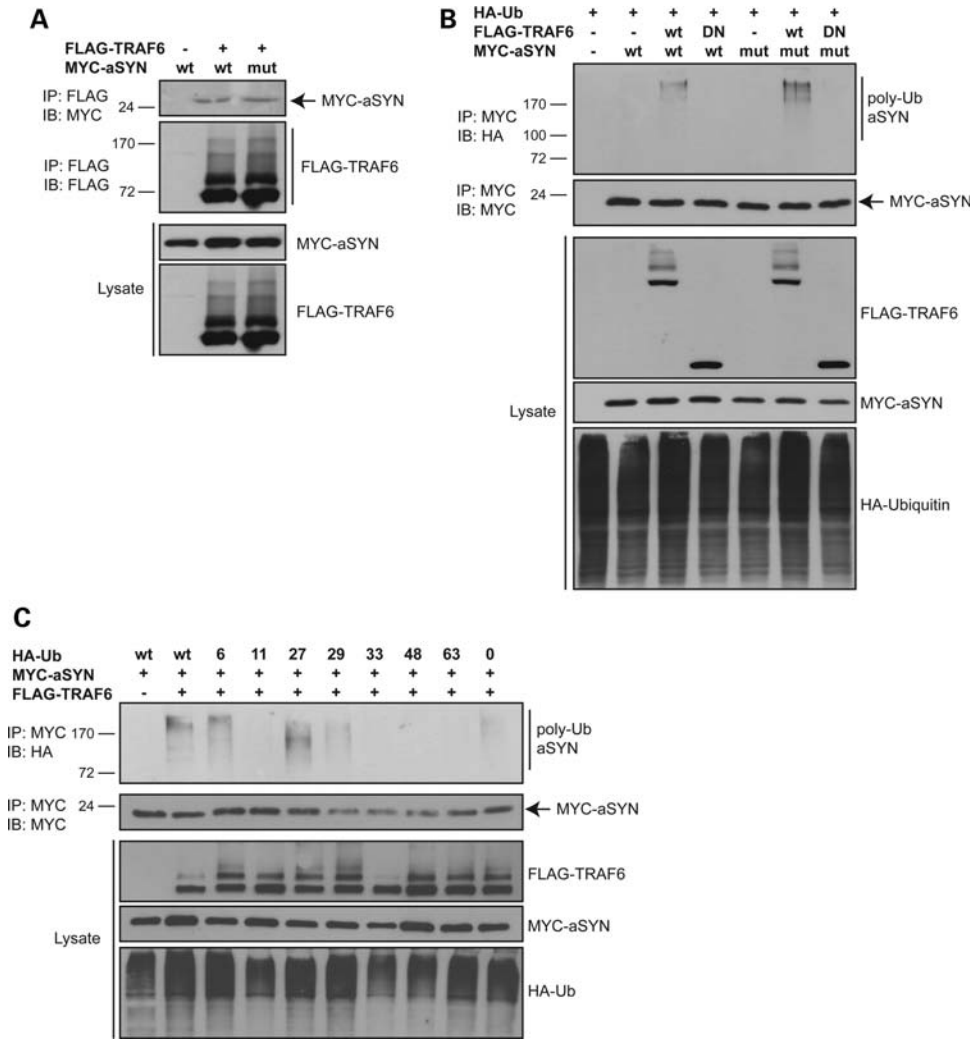

Figure 5. TRAF6 binds aSYN and enhances its ubiquitination with atypical chains. (**A**) HEK cells were transfected with FLAG–TRAF6 and MYC–aSYN wt or A53T (mut). Lysates were immunoprecipitated with anti-FLAG agarose beads and bound proteins were revealed with anti-MYC and anti-FLAG antibodies. Inputs were tested for the expression of TRAF6 and aSYN proteins. (**B**) Cells were transfected with HA–ubiquitin, MYC–aSYN (wt or A53T) and FLAG–TRAF6 (wt or DN). For *in vivo* ubiquitination assay, lysates were immunoprecipitated with anti-MYC antibody. Immunoprecipitates and lysates were analyzed with anti-MYC, anti-FLAG and anti-HA antibodies. (**C**) HA–ubiquitin mutants in which only the indicated lysine residue is available for chain formation were used. Wt and K0 ubiquitin were included as controls. *In vivo* ubiquitination of aSYN wt was performed as in (B).

been previously linked to K63-specific polyubiquitination of AD-associated protein tau (19) and in nerve growth factor-receptor signaling (18). Most importantly, TRAF6 localizes in tau-containing, intracellular aggregates in AD post-mortem brains, suggesting that TRAF6 sequestration may be a common mechanism in neurodegeneration (19).

In post-mortem brains of non-PD individuals, we show that TRAF6 protein is expressed in DA cells of SN. In the mouse brain, TRAF6 mRNA is present at comparable levels in DA cells from SN and Ventral Tegmental Area, a site that is spared in PD (32). This is consistent with the hypothesis that TRAF6 expression *per se* is not related to cellular vulnerability.

TRAF6 interacts with mutant L166P DJ-1 and aSYN to promote their ubiquitination via atypical ubiquitin chain formation involving residues K6, K27, K29 and K33. Surprisingly, none of the PD targets that we tested were modified via TRAF6 canonical activity with K63 specificity. Nonconventional ubiquitination of L166P is sufficient for its accumulation into insoluble inclusions.

In a quantitative proteomic analysis of atypical ubiquitin chains in yeast, substrates for K6, K27, K29 and K33 have been shown to accumulate upon proteasome block, although to a lower extent than for K48, suggesting their potential role in protein degradation (7). Interestingly, these four ubiquitin moieties showed some functional redundancy. Unfortunately, the low cellular concentrations of their substrates have limited so far their identification in yeast or in *ex vivo* mammalian samples (7).

TRAF6 substrate L166P DJ-1 is very unstable and its expression level, both in transfection studies and in patient lymphoblasts, is lower than wt (33). This suggests that L166P mutation may induce a loss of DJ-1 function. However, L166P disrupts DJ-1 protein conformation resulting

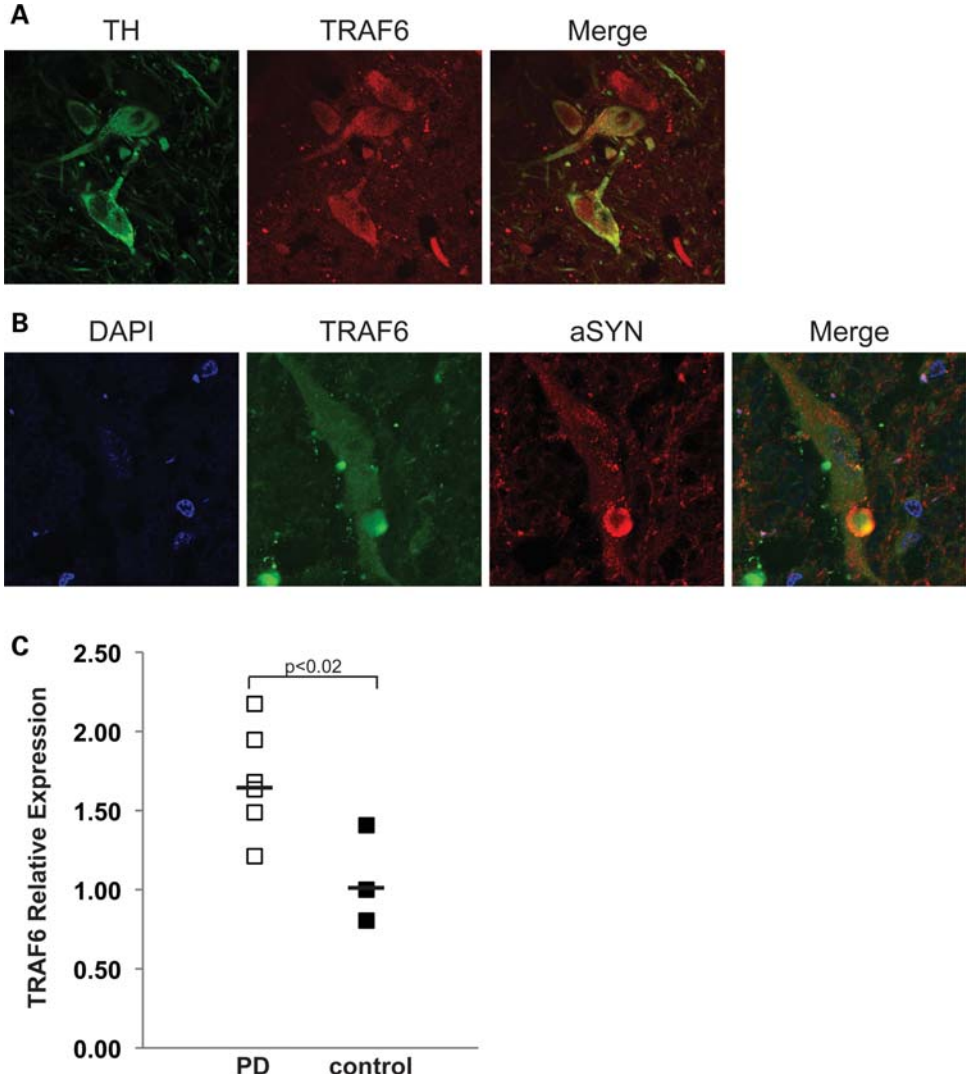

Figure 6. TRAF6 colocalizes with aSYN in LBs and accumulates in PD post-mortem brains. (**A**) Cryo-sections of post-mortem brain tissues were taken from healthy individuals and endogenous TRAF6 was visualized by immunohistochemistry. DA neurons were identified with anti-TH antibody. (**B**) TRAF6 was analyzed by immunohistochemistry in SN of PD patients. LBs were visualized with anti-aSYN antibody. (**C**) Total RNA was extracted from SN of six PD and three control brains. TRAF6 mRNA was measured by qPCR relative to β-actin. Significance between PD and control group was calculated with *t*-test.

in a misfolded protein that is prone to assemble into multimeric structures (34–36). Indeed, by gel filtration and other assays, L166P has been previously shown to be present mostly as a high-molecular-weight complex that may contain either DJ-1 oligomers and/or aggregates with other proteins (31,33,36). According to this model, L166P may be prone to aggregation in both healthy individuals heterozygous for the mutation and in PD patients. Several hypotheses may be formulated to account for these phenotypes. L166P may be recruited to cytoplasmic aggregates by TRAF6 to avoid toxicity in heterozygosity so that neurodegeneration occurs only in the absence of a functional DJ-1. In this context, wt DJ-1 may protect against cellular stress elicited by L166P. In physiological conditions, aggresomes may then be cleared *in vivo* by autophagy. The aggresome–autophagy pathway is increasingly recognized as a specialized type of induced autophagy that mediates selective clearance of misfolded and aggregated proteins under the conditions of proteotoxic stress (37,38). While TRAF6 has been recently involved in autophagy in macrophages (39), the E3 ligase parkin seems to be a key regulator of this pathway triggering L166P aggregation in an HDAC6-dependent manner (31). One can speculate that atypical ubiquitination might function in the recruitment to autophagic and/or storage vescicles as proved for K27 ubiquitination of Jun and K29 of Deltex (8,9). It must be noted that, to the best of our knowledge, no investigation of DJ-1 L166P has been done in post-mortem brains of PD patients carrying this mutation or in *knock-in* animal models.

Components of LBs are candidate aSYN interactors. Despite major efforts, the mechanisms of aSYN-induced neurodegeneration *in vivo* remain unclear. Although some genes have been isolated for their ability to suppress aSYN-mediated toxicity in invertebrate models (40–42), there is still the need to identify aSYN interactors that may regulate aSYN conformation, subcellular localization and biochemical properties.

Both SIAH (4) and CHIP (5) bind to aSYN and regulate its levels and aggregation properties (21,43,44). Here we identify TRAF6 as a new aSYN modifier through unconventional ubiquitination.

LBs contain phosphorylated, ubiquitinated and nitrated aSYN (45–47). The type of ubiquitin moieties covalently attached to aSYN in PD and control brains remains unclear. Interestingly, only 10% of aSYN is ubiquitinated with evidences for conjugation of one, two or three ubiquitins (44). Monoubiquitination by SIAH has been proposed to act as a seed for further protein aggregation (48).

In our experimental settings, we failed to trigger aSYN aggregates by TRAF6 overexpression. Its induction in cell cultures depends on many factors including a permissive cellular environment, expression of synphilin-1 (49) and a proteolytic cleavage that releases an inhibitory domain at the C-terminal (50). It will be interesting to assess whether TRAF6 may trigger aggregation of aSYN in these conditions. It also remains unclear the role of TRAF6-mediated atypical ubiquitination in the degradation of aSYN via the lysosomal/autophagy pathways (51).

Interestingly, TRAF6 expression seems increased in SN of sporadic PD brains. These data need to be validated in a larger sample size since the reproducibility of gene expression analysis of human post-mortem brains may suffer from sampling a heterogeneous tissue. If confirmed, this expression may be part of a cellular response to an excess burden of unfolded proteins, as shown for other E3 ubiquitin ligases.

However, TRAF6 may also ubiquitinate soluble aSYN in the brain and thus be important for aSYN physiological function and not necessarily for its recruitment to LBs. In this model, the increased expression of TRAF6 may be a response to its sequestration to LBs to maintain the appropriate post-translational modifications of its targets including aSYN. Further experiments are needed to verify this hypothesis.

In conclusion, our data indicate a role for TRAF6 in PD for its localization in LBs and handling of aggregation-prone misfolded proteins as atypical ubiquitin E3 ligase. These results pose new exciting questions about the role of atypical ubiquitination in cellular physiology and dysfunction.

MATERIALS AND METHODS

Further experimental details are provided as Supplementary Material.

Immunoprecipitation and western blot

For coimmunoprecipitation experiments, cells were lysed in TRAF6 (200 mM NaCl, 50 mM Tris, pH 7.5, 0.5% NP40, 10% glycerol) or aSYN (150 mM NaCl, 50 mM Tris, pH 7.5, 0.5% CHAPS) buffers supplemented with anti-protease cocktail (Roche) and 5 mM N-ethyl-maleimide (NEM). Cell lysates were incubated with anti-FLAG agarose beads (Sigma) or with the appropriate antibody. After washing, immunoprecipitated proteins were eluted with 2× sodium dodecyl sulphate (SDS) sample buffer, boiled and analyzed by western blot. The following antibodies were used: anti-FLAG 1:2000 (Sigma), anti-MYC 1:4000 (Cell Signaling), anti-HA 1:1000 (from ibridoma supernatant, kindly provided by Dr. Licio Collavin), anti-β-actin 1:5000 (Sigma). For detection, anti-mouse-horseradish peroxidase (HRP) and anti-rabbit-HRP (Dako) or protein A-HRP (Upstate) in combination with enhanced chemiluminescence (ECL) (GE Healthcare) were used.

In vivo ubiquitination assay

For *in vivo* ubiquitination assays, HEK cells were transfected with HA–ubiquitin and the indicated DJ-1, aSYN, TRAF6 or TRAF2 constructs. After transfection, cells were either left untreated or incubated with 10 μM MG132 for 3 h. Cells were then lysed with radioimmunoprecipitation assay (RIPA) buffer (150 mM NaCl, 50 mM Tris, pH 7.5, 1% Triton X-100, 1% deoxycholic acid and 0.1% SDS) and samples were briefly sonicated. After centrifugation, clear lysates were immunoprecipitated with anti-MYC, anti-FLAG or anti-GFP (Invitrogen) antibodies. Immunocomplexes were analyzed by western blot using anti-HA antibody to detect ubiquitin conjugates. For development, protein A-HRP was used.

Cell fractionation

Transfected HEK cells were lysed in a buffer containing 150 mM NaCl, 50 mM Tris, pH 7.5, and 0.2% Triton X-100, supplemented with protease inhibitor cocktail and 5 mM NEM (Sigma). Lysates were centrifuged at 20 000 *g* for 30 min at 4°C and separated into Triton X-100 soluble (supernatant) and insoluble (pellet) fractions. Insoluble pellets were resuspended in boiling sample buffer, sonicated and used for western blot analysis.

Immunocytochemistry and immunohistofluorescence

To detect insoluble aggregates of mutant DJ-1, immunocytochemistry was performed as previously described (14). After permeabilization, cells were fixed in 4% paraformaldehyde and indirect immunofluorescence was carried out following standard methods. Anti-FLAG (1:1000) and anti-ubiquitin (Dako) (1:50) antibodies were used. For detection, Alexa Fluor-405-labeled (blu) or -594-labeled (red) (Invitrogen) anti-mouse or anti-rabbit antibodies were used while GFP fluorescence was evidenced at 488 laser. Immunohistofluorescence on human post-mortem brain sections was performed as reported (52). Anti-TRAF6 antibodies were from Abnova (PAB0279) and Santa Cruz (sc-8409 and sc-7221). Mouse monoclonal (#2647) and rabbit polyclonal (#2628) anti-aSYN antibodies were from Cell Signaling. All images were collected using a confocal microscope (LEICA TCS SP2).

Post-mortem human brain samples

Brain samples are from the brain bank at the Institute of Neuropathology, Bellvitge Hospital (University of Barcelona, Spain). Samples were dissected at autopsy with the informed consent of patients or their relatives and the institutional approval of the Ethics Committee of the University of Barcelona. Brains were obtained from Caucasian, pathologically confirmed PD cases and age-matched controls (27). Briefly,

all cases of PD had suffered from classical PD, none of them had cognitive impairment and their neuropathological characterization was made according to the established criteria. Control healthy subjects showed the absence of neurological symptoms and of metabolic and vascular diseases, and the neuropathological study disclosed no abnormalities, including lack of AD and related pathology. The time between death and tissue preparation was in the range of 3–5 h. The ventral midbrain region was sectioned horizontally. The dark-pigmented zones of the SN were readily apparent from all surrounding structures and were then isolated from the ventral midbrain. SN autopsy tissues were immediately frozen for RNA extraction. For histological analysis, samples were cryoprotected with 30% sucrose in 4% formaldehyde, frozen in dry ice and stored at −80°C until use.

Quantitative real-time polymerase chain reaction

Total RNA from SN of six pathologically confirmed and three control subjects (27) was isolated using the TRIZOL reagent (Invitrogen). cDNA was obtained from 1 μg of purified RNA using the iSCRIPT™ cDNA Synhesis Kit (Bio-Rad). qPCR was performed using SYBR-Green PCR Master Mix (Applied Biosystem). Expression of TRAF6, CYLD, A20 and p62/SQSTM1 was analyzed using specific oligonucleotides.

SUPPLEMENTARY MATERIAL

Supplementary Material is available at *HMG* online.

ACKNOWLEDGEMENTS

We are indebted to all the members of the laboratory of Stefano Gustincich for discussions. We thank Prof. Peter T. Lansbury (Harvard Medical School, Cambridge, MA, USA) for aSYN cDNA, Dr. Sandro Goruppi (Tufts University, Boston, MA, USA) for TRAF2 constructs and Dr. Licio Collavin (University of Trieste, Italy) for anti-HA antibody. We thank Prof. Francesca Persichetti (University of Piemonte Orientale, Italy) for carefully reading the manuscript.

Conflict of Interest statement. None declared.

FUNDING

This work was supported by Telethon Grant GGP06268, The Giovanni Armenise-Harvard Foundation and the Italian Institute of Technology.

REFERENCES

1. Lesage, S. and Brice, A. (2009) Parkinson's disease: from monogenic forms to genetic susceptibility factors. *Hum. Mol. Genet.*, **18**, R48–R59.
2. Schlossmacher, M.G., Frosch, M.P., Gai, W.P., Medina, M., Sharma, N., Forno, L., Ochiishi, T., Shimura, H., Sharon, R., Hattori, N. *et al.* (2002) Parkin localizes to the Lewy bodies of Parkinson disease and dementia with Lewy bodies. *Am. J. Pathol.*, **160**, 1655–1667.
3. Ito, T. (2003) Dorfin localizes to Lewy bodies and ubiquitylates Synphilin-1. *J. Biol. Chem.*, **278**, 29106–29114.
4. Liani, E., Eyal, A., Avraham, E., Shemer, R., Szargel, R., Berg, D., Bornemann, A., Riess, O., Ross, C.A., Rott, R. *et al.* (2004) Ubiquitylation of synphilin-1 and alpha-synuclein by SIAH and its presence in cellular inclusions and Lewy bodies imply a role in Parkinson's disease. *Proc. Natl Acad. Sci. USA*, **101**, 5500–5505.
5. Shin, Y. (2005) The co-chaperone carboxyl terminus of Hsp70-interacting protein (CHIP) mediates alpha-synuclein degradation decisions between proteasomal and lysosomal pathways. *J. Biol. Chem.*, **280**, 23727–23734.
6. Chen, Z. and Sun, L. (2009) Nonproteolytic functions of ubiquitin in cell signaling. *Mol. Cell*, **33**, 275–286.
7. Xu, P., Duong, D.M., Seyfried, N.T., Cheng, D., Xie, Y., Robert, J., Rush, J., Hochstrasser, M., Finley, D. and Peng, J. (2009) Quantitative proteomics reveals the function of unconventional ubiquitin chains in proteasomal degradation. *Cell*, **137**, 133–145.
8. Ikeda, H. and Kerppola, T.K. (2008) Lysosomal localization of ubiquitinated Jun requires multiple determinants in a lysine-27-linked polyubiquitin conjugate. *Mol. Biol. Cell*, **19**, 4588–4601.
9. Chastagner, P., Israël, A. and Brou, C. (2006) Itch/AIP4 mediates Deltex degradation through the formation of K29-linked polyubiquitin chains. *EMBO Rep.*, **7**, 1147–1153.
10. Jiang, J., Ballinger, C.A., Wu, Y., Dai, Q., Cyr, D.M., Höhfeld, J. and Patterson, C. (2001) CHIP is a U-box-dependent E3 ubiquitin ligase: identification of Hsc70 as a target for ubiquitylation. *J. Biol. Chem.*, **276**, 42938–42944.
11. Al-Hakim, A.K., Zagorska, A., Chapman, L., Deak, M., Peggie, M. and Alessi, D.R. (2008) Control of AMPK-related kinases by USP9X and atypical Lys29/Lys33-linked polyubiquitin chains. *Biochem. J.*, **411**, 249.
12. Xu, K., Shimelis, H., Linn, D.E., Jiang, R., Yang, X., Sun, F., Guo, Z., Chen, H., Li, W., Chen, H. *et al.* (2009) Regulation of androgen receptor transcriptional activity and specificity by RNF6-induced ubiquitination. *Cancer Cell*, **15**, 270–282.
13. Pype, S., Declercq, W., Ibrahimi, A., Michiels, C., Van Rietschoten, J.G., Dewulf, N., De Boer, M., Vandenabeele, P., Huylebroeck, D. and Remacle, J.E. (2000) TTRAP, a novel protein that associates with CD40, tumor necrosis factor (TNF) receptor-75 and TNF receptor-associated factors (TRAFs), and that inhibits nuclear factor-kappa B activation. *J. Biol. Chem.*, **275**, 18586–18593.
14. Zucchelli, S., Vilotti, S., Calligaris, R., Lavina, Z.S., Biagioli, M., Foti, R., De Maso, L., Pinto, M., Gorza, M., Speretta, E. *et al.* (2009) Aggresome-forming TTRAP mediates pro-apoptotic properties of Parkinson's disease-associated DJ-1 missense mutations. *Cell Death Differ.*, **16**, 428–438.
15. Chen, Z. (2005) Ubiquitin signalling in the NF-kappaB pathway. *Nat. Cell Biol.*, **7**, 758–765.
16. Wu, H. and Arron, J. (2003) TRAF6, a molecular bridge spanning adaptive immunity, innate immunity and osteoimmunology. *Bioessays*, **25**, 1096–1105.
17. Khursigara, G., Orlinick, J.R. and Chao, M.V. (1999) Association of the p75 neurotrophin receptor with TRAF6. *J. Biol. Chem.*, **274**, 2597–2600.
18. Geetha, T., Jiang, J. and Wooten, M. (2005) Lysine 63 Polyubiquitination of the nerve growth factor receptor TrkA directs internalization and signaling. *Mol. Cell*, **20**, 301–312.
19. Babu, J., Geetha, T. and Wooten, M. (2005) Sequestosome 1/p62 shuttles polyubiquitinated tau for proteasomal degradation. *J. Neurochem.*, **94**, 192–203.
20. Lim, K.L., Chew, K.C., Tan, J.M., Wang, C., Chung, K.K., Zhang, Y., Tanaka, Y., Smith, W., Engelender, S., Ross, C.A. *et al.* (2005) Parkin mediates nonclassical, proteasomal-independent ubiquitination of Synphilin-1: implications for Lewy body formation. *J. Neurosci.*, **25**, 2002–2009.
21. Lee, J., Wheeler, T., Li, L. and Chin, L. (2007) Ubiquitination of alpha-synuclein by Siah-1 promotes alpha-synuclein aggregation and apoptotic cell death. *Hum. Mol. Genet.*, **17**, 906–917.
22. Polekhina, G., House, C.M., Traficante, N., Mackay, J.P., Relaix, F., Sassoon, D.A., Parker, M.W. and Bowtell, D.D. (2002) Siah ubiquitin ligase is structurally related to TRAF and modulates TNF-α signaling. *Nat. Struct. Biol.*, **9**, 68–75.
23. Humbert, J., Beyer, K., Carrato, C., Mate, J.L., Ferrer, I. and Ariza, A. (2007) Parkin and synphilin-1 isoform expression changes in Lewy body diseases. *Neurobiol. Dis.*, **26**, 681–687.
24. Choi, J., Levey, A.I., Weintraub, S.T., Rees, H.D., Gearing, M., Chin, L.S. and Li, L. (2004) Oxidative modifications and down-regulation of

ubiquitin carboxyl-terminal hydrolase L1 associated with idiopathic Parkinson's and Alzheimer's diseases. *J. Biol. Chem.*, **279**, 13256–13264.
25. Culpan, D., Cram, D., Chalmers, K., Cornish, A., Palmer, L., Palmer, J., Hughes, A., Passmore, P., Craigs, D., Wilcock, G.K. *et al.* (2009) TNFR-associated factor-2 (TRAF2) in Alzheimer's disease. *Neurobiol. Aging*, **30**, 1052–1060.
26. Sahara, N., Murayama, M., Mizoroki, T., Urushitani, M., Imai, Y., Takahashi, R., Murata, S., Tanaka, K. and Takashima, A. (2005) In vivo evidence of CHIP up-regulation attenuating tau aggregation. *J. Neurochem.*, **94**, 1254–1263.
27. Navarro, A., Boveris, A., Bández, M.J., Sanchez-Pinto, M.J., Gómez, C., Muntane, G. and Ferrer, I. (2009) Human brain cortex: mitochondrial oxidative damage and adaptative response in Parkinson disease and dementia with Lewy bodies. *Free Radic. Biol. Med.*, **46**, 1574–1580.
28. Wakabayashi, K., Tanji, K., Mori, F. and Takahashi, H. (2007) The Lewy body in Parkinson's disease: molecules implicated in the formation and degradation of alpha-synuclein aggregates. *Neuropathology*, **27**, 494–506.
29. Beyer, K., Domingo-Sàbat, M. and Ariza, A. (2009) Molecular pathology of lewy body diseases. *Int. J. Mol. Sci.*, **10**, 724–745.
30. Spillantini, M.G., Schmidt, M.L., Lee, V.M., Trojanowski, J.Q., Jakes, R. and Goedert, M. (1997) Alpha-synuclein in Lewy bodies. *Nature*, **388**, 839–840.
31. Olzmann, J.A., Li, L., Chudaev, M.V., Chen, J., Perez, F.A., Palmiter, R.D. and Chin, L.S. (2007) Parkin-mediated K63-linked polyubiquitination targets misfolded DJ-1 to aggresomes via binding to HDAC6. *J. Cell Biol.*, **178**, 1025–1038.
32. Biagioli, M., Pinto, M., Cesselli, D., Zaninello, M., Lazarevic, D., Roncaglia, P., Simone, R., Vlachouli, C., Plessy, C., Bertin, N. *et al.* (2009) Unexpected expression of alpha- and beta-globin in mesencephalic dopaminergic neurons and glial cells. *Proc. Natl Acad. Sci. USA*, **106**, 15454–15459.
33. Macedo, M.G., Anar, B., Bronner, I.F., Cannella, M., Squitieri, F., Bonifati, V., Hoogeveen, A., Heutink, P. and Rizzu, P. (2003) The DJ-1L166P mutant protein associated with early onset Parkinson's disease is unstable and forms higher-order protein complexes. *Hum. Mol. Genet.*, **12**, 2807–2816.
34. Olzmann, J.A., Brown, K., Wilkinson, K.D., Rees, H.D., Huai, Q., Ke, H., Levey, A.I., Li, L. and Chin, L.S. (2004) Familial Parkinson's disease-associated L166P mutation disrupts DJ-1 protein folding and function. *J. Biol. Chem.*, **279**, 8506–8515.
35. Shendelman, S., Jonason, A., Martinat, C., Leete, T. and Abeliovich, A. (2004) DJ-1 is a redox-dependent molecular chaperone that inhibits alpha-synuclein aggregate formation. *PLoS Biol.*, **2**, e362.
36. Herrera, F.E., Zucchelli, S., Jezierska, A., Lavina, Z.S., Gustincich, S. and Carloni, P. (2007) On the oligomeric state of DJ-1 protein and its mutants associated with Parkinson Disease. A combined computational and *in vitro* study. *J. Biol. Chem.*, **282**, 24905–24914.
37. Chin, L.S., Olzmann, J.A. and Li, L. (2010) Parkin-mediated ubiquitin signalling in aggresome formation and autophagy. *Biochem. Soc. Trans.*, **38**, 144–149.
38. Olzmann, J.A. and Chin, L.S. (2008) Parkin-mediated K63-linked polyubiquitination: a signal for targeting misfolded proteins to the aggresome–autophagy pathway. *Autophagy*, **4**, 85–87.
39. Subauste, C.S., Andrade, R.M. and Wessendarp, M. (2007) CD40-TRAF6 and autophagy-dependent anti-microbial activity in macrophages. *Autophagy*, **3**, 245–248.
40. Auluck, P.K., Chan, H.Y., Trojanowski, J.Q., Lee, V.M. and Bonini, N.M. (2002) Chaperone suppression of alpha-synuclein toxicity in a *Drosophila* model for Parkinson's disease. *Science*, **295**, 865–868.
41. Qiao, L., Hamamichi, S., Caldwell, K.A., Caldwell, G.A., Yacoubian, T.A., Wilson, S., Xie, Z.L., Speake, L.D., Parks, R., Crabtree, D. *et al.* (2008) Lysosomal enzyme cathepsin D protects against alpha-synuclein aggregation and toxicity. *Mol. Brain*, **1**, 17.
42. Kuwahara, T., Koyama, A., Koyama, S., Yoshina, S., Ren, C.H., Kato, T., Mitani, S. and Iwatsubo, T. (2008) A systematic RNAi screen reveals involvement of endocytic pathway in neuronal dysfunction in alpha-synuclein transgenic *C. elegans*. *Hum. Mol. Genet.*, **17**, 2997–3009.
43. Nagano, Y., Yamashita, H., Takahashi, T., Kishida, S., Nakamura, T., Iseki, E., Hattori, N., Mizuno, Y., Kikuchi, A. and Matsumoto, M. (2003) Siah-1 facilitates ubiquitination and degradation of Synphilin-1. *J. Biol. Chem.*, **278**, 51504–51514.
44. Engelender, S. (2008) Ubiquitination of alpha-synuclein and autophagy in Parkinson's disease. *Autophagy*, **4**, 372–374.
45. Hasegawa, M., Fujiwara, H., Nonaka, T., Wakabayashi, K., Takahashi, H., Lee, V.M., Trojanowski, J.Q., Mann, D. and Iwatsubo, T. (2002) Phosphorylated alpha-synuclein is ubiquitinated in alpha-synucleinopathy lesions. *J. Biol. Chem.*, **277**, 49071–49076.
46. Tofaris, G.K., Razzaq, A., Ghetti, B., Lilley, K.S. and Spillantini, M.G. (2003) Ubiquitination of alpha-synuclein in Lewy bodies is a pathological event not associated with impairment of proteasome function. *J. Biol. Chem.*, **278**, 44405–44411.
47. Anderson, J.P., Walker, D.E., Goldstein, J.M., de Laat, R., Banducci, K., Caccavello, R.J., Barbour, R., Huang, J., Kling, K., Lee, M. *et al.* (2006) Phosphorylation of Ser-129 is the dominant pathological modification of alpha-synuclein in familial and sporadic Lewy body disease. *J. Biol. Chem.*, **281**, 29739–29752.
48. Rott, R., Szargel, R., Haskin, J., Shani, V., Shainskaya, A., Manov, I., Liani, E., Avraham, E. and Engelender, S. (2008) Monoubiquitylation of alpha-synuclein by seven in absentia homolog (SIAH) promotes its aggregation in dopaminergic cells. *J. Biol. Chem.*, **283**, 3316–3328.
49. Engelender, S., Kaminsky, Z., Guo, X., Sharp, A.H., Amaravi, R.K., Kleiderlein, J.J., Margolis, R.L., Troncoso, J.C., Lanahan, A.A., Worley, P.F. *et al.* (1999) Synphilin-1 associates with alpha-synuclein and promotes the formation of cytosolic inclusions. *Nat. Genet.*, **22**, 110–114.
50. Li, W., West, N., Colla, E., Pletnikova, O., Troncoso, J.C., Marsh, L., Dawson, T.M., Jäkälä, P., Hartmann, T., Price, D.L. *et al.* (2005) Aggregation promoting C-terminal truncation of alpha-synuclein is a normal cellular process and is enhanced by the familial Parkinson's disease-linked mutations. *Proc. Natl Acad. Sci. USA*, **102**, 2162–2167.
51. Cuervo, A.M., Stefanis, L., Fredenburg, R., Lansbury, P.T. and Sulzer, D. (2004) Impaired degradation of mutant alpha-synuclein by chaperone-mediated autophagy. *Science*, **305**, 1292–1295.
52. Waldvogel, H.J., Curtis, M.A., Baer, K., Rees, M.I. and Faull, R.L. (2006) Immunohistochemical staining of post-mortem adult human brain sections. *Nat. Protoc.*, **1**, 2719–2732.

Neurobiology:

Tumor Necrosis Factor Receptor-associated Factor 6 (TRAF6) Associates with Huntingtin Protein and Promotes Its Atypical Ubiquitination to Enhance Aggregate Formation

Silvia Zucchelli, Federica Marcuzzi, Marta Codrich, Elena Agostoni, Sandra Vilotti, Marta Biagioli, Milena Pinto, Alisia Carnemolla, Claudio Santoro, Stefano Gustincich and Francesca Persichetti

J. Biol. Chem. 2011, 286:25108-25117.
doi: 10.1074/jbc.M110.187591 originally published online March 25, 2011

THE JOURNAL OF BIOLOGICAL CHEMISTRY VOL. 286, NO. 28, pp. 25108–25117, July 15, 2011

Tumor Necrosis Factor Receptor-associated Factor 6 (TRAF6) Associates with Huntingtin Protein and Promotes Its Atypical Ubiquitination to Enhance Aggregate Formation*[S]

Received for publication, September 22, 2010, and in revised form, March 24, 2011 Published, JBC Papers in Press, March 25, 2011, DOI 10.1074/jbc.M110.187591

Silvia Zucchelli[‡§¶], Federica Marcuzzi[‡], Marta Codrich[‡], Elena Agostoni[‡], Sandra Vilotti[‡], Marta Biagioli[‡¶], Milena Pinto[‡], Alisia Carnemolla[‡], Claudio Santoro[‖], Stefano Gustincich[‡§¶], and Francesca Persichetti[‡1]**

*From the [‡]Sector of Neurobiology, International School for Advanced Studies (SISSA), via Bonomea 265, 34136 Trieste, Italy, the [§]SISSA Unit, Italian Institute of Technology, via Bonomea 265, 34136 Trieste, Italy, [¶]The Giovanni Armenise-Harvard Foundation Laboratory, SISSA, via Bonomea 265, 34136 Trieste, Italy, the [‖]Department of Medical Sciences, University of Eastern Piedmont, Viale Solari 17, 28100 Novara, Italy, and the **Department of Environmental and Life Sciences, University of Eastern Piedmont, Viale T. Michel 11, 15121 Alessandria, Italy*

Huntington disease (HD) is a neurodegenerative disorder caused by an expansion of polyglutamines in the first exon of huntingtin (*HTT*), which confers aggregation-promoting properties to amino-terminal fragments of the protein (N-HTT). Mutant N-HTT aggregates are enriched for ubiquitin and contain ubiquitin E3 ligases, thus suggesting a role for ubiquitination in aggregate formation. Here, we report that tumor necrosis factor receptor-associated factor 6 (TRAF6) binds to WT and polyQ-expanded N-HTT *in vitro* as well as to endogenous full-length proteins in mouse and human brain *in vivo*. Endogenous TRAF6 is recruited to cellular inclusions formed by mutant N-HTT. Transient overexpression of TRAF6 promotes WT and mutant N-HTT atypical ubiquitination with Lys[6], Lys[27], and Lys[29] linkage formation. Both interaction and ubiquitination seem to be independent from polyQ length. In cultured cells, TRAF6 enhances mutant N-HTT aggregate formation, whereas it has no effect on WT N-HTT protein localization. Mutant N-HTT inclusions are enriched for ubiquitin staining only when TRAF6 and Lys[6], Lys[27], and Lys[29] ubiquitin mutants are expressed. Finally, we show that TRAF6 is up-regulated in post-mortem brains from HD patients where it is found in the insoluble fraction. These results suggest that TRAF6 atypical ubiquitination warrants investigation in HD pathogenesis.

Huntington disease (HD)[2] is a dominantly inherited neurodegenerative disorder caused by the expansion of a polymorphic CAG sequence in the first exon of the gene encoding for huntingtin (HTT) protein (1). The onset of HD symptoms, including motor dysfunction and cognitive decline, occurs when the length of CAG exceeds 36 repeats (2). CAG triplets are translated into a series of uninterrupted glutamine residues (polyQ) at the N terminus of HTT, a ubiquitously expressed protein of ~350 kDa. HTT is found both in the nucleus and in the cytoplasm where it associates with a variety of organelles, including endoplasmic reticulum, Golgi apparatus, and mitochondria (3–5). This widespread subcellular localization, associated with the ability to interact with a large number of proteins, implicates HTT in diverse cellular activities ranging from transcription and energy metabolism to vesicle trafficking (6).

The elongation of the polyQ sequence in HTT protein induces HD pathogenesis largely through a gain-of-function mechanism. One hallmark of HD is the presence of neuronal aggregates that contain N-terminal fragments of polyQ HTT (N-HTT). Aggregates or inclusions are found primarily in the striatum and in the cortex of HD patients and are located mainly in nuclear, perinuclear, and cytoplasmic regions of affected neurons (7). Although it is still unclear whether inclusions are protective or detrimental for cell viability, their formation seems to be strikingly connected to the propensity of polyQ N-HTT to misfold. In addition to mutant N-HTT, inclusions are enriched for components of the protein quality control machinery, such as ubiquitin, proteasome subunits, and chaperones (7, 8).

An extensive proteomic study has demonstrated that global changes to the ubiquitin system are associated with HD pathology (9). Although the E3 ligase Hdr1 and the ubiquitin-conjugating enzymes E2–25K interact and ubiquitinate both WT and mutant HTT (10, 11), parkin and CHIP (C terminus of Hsc70-interacting protein) selectively act on the mutant protein (12, 13). All of these are localized in the aggregates of HD post-mortem brains and are able to decrease aggregate formation *in vitro*.

Ubiquitin contains seven lysine residues, and it is assumed that all of these can be involved in the formation of polyubiquitin chains on target proteins. Canonical Lys[48]- and Lys[63]-linked polyubiquitination has been related respectively to proteasome degradation of the substrate and to cell signaling or aggresome formation (14). The role of nonconventional chains via Lys[6], Lys[11], Lys[27], Lys[29], and Lys[33] is much less clear (15). It has been

* This work was supported by the Telethon Foundation of Italy (Grant GGP07185) and the Italian Institute of Technology.
⌘ *Author's Choice*—Final version full access.
[S] The on-line version of this article (available at http://www.jbc.org) contains supplemental Figs. S1 and S2.
[1] To whom correspondence should be addressed: Dipartimento di Scienze dell'Ambiente e della Vita, Universita' degli Studi del Piemonte Orientale, Viale T. Michel 11, 15121 Alessandria, Italy. Tel.: 39-040-3787-774; Fax: 39-040-3787-702; E-mail: francesca.persichetti@mfn.unipmn.it.
[2] The abbreviations used are: HD, Huntington disease; HTT, huntingtin; polyQ, polyglutamine; N-HTT, amino-terminal fragment of huntingtin; TRAF6, TNF receptor-associated factor 6; PD, Parkinson disease; DN, deleted of the N terminus.

shown that Lys^{6}-specific modification can protect substrates from proteolysis (16, 17) or regulate their enzymatic activity (18). Similarly, nondegradative functions have been associated with Lys^{27} and Lys^{29} chains, which have been shown to control subcellular localization and activity of targeted proteins (19–21).

Tumor necrosis factor receptor-associated factor 6 (TRAF6) is an E3 ubiquitin ligase that promotes Lys^{63}-specific chain assembly in the signal transduction pathway that leads ultimately to NFκB activation (22). In the brain, TRAF6 activity has been associated with the transduction cascade of the neurotrophin receptors p75 and TrkA (23, 24). Interestingly, TRAF6 localizes to Tau inclusions and Lewy bodies in brains of Alzheimer disease and Parkinson disease (PD) patients, respectively (25, 26), supporting the idea that E3 ligases tend to accumulate at the site of protein inclusions. Furthermore, TRAF6 was found to promote atypical Lys^{6}-, Lys^{27}-, and Lys^{29}-mediated poly-ubiquitination of mutant DJ-1 and α-synuclein, proteins relevant for PD pathogenesis. Atypical ubiquitin ligase activity of TRAF6 was shown to induce mutant DJ-1 aggregation (26).

In the current study, we provide evidence that TRAF6 interacts with and ubiquitinates WT and mutant HTT. In analogy to PD targets, TRAF6 promotes an atypical mode of polyubiquitin chain formation onto N-HTT proteins with selective choice of Lys^{6}, Lys^{27}, and Lys^{29} linkages. We also show that both overexpressed and endogenous TRAF6 is recruited at the site of mutant N-HTT aggregates. Furthermore, TRAF6-mediated ubiquitination stimulates the formation of mutant N-HTT inclusions. Only when atypical Lys^{6}, Lys^{27}, and Lys^{29} ubiquitins are expressed, N-HTT aggregates are strongly positive for ubiquitin. Finally, in post-mortem brains of HD patients, TRAF6 expression is induced, and the protein preferentially accumulates in the insoluble fraction. Altogether, our data imply a novel role for TRAF6 and atypical ubiquitination in HD pathogenesis.

EXPERIMENTAL PROCEDURES

Plasmids and Cells—N-HTT-GFP Gln^{21} and Gln^{150} constructs were described previously (27). N-HTT-GFP Gln^{60} was a serendipitous construct obtained during Gln^{150} plasmid preparation. It was sequence-verified and controlled during each preparation. FLAG-TRAF6 (WT and DN) and HA-ubiquitin (WT and mutants) were described elsewhere (26).

HEK 293 cells (Sigma) were maintained in culture in DMEM (Invitrogen) with 10% FBS (Sigma). Transfections were performed with the standard calcium phosphate method or with Lipofectamine 2000 (Invitrogen), as required.

Immunoprecipitation and Western Blot—For co-immunoprecipitation experiments, cells were lysed in TRAF6 buffer (200 mM NaCl, 50 mM Tris, pH 7.5, 0.5% Nonidet P-40, 10% glycerol) supplemented with anti-protease mixture (Roche Applied Science) and 5 mM *N*-ethylmaleimide. Cell lysates were incubated with anti-FLAG-agarose beads (Sigma) or with anti-GFP antibody (Invitrogen). For co-immunoprecipitation of endogenous proteins anti-HTT mouse monoclonal (Chemicon, catalog nos. MAB 2166 and MAB 5490) and rabbit polyclonal HP1 (27) antibodies were used. Cortex was dissected from homozygous Hdh^{Q111} knock-in mice (28) or control littermates, snap-frozen on liquid nitrogen, and stored at −80 °C. Parietal cortex from HD patients was used for co-immunoprecipitation of endogenous proteins in the human brain sample. Lysates were prepared homogenizing tissue in modified TRAF6 buffer (150 mM NaCl, 50 mM Tris, pH 7.5, 0.5% Nonidet P-40, 10% glycerol) supplemented with anti-protease mixture. Total protein content was measured, and an equivalent amount was used for co-immunoprecipitation. After washing, immunoprecipitated proteins were eluted with 2× SDS sample buffer, boiled, and analyzed by Western blot. The following antibodies were used: anti-FLAG (1:2000; Sigma), anti-GFP (1:1000; Invitrogen), anti-HA (1:1000; from hybridoma supernatant, kindly provided by Dr. Licio Collavin), anti-HTT (Chemicon, catalog no. MAB 2166), anti-TRAF6 (Santa Cruz Biotechnology, catalog no. sc-7221), and anti-β-actin (1:5000; Sigma). For detection, anti-mouse-HRP and anti-rabbit-HRP (Dako) or protein A-HRP (Upstate) in combination with ECL (GE Healthcare) were used. For total protein extracts, cells were lysed directly in 2× SDS sample buffer and analyzed by Western blot.

Cell-based Ubiquitination Assay—For cell-based ubiquitination assays, HEK cells were transfected with HA-ubiquitin, FLAG-TRAF6 (WT or DN), and N-HTT-GFP constructs. After transfection, cells were lysed with radioimmune precipitation assay buffer (150 mM NaCl, 50 mM Tris, pH 7.5, 1% Triton X-100, 1% deoxycholic acid, 0.1% SDS), and samples were briefly sonicated. After centrifugation, clear lysates were immunoprecipitated with anti-GFP or anti-FLAG antibodies. Immunocomplexes were analyzed by Western blot using anti-HA antibody to detect ubiquitin conjugates. For development, protein A-HRP was used.

Immunocytochemistry—Indirect immunofluorescence was carried out following standard methods (29). Anti-FLAG (1:1000; SIGMA), anti-ubiquitin (1:50; Dako) and anti-TRAF6 (1:100; catalog no. sc-8409, Santa Cruz Biotechnology) antibodies were used. For detection, Alexa Fluor 405 (blue) or 594 (red) (Invitrogen) labeled anti-mouse or anti-rabbit antibodies were used. All images were collected using a confocal microscope (Leica TCS SP2). The analysis of aggregates was performed on high resolution images using ImageJ software. At least 200 cells from two independent experiments were counted and scored for percentage of cells with aggregates. For the analysis of aggregate size, only cells ($n = 200$) with comparable levels of TRAF6 expression, as determined by fluorescence intensity normalized to cell area, were used. N-HTT cytoplasmic staining was quantified on the same cells on a randomly selected area. Background fluorescence was quantified from an area placed outside the cells and was subtracted to each signal.

Human Post-mortem Brain Samples—Control and HD post-mortem brain tissues used in this study were collected by the Harvard Brain Tissue Resource Center, McLean Hospital (Belmont, MA) and described previously (30). HD brains were assigned Vonsattel grade 3 pathology (31). Post-mortem intervals were from 12 to 32 h for controls and from 8 to 30 h for HD

brains. Total proteins were extracted from parietal cortex in 10% SDS. Fractionation in soluble and insoluble protein extracts was performed from the cortex as follows; soluble fractions were extracted in 150 mM sucrose, 15 mM Hepes, pH 7.9, 60 mM KCl, 15 mM NaCl, 5 mM EDTA, 1 mM EGTA, 1% Triton X-100), supplemented with protease inhibitors (Roche Applied Science). After centrifugation, the soluble fraction was removed, and the insoluble fractions were extracted from pel-

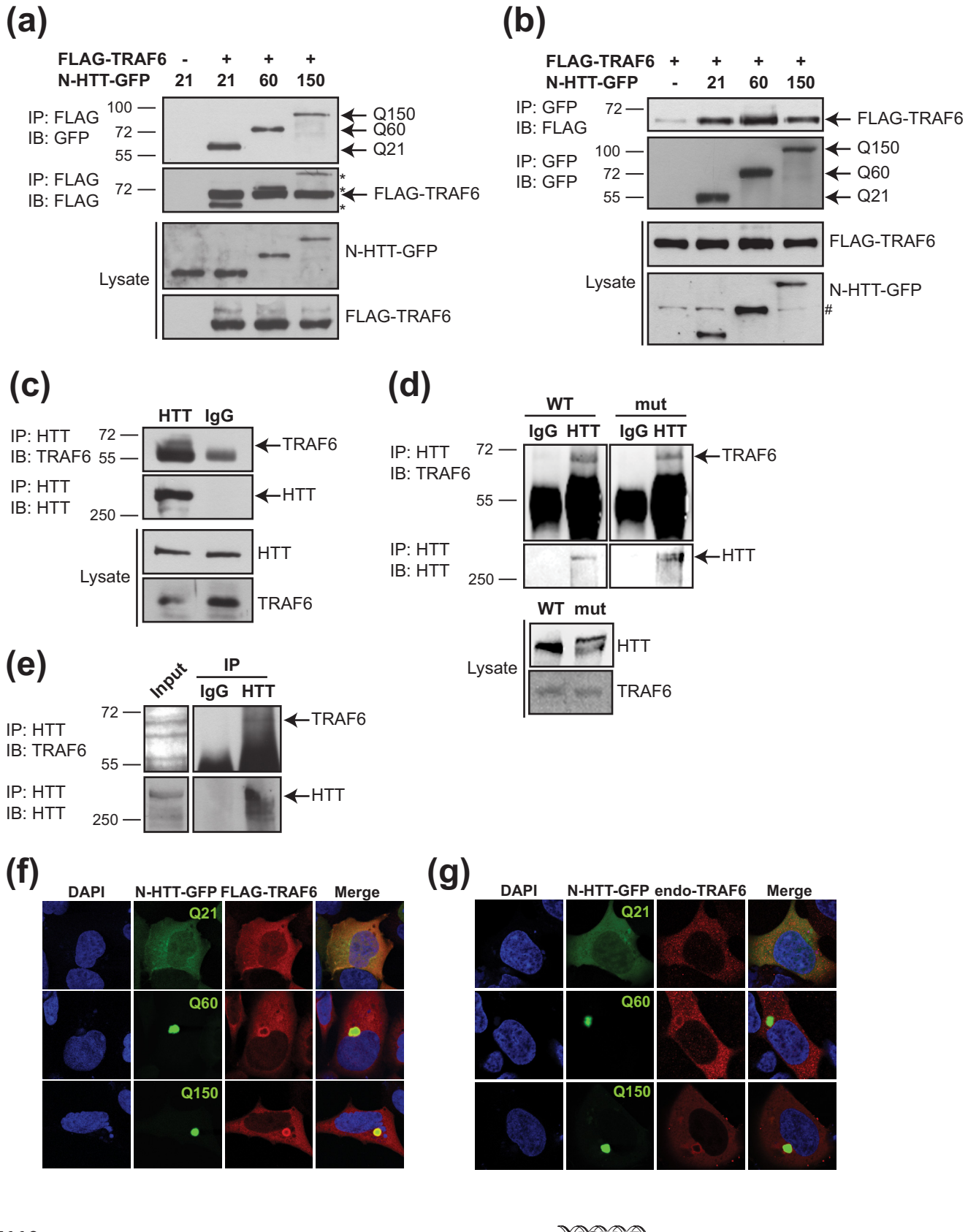

lets in 10% SDS. For Western blot analysis, anti-TRAF6 polyclonal (Santa Cruz Biotechnology, catalog no. sc-7221) and monoclonal (Santa Cruz Biotechnology, catalog no. sc-8409) antibodies were used.

Quantitative Real-time PCR—Total RNA from cortex of pathologically confirmed HD and control subjects was isolated using the TRIzol reagent (Invitrogen). cDNA was obtained from 1 μg of purified RNA using the iSCRIPT^{TM} cDNA Synthesis Kit (Bio-Rad). Quantitative real-time PCR was performed using SYBR-Green PCR Master Mix (Applied Biosystem). Expression of TRAF6 was analyzed as already described (26).

Statistical Analysis—All experiments were repeated in duplicate or more. Confocal images were analyzed with ImageJ software. Western blot scans were quantified with Adobe Photoshop CS3. Data represent the mean with standard deviation. When necessary, each group was compared individually with reference to the control group using Student's *t* test (Microsoft Excel software).

RESULTS

E3 Ubiquitin Ligase TRAF6 Interacts with WT and Mutant HTT and Associates with Polyglutamine Aggregates—To evaluate whether TRAF6 might have a role in HD, we studied its ability to bind huntingtin amino-terminal fragments (residues 1–171) fused to green fluorescent protein (N-HTT-GFP), with either a physiological (Gln^{21}), or short (Gln^{60}) or long (Gln^{150}) pathological polyQ stretch. N-HTT-GFP constructs were transfected in HEK 293 cells with FLAG-TRAF6 or FLAG-empty vector, as control. Immunoprecipitation of transfected cell lysates revealed a specific binding between TRAF6 and N-HTT with no evident selectivity for polyQ length (Fig. 1*a*). Reverse co-immunoprecipitation of transfected proteins confirmed that TRAF6 physically associated with N-HTT with a physiological and pathological polyQ stretch (Fig. 1*b*).

We then performed co-immunoprecipitation experiments in HEK 293 cells on endogenous proteins proving TRAF6 interaction with full-length WT HTT *in vitro* (Fig. 1*c*). The cortex from control WT and *Hdh*^{Q111} knock-in mice were also analyzed, showing that TRAF6 specifically binds full-length HTT *in vivo* with no preference for WT or expanded polyQ-containing protein (Fig. 1*d*). This interaction was confirmed *in vivo* in the parietal cortex from HD post-mortem brains (Fig. 1*e*).

We then analyzed TRAF6 localization in cells that express WT or mutant N-HTT. WT N-HTT was located both in the cytoplasm and the nucleus, with a diffused staining throughout the cell. TRAF6 was mainly present in the cytoplasm and partially in the nucleus, where it co-localized with WT N-HTT (Fig. 1, *f* and *g*). Similar data were obtained with overexpressed and endogenous TRAF6. Overexpression of WT N-HTT did not alter TRAF6 cellular localization (data not shown). When transfected in cells, mutant N-HTT-GFP (Gln^{60} and Gln^{150}) developed fluorescent aggregates, as expected, located in the cytoplasm and concentrated in perinuclear regions. The presence of mutant N-HTT aggregates induced the recruitment of TRAF6 at the site of N-HTT inclusions, with a more prominent accumulation at the border (Fig. 1, *f* and *g*).

Altogether, these results demonstrate that TRAF6 binds huntingtin *in vitro* and *in vivo* in a polyQ length-independent

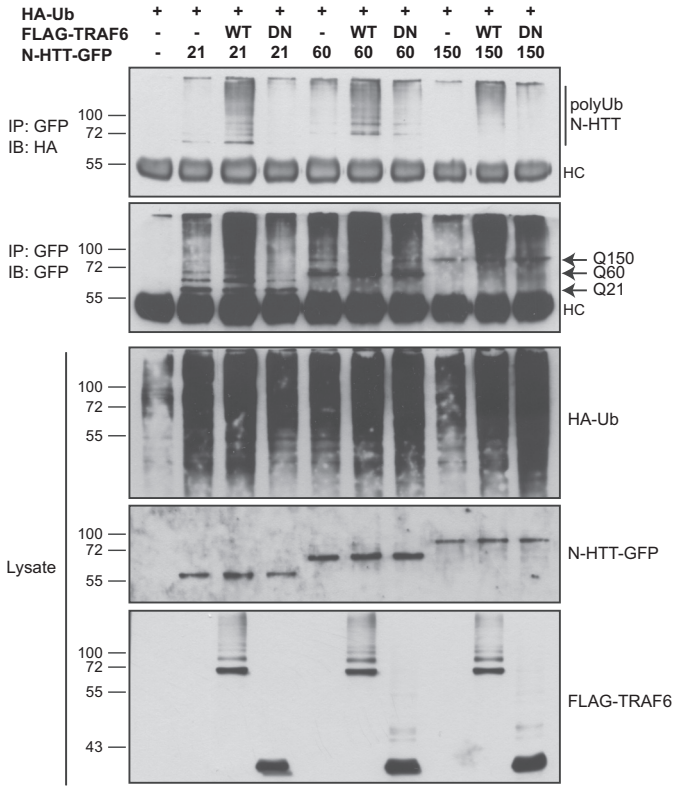

FIGURE 2. **TRAF6 enhances ubiquitination of WT and mutant N-HTT.** For ubiquitination assay, HEK 293 cells were transfected with HA-ubiquitin and N-HTT-GFP Gln^{21} (Q21), Gln^{60} (Q60), and Gln^{150} (Q150) constructs with WT or DN FLAG-TRAF6. Lysates were immunoprecipitated (*IP*) with anti-GFP antibody, and ubiquitinated N-HTT protein was revealed with anti-HA. Input lysates were analyzed with anti-HA, anti-GFP, and anti-FLAG antibodies. Molecular mass markers (kDa) are indicated on the *left*. *HC*, heavy chain; *IB*, immunoblot; *Ub*, ubiquitin.

FIGURE 1. **TRAF6 interacts with WT and mutant N-HTT *in vitro* and full-length proteins *in vivo* and accumulates in mutant N-HTT aggregates.** *a*, HEK 293 cells were transfected with FLAG-TRAF6, and the huntingtin N-terminal fragment fused to GFP (N-HTT-GFP) with WT (Gln^{21}, Q21) or mutated (Gln^{60}, Q60 and Gln^{150}, Q150) polyglutamine expansion. Lysates were immunoprecipitated (*IP*) with anti-FLAG beads, and bound proteins were revealed by immunoblot (*IB*) with anti-GFP, Q150 and anti-FLAG antibodies. Lysates were tested for the expression of TRAF6 and N-HTT proteins. Molecular mass markers (kDa) are indicated on the *left*. *b*, cells were transfected with FLAG-TRAF6 and N-HTT-GFP constructs as indicated. Lysates were immunoprecipitated with anti-GFP. Bound proteins and lysates were analyzed with anti-FLAG and anti-GFP antibodies. An *asterisk* represents N-HTT bands from previous development of the same gel. # represents an unspecific band. *c*, HEK 293 cell lysates were immunoprecipitated with anti-HTT or control IgG (as indicated), and bound endogenous proteins were revealed with anti-TRAF6 and anti-HTT antibodies. *d*, the cortex from WT and homozygous *Hdh*^{Q111} (*mut*) mice was dissected, lysed, and used for immunoprecipitation of endogenous TRAF6 and full-length HTT proteins. *e*, the parietal cortex from HD post-mortem brain was lysed and processed for co-immunoprecipitation of endogenous proteins as in *d*. *f*, HEK 293 cells were transfected as in *a*. TRAF6 was visualized by indirect immunofluorescence with anti-FLAG antibody (*red*). N-HTT was visible by GFP autofluorescence (*green*). Nuclei were visualized with DAPI (*blue*). *g*, cells were transfected with N-HTT-GFP constructs. Endogenous TRAF6 was stained with anti-TRAF6 antibody (*red*).

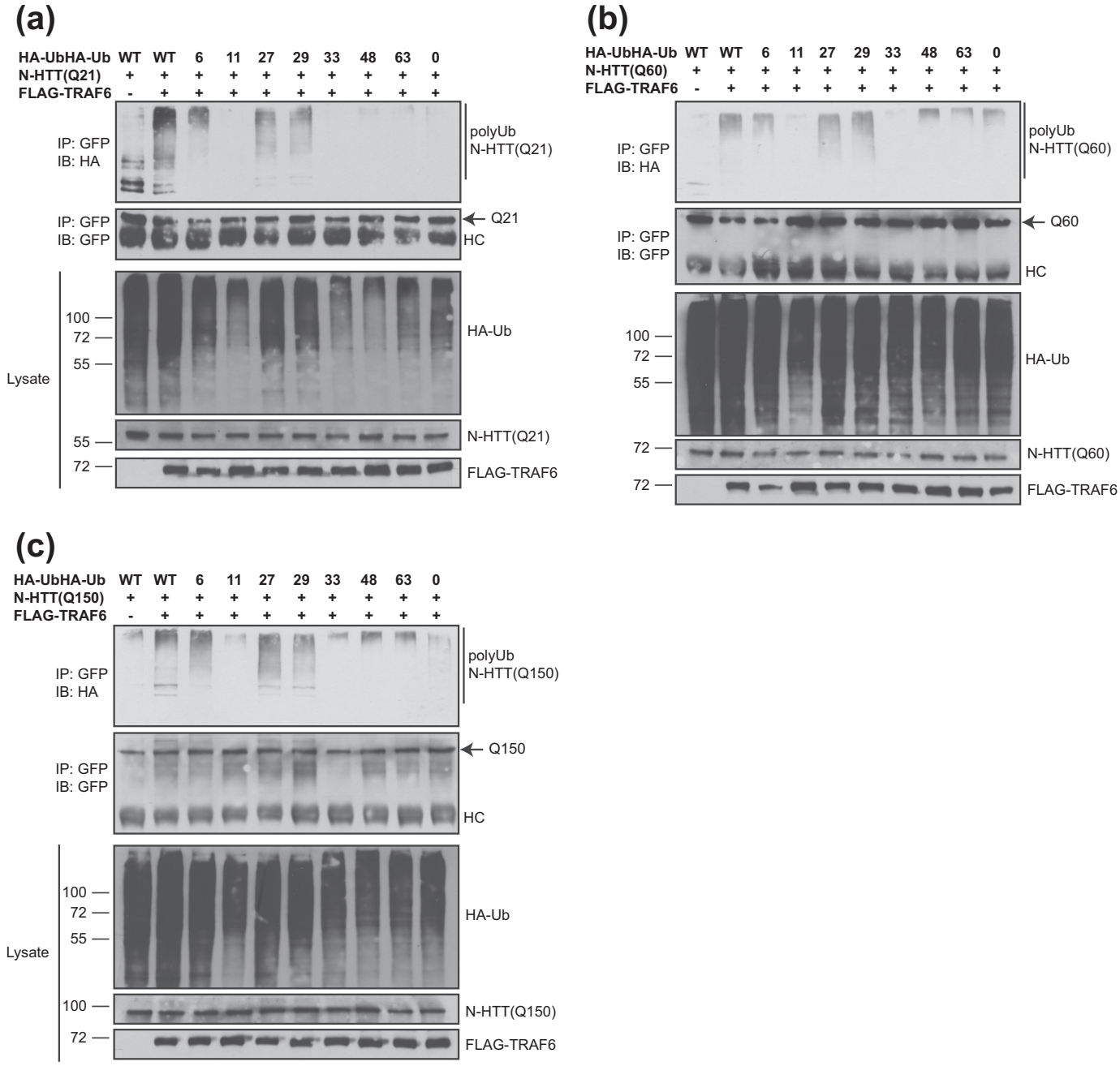

FIGURE 3. **TRAF6 promotes atypical ubiquitination of WT and mutant N-HTT.** HA-ubiquitin (*Ub*) mutants were used in which only the indicated lysine is available for chain formation. WT and Lys^0 ubiquitin were included as controls. HEK 293 cells were transfected with HA-ubiquitin mutant (as indicated), FLAG-TRAF6, and N-HTT-GFP Gln^{21} (Q21) (*a*), Gln^{60} (Q60) (*b*), and Gln^{150} (Q150) (*c*). Ubiquitination was monitored with anti-HA, anti-GFP, and anti-FLAG antibodies. *IB*, immunoblot; *IP*, immunoprecipitation; *HC*, heavy chain.

manner. Furthermore, mutant protein can sequester TRAF6 into cellular aggregates.

TRAF6 Facilitates Atypical Polyubiquitination of WT and Mutant N-HTT—The interaction between TRAF6 and N-HTT and their co-localization in polyglutamine aggregates raised the possibility that N-HTT might be target of TRAF6 E3 ubiquitin ligase activity. To test this hypothesis, we performed ubiquitination assay in HEK 293 cells. Cells were transfected with HA-ubiquitin, N-HTT-GFP with 21, 60, or 150 polyQ segment and with or without FLAG-TRAF6. A TRAF6 mutant deleted of the N-terminal E3 ligase domain (DN) also was included as control. We found that overexpression of WT TRAF6, but not of DN mutant, facilitated the formation of high molecular weight polyubiquitinated forms of N-HTT (Fig. 2). TRAF6 activity was evident toward N-HTT with physiological length of polyQ stretch (Gln^{21}) and for pathological mutants (Gln^{60} and Gln^{150}). Therefore, TRAF6 ubiquitin-ligase activity did not seem to be polyQ-dependent, as already seen for its binding capability.

Because we have shown recently that TRAF6 can promote unconventional ubiquitin linkages on target proteins (26), we investigated the mode of polyubiquitination mediated by TRAF6 onto N-HTT. We thus took advantage of a set of ubiquitin mutants that we have generated with only one lysine avail-

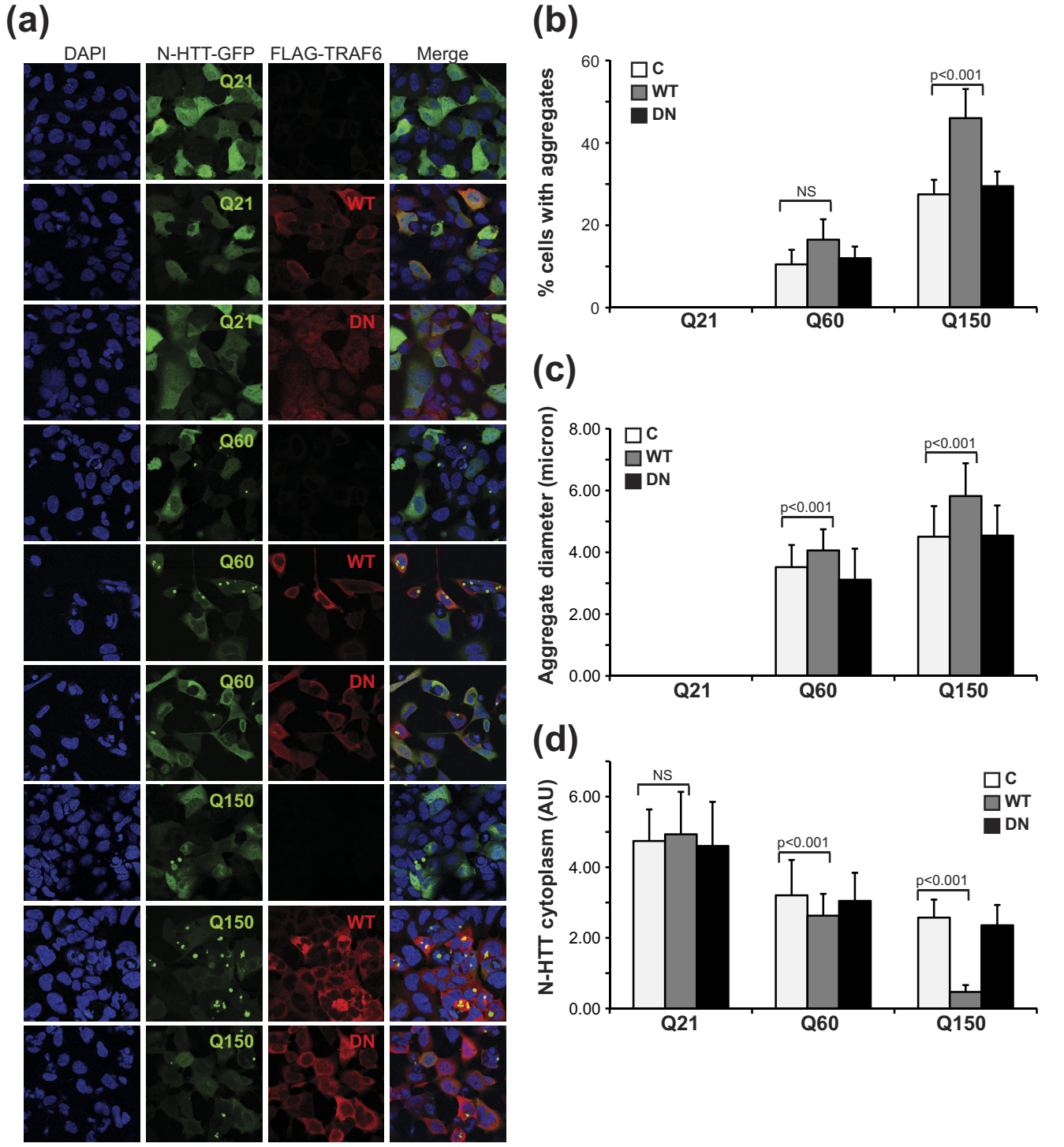

FIGURE 4. **TRAF6 enhances aggregate formation.** *a*, HEK 293 cells were transfected with N-HTT-GFP alone (*C*, control), or with FLAG-TRAF6 (WT or DN), as indicated. Immunofluorescence was performed with anti-FLAG (*red*) antibody. Nuclei were visualized with DAPI (*blue*). GFP was followed by autoflorescence. Confocal images from two independent experiments were scored for percentage of cells with aggregates (*b*), aggregate average size (*c*), and N-HTT cytoplasmic diffuse staining (*d*). At least 200 cells per experimental condition were counted. Data were analyzed with ImageJ software. Statistical analysis was performed with a *t* test. *NS*, not significant. *AU*, arbitrary units.

able for chain formation (remaining lysine residues were substituted with arginine). An ubiquitin mutant with all lysines substituted with arginine was also included as negative control (Lys^0). Cell-based ubiquitination assay was performed with all N-HTT constructs with or without TRAF6 and in combination with ubiquitin mutants. TRAF6 promoted a robust polyubiquitination of WT N-HTT in the presence of Lys^6, Lys^{27}, and Lys^{29} mutants. Background signals were observed with Lys^0 mutant (Fig. 3*a*). Similar results were obtained with mutant N-HTT with short (Gln^{60}) or long (Gln^{150}) polyQ stretch (Fig. 3, *b* and *c*).

Therefore, we conclude that TRAF6 promotes an atypical polyubiquitination of WT and mutant N-HTT that is inde-

pendent from polyQ length. Lys^{6}, Lys^{27}, and Lys^{29} are the preferred lysine residues for linkage formation.

TRAF6-mediated Ubiquitination Increases Mutant N-HTT Aggregates—When expressed in cells, Gln^{60} and Gln^{150} mutant, but not Gln^{21} N-HTT, generated aggregates, with an average size and number that correlate with polyQ length. We examined the influence of TRAF6-mediated ubiquitination on mutant N-HTT aggregation by transient transfection in HEK 293 cells. We included WT N-HTT as an internal reference in all our experiments. Only cells with comparable levels of TRAF6 expression (WT and DN), as determined by fluorescence intensity normalized to cell area, were used for analysis of aggregate number and size. The residual diffuse cytoplasmic staining was also quantified as additional indication of protein segregation into aggregates. TRAF6 overexpression had no influence on WT N-HTT cellular localization, with a diffuse cytoplasmic and nuclear staining as expected (Fig. 4*a*). Mutant N-HTT formed cytoplasmic and perinuclear aggregates, whose number and size correlated with polyQ length (Fig. 4*a*). Overexpression of TRAF6 increased the percentage of cells with aggregates and promoted the formation of inclusions with an average larger size (Fig. 4, *b* and *c*). This is likely due to a redistribution of the mutant protein to inclusions, as total protein levels were not affected by TRAF6 (supplemental Fig. S1) (compatible with a nondegradative role of atypical ubiquitination) and diffuse cytoplasmic staining decreased when aggregate number and size increased (Fig. 4*d*). The expression of TRAF6 DN mutant had no effect on percentage, size, and distribution of N-HTT aggregates, thus indicating that TRAF6 E3 ligase activity is required for its function on mutant N-HTT inclusion formation.

Because TRAF6 is recruited at the site of N-HTT aggregates and affects inclusion formation, we asked whether mutant protein might affect TRAF6 E3 ligase activity. To do so, we followed TRAF6 autoubiquitination by immunoprecipitation assay. We included WT N-HTT as an internal control. We found no differences in the levels of ubiquitinated TRAF6 when Gln^{21}, Gln^{60}, or Gln^{150} N-HTT was expressed (supplemental Fig. S2). Altogether, these data suggest a scenario in which TRA6-mediated ubiquitination may control N-HTT recruitment into aggregate structures without affecting its steady-state levels.

TRAF6-mediated Atypical Ubiquitination Is Involved in Mutant N-HTT Aggregates—To functionally link TRAF6-mediated atypical ubiquitination with mutant N-HTT aggregates, HEK 293 cells were transfected with HA-ubiquitin, FLAG-TRAF6, and N-HTT-GFP Gln^{150}. Aggregates were analyzed by double immunofluorescence coupled with GFP autofluorescence. First, we set the system using WT ubiquitin (Fig. 5*a*). Overexpression of ubiquitin *per se* enhanced N-HTT inclusion formation, as expected for the well established role of the UPS in mutant N-HTT aggregation. Nonetheless, under these conditions, ubiquitin staining was diffuse throughout the cell and did not accumulate at the site of N-HTT inclusions (Fig. 5*a*, *upper panels*). When TRAF6 was added to the system, all of the components coalesced into the aggregates, which appeared strongly stained with both ubiquitin and TRAF6 (Fig. 5*a*, *lower panels*). To prove that TRAF6 action on mutant N-HTT aggregates involved atypical ubiquitination, we carried out analogous experiments with ubiquitin mutants that were shown to be involved in N-HTT ubiquitination (Lys^{6}, Lys^{27}, and Lys^{29}). As control, we used a Lys^{11} mutant that mediates polychain formation but is not used by TRAF6. Lys^{6}, Lys^{27}, and Lys^{29} were able to recapitulate the phenotype observed with WT ubiquitin (Fig. 5*b*). On the contrary, the Lys^{11} mutant did not accumulate into N-HTT inclusions. Together, these data provide evidence that TRAF6-mediated atypical activity is involved in controlling the composition of mutant N-HTT aggregates.

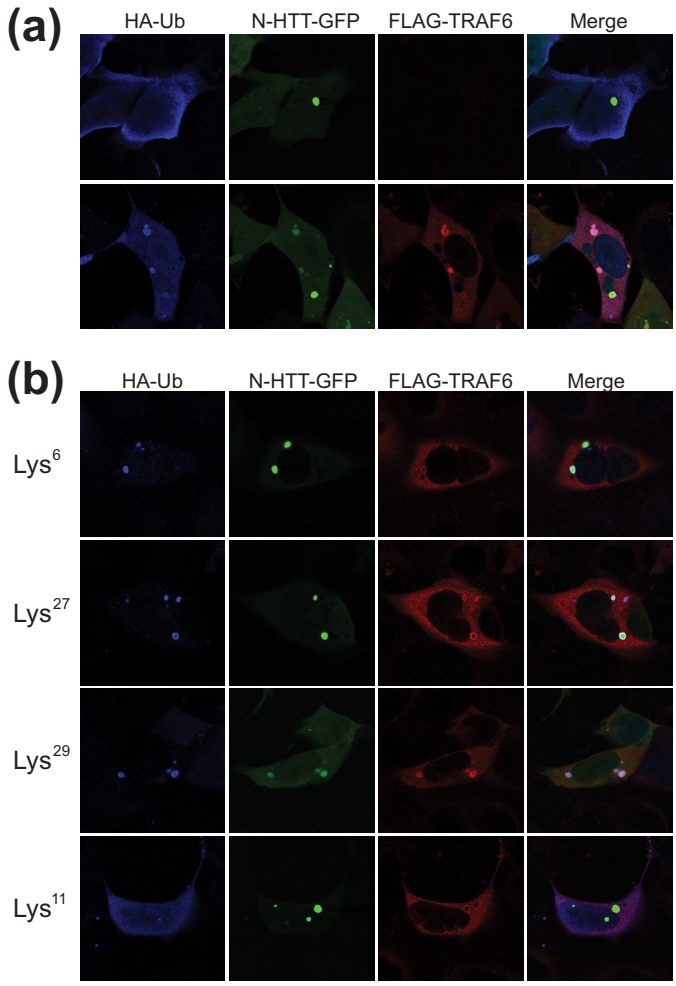

FIGURE 5. **Atypical ubiquitination by TRAF6 is localized at the aggregates.** *a*, HEK 293 cells were transfected with Gln^{150} N-HTT-GFP with FLAG-TRAF6 and HA-ubiquitin (*Ub*) WT. Localization of ubiquitin (*blue*) and TRAF6 (*red*) at N-HTT aggregates were analyzed by double immunofluorescence coupled with GFP autofluorescence. *b*, cells were transfected with Gln^{150} N-HTT-GFP, FLAG-TRAF6, and HA-ubiquitin mutants Lys^{6}, Lys^{27}, Lys^{29}, and Lys^{11} as indicated. Aggregates were analyzed by immunofluorescence as in *a*.

TRAF6 Is Up-regulated in Post-mortem Brains from HD Patients and Accumulates in Insoluble Protein Fraction—To obtain further evidence supporting the role of TRAF6 in HD pathogenesis, we assessed the expression of TRAF6 in human post-mortem brains from patients and age-matched healthy controls. First, TRAF6 mRNA expression was monitored by quantitative real-time PCR in RNA extracted from parietal cortex of controls and HD (Vonsattel grade 3 neuropathology) brains. TRAF6 mRNA levels were significantly

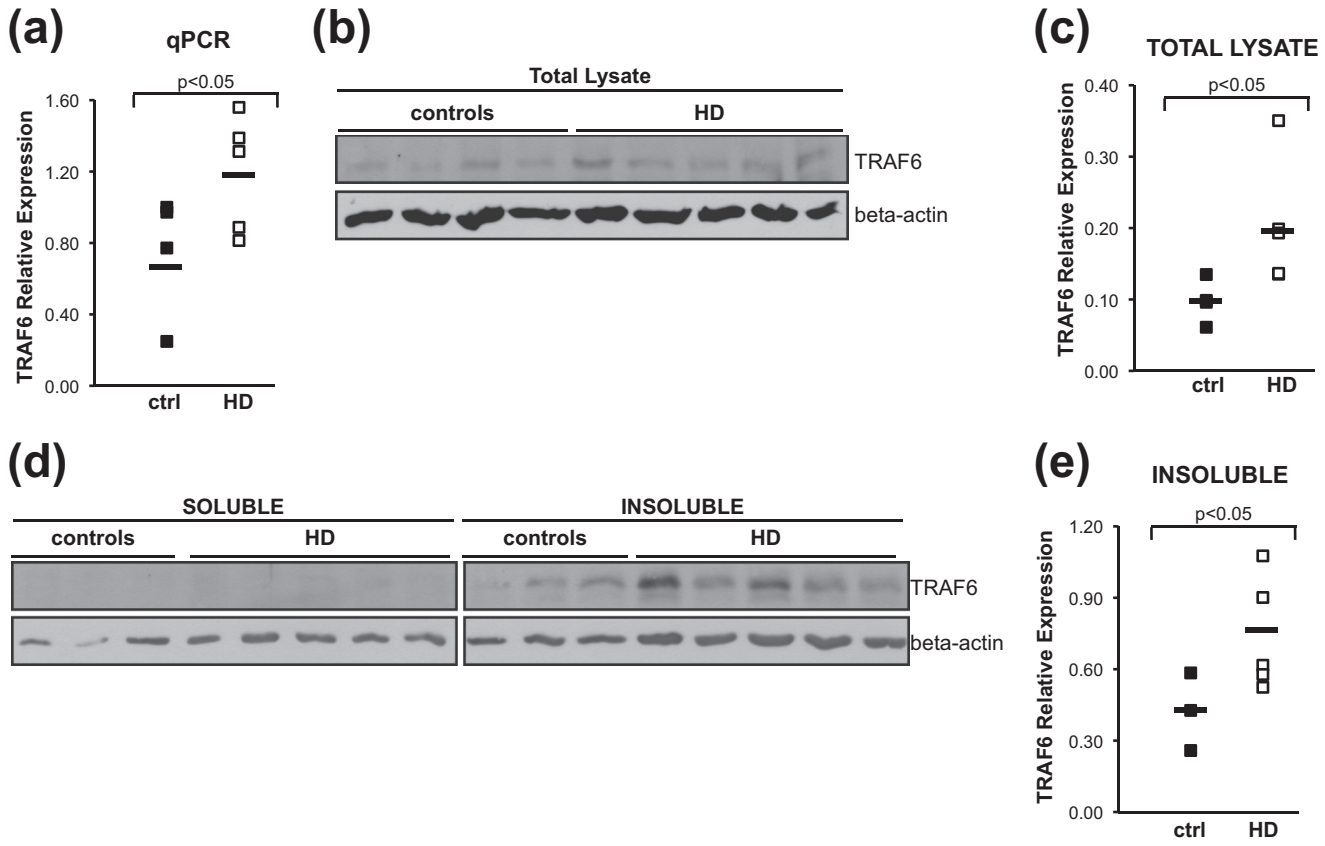

FIGURE 6. **In HD post-mortem brain, TRAF6 expression is increased, and TRAF6 protein accumulates in the insoluble fraction.** *a*, total RNA was extracted from parietal cortex of HD and control brains. TRAF6 mRNA was measured by quantitative real-time PCR relative to β-actin. *b*, total protein lysates from HD and controls were prepared, and endogenous TRAF6 expression was monitored with anti-TRAF6 antibody. Loading was normalized by protein quantification and verified with anti-β-actin antibody. Representative images from three independent experiments are shown. *c*, densitometric analysis of protein bands was performed using Adobe Photoshop CS3. Expression of endogenous TRAF6 in total lysates was normalized relative to β-actin. Statistical analysis was performed with a Student's *t* test. *d*, soluble and insoluble fractions from HD and control brains were prepared and analyzed for TRAF6 distribution. Lysates were normalized for total protein content. Anti-TRAF6 and actin antibodies were used. Images are representative of three independent experiments. *e*, quantification of TRAF6 expression in insoluble fraction was done as described in *c*.

up-regulated in HD compared with controls, with an average increase of 1.6-fold (Fig. 6*a*). We then tested whether TRAF6 up-regulation also was present at the protein level. Samples dissected from the parietal cortex of HD and control patients were used to prepare total protein extracts. Lysates were analyzed by Western blotting. To avoid artifacts due to unspecific signals, experiments were carried out using two different, commercially available anti-TRAF6 antibodies. Endogenous TRAF6 protein was slightly up-regulated in HD *versus* control samples (Fig. 6*b*). Quantification of TRAF6 signal demonstrated that the increase was statistically significant (Fig. 6*c*).

Because we found that mutant N-HTT promotes TRAF6 accumulation at the aggregates in cell culture system, TRAF6 distribution was studied in soluble and insoluble protein fractions prepared from human brain samples. Loading was normalized for total protein quantity in each of the two fractions. In HD and controls, TRAF6 was present mainly in the insoluble fraction. In this compartment, there was a statistically significant accumulation of TRAF6 in HD *versus* controls. Altogether, these data suggest an effect of mutant huntingtin on TRAF6 expression and solubility.

DISCUSSION

The ubiquitin proteasome system is under intense scrutiny in the study of neurodegenerative diseases. Different E2 conjugating enzymes and E3 ligases have been shown to ubiquitinate aggregate-prone mutant proteins via Lys^{48} and Lys^{63} moieties.

In the present study, we have found that the E3 ubiquitin ligase TRAF6 interacts with WT and mutant N-HTT *in vitro* as well as with endogenous full-length proteins *in vivo* and ubiquitinates both WT and mutant N-HTT through conjugation of atypical ubiquitin chains linked at Lys^6, Lys^{27}, and Lys^{29}.

Unconventional ubiquitination recently has provided new moieties to regulate cell signaling, intracellular trafficking, and biochemical activities (15). A variety of cellular functions have been associated to atypical ubiquitination with Lys^6, Lys^{27}, and Lys^{29} linkages that include protein degradation, regulation of proteasome activity as well as control of target protein localization and function. The E3 ubiquitin ligase parkin, found mutated in genetic cases of PD, is an HTT interactor that has been shown to act with atypical Lys^{27} linkage on mitochondrial target VDAC1 to control mitophagy (32). Transcriptional activity of androgen receptor, another polyQ containing protein, is regulated by Lys^6 and Lys^{27} ubiquitination through modulation of cofactor recruitment to a

subset of androgen receptor target genes (21). In both cases, atypical ubiquitination regulates protein function without affecting its degradation rate.

Interestingly, we found that both WT and mutant N-HTT are ubiquitinated with no evident selectivity for polyQ length. It is conceivable to hypothesize that atypical ubiquitination of N-HTT might exert diverse functions when associated to WT or mutant polyQ stretch even if the mode of ubiquitination is maintained. Although the ubiquitination of mutant N-HTT by TRAF6 was found to induce aggregate formation, the role of this post-translational modification in WT N-HTT is unclear and deserves further investigation.

Recent data have proven the accumulation of ubiquitinated proteins with unconventional ubiquitin linkages in the brain of HD mouse models (9). In HD, it is well established that neuronal inclusions that contain mutant HTT in human post-mortem brains and in mouse models are stained heavily for ubiquitin (7, 33). *In vitro*, our data demonstrated that atypical ubiquitin, N-HTT, and TRAF6 were all localized to the aggregates. Differently from all of the ubiquitin ligases studied so far in HD, TRAF6 promoted aggregate formation and segregated ubiquitin at the site of N-HTT inclusion. This is in agreement with previous studies showing that TRAF6 elicited aggresome formation of the PD-associated mutant DJ-1 L166P (26).

An important debate is ongoing on the effects of aggregate formation on cell viability *in vivo*. Among the various functional consequences, it has been hypothesized that inclusions can act as a sink for prosurvival proteins, thus depleting the neuronal cell of soluble, active molecules. In HD postmortem brains, we found that TRAF6 was up-regulated and accumulated in the insoluble protein fraction. For the majority of the ubiquitin ligases found trapped in cellular inclusions, a concomitant increase in expression has been measured in post-mortem brains, suggesting a homeostasis response aimed to preserve a physiological concentration of the molecule. Under this model, we speculate that TRAF6 sequestration *in vivo* may deplete soluble TRAF6 in neurons impairing some of its physiological functions.

In vitro TRAF6 was able to increase both the number and size of intracellular aggregates via an atypical mode of ubiquitination. In general, larger aggregates tend to be disposed by the autophagy/lysosomal pathway. TRAF6 recently has been shown to be involved in autophagy via its Lys^{63}-specific activity on Beclin-1 in the context of innate immunity (34). Furthermore, TRAF6 was able to bind p62/SQSTM1 (25), which anchors aggregated structures to LC3 and autophagosomes. Importantly, p62 is a component of the ubiquitinated proteins found in the inclusions of exon 1 mice and in cells overexpressing the N-terminal fragment of mutant HTT (35, 36). Because Lys^{27} ubiquitination of Jun and Lys^{29} of Deltex have been recently involved in their recruitment to autophagic and/or storage vesicles (20, 37), it will be interesting to study whether TRAF6 atypical ubiquitin ligase activity has an impact on autophagy in neurodegenerative disorders. It recently has been demonstrated that, similarly to Lys^{63}, Lys^{27}-linked ubiquitin chains are recognized by p62/SQSTM1 to label target proteins for autophagy (32). Our preliminary results (data not shown) indicate that TRAF6 is able to bind LC3 in transfected cells, further supporting our hypothesis that TRAF6 and atypical ubiquitination may favor alternative fates of misfolded aggregated proteins.

In the future, the generation of reagents to discriminate among Lys^{6}, Lys^{27}, and Lys^{29} ubiquitin chains and the improvement of proteomic techniques to be used on small amount of human autoptic samples will definitely help the study of atypical ubiquitination in various cellular processes *in vivo* and from diseased brains.

Acknowledgments—We are indebted to all members of the Persichetti and Gustincich laboratories for thought-provoking discussions and to Cristina Leonesi for technical support. We thank Professors Marcy MacDonald (Boston, USA) and Giannino Del Sal (Trieste, Italy) for helpful comments.

REFERENCES

1. Huntington's Disease Collaborative Research Group (1993) *Cell* **72,** 971–983
2. Hendricks, A. E., Latourelle, J. C., Lunetta, K. L., Cupples, L. A., Wheeler, V., MacDonald, M. E., Gusella, J. F., and Myers, R. H. (2009) *Am. J. Med. Genet. A* **149A,** 1375–1381
3. Hilditch-Maguire, P., Trettel, F., Passani, L. A., Auerbach, A., Persichetti, F., and MacDonald, M. E. (2000) *Hum. Mol. Genet.* **9,** 2789–2797
4. Panov, A. V., Gutekunst, C. A., Leavitt, B. R., Hayden, M. R., Burke, J. R., Strittmatter, W. J., and Greenamyre, J. T. (2002) *Nat. Neurosci.* **5,** 731–736
5. Velier, J., Kim, M., Schwarz, C., Kim, T. W., Sapp, E., Chase, K., Aronin, N., and DiFiglia, M. (1998) *Exp. Neurol.* **152,** 34–40
6. Zuccato, C., Valenza, M., and Cattaneo, E. (2010) *Physiol. Rev.* **90,** 905–981
7. DiFiglia, M., Sapp, E., Chase, K. O., Davies, S. W., Bates, G. P., Vonsattel, J. P., and Aronin, N. (1997) *Science* **277,** 1990–1993
8. Wyttenbach, A., Carmichael, J., Swartz, J., Furlong, R. A., Narain, Y., Rankin, J., and Rubinsztein, D. C. (2000) *Proc. Natl. Acad. Sci. U.S.A.* **97,** 2898–2903
9. Bennett, E. J., Shaler, T. A., Woodman, B., Ryu, K. Y., Zaitseva, T. S., Becker, C. H., Bates, G. P., Schulman, H., and Kopito, R. R. (2007) *Nature* **448,** 704–708
10. de Pril, R., Fischer, D. F., Roos, R. A., and van Leeuwen, F. W. (2007) *Mol. Cell. Neurosci.* **34,** 10–19
11. Yang, H., Zhong, X., Ballar, P., Luo, S., Shen, Y., Rubinsztein, D. C., Monteiro, M. J., and Fang, S. (2007) *Exp. Cell Res.* **313,** 538–550
12. Jana, N. R., Dikshit, P., Goswami, A., Kotliarova, S., Murata, S., Tanaka, K., and Nukina, N. (2005) *J. Biol. Chem.* **280,** 11635–11640
13. Tsai, Y. C., Fishman, P. S., Thakor, N. V., and Oyler, G. A. (2003) *J. Biol. Chem.* **278,** 22044–22055
14. Chen, Z. J., and Sun, L. J. (2009) *Mol. Cell* **33,** 275–286
15. Ikeda, F., and Dikic, I. (2008) *EMBO Rep.* **9,** 536–542
16. Cripps, D., Thomas, S. N., Jeng, Y., Yang, F., Davies, P., and Yang, A. J. (2006) *J. Biol. Chem.* **281,** 10825–10838
17. Shang, F., Deng, G., Liu, Q., Guo, W., Haas, A. L., Crosas, B., Finley, D., and Taylor, A. (2005) *J. Biol. Chem.* **280,** 20365–20374
18. Ben-Saadon, R., Zaaroor, D., Ziv, T., and Ciechanover, A. (2006) *Mol. Cell* **24,** 701–711
19. Al-Hakim, A. K., Zagorska, A., Chapman, L., Deak, M., Peggie, M., and Alessi, D. R. (2008) *Biochem. J.* **411,** 249–260
20. Ikeda, H., and Kerppola, T. K. (2008) *Mol. Biol. Cell* **19,** 4588–4601
21. Xu, K., Shimelis, H., Linn, D. E., Jiang, R., Yang, X., Sun, F., Guo, Z., Chen, H., Li, W., Chen, H., Kong, X., Melamed, J., Fang, S., Xiao, Z., Veenstra, T. D., and Qiu, Y. (2009) *Cancer Cell* **15,** 270–282
22. Chen, Z. J. (2005) *Nat. Cell Biol.* **7,** 758–765
23. Geetha, T., Jiang, J., and Wooten, M. W. (2005) *Mol. Cell* **20,** 301–312
24. Khursigara, G., Orlinick, J. R., and Chao, M. V. (1999) *J. Biol. Chem.* **274,** 2597–2600

25. Babu, J. R., Geetha, T., and Wooten, M. W. (2005) *J. Neurochem.* **94,** 192–203
26. Zucchelli, S., Codrich, M., Marcuzzi, F., Pinto, M., Vilotti, S., Biagioli, M., Ferrer, I., and Gustincich, S. (2010) *Hum. Mol. Genet.* **19,** 3759–3770
27. Persichetti, F., Trettel, F., Huang, C. C., Fraefel, C., Timmers, H. T., Gusella, J. F., and MacDonald, M. E. (1999) *Neurobiol. Dis.* **6,** 364–375
28. White, J. K., Auerbach, W., Duyao, M. P., Vonsattel, J. P., Gusella, J. F., Joyner, A. L., and MacDonald, M. E. (1997) *Nat. Genet.* **17,** 404–410
29. Zucchelli, S., Vilotti, S., Calligaris, R., Lavina, Z. S., Biagioli, M., Foti, R., De Maso, L., Pinto, M., Gorza, M., Speretta, E., Casseler, C., Tell, G., Del Sal, G., and Gustincich, S. (2009) *Cell. Death Differ.* **16,** 428–438
30. Fossale, E., Wheeler, V. C., Vrbanac, V., Lebel, L. A., Teed, A., Mysore, J. S., Gusella, J. F., MacDonald, M. E., and Persichetti, F. (2002) *Hum. Mol. Genet.* **11,** 2233–2241
31. Vonsattel, J. P., Myers, R. H., Stevens, T. J., Ferrante, R. J., Bird, E. D., and Richardson, E. P., Jr. (1985) *J. Neuropathol. Exp. Neurol.* **44,** 559–577
32. Geisler, S., Holmström, K. M., Skujat, D., Fiesel, F. C., Rothfuss, O. C., Kahle, P. J., and Springer, W. (2010) *Nat. Cell. Biol.* **12,** 119–131
33. Sieradzan, K. A., Mechan, A. O., Jones, L., Wanker, E. E., Nukina, N., and Mann, D. M. (1999) *Exp. Neurol.* **156,** 92–99
34. Shi, C. S., and Kehrl, J. H. (2010) *Sci. Signal.* **3,** ra42
35. Bjørkøy, G., Lamark, T., Brech, A., Outzen, H., Perander, M., Overvatn, A., Stenmark, H., and Johansen, T. (2005) *J. Cell Biol.* **171,** 603–614
36. Nagaoka, U., Kim, K., Jana, N. R., Doi, H., Maruyama, M., Mitsui, K., Oyama, F., and Nukina, N. (2004) *J. Neurochem.* **91,** 57–68
37. Chastagner, P., Israël, A., and Brou, C. (2006) *EMBO Rep.* **7,** 1147–1153

OPEN ACCESS Freely available online

PLoS one

Parkinson's Disease DJ-1 L166P Alters rRNA Biogenesis by Exclusion of TTRAP from the Nucleolus and Sequestration into Cytoplasmic Aggregates via TRAF6

Sandra Vilotti[1], Marta Codrich[1], Marco Dal Ferro[2,3], Milena Pinto[1], Isidro Ferrer[4,5], Licio Collavin[2,3], Stefano Gustincich[1,4,5]*, Silvia Zucchelli[1,4,5]*

1 SISSA, Sector of Neurobiology, Trieste, Italy, **2** Laboratorio Nazionale Consorzio Interuniversitario Biotecnologie, Trieste, Italy, **3** Department of Life Sciences (DSV), University of Trieste, Trieste, Italy, **4** Institute of Neuropathology, Institut d'Investigacio Biomedica de Bellvitge, University Hospital Bellvitge, University of Barcellona, Llbregat, Spain, **5** SISSA Unit, Italian Institute of Technology (IIT), Trieste, Italy

Abstract

Mutations in PARK7/DJ-1 gene are associated to autosomal recessive early onset forms of Parkinson's disease (PD). Although large gene deletions have been linked to a loss-of-function phenotype, the pathogenic mechanism of missense mutations is less clear. The L166P mutation causes misfolding of DJ-1 protein and its degradation. L166P protein may also accumulate into insoluble cytoplasmic aggregates with a mechanism facilitated by the E3 ligase TNF receptor associated factor 6 (TRAF6). Upon proteasome impairment L166P activates the JNK/p38 MAPK apoptotic pathway by its interaction with TRAF and TNF Receptor Associated Protein (TTRAP). When proteasome activity is blocked in the presence of wild-type DJ-1, TTRAP forms aggregates that are localized to the cytoplasm or associated to nucleolar cavities, where it is required for a correct rRNA biogenesis. In this study we show that in post-mortem brains of sporadic PD patients TTRAP is associated to the nucleolus and to Lewy Bodies, cytoplasmic aggregates considered the hallmark of the disease. In SH-SY5Y neuroblastoma cells, misfolded mutant DJ-1 L166P alters rRNA biogenesis inhibiting TTRAP localization to the nucleolus and enhancing its recruitment into cytoplasmic aggregates with a mechanism that depends in part on TRAF6 activity. This work suggests that TTRAP plays a role in the molecular mechanisms of both sporadic and familial PD. Furthermore, it unveils the existence of an interplay between cytoplasmic and nucleolar aggregates that impacts rRNA biogenesis and involves TRAF6.

Citation: Vilotti S, Codrich M, Dal Ferro M, Pinto M, Ferrer I, et al. (2012) Parkinson's Disease DJ-1 L166P Alters rRNA Biogenesis by Exclusion of TTRAP from the Nucleolus and Sequestration into Cytoplasmic Aggregates via TRAF6. PLoS ONE 7(4): e35051. doi:10.1371/journal.pone.0035051

Editor: Ferdinando Di Cunto, University of Turin, Italy

Received November 16, 2011; **Accepted** March 8, 2012; **Published** April 20, 2012

Funding: The following fundings have supported this work: Telethon Grant GGP06268; The Giovanni Armenise-Harvard Foundation; and the Italian Institute of Technology. The funders had no role in study design, data collection and analysis, decision to publish, or preparation of the manuscript.

Competing Interests: The authors have declared that no competing interests exist.

* E-mail: gustinci@sissa.it (SG); silvia.zucchelli@sissa.it (SZ)

Introduction

The accumulation of misfolded proteins is a common feature to a wide range of neurodegenerative diseases [1]. A neuropathological hallmark of Parkinson's disease (PD) is the presence of proteinaceous aggregates, known as Lewy Bodies (LBs), in the cytoplasm of dopaminergic (DA) neurons of the Substantia Nigra, the major target of neurodegeneration. In Huntington's disease (HD), N-terminal fragments of mutant huntingtin (N-HTT) form intracellular aggregates in the brain [2].

Several evidences implicate malfunction of the ubiquitin-proteasome system (UPS) in both idiopatic and familial PD [3]. Key UPS elements are altered in PD post-mortem brains [4], while synthetic proteasome inhibitors preferentially affect catecholaminergic neurons *in vitro* and *in vivo* leading to cell death [5,6].

DJ-1 is a ubiquitously expressed protein that is mutated in autosomal recessive early onset forms of PD (PARK7) [7]. DJ-1 is an anti-oxidant protein [8] involved in mitochondrial integrity [9], autophagy [10] and hypoxia [11,12]. Together with phenotypes due to large gene deletions, the exact pathogenic mechanism of PD-causing missense mutations remains unclear. In the most studied case, L166P disrupts DJ-1 protein activity and dimer formation, resulting in a misfolded protein that undergoes degradation [13]. However, mutant DJ-1 may also accumulate into insoluble cytoplasmic aggregates [14,15] and acquire a gain-of-function property that may co-exist with its loss of physiological activity, as previously found for mutant HTT in HD [16] and superoxide dismutase 1 (SOD1) missense mutations in amyotrophic lateral sclerosis (ALS) [17].

The formation of L166P-containing aggregates is facilitated by atypical ubiquitination carried out by the TNF associated protein 6 (TRAF6) [15], a component of LBs in PD post-mortem brains. Interestingly, TRAF6 activity also triggers aggregate formation of mutant HTT suggesting a broader role of this E3 ligase in neurodegenerative diseases [18].

TRAF and TNF Receptor Associated Protein (TTRAP) is a 5′-tyrosyl DNA phosphodiesterase that repairs topoisomerase-2-induced DNA breaks [19]. In physiological conditions in neurons TTRAP is a nuclear protein associated to PML Nuclear Bodies (PML-NBs) [20]. It was originally described as involved in signal transduction for its interaction with TNF receptors (TNFR) family members and TNFR-associated factors (TRAFs), including TRAF6 [21], as well as in transcriptional regulation for its binding to ETS-related proteins [22]. TTRAP has been linked to

PD for its ability to specifically interact with L166P DJ-1. When UPS activity is inhibited, TTRAP mediates L166P toxicity via JNK/p38 MAPK pathways providing the molecular basis for L166P gain-of-function properties [23]. Interestingly, TTRAP forms aggregates both in the cytoplasm and in nucleolar cavities, a region of the nucleolus devoid of ribosomal markers [24]. Under these conditions, TTRAP is neuroprotective and required for a correct rRNA biogenesis [20].

The structure and function of the nucleolus have been recently found altered in PD and essential to the survival of DA neurons *in vivo* [25,26].

In this paper we show that in PD post-mortem brains TTRAP is associated to LBs in the cytoplasm or accumulated in the nucleolus in a portion of surviving DA neurons. In a cellular model of familial PD linked to mutant DJ-1 L166P, accumulation of misfolded proteins impairs rRNA biogenesis *in vitro* by inhibiting TTRAP localization into nucleolar cavities. This is concomitant with an increase in the number and size of cytoplasmic aggregates containing both L166P and TTRAP. This phenotype depends, at least in part, on TRAF6 E3 ligase activity.

Materials and Methods

Human post-mortem brains

Brain samples were obtained from the brain bank at the Institute of Neuropathology, Bellvitge Hospital (University of Barcelona, Spain). Samples were dissected at autopsy with the informed consent of patients or their relatives and the institutional approval of the Ethics Committee of the University of Barcelona. Brains were obtained from Caucasian, pathologically confirmed PD cases and age-matched controls [27]. Briefly, all cases of PD had suffered from classical PD, none of them had cognitive impairment and their neuropathological characterization was made according to established criteria. Control healthy subjects showed absence of neurological symptoms and of metabolic and vascular diseases, and the neuropathological study disclosed no abnormalities, including lack of Alzheimer disease and related pathology. The time between death and tissue preparation was in the range of 3 to 5 hours. The ventral midbrain region was sectioned horizontally. The dark pigmented zones of the Substantia Nigra were readily apparent from all surrounding structures and were then isolated from the ventral midbrain. For histological analysis, samples were cryoprotected with 30% sucrose in 4% formaldehyde, frozen in dry ice and stored at -80°C until use.

Immunohistochemistry

Immunohistochemistry was performed on three controls and six PD human post-mortem brains. Only Substantia Nigra was dissected and analyzed. Tissue processing and histology were performed as previously described [15]. The following primary antibodies were used: anti-TTRAP (1:50) [23] and anti-alpha-synuclein (1:100, Cell Signaling Technology). Nuclei were visualized with DAPI. DA neurons in the Substantia Nigra were identified by neuromelanin staining with transmitted light.

Cell culture and transfections

Human neuroblastoma SH-SY5Y cells (*ATCC*) were maintained in culture as suggested by the vendor. SH-SY5Y cells stably transfected with pCDNA3-FLAG-DJ-1 wt and L166P or empty vector control and with pSuperior-siDJ-1 or pSuperior-Scramble were previously described [11,23]. All stably transfected SH-SY5Y cells were kept in culture with neomycin selection. Proteasome inhibition was performed for 16 hours with 5 μM MG132 (z-Leu-Leu-al) (Sigma Aldrich). DJ-1 silencing was obtained by adding 2.5 μg/ml of Doxycicline Hyclate (Sigma Aldrich) every 48 hours for a total of 10 days. GFP-TRAF6 (wt and DN) and N-HTT-GFP Gln^{21} and Gln^{150} were previously described [15,18]. Transfections were performed with Lipofectamine reagent (Invitrogen).

For silencing endogenous TRAF6 specific oligonucleotides (Sigma Aldrich, EHU147511) were transiently transfected with Oligofectamine (Invitrogen). Immunofluorescence and western blot experiments were performed 72 hours after transfection.

Immunofluorescence

For immunofluorescence experiments, cells were fixed in 4% paraformaldehyde directly added to culture medium for 10 minutes, then washed in PBS two times, treated with 0.1 M glycine for 4 minutes in PBS and permeabilized with 0,1% Triton X-100 in PBS for another 4 minutes. After washing with PBS and blocking with 0.2% BSA, 1% NGS, 0,1% Triton X-100 in PBS (blocking solution), cells were incubated with the indicated antibodies diluted in blocking solution for 90 minutes at room temperature. To detect insoluble TTRAP, immunocytochemistry was performed as described earlier [23].

We used anti-FLAG (1:1000, Sigma Aldrich), anti-TTRAP (1:100), anti-NPM (1:100, Invitrogen), anti-Nucleolin (1:100, Invitrogen), anti-PML (PG-M3) (1:100, Santa Cruz Biotechnology), anti-p53 (DO1, Santa Cruz Biotechnology). For detection, cells were incubated with Alexa Fluor-488 or -594 (Molecular Probes, Invitrogen) labeled anti-mouse or anti-rabbit secondary antibodies. For nuclear staining, cells were incubated with DAPI (1 μg/ml) for 5 minutes. Triple immunofluorescence was performed using Zenon technology: anti-NPM antibody was labeled with Zenon Alexa Fluor 405 Mouse IgG(1) labeling reagent (Invitrogen), according to manufacturer's instructions. Cells were washed and mounted with Vectashield mounting medium (Vector). All images were collected using a confocal laser scanning microscopy LEICA TCS SP2. The analysis of aggregates was performed on high-resolution images using ImageJ software. At least 100 cells from two independent experiments were counted and scored for percentage of cells with aggregates and average aggregate size.

RNA isolation, reverse transcription and qPCR

Total RNA was isolated using the TRIZOL reagent (Invitrogen) following the manufacturer's instructions. Single strand cDNA was obtained from 1 μg of purified RNA using the iSCRIPT^{TM} cDNA Synthesis Kit (Bio-Rad) according to manufacturer's instructions. Quantitative real time PCR (qPCR) was performed using SYBR-Green PCR Master Mix (Applied Biosystem) and an iCycler IQ Real time PCR System (Bio-Rad). Primers for rRNA biogenesis A0, 1 and 4 [20], and for housekeeping genes beta-actin and GAPDH [15] were previously described.

^{32}P-orthophosphate in vivo labeling and RNA analysis

Metabolic labeling and analysis of rRNA was carried out as previously described [20]. Briefly, mutant DJ-1 L166P and empty control cells were treated with 5 μM MG132 for 16 h or left untreated. Drug was maintained in the medium during the whole time of the procedure. Cells were incubated with phosphate-free medium supplemented with 10% dialyzed FBS (labeling medium) for 1 h prior to labeling with ^{32}P-orthophosphate (15 μCi/ml) in labeling medium for 1 h (pulse). Medium was then replaced with complete medium for 3 h (chase). Total RNA was extracted using TRIZOL reagent (Invitrogen) and 1 μg of purified RNA was separated on 1% agarose-formaldehyde gel. After electrophoresis,

28S and 18S rRNA forms were controlled under UV light and gels were dried. rRNA species were detected by autoradiography.

Proliferation and viability assays

Cell proliferation was measured by flow-cytometry (FACS) upon propidium iodide staining. Briefly, SH-SY5Y cells stably transfected with L166P and control cells were either left untreated or treated with 5 μM MG132 for 16 hours. After treatment, cells were collected, fixed with ice-cold 70% ethanol, treated with RNase A (0.2 mg/ml), and stained with propidium iodide (0.04 mg/ml). Samples were analyzed on a flow cytometer (FacsCalibur, BD). FACS data were processed using FlowJo software, and cell cycle profiles were determined using the Watson pragmatic model (Tree Star).

Cell viability was measured using WST-1 reagent (Roche), following manufacturer's instructions and reading absorbance at 440 nm using a standard spectrophotometer. Percentage of live cells after treatment with 5 μM MG132 for 16 hours was calculated relative to DMSO-treated cells (set as 100% for each cell line).

Cell fractionation and Western blot analysis

SH-SY5Y stable cells were lysed in a buffer containing 150 mM NaCl, 50 mM Tris pH 7.5 and 0.2% TRITON X-100, supplemented with protease inhibitor cocktail (Roche). Lysates were centrifuged at 20 000 g for 30 min at 4°C and separated into Triton X-100 soluble (supernatant) and insoluble (pellet) fractions. Insoluble pellets were resuspended in boiling sample buffer, sonicated and used for western blot analysis. The following antibodies were used: anti-FLAG 1:2000 (Sigma), anti-TTRAP 1:1000, anti-TRAF6 (Santa Cruz), anti-beta-actin 1:5000 (Sigma). For detection, anti-mouse-HRP or anti-rabbit-HRP (Dako) in combination with ECL (GE Healthcare) were used.

Statistical analysis

All experiments were repeated in triplicate or more. For stably transfected cells, at least two independent clones were used for each cell line in all experiments. Data represent the mean with standard deviation. When necessary, each group was compared individually with reference control group using Student's *t*-Test (Microsoft Excel software).

Results

TTRAP is present in cytoplasmic LBs and in the nucleolus of surviving dopaminergic neurons of PD post-mortem brains

To study TTRAP localization in sporadic PD, we performed immunohistochemical analysis in human post-mortem brains. A total of six PD patients and three controls were examined (Figure 1A). In normal conditions, TTRAP is expressed mainly in the nucleus of DA neurons, identified for the presence of neuromelanin. A weaker cytoplasmic staining is observed. Low levels of TTRAP expression can also be found in non-DA neurons. No staining was detected when control rabbit immunoglobulins were used (data not shown). In human brain sections of sporadic PD cases TTRAP expression was heterogeneous throughout mesencephalic cells identifying at least four phenotypes. While a small quantity of cells (15–20%) presented a nuclear distribution as in controls, in the majority of DA neurons (80%) TTRAP was exclusively relocalized to the cytoplasm, almost completely emptying the nucleus. In about 1–20% of the cells, TTRAP accumulated in large cytoplasmic aggregates. Double immunohistochemical analysis using anti-alpha-synuclein antibody demonstrated that these are *bona fide* LBs (Figure 1B). The patient-to-patient variability, in conjunction with an uneven distribution of aggregates in the Substantia Nigra, reflected the heterogeneous distribution of LBs in post-mortem brains. In addition, in 1–2% of surviving DA neurons, TTRAP diffuse cytoplasmic localization was concomitant with the presence of TTRAP in the nucleolus, as shown by lack of DAPI staining.

Altogether these data show that TTRAP is present in cytoplasmic LBs as well as in the nucleolus in surviving dopaminergic neurons of sporadic PD brains.

L166P mutant DJ-1 inhibits TTRAP localization in nucleolar cavities

When SH-SY5Y neuroblastoma cells are treated with proteasome inhibitors *in vitro*, TTRAP forms aggresome-like structures in the cytoplasm and in the nucleolus where it participates in rRNA biogenesis [20,23]. In these conditions it binds L166P, the protein product of the most studied missense DJ-1 mutation in familial PD. To test whether L166P binding might have an effect on TTRAP localization, SH-SY5Y cells stably expressing FLAG-tagged wt DJ-1 or PD-associated L166P were treated with MG132. When nucleoli were visualized with the marker Nucleophosmin (NPM), TTRAP was detected in the nucleolus of about 60% of control cells upon proteasome block (Figure 2A, 2B) [20]. This localization was also observed when more specific inhibitors of proteasome activity were used like epoxomicin and lactacystin (Figure S1). No staining was observed in cells with knock-down TTRAP expression (Figure S1). While overexpression of wt DJ-1 had no effect on TTRAP nucleolar localization, the presence of misfolded L166P mutant almost completely inhibited TTRAP recruitment to the nucleolus (Figure 2A, 2B and figure S2). No differences in TTRAP localization were observed in untreated conditions, thus indicating that overexpression of wt or mutant DJ-1 per se does not alter TTRAP subcellular distribution (Figure 2B and Figure S2). Since L166P DJ-1 is expressed at lower levels than wt protein and is generally associated to a loss-of-function phenotype, we asked whether silencing DJ-1 expression in SH-SY5Y cells could recapitulate the phenotype observed in L166P expressing cells. We performed similar immuno-fluorescence experiments in SH-SY5Y cells with inducible loss of DJ-1 expression [11] by using two independent siDJ-1 (A, B) and scramble (a, b) clones. The lack of DJ-1 protein did not affect TTRAP localization, neither in untreated or MG132-treated cells (Figure 2C, 2D, 2E and Figure S3).

To evaluate whether TTRAP exclusion from the nucleolus was a phenotype common to other misfolded proteins involved in neurodegenerative diseases, we studied TTRAP localization in a cellular model of Huntington's disease. SH-SY5Y cells were transfected with huntingtin amino-terminal fragment (residues 1–171) fused to green fluorescent protein (N-HTT-GFP) with either a physiological (Gln^{21}) or a pathological (Gln^{150}) polyglutamine (polyQ) stretch. N-HTT aggregates triggered by polyQ expansion inhibited TTRAP nucleolar localization upon proteasome impairment (Figure 2F, 2G), while no effects were observed when wt Gln^{21} N-HTT was used.

These data indicate that misfolding-causing mutations in neurodegenerative diseases impact TTRAP nucleolar localization upon proteasome inhibition.

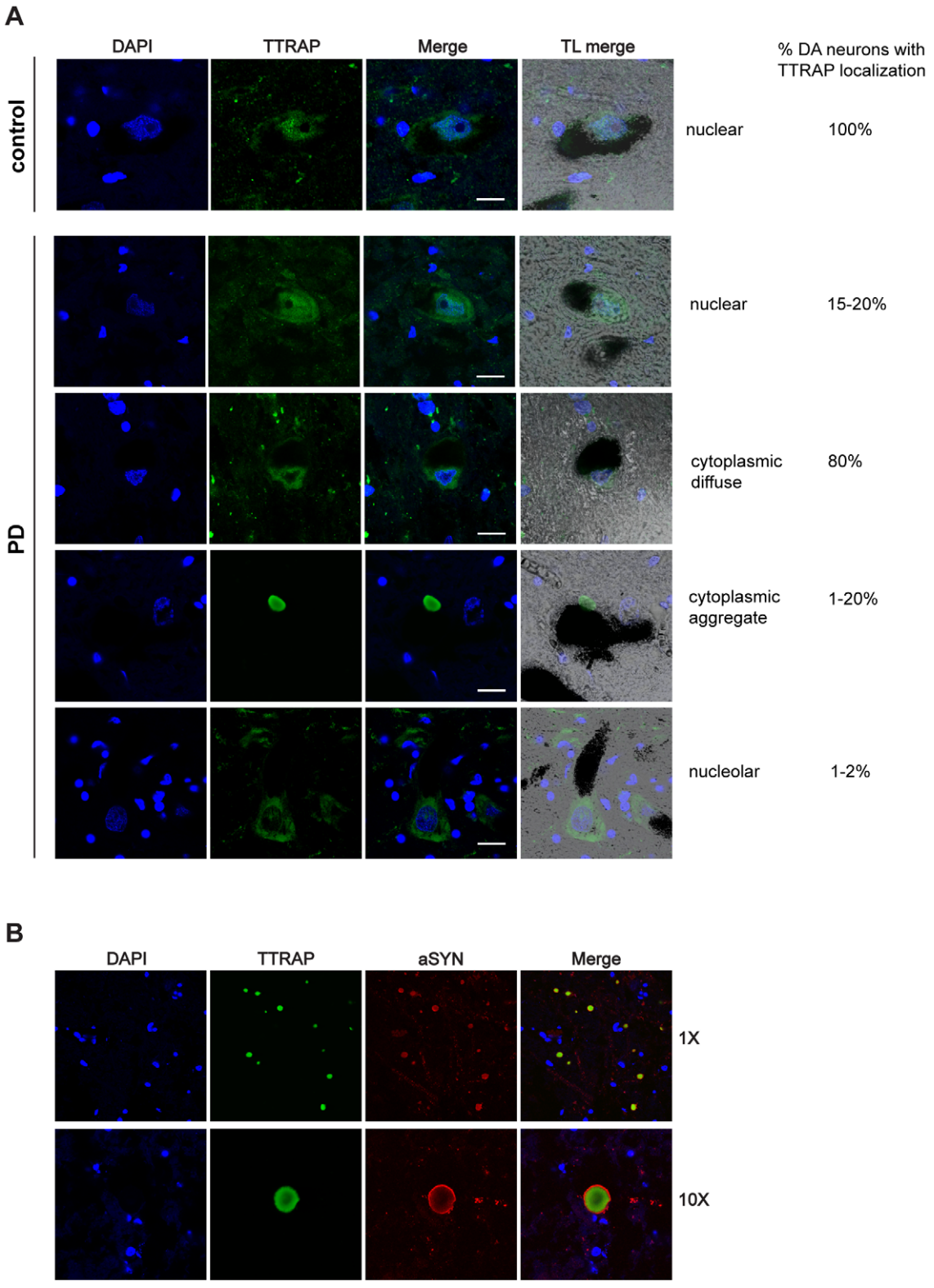

Figure 1. TTRAP is present in cytoplasmic Lewy bodies and in the nucleolus in surviving dopaminergic neurons in PD *post-mortem* brains. (A) TTRAP localization in normal and PD dopaminergic neurons. Cryo-sections of post-mortem brain tissues were taken from Substantia Nigra of healthy individuals and PD patients, as indicated. Immunohistochemistry was performed with anti-TTRAP antibody (green). Nuclei were stained with DAPI (blue). Dopaminergic neurons were identified by neuromelanin (black) in transmitted light (TL). Overlays of fluorescence (merge) and fluorescence with TL (TL merge) are shown. Panels are representative images showing TTRAP nuclear, cytoplasmic diffused, cytoplasmic aggregated and nucleolar localization. The percentage of dopaminergic neurons with nuclear, cytoplasmic or nucleolar TTRAP staining is indicated on the right. Bars, 15 μM. (B) TTRAP-containing cytoplasmic aggregates are Lewy bodies. Immunohistochemistry of Substantia Nigra from PD brains was performed with anti-TTRAP (green) and anti-alpha-synuclein (red) antibodies. Images at low (1×) and high (10×) magnification are shown.
doi:10.1371/journal.pone.0035051.g001

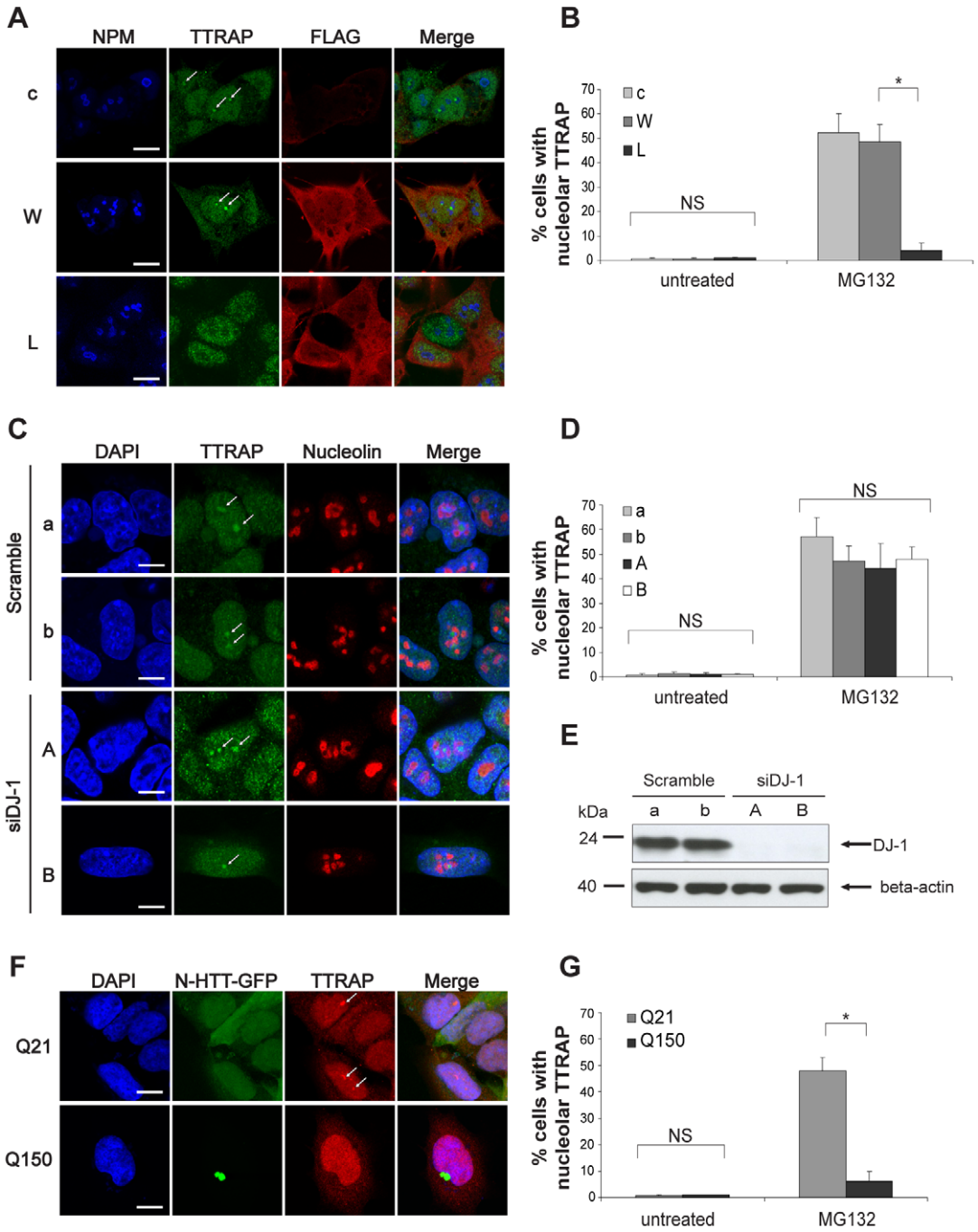

Figure 2. Mutant DJ-1 L166P inhibits TTRAP nucleolar localization after proteasome inhibition. (A) TTRAP nucleolar localization is inhibited in L166P expressing cells. SH-SY5Y cells stably transfected with empty vector (c), FLAG-DJ-1 wt (W) or L166P (L) were treated with 5 μM MG132 for 16 h. Triple immunofluorescence was performed with anti-NPM (blue), anti-TTRAP (green) and anti-FLAG (red) antibodies. Images are representatives of three independent experiments. Data have been confirmed on two independent clones for each cell line. Bars, 10 μm. (B) Quantification of TTRAP nucleolar localization. Cells as in A. At least 200 cells from two independent experiments were counted and scored for TTRAP in the nucleolus (*, $p<0.05$). (C) Localization of TTRAP is unaffected in cells depleted of endogenous DJ-1. SH-SY5Y cells stably expressing an inducible short-hairpin RNA targeting DJ-1 (siDJ-1, clones A and B) or a scramble shRNA control (scramble, clones a and b) were treated with doxycycline for 10 days to induce silencing of DJ-1 expression. Then cells were treated with 5 μM MG132 for 16 h. Immunofluorescence was performed with anti-TTRAP (green) and anti-NCL (red) antibodies. Nuclei were visualized with DAPI (blue). Images are representatives of two independent experiments. Bars, 10 μm. (D) Quantification of TTRAP nucleolar localization in siDJ-1 cells. Data were collected as in B. (NS, not-significant). (E) DJ-1 is efficiently depleted in siDJ-1 cells. Total protein lysates were prepared from cells as in C. Levels of endogenous DJ-1 were measured by western blot with anti-DJ-1 antibody. Beta-actin was detected as loading control. (F) TTRAP nucleolar localization is altered by mutant huntingtin. SH-SY5Y cells were transfected with huntingtin N-terminal fragment fused to GFP with WT (Gln^{21}, Q21) or mutated (Gln^{150}, Q150) polyglutamine expansion. Endogenous TTRAP was visualized by indirect immunofluorescence (red). N-HTT was visible by GFP autofluorescence. Nuclei were visualized with DAPI (blue). Bars, 10 μm. (F) Quantification of TTRAP nucleolar localization in N-HTT expressing cells. Data were collected as in B on GFP-positive cells (*, $p<0.05$; NS, not-significant).
doi:10.1371/journal.pone.0035051.g002

L166P alters rRNA biogenesis in response to proteasome inhibition

Since we have previously found that nucleolar TTRAP regulates rRNA biogenesis in conditions of proteasome inhibition [20], we analyzed the levels of precursor rRNA molecules (pre-rRNA) and of rRNA processing intermediates in SH-SY5Y stable cells for wt DJ-1, mutant L166P and empty vector as control. Cells were treated with MG132 and rRNA biogenesis was measured by qPCR with A0, 1 and 4 primers as previously described [28,29,30] [20]. A scheme of rRNA processing events and positioning of qPCR primers on processing intermediates is shown in figure 3A. In untreated conditions, A0, 1 and 4 probes detected no changes dependent on wt or mutant DJ-1 overexpression (Figure 3B). Upon proteasome inhibition, the levels of pre-rRNA containing A0 sites were significantly increased ($p<0.05$). This pattern was maintained in cells expressing wt DJ-1. On the contrary, concomitant with the disappearance of nucleolar TTRAP, in L166P cells the quantity of A0 sites was strongly reduced ($p<0.05$). Furthermore, the amount of rRNA processing intermediates, measured by oligonucleotides targeting 1 and 4 cleavage sites, dramatically increased in L166P cells compared to wt DJ-1 and controls (Figure 3B). No detectable alterations in pre-rRNA levels were observed in inducible si-DJ-1 cells (Figure S4). Importantly, no gross alterations in the structure of nucleoli were induced by overexpression of L166P as proved with NPM staining (Figure S5).

To further investigate ribosome biogenesis in mutant DJ-1 cells, we measured nascent rRNA by pulse-chase labeling with ^{32}P-orthophosphate. Untreated cells were used as controls. Metabolically labeled rRNA species were visualized by autoradiography (Figure 3C, upper panel) and loading was verified with ethidium bromide (Figure 3C, lower panel). No differences in rRNA processing were detected in untreated conditions between control and mutant DJ-1 cells, thus confirming qPCR data. While proteasome inhibition caused a marked reduction of 28S and 18S mature forms in both cell lines, mutant DJ-1 L166P expression caused an increase in pre-rRNA precursors (47S/45S) and an accumulation of the 32S processing intermediate.

Altogether, these results suggest that misfolded DJ-1 expression has an impact both on the initial events of transcription and on the conversion of intermediate to mature forms (47S to 45S and 32S to 28S). This phenotype resembles the one observed in neuroblastoma cells lacking TTRAP expression [20]. Analysis of cell proliferation in untreated and treated conditions could not detect any difference between control and mutant cells (Figure S6). A small, but significant, decrease in cell viability could be observed in L166P cells exposed to MG132 as compared to control cells (Figure S6).

L166P-mediated exclusion of TTRAP from nucleolar cavities does not depend on PML

The presence of PML and the integrity of PML-NBs in nucleolar cavities are fundamental for TTRAP to be recruited to the nucleolus in response to proteasome inhibition [20]. Therefore, we asked whether L166P-mediated exclusion of TTRAP from nucleolar cavities might depend on L166P action on PML-NBs. SH-SY5Y cells expressing wt, L166P or an empty vector were treated with MG132 and PML localization was followed by immunofluorescence using NPM as nucleolar marker (Figure 4A). The number of cells with nucleolar PML-NBs was scored in duplicates in two independent clones for each cell line (at least 100 cells per experiment) (Figure 4B). Total levels of PML protein were measured by western blot analysis (Figure 4C, 4D). We found that L166P, similarly to wt and control cells, did not impact PML expression or PML-NBs accumulation in nucleolar cavities. Therefore, L166P inhibition of TTRAP nucleolar accumulation is independent from PML. To further support this model, we also checked whether MG132-induced nucleolar localization of p53, another marker of nucleolar cavities, was altered by L166P. Similarly to PML staining, we couldn't observe any change in p53 localization induced by overexpression of misfolded mutant DJ-1, or in controls (Figure 4E, 4F). No changes in TTRAP, PML and p53 localization were observed in untreated cells (Figure S7).

Altogether our data indicate that L166P overexpression does not impact the overall structure of nucleolar cavities but specifically alters nucleolar localization of L166P-binding protein TTRAP.

L166P enhances TTRAP accumulation into insoluble cytoplasmic aggresomes

As MG132 treatment accumulates TTRAP into cytoplasmic insoluble aggresome-like structures [23], we analyzed TTRAP localization in cells that express wt DJ-1 or L166P after permeabilization with Triton X-100 before fixation. In all cell lines analyzed, endogenous TTRAP formed aggresome-like structures in the cytoplasm, as expected (Figure 5A), whereas no aggresomes were visible in untreated conditions (data not shown). Interestingly, overexpression of L166P increased the percentage of cells with TTRAP-containing cytoplasmic aggregates and promoted the formation of inclusions with an average larger size (Figure 5A, 5B, 5C).

In about half of SH-SY5Y cells stably transfected with DJ-1 wt or empty vector, TTRAP was also present in the insoluble fraction of the nucleolus. As expected, TTRAP accumulation in insoluble nucleolar granules was almost completely inhibited in presence of L166P mutant (Figure 5A). Interestingly, L166P itself was present in TTRAP-positive cytoplasmic aggregates (figure 5A), whereas no DJ-1 aggregates were visible in wt overexpressing cells.

Since mutant L166P promotes TTRAP accumulation in cytoplasmic aggregates upon MG132 treatment, we analyzed TTRAP distribution into insoluble fractions by western blot analysis, proving a more evident accumulation in L166P-expressing cells (Figure 5D) [23].

Altogether, these data demonstrate that L166P depletes TTRAP from nucleolar cavities and enhances its recruitment into L166P-containing insoluble cytoplasmic aggregates.

TRAF6 E3 ligase activity contributes to L166P-mediated exclusion of TTRAP from nucleolar cavities

Since TTRAP and L166P co-localize in cytoplasmic insoluble inclusions, we hypothesized that factors that promote L166P aggregation might control TTRAP distribution between the cytoplasm and the nucleolus. In a previous work, we have shown that atypical ubiquitination by the E3 ligase TRAF6 enhances L166P aggregate formation [15]. Therefore, we tested whether TRAF6 E3 ligase activity might contribute to L166P-induced TTRAP mislocalization. To this purpose we took advantage of a TRAF6 mutant deleted of the N-terminal E3 ligase RING domain (TRAF6 DN), that acts as dominant negative [31]. We transfected SH-SY5Y cells stably expressing L166P with TRAF6 DN or wt fused to GFP (Figure 6A, 6B). Cells expressing wt DJ-1 or empty vector were used as controls. TTRAP localization in nucleolar cavities was scored only in those cells with equivalent expression of transfected constructs. Overexpression of wt TRAF6 had no effect on TTRAP exclusion from nucleolar cavities induced by L166P. Instead, TTRAP nucleolar localization was restored in about 20%

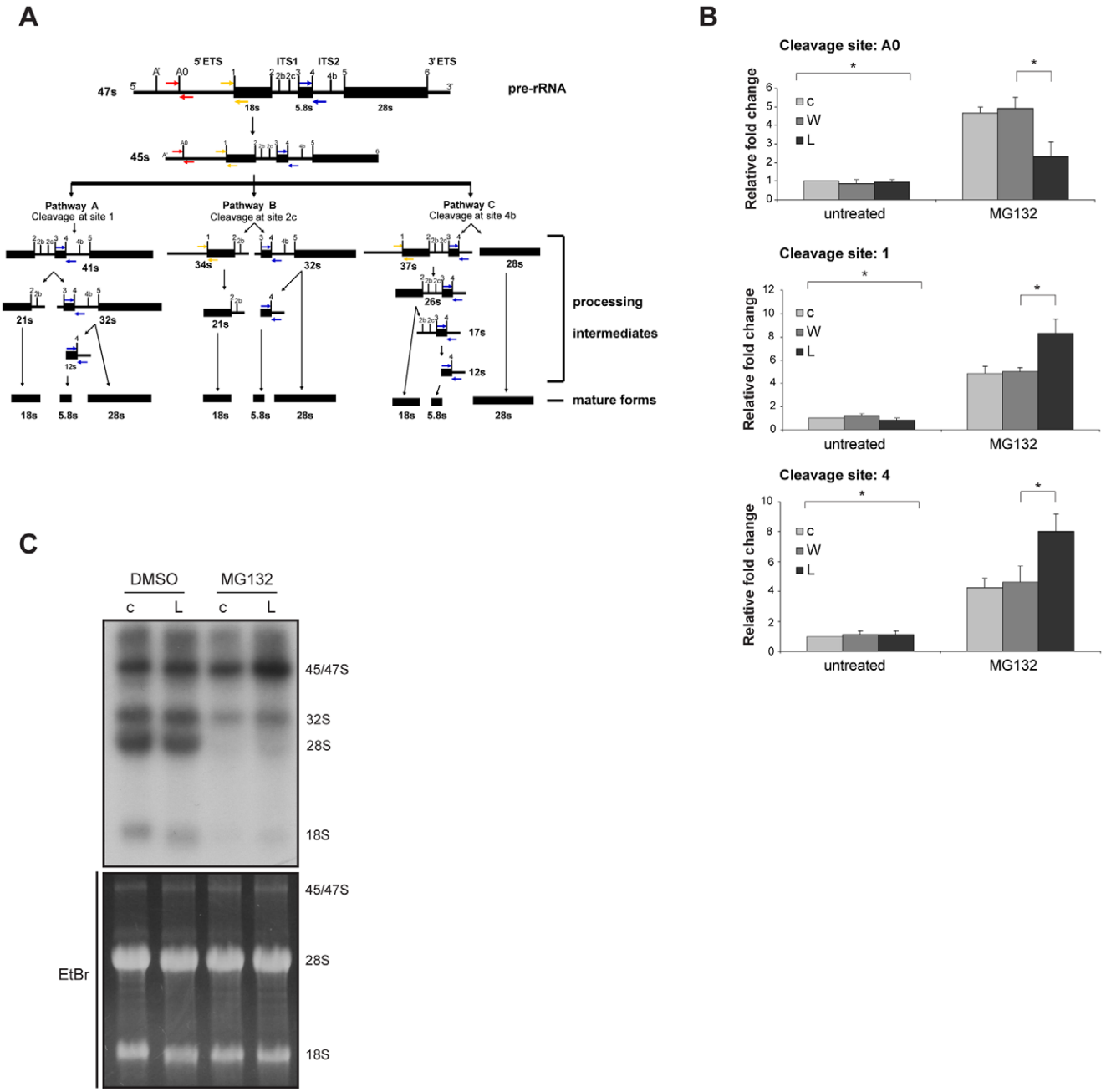

Figure 3. Processing of rRNA is altered in L166P overexpressing cells. (A) Schematic diagram showing pre-rRNA structure and processing steps. Positioning of A0, 1 and 4 cleavage sites on rRNA processing intermediates is shown. ETS, external transcribed spacer; ITS, internal transcribed spacer. (B) Analysis of steady-state levels of rRNA precursor and processing intermediates. SH-SY5Y cells stably expressing wt DJ-1 (W), L166P (L) and empty vector (c) were treated with Bars, 5 μM MG132 for 16 h, or left untreated. Total RNA was extracted and levels of pre-rRNA and processing intermediates were analyzed by qPCR with primers targeting A0 , 1 and 4 cleavage sites. Standard deviations are calculated on four replicas from two independent experiments. *, $p<0.05$. (C) Analysis of rRNA processing by metabolic labeling. L166P (L) and control (c) cells were treated as in A. After treatment, cells were pulse-labeled with ^{32}P-orthophosphate for 1 h and chased with cold medium for 3 h. RNA was extracted and equal quantities were separated on denaturing agarose gel. Nascent rRNA was visualized by autoradiography after gel drying (upper panel). rRNA processing intermediates and mature forms are indicated on the right. Loading was verified with ethidium bromide staining (lower panel).
doi:10.1371/journal.pone.0035051.g003

of cells when TRAF6 DN was used (Figure 6A, 6B). This phenotype was only partially penetrant. Overexpression of TRAF6 or TRAF6 DN in stable cells for wt DJ-1 or empty vector had no effects on TTRAP localization (Figure 6B). No differences in TTRAP localization were observed in untreated condition (Figure S8), thus indicating that overexpression of wt or mutant TRAF6 per se does not alter TTRAP subcellular distribution.

To further support the role of TRAF6 in excluding TTRAP from nucleolar cavities, endogenous TRAF6 was silenced in L166P-expressing cells with specific siRNA oligonucleotides. Scramble siRNA and wt DJ-1 cells were used as controls.

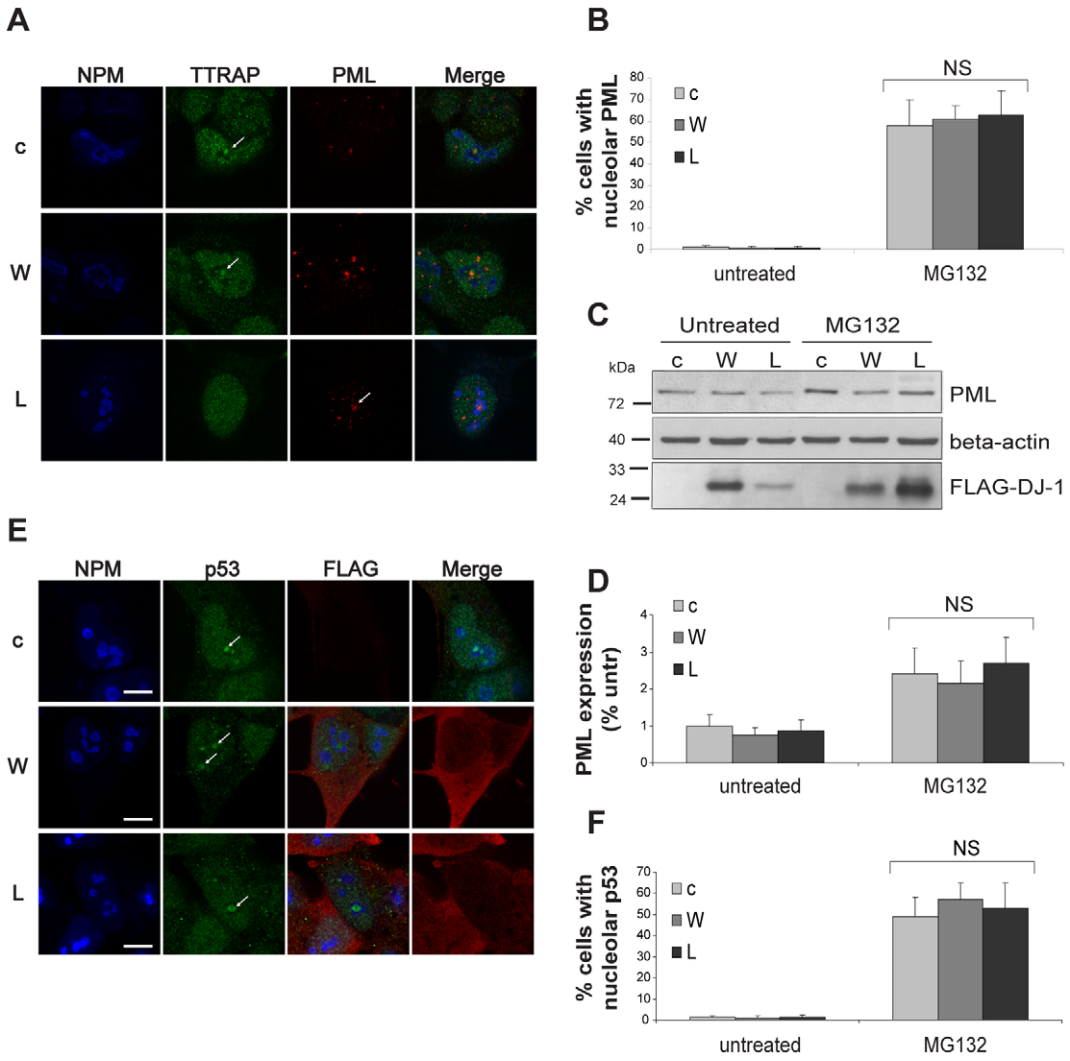

Figure 4. Mutant DJ-1 L166P does not inhibit nucleolar localization of PML and p53 upon proteotoxic stress. (A) Nucleolar localization of PML. SH-SY5Y cells stably expressing wt DJ-1 (W), L166P (L) or empty vector (c) were treated with 5 μM MG132 for 16 h. Endogenous TTRAP (green), PML (red) and NPM (blue) localization was analyzed by triple immunofluorescence. Images are representatives of two separate experiments performed on two independent clones for each cell line. (B) Quantification of PML nucleolar localization. Cells were treated as in A. 200 cells from two independent experiments were counted and scored for PML in the nucleolus (*, $p<0.05$). (C) Mutant DJ-1 L166P does not affect levels of endogenous PML. SH-SY5Y cells stably expressing wt DJ-1 (W), L166P (L) or empty vector (c) were treated with 5 μM MG132 for 16 h or left untreated, as indicated. The expression of endogenous PML and overexpressed FLAG-DJ-1 were measured with anti-PML and anti-FLAG antibodies, respectively. Beta-actin was detected as loading control. (D) Quantification of PML levels. Densitometric analysis of protein bands was performed on two independent experiments. Relative expression of endogenous PML was normalized to beta-actin. Data are expressed as the percentage of untreated condition in empty cells (c). (E) Nucleolar localization of p53. Cells were exactly as in A. Localization of endogenous p53 (green), NPM (blue) and FLAG-DJ-1 (red) were analyzed by triple immunofluorescence. Bars, 10 μm. (F) Quantification of p53 nucleolar localization. Analysis was performed as in B (NS, non significant).
doi:10.1371/journal.pone.0035051.g004

Knocking-down TRAF6 expression recapitulated the phenotype observed with TRAF6-DN, with partial recovery of nucleolar TTRAP localization (Figure 6C, 6D and 6E). In line with partial rescue of TTRAP nucleolar localization, knockdown of TRAF6 could also partially recover rRNA biogenesis defects in mutant DJ-1 cells exposed to proteasome inhibition, although not all processing intermediates were affected to the same extent (Figure S9); this observation is also compatible with a DJ-1/TTRAP independent role of TRAF6 in regulating ribosome biogenesis in response to proteotoxic stress.

In any case, our data indicate that TRAF6 E3 ligase activity contributes to TTRAP partitioning between cytoplasmic and nucleolar aggregates in the presence of misfolded mutant DJ-1.

Discussion

L166P presents a structural rearrangement that interferes with dimer formation favoring oligomerization and protein instability [13,32]. This led to the hypothesis that DJ-1 deletions and missense mutations share a common phenotype based on a loss-of-function model. However, increasing evidences indicate that missense mutations like L166P may also present gain-of-function properties. L166P has exerted dominant-negative effects on the antioxidant wt DJ-1 activity [33]. Gene profiling experiments in DJ-1 KO and in L166P-NIH3T3 cells [34] have shown that L166P affects the expression of a larger number of genes with no common genes between these two conditions. Furthermore, tau

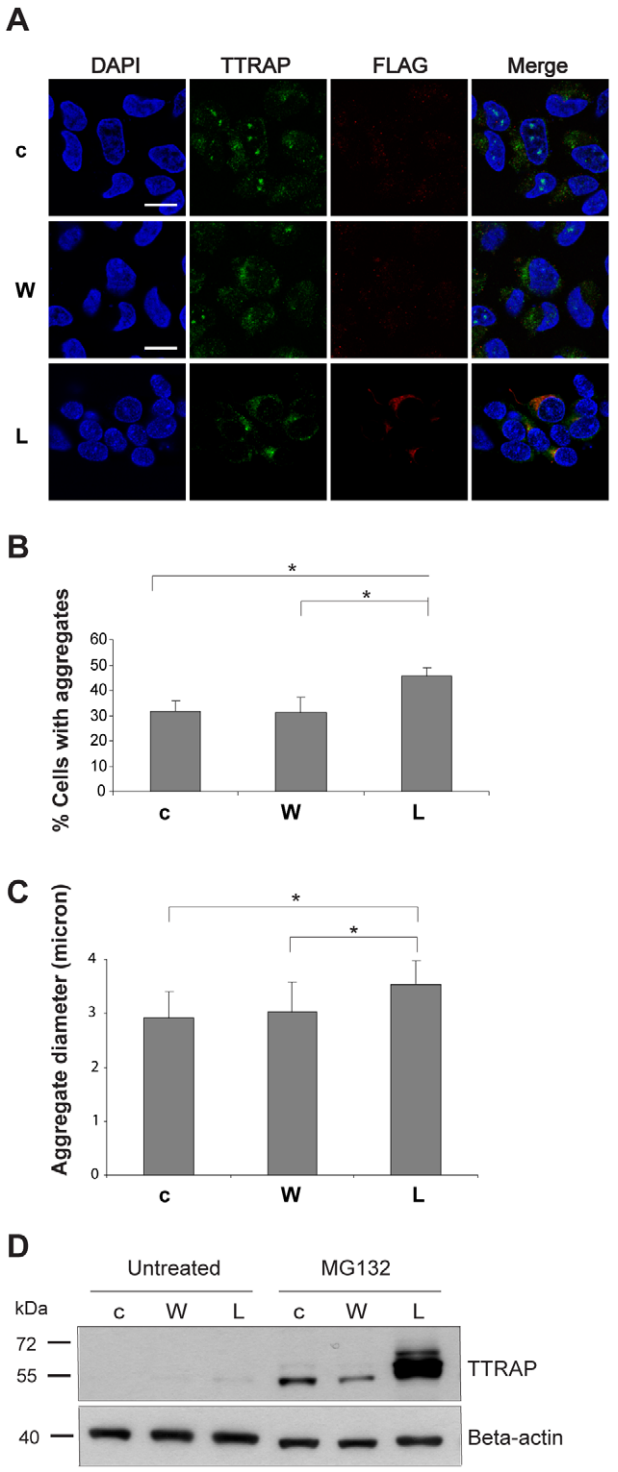

Figure 5. L166P enhances TTRAP accumulation into insoluble cytoplasmic aggresomes. (A) Cytoplasmic localization of TTRAP. SH-SY5Y cells stably expressing wt DJ-1 (W), L166P (L) or empty vector (c) were treated with 5 μM MG132 for 16 h. Before fixation, cells were permeabilized with Triton X-100 and double immunofluorescence was performed with TTRAP (green) and anti-FLAG (red) antibodies. Nuclei were visualized with DAPI. Confocal images from two independent experiments were scored for percentage of cells with aggregates (B), and aggregate average size (C). At least 50 cells per experimental condition were counted (*, $p<0.05$). (D) Mutant DJ-1 L166P promotes accumulation of TTRAP in insoluble fraction. Cells were as in A. After treatment with MG132, cells were lysed, and Triton X-100 insoluble fraction was prepared. Endogenous TTRAP was analyzed by western blotting with anti-TTRAP antibody. Protein loading was controlled by beta-actin.
doi:10.1371/journal.pone.0035051.g005

promoter was directly upregulated by L166P, in conditions when wt DJ-1 was acting as a repressor. In this context, we have previously shown that upon proteasome impairment L166P blocked the neuroprotective property of TTRAP to MG132 treatment inducing JNK and p38 MAPKs apoptotic pathways [23].

Here we provide evidences for a novel pathogenic mechanism of mutant DJ-1 mediated by the sequestration of TTRAP. Upon proteasome inhibition, L166P triggers alterations of rRNA biogenesis by selectively excluding TTRAP from nucleolar cavities and sequestering it into cytoplasmic aggregates. Inhibition of TTRAP nucleolar localization by accumulated misfolded proteins is not restricted to mutant DJ-1, but can also be observed for aggregates of mutant huntingtin.

rRNA biogenesis is a complex process that requires the transcription of rDNA genes by polymerase I, nucleolytic cleavages and chemical modification of precursor rRNAs and ultimately leads to the assembly of mature ribosomes [35]. It is subjected to rigorous quality control mechanisms [36,37] and stressful events elicit homeostatic responses that involve the majority of its steps [38,39]. We have previously found that TTRAP regulates rRNA biogenesis under proteasome impairment. TTRAP down-regulation leads to a decrease of pre-rRNA and a concomitant increase of processing species thus suggesting it might function at multiple steps [20]. Accumulation of processing intermediates might be due to impaired cleavage or to reduced degradation of cleaved fragments, while the effects on pre-rRNA levels may unveil a role of TTRAP at rDNA loci or may be secondary to changes in rRNA processing [40].

Here we show that misfolded mutant DJ-1 expression recapitulates this phenotype affecting the initial events of transcription and the conversion of intermediate to mature forms (47S to 45S and 32S to 28S). While both qPCR and pulse-chase labeling with ^{32}P-orthophosphate indicate an increase in the amount of rRNA processing intermediates, the quantity of A0 sites was strongly reduced when measured with qPCR while seemed increased in pulse-chase experiment. To reconcile these data we hypothesize that PCR amplification of the 5′ ETS region of rRNA precursors may detect illegitimate small RNA species due to abortive transcription initiation that are not visible by gel electrophoresis.

Several human genetic diseases, collectively defined as ribosomopathies, are caused by mutations in genes involved rRNA biogenesis and ribosome assembly [41]. Surprisingly, few studies so far have analyzed the status of protein synthesis, ribosome biogenesis and of the nucleolus in human post-mortem brains of neurodegenerative diseases. Alteration of protein synthesis capability due to ribosome dysfunction has been shown to be an early event in Alzheimer's disease [42]. A nucleolar protein involved in ribosome biogenesis was found induced in post-mortem brains of Huntington's disease patients [43]. Nucleolin was identified as an interactor of the PD-associated proteins DJ-1 and alpha-synuclein and its protein expression was found reduced in Substantia Nigra of human PD brains [25]. More recently, genetic ablation of rRNA transcription caused an alteration of the nucleolus architecture and ultimately neurodegeneration both in hippocampal and dopaminergic neurons [26,44].

An analysis of rRNA biogenesis in post-mortem brains of familial PD cases and in animal models of the disease is thus

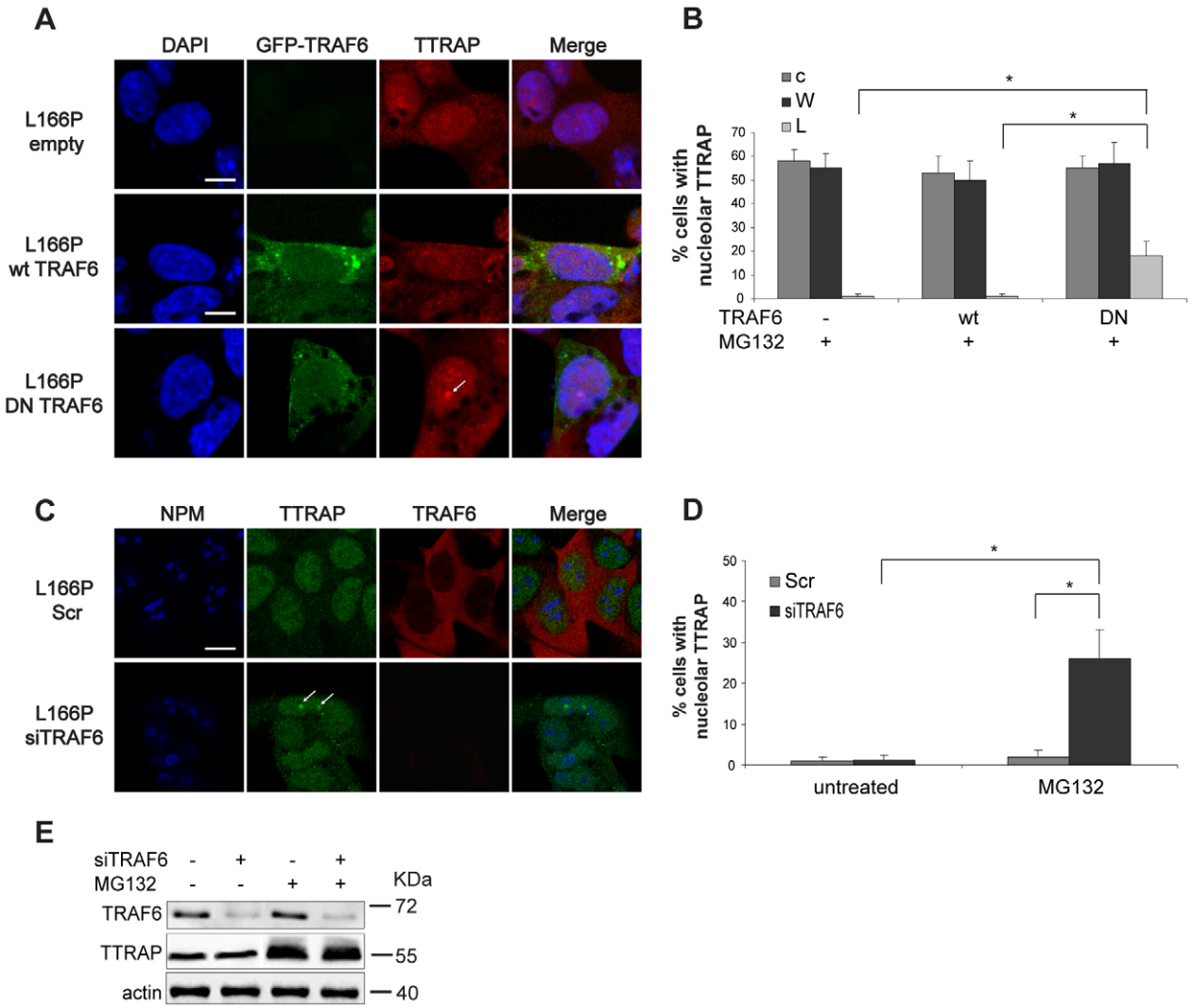

Figure 6. TRAF6 E3 ligase activity contributes to L166P-mediated exclusion of TTRAP from nucleolar cavities. (A) Expression of TRAF6 DN partially rescues TTRAP nucleolar localization in L166P cells. SH-SY5Y cells stably expressing mutant DJ-1 were transfected with GFP-tagged TRAF6 (wt or deleted of the N-terminus, DN), or with empty vector control, as indicated. After 24 h from transfection, cells were treated for 16 h with MG132. TTRAP localization was followed by indirect immunofluorescence coupled with GFP autofluorescence. Bars, 10 μm. (B) Quantification of TTRAP nucleolar localization. Cells were as in A. At least 100 transfected cells with comparable GFP levels from two independent experiments were counted and scored for TTRAP in the nucleolus (*, $p<0.05$). (C) Knock-down endogenous TRAF6 expression partially rescues TTRAP nucleolar localization. SH-SY5Y cells stably transfected with mutant DJ-1 L166Pwere transfected with siRNA oligonucleotides targeting endogenous TRAF6 (siTRAF6) or with a scramble control siRNA (Scr). After 72 h from transfection, cells were treated for 16 h with MG132. Immunofluorescence was performed with anti-TTRAP (green), anti-TRAF6 (red), anti-NPM (blue). Bars, 15 μm. (D) Quantification of TTRAP nucleolar localization. Cells were as in C. Analysis was performed as in B on cells with reduced TRAF6 expression (*, $p<0.05$). (E) Total cell lysates were prepared from SH-SY5Y cells transfected as in C. Cells were treated with MG132 for 16 h or left untreated. Expression of endogenous TRAF6 and TTRAP was measured with specific antibodies. Protein loading was controlled by beta-actin. Molecular weight markers (MWM) are indicated for each gel (kDa). Images are representative of two independent experiments.
doi:10.1371/journal.pone.0035051.g006

needed. Interestingly, the association of TTRAP to the nucleolus of DA cells in sporadic PD brains increases the list of changes in the nucleolar composition in PD. Their functional effects remain to be investigated.

Recently, nucleolar aggregates have been identified as a novel form of nuclear stress bodies that occupy nucleolar cavities [20,28]. They contain polyadenylated RNA, unconjugated ubiquitin and several nucleoplasmic proteasome target proteins [28]. Their formation was relieved by an excess of free cytoplasmic ubiquitin and occurred with both wt and triple mutant ubiquitins lacking K48, K29 and K63 lysines, proving that atypical ubiquitination is involved. This led to the hypothesis that a cross-talk between cytoplasmic and nucleolar aggregates regulates the subcellular localization of atypically ubiquitinated misfolded proteins.

The partitioning of TTRAP between nucleolar and cytoplasmic aggregates is modulated by TRAF6. This E3 ligase binds both TTRAP and mutant DJ-1 promoting atypical ubiquitination of L166P and its accumulation in cytoplasmic aggregates [15]. When TRAF6 ligase activity is lacking, L166P inclusions are smaller and TTRAP is relieved to relocate, at least in part, into the nucleolus. Other E3 ubiquitin ligases, such as parkin [45], have been

demonstrated to act on mutant DJ-1, possibly accounting for additional TRAF6-independent regulation. TRAF6, as other E3 ubiquitin ligases, is accumulated in LBs [15]. In this context, the aberrant localization of TTRAP in LBs and in the nucleolus of sporadic PD post-mortem brains may suggest the existence of this regulatory pathway *in vivo*. On the other hand, the impact of TTRAP sequestration and consequent alteration in rRNA biogenesis in familial cases will ultimately depend on the level of L166P protein, which remains unknown. In summary this work demonstrates a novel role for misfolded mutant DJ-1 in the homeostasis of rRNA biogenesis and suggests the existence of a functional interplay between cytoplasmic and nucleolar aggregates that may regulate nucleolar functions in neurodegenerative diseases.

Supporting Information

Figure S1 Quantitative analysis of TTRAP nucleolar localization. (A) TTRAP localizes to the nucleolus upon proteotoxic stress. SH-SY5Y cells were treated with increasing concentration of Epoxomycin or Lactacystin, as indicated. Untreated cells were used as controls. TTRAP was visualized with indirect immunofluorescence with anti-TTRAP antibody (green). Nuclei were visualized with DAPI (blue). Nucleolar TTRAP was scored in DAPI-negative regions in >100 cells. Representative images are shown for cells treated with 1 μM Epoxomycin and 25 μM Lactacystin. (*, $p<0.05$). (B) TTRAP staining is specific. SH-SY5Y cells stably expressing a short-hairpin RNA targeting TTRAP (siTTRAP #1 and #2) or a scrambled shRNA control (scramble #1 and #2) were treated for 16 h with 5 μM MG132. TTRAP (green) and nuclei (blue) were stained as in A.
(TIF)

Figure S2 Altered TTRAP nucleolar localization in L166P mutant cells upon treatment with MG132. SH-SY5Y cells stably transfected with empty vector (c), FLAG-DJ-1 wt (W) or L166P (L) were treated with 5 μM MG132 for 16 h or left untreated. TTRAP localization was analyzed by immunofluorescence with anti-TTRAP (green) and anti-FLAG (red) antibodies. Nuclei were visualized by DAPI staining (blue). Low magnification images are shown. Nucleolar TTRAP is evident in DAPI-negative regions of the nucleus (white arrows). Images are representatives of three independent experiments from two independent clones for each cell line.
(TIF)

Figure S3 Analysis of DJ-1 expression in siDJ-1 and scramble SH-SY5Y cells. SH-SY5Y cells stably expressing a doxycyclin-inducible short-hairpin targeting DJ-1 (siDJ-1, clones A and B) or a scramble shRNA control (scramble, a and b) were treated with doxycycline for 10 days. Endogenous DJ-1 expression was analyzed by immunofluorescence with anti-DJ-1 antibody.
(TIF)

Figure S4 Depletion of DJ-1 does not alter transcription and processing of ribosomal RNA. SH-SY5Y stably expressing a doxycyclin-inducible shRNA targeting DJ-1 (siDJ-1, clones A and B) or a scramble shRNA control (scramble, a and b) were induced 10 days with doxyciclin and then treated with 5 μM MG132 for 16 h, or left untreated. Total RNA was extracted and levels of pre-rRNA and processing intermediates were analyzed by qPCR. Amplicons are those described in figure 3. Standard deviations are calculated from two independent experiments. Differences between a, b, A and B are not statistically significant (*, $P<0.05$. NS, not significant).
(TIF)

Figure S5 Analysis of the effects of wild-type and mutant DJ-1 on nucleolar integrity. SH-SY5Y cells stably expressing wt DJ-1 (W), L166P (L) or empty vector (c) were treated with 5 μM MG132 for 16 h. Immunofluorescence was performed with anti-NPM antibody and NPM nucleoplasmic staining was measured with ImageJ software on a randomly selected area. Background fluorescence was quantified from an area placed outside the cells and was subtracted for each signal. At least 100 cells from two separate experiments were counted (NS, not statistically significant). Representative zoomed images are shown for each cell line.
(TIF)

Figure S6 Analysis of the effects of mutant DJ-1 L166P on cell proliferation and viability. (A) Expression of L166P does not affect the cell cycle. SH-SY5Y cells stably expressing the L166P mutant and control cells were treated for 16 h with 5 μM MG132, or DMSO as control. Cell proliferation was analyzed by flow-cytometry (FACS) after propidium iodide (PI) staining. Graphs show the overlay of representative FACS profiles for each sample. (B) Quantification of the cell cycle distribution in control and L166P cells treated as in A. Data are from three independent experiments (error bars, standard deviation). (C) Expression of L166P DJ-1 moderately sensitizes cells to death induced by proteasome inhibition. Identical numbers of L166P and control cells were seeded in 96-well plates. After 24 hours, cells were treated with DMSO or 5 μM MG132 for additional 16 h. Cell viability was measured by WST-1 assay. Data are normalized to WST activity in untreated cells. Standard deviations are calculated from four independent experiments (*, $p<0.05$).
(TIF)

Figure S7 Localization of PML and p53 is not affected by the expression of DJ-1 L166P mutant in untreated cells. (A) Localization of PML. SH-SY5Y cells stably expressing FLAG-tagged DJ-1 wt (W), or mutant (L) or empty vector (c) were stained by triple immunofluorescence with anti-TTRAP (green), anti-PML (red) and anti-NPM (blue) antibodies. (B) Localization of p53. Cells were stained by triple immunofluorescence with anti-NPM (blue), anti-p53 (green) and anti-FLAG (red) antibodies. Bars, 10 μm.
(TIF)

Figure S8 TRAF6 expression does not alter TTRAP localization in untreated cells. SH-SY5Y stably expressing L166P were transfected with GFP-TRAF6 (wt and DN), as indicated. Cells were left untreated. TTRAP localization was analyzed by immunofluorescence with anti-TTRAP (red) antibody. Bars, 10 μm.
(TIF)

Figure S9 Analysis of rRNA biogenesis in mutant DJ-1 L166P cells with knock-down of TRAF6 expression. SH-SY5Y cells stably transfected with mutant DJ-1 L166P were transfected with oligonucleotides targeting endogenous TRAF6 (siRNA TRAF6) or a scramble control sequence (siRNA Scramble). After 72 h from transfection, cells were treated for 16 h with MG132 or DMSO as control. Total RNA was extracted and levels of pre-rRNA and processing intermediates were analyzed by qPCR with primers targeting A0, 1 and 4 cleavage sites, as indicated. Efficiency of TRAF6 knock-down was monitored with specific primers (TRAF6). Standard deviations are calculated from four independent experiments (*, $P<0.05$).
(TIF)

Acknowledgments

We are indebted to Prof. F. Persichetti (University of Eastern Piedmont, Italy) and all the members of the SG lab for thought-provoking discussions. We thank Cristina Leonesi for technical support.

Author Contributions

Conceived and designed the experiments: SV MC MDF MP IF LC SG SZ. Performed the experiments: SV MC MDF MP. Analyzed the data: SV MC MDF MP IF LC SG SZ. Contributed reagents/materials/analysis tools: SV MDF MP LC IF SG SZ. Wrote the paper: SV LC SG SZ.

References

1. Lesage S, Brice A (2009) Parkinson's disease: from monogenic forms to genetic susceptibility factors. Hum Mol Genet 18: R48–59.
2. DiFiglia M, Sapp E, Chase KO, Davies SW, Bates GP, et al. (1997) Aggregation of huntingtin in neuronal intranuclear inclusions and dystrophic neurites in brain. Science 277: 1990–1993.
3. Betarbet R, Sherer TB, Greenamyre JT (2005) Ubiquitin-proteasome system and Parkinson's diseases. Exp Neurol 191 Suppl 1: S17–27.
4. McNaught KS, Belizaire R, Isacson O, Jenner P, Olanow CW (2003) Altered proteasomal function in sporadic Parkinson's disease. Exp Neurol 179: 38–46.
5. Petrucelli L, O'Farrell C, Lockhart PJ, Baptista M, Kehoe K, et al. (2002) Parkin protects against the toxicity associated with mutant alpha-synuclein: proteasome dysfunction selectively affects catecholaminergic neurons. Neuron 36: 1007–1019.
6. Rideout HJ, Lang-Rollin IC, Savalle M, Stefanis L (2005) Dopaminergic neurons in rat ventral midbrain cultures undergo selective apoptosis and form inclusions, but do not up-regulate iHSP70, following proteasomal inhibition. J Neurochem 93: 1304–1313.
7. Bonifati V, Rizzu P, van Baren MJ, Schaap O, Breedveld GJ, et al. (2003) Mutations in the DJ-1 gene associated with autosomal recessive early-onset parkinsonism. Science 299: 256–259.
8. Andres-Mateos E, Perier C, Zhang L, Blanchard-Fillion B, Greco TM, et al. (2007) DJ-1 gene deletion reveals that DJ-1 is an atypical peroxiredoxin-like peroxidase. Proc Natl Acad Sci U S A 104: 14807–14812.
9. Hao LY, Giasson BI, Bonini NM (2010) DJ-1 is critical for mitochondrial function and rescues PINK1 loss of function. Proc Natl Acad Sci U S A 107: 9747–9752.
10. Thomas KJ, McCoy MK, Blackinton J, Beilina A, van der Brug M, et al. (2011) DJ-1 acts in parallel to the PINK1/parkin pathway to control mitochondrial function and autophagy. Hum Mol Genet 20: 40–50.
11. Foti R, Zucchelli S, Biagioli M, Roncaglia P, Vilotti S, et al. (2010) Parkinson disease-associated DJ-1 is required for the expression of the glial cell line-derived neurotrophic factor receptor RET in human neuroblastoma cells. J Biol Chem 285: 18565–18574.
12. Vasseur S, Afzal S, Tardivel-Lacombe J, Park DS, Iovanna JL, et al. (2009) DJ-1/PARK7 is an important mediator of hypoxia-induced cellular responses. Proc Natl Acad Sci U S A 106: 1111–1116.
13. Herrera FE, Zucchelli S, Jezierska A, Lavina ZS, Gustincich S, et al. (2007) On the oligomeric state of DJ-1 protein and its mutants associated with Parkinson Disease. A combined computational and in vitro study. J Biol Chem 282: 24905–24914.
14. Olzmann JA, Li L, Chudaev MV, Chen J, Perez FA, et al. (2007) Parkin-mediated K63-linked polyubiquitination targets misfolded DJ-1 to aggresomes via binding to HDAC6. J Cell Biol 178: 1025–1038.
15. Zucchelli S, Codrich M, Marcuzzi F, Pinto M, Vilotti S, et al. (2010) TRAF6 promotes atypical ubiquitination of mutant DJ-1 and alpha-synuclein and is localized to Lewy bodies in sporadic Parkinson's disease brains. Hum Mol Genet 19: 3759–3770.
16. Cattaneo E, Rigamonti D, Goffredo D, Zuccato C, Squitieri F, et al. (2001) Loss of normal huntingtin function: new developments in Huntington's disease research. Trends Neurosci 24: 182–188.
17. Sau D, De Biasi S, Vitellaro-Zuccarello L, Riso P, Guarnieri S, et al. (2007) Mutation of SOD1 in ALS: a gain of a loss of function. Hum Mol Genet 16: 1604–1618.
18. Zucchelli S, Marcuzzi F, Codrich M, Agostoni E, Vilotti S, et al. (2011) Tumor Necrosis factor receptor associated factor 6 (TRAF6) associates with huntingtin protein and promotes its atypical ubiquitination to enhance aggregate formation. J Biol Chem.
19. Cortes Ledesma F, El Khamisy SF, Zuma MC, Osborn K, Caldecott KW (2009) A human 5′-tyrosyl DNA phosphodiesterase that repairs topoisomerase-mediated DNA damage. Nature 461: 674–678.
20. Vilotti S, Biagioli M, Foti R, Dal Ferro M, Lavina ZS, et al. (2011) The PML nuclear bodies-associated protein TTRAP regulates ribosome biogenesis in nucleolar cavities upon proteasome inhibition. Cell Death Differ.
21. Pype S, Declercq W, Ibrahimi A, Michiels C, Van Rietschoten JG, et al. (2000) TTRAP, a novel protein that associates with CD40, tumor necrosis factor (TNF) receptor-75 and TNF receptor-associated factors (TRAFs), and that inhibits nuclear factor-kappa B activation. J Biol Chem 275: 18586–18593.
22. Pei H, Yordy JS, Leng Q, Zhao Q, Watson DK, et al. (2003) EAPII interacts with ETS1 and modulates its transcriptional function. Oncogene 22: 2699–2709.
23. Zucchelli S, Vilotti S, Calligaris R, Lavina ZS, Biagioli M, et al. (2009) Aggresome-forming TTRAP mediates pro-apoptotic properties of Parkinson's disease-associated DJ-1 missense mutations. Cell Death Differ 16: 428–438.
24. Kruger T, Scheer U (2010) p53 localizes to intranucleolar regions distinct from the ribosome production compartments. J Cell Sci 123: 1203–1208.
25. Caudle WM, Kitsou E, Li J, Bradner J, Zhang J (2009) A role for a novel protein, nucleolin, in Parkinson's disease. Neurosci Lett 459: 11–15.
26. Rieker C, Engblom D, Kreiner G, Domanskyi A, Schober A, et al. (2011) Nucleolar disruption in dopaminergic neurons leads to oxidative damage and parkinsonism through repression of mammalian target of rapamycin signaling. J Neurosci 31: 453–460.
27. Navarro A, Boveris A, Bandez MJ, Sanchez-Pino MJ, Gomez C, et al. (2009) Human brain cortex: mitochondrial oxidative damage and adaptive response in Parkinson disease and in dementia with Lewy bodies. Free Radic Biol Med 46: 1574–1580.
28. Latonen L, Moore HM, Bai B, Jaamaa S, Laiho M (2011) Proteasome inhibitors induce nucleolar aggregation of proteasome target proteins and polyadenylated RNA by altering ubiquitin availability. Oncogene.
29. Murayama A, Ohmori K, Fujimura A, Minami H, Yasuzawa-Tanaka K, et al. (2008) Epigenetic control of rDNA loci in response to intracellular energy status. Cell 133: 627–639.
30. Schmitz KM, Mayer C, Postepska A, Grummt I (2010) Interaction of noncoding RNA with the rDNA promoter mediates recruitment of DNMT3b and silencing of rRNA genes. Genes Dev 24: 2264–2269.
31. Schultheiss U, Puschner S, Kremmer E, Mak TW, Engelmann H, et al. (2001) TRAF6 is a critical mediator of signal transduction by the viral oncogene latent membrane protein 1. EMBO J 20: 5678–5691.
32. Macedo MG, Anar B, Bronner IF, Cannella M, Squitieri F, et al. (2003) The DJ-1L166P mutant protein associated with early onset Parkinson's disease is unstable and forms higher-order protein complexes. Hum Mol Genet 12: 2807–2816.
33. Kim RH, Smith PD, Aleyasin H, Hayley S, Mount MP, et al. (2005) Hypersensitivity of DJ-1-deficient mice to 1-methyl-4-phenyl-1,2,3,6-tetrahydropyrindine (MPTP) and oxidative stress. Proc Natl Acad Sci U S A 102: 5215–5220.
34. Wang C, Ko HS, Thomas B, Tsang F, Chew KC, et al. (2005) Stress-induced alterations in parkin solubility promote parkin aggregation and compromise parkin's protective function. Hum Mol Genet 14: 3885–3897.
35. Henras AK, Soudet J, Gerus M, Lebaron S, Caizergues-Ferrer M, et al. (2008) The post-transcriptional steps of eukaryotic ribosome biogenesis. Cell Mol Life Sci 65: 2334–2359.
36. Dez C, Houseley J, Tollervey D (2006) Surveillance of nuclear-restricted pre-ribosomes within a subnucleolar region of Saccharomyces cerevisiae. EMBO J 25: 1534–1546.
37. LaRiviere FJ, Cole SE, Ferullo DJ, Moore MJ (2006) A late-acting quality control process for mature eukaryotic rRNAs. Mol Cell 24: 619–626.
38. Blaise R, Masdehors P, Lauge A, Stoppa-Lyonnet D, Alapetite C, et al. (2001) Chromosomal DNA and p53 stability, ubiquitin system and apoptosis in B-CLL lymphocytes. Leuk Lymphoma 42: 1173–1180.
39. Stavreva DA, Kawasaki M, Dundr M, Koberna K, Muller WG, et al. (2006) Potential roles for ubiquitin and the proteasome during ribosome biogenesis. Mol Cell Biol 26: 5131–5145.
40. Schmid M, Jensen TH (2008) The exosome: a multipurpose RNA-decay machine. Trends Biochem Sci 33: 501–510.
41. Narla A, Ebert BL (2010) Ribosomopathies: human disorders of ribosome dysfunction. Blood 115: 3196–3205.
42. Ding Q, Markesbery WR, Chen Q, Li F, Keller JN (2005) Ribosome dysfunction is an early event in Alzheimer's disease. J Neurosci 25: 9171–9175.
43. Carnemolla A, Fossale E, Agostoni E, Michelazzi S, Calligaris R, et al. (2009) Rrs1 is involved in endoplasmic reticulum stress response in Huntington disease. J Biol Chem 284: 18167–18173.
44. Parlato R, Kreiner G, Erdmann G, Rieker C, Stotz S, et al. (2008) Activation of an endogenous suicide response after perturbation of rRNA synthesis leads to neurodegeneration in mice. J Neurosci 28: 12759–12764.
45. Olzmann J, Li L, Chudaev M, Chen J, Perez F, et al. (2007) Parkin-mediated K63-linked polyubiquitination targets misfolded DJ-1 to aggresomes via binding to HDAC6. The Journal of Cell Biology 178: 1025–1038.

Biochimica et Biophysica Acta xxx (2013) xxx–xxx

Contents lists available at SciVerse ScienceDirect

Biochimica et Biophysica Acta

journal homepage: www.elsevier.com/locate/bbapap

Hemoglobin is present as a canonical $\alpha_2\beta_2$ tetramer in dopaminergic neurons☆,☆☆

Roberta Russo [a,1], Silvia Zucchelli [b,1], Marta Codrich [b], Federica Marcuzzi [b], Cinzia Verde [a,c,*], Stefano Gustincich [b,**]

[a] Institute of Protein Biochemistry, CNR, Via Pietro Castellino 111, 80131 Naples, Italy
[b] SISSA, Area of Neuroscience, via Bonomea 265, 34136 Trieste, Italy
[c] Roma 3 University, Department of Biology, Viale Marconi 446, 00146 Rome, Italy

ARTICLE INFO

Article history:
Received 14 February 2013
Received in revised form 29 April 2013
Accepted 8 May 2013
Available online xxxx

Keywords:
Dopaminergic neurons
Hemoglobin
Mouse
Native structure

ABSTRACT

Hemoglobin is the oxygen carrier in blood erythrocytes. Oxygen coordination is mediated by $\alpha_2\beta_2$ tetrameric structure via binding of the ligand to the heme iron atom. This structure is essential for hemoglobin function in the blood. In the last few years, expression of hemoglobin has been found in atypical sites, including the brain. Transcripts for α and β chains of hemoglobin as well as hemoglobin immunoreactivity have been shown in mesencephalic A9 dopaminergic neurons, whose selective degeneration leads to Parkinson's disease. To gain further insights into the roles of hemoglobin in the brain, we examined its quaternary structure in dopaminergic neurons *in vitro* and *in vivo*. Our results indicate that (*i*) in mouse dopaminergic cell line stably over-expressing α and β chains, hemoglobin exists as an $\alpha_2\beta_2$ tetramer; (ii) similarly to the over-expressed protein, endogenous hemoglobin forms a tetramer of 64 kDa; (iii) hemoglobin also forms high molecular weight insoluble aggregates; and (iv) endogenous hemoglobin retains its tetrameric structure in mouse mesencephalon *in vivo*. In conclusion, these results suggest that neuronal hemoglobin may be endowed with some of the biochemical activities and biological function associated to its role in erythroid cells. This article is part of a Special Issue entitled: Oxygen Binding and Sensing Proteins.

1. Introduction

Hemoglobin (Hb) is the major heme-containing protein of erythrocytes, where it mediates the transport of oxygen and carbon dioxide in the blood. Hb is an assembly of four globular protein subunits each containing a heme moiety. In adult humans the most common type of Hb is a hetero-tetramer consisting of two α and two β subunits held together by non-covalent interactions ($\alpha_2\beta_2$). The expression of α and β chains and their post-translational assembly into $\alpha_2\beta_2$ tetramers is fundamental for Hb to function. As a consequence, strong evolutionary pressure has favored the expression of equal amounts of α and β chains, supporting the evidence that all the functional properties displayed by Hb, as cooperativity, pH sensitivity, and anionic regulation, occur only in the $\alpha_2\beta_2$ tetramers [1].

It has long been thought that Hb expression is restricted to erythrocytes and precursor cells of the erythroid lineage. This notion has been extensively revised in recent years. Hb α and β chains have been found co-expressed in alveolar cells [2], mesangial cells of the kidney [3], retinal ganglion cells [4], hepatocytes [5], and neurons [6–8]. Endothelial and peripheral catecholaminergic cells express exclusively the α chain [9] while macrophages present the β chain only [10]. Importantly, Hb expression has been associated to various types of cancer [11–13].

In the brain, Hb can be detected in mesencephalic A9 dopaminergic neurons, whose selective degeneration is the primary cause of Parkinson's disease [14], in cortical and hippocampal astrocytes as well as in virtually all mature oligodentrocytes [6]. Similar pattern of Hb staining is present in mouse, rat and human central nervous systems [6,7]. Importantly, altered Hb levels have been observed in neurodegenerative diseases *post-mortem* brains. Hb expression is increased in pyramidal neurons in the cortex of multiple sclerosis's patients [15], whereas it is decreased in neurons of Alzheimer's and Parkinson disease brains [16]. Elevated levels of Hb can be found in extracellular amyloid plaques and aged brains, possibly due to compromised brain-blood barrier [17].

The specific function of Hb in neurons remains unclear. We have previously showed that Hb regulates genes involved in oxygen homeostasis and oxidative phosphorylation, linking Hb expression to mitochondrial activity [6]. This is particularly relevant in the context of mesencephalic A9 dopaminergic neurons, since these cells specifically express genes involved in energy metabolism and

☆☆ This article is part of a Special Issue entitled: Oxygen Binding and Sensing Proteins.

* Correspondence to: C. Verde, Institute of Protein Biochemistry, National Research Council, Via Pietro Castellino 111, 80131, Naples, Italy. Tel./fax: +39 081 6132710.
** Correspondence to: S. Gustincich, SISSA, Sector of Neurobiology, Via Bonomea 265, 34136 Trieste, Italy. Tel.: +39 040 3787 705; fax: +39 040 3787 702.
E-mail addresses: c.verde@ibp.cnr.it (C. Verde), gustinci@sissa.it (S. Gustincich).

[1] These two authors contributed equally to this work.

1570-9639/$ – see front matter © 2013 The Authors. Published by Elsevier B.V. All rights reserved.
http://dx.doi.org/10.1016/j.bbapap.2013.05.005

mitochondrial function and present a high metabolic rate and oxidative stress [18,19]. These features are believed to be important for cells' selective vulnerability in Parkinson disease.

In red blood cells Hb functions are achieved through tetrameric structure, but so far no evidence is available for neuronal Hb.

To gain further insights into the biochemical activities and biological functions of Hb in the brain, we have examined the quaternary structure of Hb in dopaminergic neurons *in vitro* and *in vivo*. In this study, we demonstrate for the first time that Hb exhibits a $\alpha_2\beta_2$ hetero-tetrameric state in mouse and human neuronal cell lines as well as in mouse mesencephalon. These results may have important implications in the physiology and pathology of the brain given the many defined roles inherent to the structure of Hb including gas exchange, NO metabolism, and protection against oxidative and nitrosative stress.

2. Materials and methods

2.1. Cell culture

Mouse dopaminergic neuroblastoma iMN9D cells were maintained in culture using Dulbecco's Modified Eagle Medium (DMEM)/ F12 medium (Invitrogen) supplemented with 10% fetal bovine serum (Sigma-Aldrich), 100 μg/mL penicillin and 100 μg/mL streptomycin. Neuro2a mouse neuroblastoma cells were cultured in Eagle's minimal essential medium (EMEM) with 10% fetal bovine serum (FBS), 1% GlutaMAX, 1% non-essential amino acids (NEAA) and antibiotics.

2.2. Cell lysis, protein extraction and protein assay

Cells were harvested and lysed by osmotic shock in Nonidet P-40 (NP-40) lysis buffer (150 mM NaCl, 50 mM Tris-Cl pH 7.5 and 0.5% NP-40) with the addition of protease inhibitor mixture (Roche). Lysates were then cleared by centrifugation (14,000 ×*g*, 30 min, 4 °C) and supernatants were transferred in new tubes. The total amount of solubilized protein was estimated with the Bio-Rad protein assay kit, according to the manufacturer's instructions. Insoluble proteins were also collected upon resuspending the pellets in sample buffer. Soluble and insoluble protein extracts were used for Western blot analysis. For competition assay, the anti-Hb (1:1000, Cappel) antibody was incubated with purified human Hb (HbA) (Sigma-Aldrich) at 1 mg/mL for 2 h at 4 °C. Nitrocellulose membranes were then incubated for 2 h at room temperature with the appropriate antibody–protein solutions, and subjected to Western blot detection as already described.

2.3. Native PAGE Electrophoresis

Native PAGE was performed on gradient polyacrylamide gel electrophoresis (10–12–17% of acrylamide) for approximately 3 h. Standard proteins were loaded using Native Mark Unstained Protein Standard (Sigma-Aldrich). The proteins supplied in the kit have a molecular mass range of 14.2–545 kDa.

For Western Blot analysis, proteins were transferred to nitrocellulose membrane (GE Healthcare). Membrane was blocked with 5% non-fat milk in Tris buffered saline (TBS) solution (TBS + 0.1% Tween-20), then incubated with primary antibodies overnight at 4 °C or at room temperature for 2 h. Proteins were detected by horseradish peroxidase (HRP)-conjugated secondary antibodies and enhanced chemiluminescence reagents (ECL) (GE Healthcare).

2.4. Primary antibodies

The following antibodies were used in this study for Western blot: anti-FLAG (1:1000, Sigma-Aldrich), anti-MYC (1:2000, Cell Signaling), anti-Hb (1:1000, Cappel), anti-β-actin (1:5000, Sigma). For detection, anti-mouse-HRP or anti-rabbit-HRP (Dako) in combination with ECL (GE Healthcare) was used.

2.5. In-cell cross-linking

Cells were extensively washed with ice-cold phosphate-buffered saline (PBS) (pH 8.0) to remove amine-containing culture media. Cells were incubated with 5 mM of the homobifunctional amine-reactive crosslinking reagent disuccinimidyl suberate (DSS) (Pierce Biotechnology) for 30, 60 or 360 min at room temperature. The reaction was quenched by incubation with 50 mM Tris-HCl, pH 7.5, for 15 min at room temperature. Samples were diluted in loading buffer and separated on homogenous 10–12–17% SDS–PAGE gels. The electrophoresis and Western blot were conducted as previously described for native PAGE and analyzed with an anti-Hb antibody.

2.6. Animals

All animal experiments were performed in accordance with European guidelines for animal care and following SISSA Ethical Committee permissions and SISSA veterinary service. Mice were housed and bred in SISSA non-specific pathogen free (SPF) animal facility, with 12 h dark/light cycles and controlled temperature and humidity. Mice had *ad libitum* access to food and water.

2.7. Extraction of native Hb from mouse midbrain

C57BL6 mice ($n = 4$), 12 months-old, were deeply anesthetized with a single intra-peritoneal injection of urethane (ethyl carbamate, Sigma, Cat. No. U2500) at the dose of 2 g/kg. Prior to brain sample collection, mice were extensively perfused with saline buffer through the circulatory system. Briefly, a cannula tip was inserted through the left ventricle and connected to a perfusion apparatus that utilizes a pump with fixed pressure flow to quickly reach every organ using the natural vascular network. The perfusion pump was set to match physiological pressure. After perfusion, mice were sacrificed by cervical dislocation and the ventral midbrain was dissected and immediately frozen in liquid nitrogen. Tissues were homogenized briefly with the aid of a mechanical homogenizer in NP-40 lysis buffer (150 mM NaCl, 50 mM Tris-Cl pH 7.5 and 0.5% NP-40) and complete protease inhibitor cocktail (Roche). Extraction volume was 1.5 mL. All steps were performed at 4 °C, in the absence of any detergent or denaturant. Following homogenization, the samples were subjected to centrifugation at 350 ×*g* for 20 min at 4 °C, and the supernatants and pellets were collected. Protein concentration was determined in the total lysate with the Bio-Rad protein assay kit, according to the manufacturer's instructions. The samples were maintained on ice at all times during preparation, avoiding freezing and thawing steps. Total lysate (TL), pellet (P) and supernatants (S) were loaded on SDS–PAGE and native Page as previously described.

3. Results and discussion

3.1. Hemoglobin is an $\alpha_2\beta_2$ tetramer in murine dopaminergic iMN9D cells

In the blood, functional Hb folds as a tetramer composed by two α and two β chains. To study the structure of Hb in neurons, we first determined the assembly of α and β chains in mouse dopaminergic iMN9D cells, a well-accepted *in vitro* model to study dopaminergic cell physiology and dysfunctions [20]. In a previous study we generated iMN9D cells stably expressing tagged version of α and β chains of mouse Hb [6]. Since most antibodies raised against mouse Hb do not discriminate between the two chains, we used anti-FLAG and anti-MYC monoclonals to determine the presence of each chain within Hb quaternary structure. In contrast to SDS–PAGE, native PAGE is performed in non-denaturing conditions and thus permits separation of intact non-covalent protein complexes [21,22]. We used this technique to determine the native molecular mass of Hb extracted from iMN9D cells expressing FLAG-α and MYC-β chains. As control, we included protein extracts prepared from

Please cite this article as: R. Russo, et al., Hemoglobin is present as a canonical $\alpha_2\beta_2$ tetramer in dopaminergic neurons, Biochim. Biophys. Acta (2013), http://dx.doi.org/10.1016/j.bbapap.2013.05.005

iMN9D cells stably transfected with an empty vector. Both anti-FLAG and anti-MYC antibodies detected a single band with an estimated mass of ~64 kDa, based on its mobility relative to native molecular weight markers (Fig. 1). As expected, no bands were observed in cells expressing an empty control vector. These data indicate that over-expressed Hb folds as a tetramer that contains two α and β chains. Interestingly, high molecular weight (HMW) complexes have been also detected. The same result was obtained when the lysates were probed with an anti-Hb specific antibody, thus confirming that anti-tag monoclonals detected Hb-containing bands.

Altogether these data demonstrate that Hb, when overexpressed in mouse dopaminergic cell line, is present as $\alpha_2\,\beta_2$ tetramer.

3.2. In-cell cross-linking assay

Since the migration of a protein on native PAGE does not depend solely on its mass but also on its conformation and charge, we stabilized α and β subunits within Hb with the bifunctional cross-linking reagent disuccinimidyl suberate (DSS). Protein chains that are in quaternary structure become covalently linked and their molecular mass can be determined by denaturing SDS–PAGE. We first examined DSS-mediated cross-linking on freshly prepared protein lysates, using a standard protocol [23]. Under these conditions, we noticed that the efficiency of chemical ligation was extremely low and only dimers could be observed (data not shown). The presence of α/β heterodimers upon *in vitro* cross-linking nonetheless confirms previous data showing physical interaction between the two chains by co-immunoprecipitation experiments [6].

To improve the efficacy of DSS ligation, we resorted to in-cell cross-linking. DSS is a membrane permeable molecule, and therefore can be added directly to the cell culture medium. Under these conditions, the proximity-induced cross-linking took place in the protein own cellular milieu. We applied in-cell cross-linking to iMN9D cells stably expressing tagged α and β chains of Hb or to empty vector-expressing cells as control. After protein extraction, lysates were subjected to SDS–PAGE followed by immuno-blot analysis. Anti-FLAG and anti-MYC monoclonals detected multiple unspecific bands and high background in denaturing conditions (data not shown), so anti-Hb antibody was used for detection. As shown in Fig. 2A, a protein band could be observed at about 32 kDa, compatible with the molecular size of covalently linked globin dimers thus confirming data obtained with previous protocols. We also observed SDS-stable Hb bands migrating at the expected positions of a trimer (~48 kDa) and tetramer (~64 kDa). Relative ratio between trimer and tetramer bands was strongly in favor of a trimeric structure, probably as a consequence of facilitated cross-linking for less complex structures as observed with α/β heterodimers. This conclusion is also supported by titration assays, showing an increasing proportion of oligomers (trimer and tetramers) with decreasing levels of monomers along with longer incubation times (Fig. 2B).

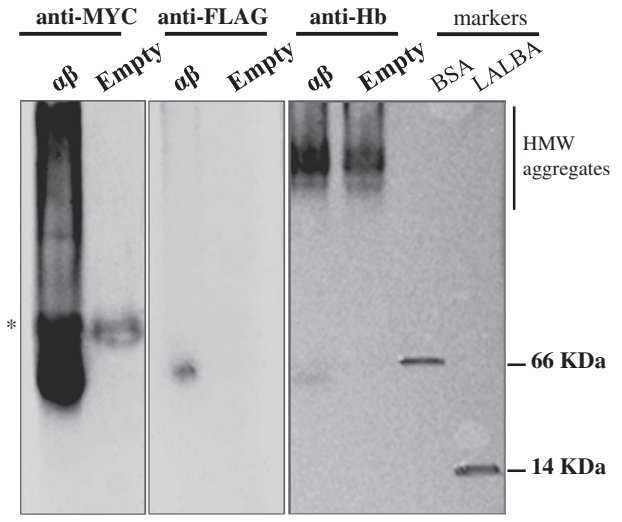

Fig. 1. Hb overexpressed in iMN9D dopaminergic cells is present as $\alpha_2\beta_2$. Native PAGE of dopaminergic iMN9D cells over-expressing FLAG-tagged α and MYC-tagged β chains. Lysates from iMN9D cells expressing empty vector were included as control. Purified proteins were used as markers, as indicated (BSA, bovine serum albumin; LALBA, α-lactalbumin). Relative molecular weights are indicated on the right (kDa). Anti-MYC, anti-FLAG and anti-Hb antibodies were used for immune-staining, as indicated. The asterisk indicates non-specific band. Images are representative of four independent experiments.

It has to be noted that bands of lower intensities but same molecular weight could be observed in empty control cells (Fig. 2A). Since these are revealed with an anti-Hb antibody, these data indicate that endogenous Hb protein is expressed in dopaminergic neuronal iMN9D cells. Importantly, chemical cross-linking indicates that the endogenous Hb can be detected as trimer and tetramer.

Altogether, these experiments further prove that overexpressed Hb has an $\alpha_2\beta_2$ fold and support the existence of native tetramers in dopaminergic neuronal cells.

3.3. Endogenous hemoglobin is a tetramer in neuronal cell lines

To further study the status of endogenous Hb, we used native PAGE to examine the protein expressed in dopaminergic (iMN9D) and in a non-dopaminergic (Neuro2a) neuronal cell lines. We choose Neuro2a since we have previously detected the expression of globin α and β chains mRNAs by RT-PCR (data not shown). Soluble extracts were separated from detergent-insoluble proteins to determine the distribution of Hb and its folding within biochemically-defined sub-cellular fractions. A clear band at ~64 kDa, corresponding to Hb tetramer, was observed in the soluble fractions of iMN9D as well as Neuro2a cells (Fig. 3A). Signal specificity was verified by competition assay, using purified HbA to compete for binding (Fig. 3A). Interestingly, both cell lines presented HMW complexes where multiple species could be detected.

To gain further insights into the existence of HMW aggregates of endogenous Hb in neuronal cells, we prepared detergent-insoluble fractions from iMN9D and Neuro2a cells. As shown in Fig. 3B, when equal amounts of total proteins were loaded, insoluble fractions revealed a much fainter signal at ~64 kDa, as expected for a globular soluble protein. The band corresponding to tetrameric Hb was almost undetectable. Instead, a clear smear in the region of HMW could be measured, thus indicating that Hb exists as part of large insoluble aggregates in neuronal cells *in vitro*.

Insoluble aggregates play an important role in neurodegenerative diseases, albeit their exact contribution to neuronal cell death is always under intense debate. Endogenous Hb has been detected in proteinaceous aggregates in human post-mortem brains from Alzheimer's disease [24], Parkinson's disease and Dementia with Lewy Body disease [16] patients as well as in neurofibrillary tangles in mouse models of familial Alzheimer's disease [17]. It will be interesting in the future to assess whether Hb aggregates are neuroprotective or neurotoxic and what are the molecular mechanisms underlying their formation.

3.4. Endogenous hemoglobin is expressed as a tetramer in vivo in the mouse brain

We then sought to assess the quaternary structure of endogenous Hb expressed in the mouse ventral midbrain, the region that is enriched of dopaminergic neurons and whose selective degeneration leads to Parkinson's disease. The ventral midbrain region was dissected from 12-months old C57BL6 mice. To preserve the native conformation of the proteins and to prevent breakdown of potential higher protein assemblies, the lysis buffer used to homogenize the tissues was free of detergents and denaturing agents. Total lysate (TL) was then separated by centrifugation into detergent-insoluble pellet (P) and supernatant

Please cite this article as: R. Russo, et al., Hemoglobin is present as a canonical $\alpha_2\beta_2$ tetramer in dopaminergic neurons, Biochim. Biophys. Acta (2013), http://dx.doi.org/10.1016/j.bbapap.2013.05.005

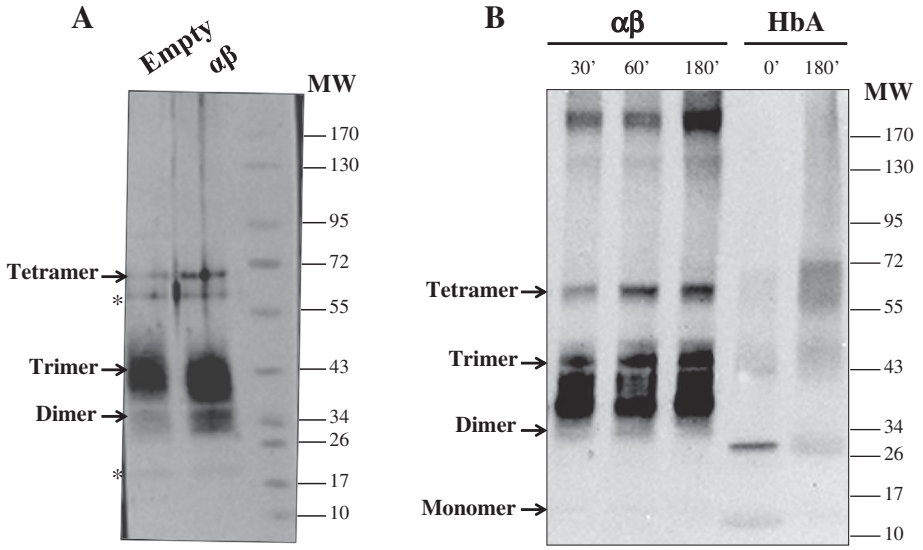

Fig. 2. In-cell cross-linking analysis of Hb structure. A) iMN9D cells overexpressing tagged α and β chains or empty control cells were treated with chemical cross-linker DSS while in culture. Equal amounts of total proteins were loaded on SDS–PAGE and analyzed by Western blotting using anti-Hb antibody. Hb staining is visible in empty cells, indicating the endogenous protein. Asterisks indicate non-specific bands. Images are representative of three independent experiments. B) iMN9D cells stably expressing α and β chains were incubated with chemical cross-linker DSS for the indicated time. After cell lysis, equal amounts of proteins were processed as in A. Purified HbA was included as control. Molecular weight markers are indicated for each gel (kDa). Monomeric, dimeric, trimeric and tetrameric species are indicated by arrows.

detergent-soluble (S) fractions. TL, S and P were loaded on native PAGE along with protein standards. Purified recombinant HbA was also included as control. Immunoblotting with Hb-specific antibody revealed that *in vivo* endogenous Hb from mouse ventral midbrain migrates with an apparent molecular weight of 64 kDa similarly to the purified recombinant protein (Fig. 4). Tetrameric Hb could be observed at similar levels in TL and S fractions. Interestingly, a smaller but detectable amount of Hb was associated to soluble HMW aggregates. Competition experiment verified that bands corresponding to tetrameric and HMW-associated Hb were indeed specific. Surprisingly, fraction P did not contain any Hb neither as tetramer or HMW aggregate (data not shown). All samples contained monomeric and dimeric species under denaturing conditions (data not shown).

To our knowledge this is the first time that native Hb from mouse brain is shown to exist as a tetramer *in vivo*. Recent studies indicate that upon aging, Hb levels are increased in neurons and the protein co-localizes with proteinaceous aggregates [16,24]. We could not find HMW insoluble aggregates of Hb *in vivo*, albeit these forms could be easily detectable in soluble fraction in the brain as well as in the insoluble fractions in neuronal cell lines. It remains to be assessed whether Hb retains its tetrameric structure and/or form intracellular insoluble aggregates when pathological conditions occur.

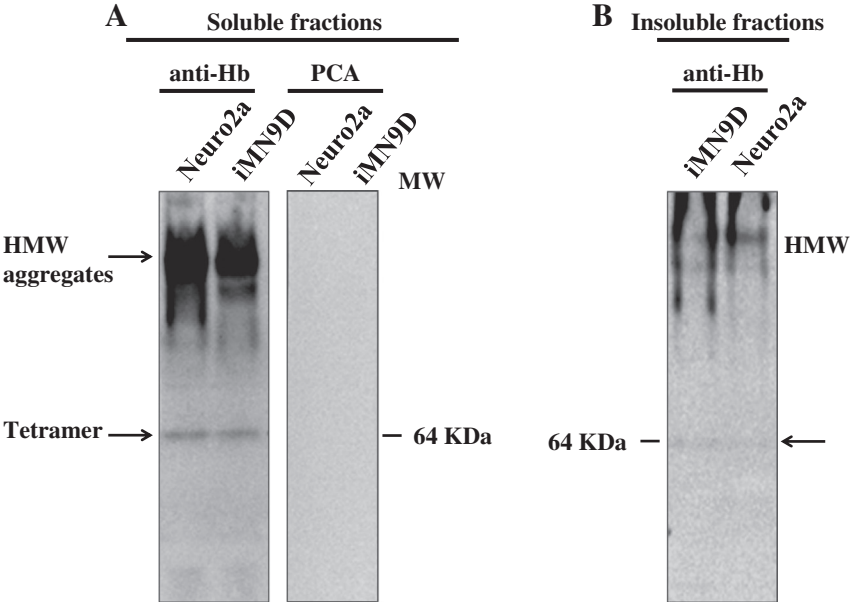

Fig. 3. Biochemical analysis of native endogenous hemoglobin in neuronal cell lines. A) Endogenous Hb is a tetramer in neuroblastoma cells. Dopaminergic (iMN9D) and non-dopaminergic (Neuro2a) neuronal cells were lysed and detergent-soluble proteins were recovered after centrifugation. Total protein content was determined with the Bio-Rad protein assay kit. Equal quantities were loaded on native PAGE and endogenous Hb was visualized by Western blot with anti-Hb antibody. Purified recombinant human Hb was used for protein competition assay (PCA). Relative molecular weight (MW) is indicated on the right (kDa). Tetramers and high molecular weight (HMW) aggregates are shown by arrows. Images are representative of three independent experiments. B) HMW aggregates containing Hb are present in the detergent-insoluble fraction of neuronal cells lines. iMN9D and Neuro2a cells were lysated as in A. After centrifugation, pellet was recovered and analyzed by native PAGE. Endogenous Hb was detected using anti-Hb antibody.

Please cite this article as: R. Russo, et al., Hemoglobin is present as a canonical $\alpha_2\beta_2$ tetramer in dopaminergic neurons, Biochim. Biophys. Acta (2013), http://dx.doi.org/10.1016/j.bbapap.2013.05.005

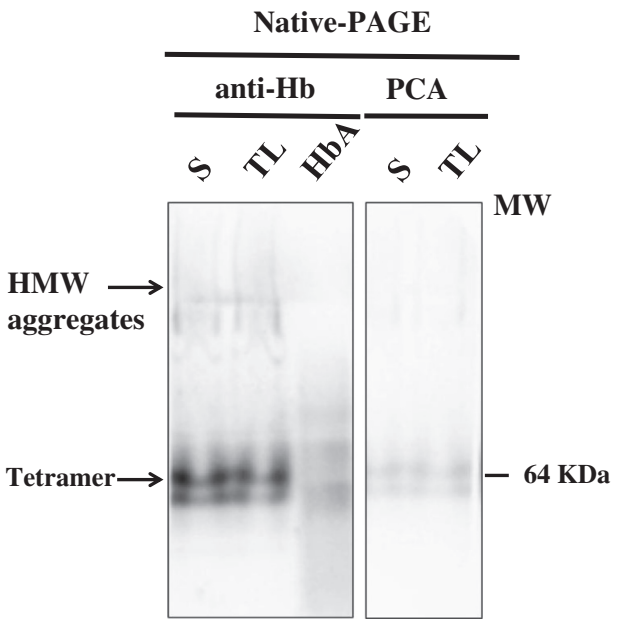

Fig. 4. Endogenous Hb is a tetramer *in vivo* in the mouse brain. Native Hb was extracted from the ventral midbrain of 12-months old C57BL6 mice. Tissue homogenization was performed under non-reducing and non-denaturing conditions. Total lysate (TL), detergent soluble (S) and insoluble (P) fractions were separated. Equal quantities of proteins were loaded on native PAGE. Purified recombinant HbA was included as control. Specificity of bands was assessed by competition assay (PCA). Relative molecular weight (MW) is indicated on the right (kDa). Hb tetramer is indicated by an arrow. The image is representative of two independent tissue preparations from four C57BL6 mice.

4. Conclusions

Hb is the main component of erythrocytes in the blood, where it serves as a molecular cargo of oxygen and carbon dioxide to and from tissues. The assembly of $\alpha_2\beta_2$ tetramer is essential for Hb to function as oxygen carrier in the blood. In recent years, expression of Hb has been observed in cell types other than erythrocytes, including dopaminergic neurons in the mouse [6] and human brain [16]. The exact function and structure of Hb in neurons is presently unknown.

Using native PAGE and in-cell cross-linking, we demonstrate that Hb is present as $\alpha_2\beta_2$ tetramer when overexpressed in dopaminergic iMN9D cell line. The canonical $\alpha_2\beta_2$ structure can also be observed for endogenous Hb expressed by dopaminergic and non-dopaminergic neuronal cell lines. Importantly, native Hb exists as a 64 kDa tetramer in mouse ventral midbrain *in vivo*.

This work suggests that neuronal Hb may retain some of the biochemical activities and biological functions of Hb of erythroid lineage laying down the foundation for a better understanding of its role in brain physiology and in neurodegenerative diseases.

Abbreviations

Hb	hemoglobin
SDS–PAGE	sodium dodecyl sulfate polyacrylamide gel electrophoresis
kDa	kilo Dalton
HMW	high molecular weight
DSS	disuccinimidyl suberate
DMEM	Dulbecco's modified Eagle's medium
EMEM	Eagle's minimal essential medium

Acknowledgments

We are indebted to all the members of the SG lab for thought-provoking discussions and to Cristina Leonesi for technical support. This work was supported by the Italian Ministry of Education, University and Research (FIRB grant prot. RBAP11FRE9) and by the European Territorial Cooperation program for Italy-Slovenia cross-border cooperation 2007–2013 (MINA, CUP D35C12002830003) to S.G. and by the Italian National Programme for Antarctic Research (PNRA) to C.V.

References

[1] M.F. Perutz, Mechanisms regulating the reactions of human hemoglobin with oxygen and carbon monoxide, Ann. Rev. Physiol. 52 (1990) 1–25.
[2] D.A. Newton, K.M. Rao, R.A. Dluhy, J.E. Baatz, Hemoglobin is expressed by alveolar epithelial cells, J. Biol. Chem. 281 (2006) 5668–5676.
[3] H. Nishi, R. Inagi, H. Kato, M. Tanemoto, I. Kojima, D. Son, T. Fujita, M. Nangaku, Hemoglobin is expressed by mesangial cells and reduces oxidant stress, J. Am. Soc. Nephrol. 19 (2008) 1500–1508.
[4] G. Tezel, X. Yang, C. Luo, J. Cai, A.D. Kain, D.W. Powell, M.H. Kuehn, W.M. Pierce, Hemoglobin expression and regulation in glaucoma: insights into retinal ganglion cell oxygenation, Invest. Ophthalmol. Vis. Sci. 51 (2010) 907–919.
[5] W. Liu, S.S. Baker, R.D. Baker, N.J. Nowak, L. Zhu, Upregulation of hemoglobin expression by oxidative stress in hepatocytes and its implication in nonalcoholic steatohepatitis, PLoS One 6 (2011) e24363.
[6] M. Biagioli, M. Pinto, D. Cesselli, M. Zaninello, D. Lazarevic, P. Roncaglia, R. Simone, C. Vlachouli, C. Plessy, N. Bertin, A. Beltrami, K. Kobayashi, V. Gallo, C. Santoro, I. Ferrer, S. Rivella, C.A. Beltrami, P. Carninci, E. Raviola, S. Gustincich, Unexpected expression of alpha- and beta-globin in mesencephalic dopaminergic neurons and glial cells, Proc. Natl. Acad. Sci. U. S. A. 106 (2009) 15454–15459.
[7] F. Richter, B.H. Meurers, C. Zhu, V.P. Medvedeva, M.F. Chesselet, Neurons express hemoglobin alpha- and beta-chains in rat and human brains, J. Comp. Neurol. 515 (2009) 538–547.
[8] D.W. Schelshorn, A. Schneider, W. Kuschinsky, D. Weber, C. Kruger, T. Dittgen, H.F. Burgers, F. Sabouri, N. Gassler, A. Bach, M.H. Maurer, Expression of hemoglobin in rodent neurons, J. Cereb. Blood Flow Metab. 29 (2009) 585–595.
[9] A.C. Straub, A.W. Lohman, M. Billaud, S.R. Johnstone, S.T. Dwyer, M.Y. Lee, P.S. Bortz, A.K. Best, L. Columbus, B. Gaston, B.E. Isakson, Endothelial cell expression of haemoglobin alpha regulates nitric oxide signalling, Nature 491 (2012) 473–477.
[10] L. Liu, M. Zeng, J.S. Stamler, Hemoglobin induction in mouse macrophages, Proc. Natl. Acad. Sci. U. S. A. 96 (1999) 6643–6647.
[11] M. Capulli, A. Angelucci, K. Driouch, T. Garcia, P. Clement-Lacroix, F. Martella, L. Ventura, M. Bologna, S. Flamini, O. Moreschini, R. Lidereau, E. Ricevuto, M. Muraca, A. Teti, N. Rucci, Increased expression of a set of genes enriched in oxygen binding function discloses a predisposition of breast cancer bone metastases to generate metastasis spread in multiple organs, J. Bone Miner. Res. 27 (2012) 2387–2398.
[12] T.A. Gorr, D. Wichmann, C. Pilarsky, J.P. Theurillat, A. Fabrizius, T. Laufs, T. Bauer, M. Koslowski, S. Horn, T. Burmester, T. Hankeln, G. Kristiansen, Old proteins — new locations: myoglobin, haemoglobin, neuroglobin and cytoglobin in solid tumours and cancer cells, Acta Physiol (Oxf.) 202 (2011) 563–581.
[13] X. Li, Z. Wu, Y. Wang, Q. Mei, X. Fu, W. Han, Characterization of adult alpha- and beta-globin elevated by hydrogen peroxide in cervical cancer cells that play a cytoprotective role against oxidative insults, PLoS One 8 (2013) e54342.
[14] E. Hirsch, A.M. Graybiel, Y.A. Agid, Melanized dopaminergic neurons are differentially susceptible to degeneration in Parkinson's disease, Nature 334 (1988) 345–348.
[15] L. Broadwater, A. Pandit, R. Clements, S. Azzam, J. Vadnal, M. Sulak, V.W. Yong, E.J. Freeman, R.B. Gregory, J. McDonough, Analysis of the mitochondrial proteome in multiple sclerosis cortex, Biochim. Biophys. Acta 1812 (2011) 630–641.
[16] I. Ferrer, A. Gomez, M. Carmona, G. Huesa, S. Porta, M. Riera-Codina, M. Biagioli, S. Gustincich, E. Aso, Neuronal hemoglobin is reduced in Alzheimer's disease, argyrophilic grain disease, Parkinson's disease, and dementia with Lewy bodies, J. Alzheimers Dis. 23 (2011) 537–550.
[17] J.Y. Chuang, C.W. Lee, Y.H. Shih, T. Yang, L. Yu, Y.M. Kuo, Interactions between amyloid-beta and hemoglobin: implications for amyloid plaque formation in Alzheimer's disease, PLoS One 7 (2012) e33120.
[18] C.Y. Chung, H. Seo, K.C. Sonntag, A. Brooks, L. Lin, O. Isacson, Cell type-specific gene expression of midbrain dopaminergic neurons reveals molecules involved in their vulnerability and protection, Hum. Mol. Genet. 14 (2005) 1709–1725.
[19] J.G. Greene, R. Dingledine, J.T. Greenamyre, Gene expression profiling of rat midbrain dopamine neurons: implications for selective vulnerability in parkinsonism, Neurobiol. Dis. 18 (2005) 19–31.
[20] E. Hermanson, B. Joseph, D. Castro, E. Lindqvist, P. Aarnisalo, A. Wallen, G. Benoit, B. Hengerer, L. Olson, T. Perlmann, Nurr1 regulates dopamine synthesis and storage in MN9D dopamine cells, Exp. Cell Res. 288 (2003) 324–334.
[21] H. Schagger, W.A. Cramer, G. von Jagow, Analysis of molecular masses and oligomeric states of protein complexes by blue native electrophoresis and isolation of membrane protein complexes by two-dimensional native electrophoresis, Anal. Biochem. 217 (1994) 220–230.
[22] W. Vandenberghe, R.A. Nicoll, D.S. Bredt, Stargazin is an AMPA receptor auxiliary subunit, Proc. Natl. Acad. Sci. U. S. A. 102 (2005) 485–490.
[23] F.E. Herrera, S. Zucchelli, A. Jezierska, Z.S. Lavina, S. Gustincich, P. Carloni, On the oligomeric state of DJ-1 protein and its mutants associated with Parkinson Disease. A combined computational and in vitro study, J. Biol. Chem. 282 (2007) 24905–24914.
[24] C.W. Wu, P.C. Liao, L. Yu, S.T. Wang, S.T. Chen, C.M. Wu, Y.M. Kuo, Hemoglobin promotes Abeta oligomer formation and localizes in neurons and amyloid deposits, Neurobiol. Dis. 17 (2004) 367–377.